

Autonomous High-Speed Overtaking in Structured Environments



Shilp Dixit

Supervisors: Dr. Saber Fallah
Dr. Umberto Montanaro

Examiners: Prof. Mark Cannon
Prof. John F Watts

Mechanical Engineering Sciences
University of Surrey

This dissertation is submitted for the degree of
Doctor of Philosophy

Faculty of Engineering and
Physical Sciences (FEPS)

December 2019

To my grandparents

śrīmatī Mahālakṣmī Dīkṣita & śrī Harivallabha Dīkṣita
śrīmatī Sulocanā Dvivedī & Dr. Prāṇaśamkara Dvivedī

and my parents

śrīmatī Latā Dīkṣita & śrī Subodha Candra Dīkṣita

समानी व आकूति: समाना हृदयानि वः ।
समानमस्तु वो मनो यथा वः सुसहासति ॥८:४९:४॥

— ऋग्वेद्

United be your purpose, harmonious be your feelings, collected be your mind, in the same way as all the various aspects of the universe exist in togetherness, wholeness..

— *Rgveda* 8:49:4

Declaration

I hereby declare that except where specific reference is made to the work of others, the contents of this dissertation are original and have not been submitted in whole or in part for consideration for any other degree or qualification in this, or any other university. This dissertation is my own work and contains nothing which is the outcome of work done in collaboration with others, except as specified in the text and Acknowledgements.

Shilp Dixit
December 2019

Acknowledgements

My journey through this PhD has been a truly life-changing experience which would not have been possible without the guidance, help, and support that I received from many people.

First and foremost I wish to say a very big thank you to my supervisor Dr. Saber Fallah who gave me an opportunity to work on this exciting project and become a part of his research lab. We have spent many hours discussing the various technical aspects of the work, applying polishing touches to the papers, and finalising the project deliverables in his office and I am truly grateful that he gave me freedom to explore the different facets of the thesis while being supportive. He has also encouraged me to grow professionally by letting me explore other opportunities via research assistantships and external projects.

A very special thank you to my co-supervisor Dr. Umberto Montanaro for his support and guiding me through the various phases of the PhD. His passion for mathematics and control engineering is contagious and I am thankful of all his help with writing mathematical proofs and technical papers. I sincerely thank him for his mentorship that helped me improve my ability for formulate mathematical problems and showed me the way to become a more rounded researcher. I fondly look back at the many riveting discussions we had over the years on topics beyond control engineering which presented me with a different perspective and played a key role in my development as an individual. Without his guidance and constant feedback this PhD would not have been achievable.

I gratefully acknowledge Jaguar Land Rover and the entire CARMA team for the financial support and in making the project come to life. As the PI of the CARMA team, Professor Mehrdad Dianati's valuable feedback and encouragement to extract the best output from our work helped immensely in pushing us to become the best possible researcher and I am thankful to him for imbibing this quality within the group. Thank you to David Oxtoby and Tom Mizutani from JLR for all their support with the knowledge transfer and publications throughout the duration of the PhD. I am also grateful to Mete Türedi and Maxime Penet for their tremendous help with moving towards the implementation of the steering controller on a test vehicle. Their

patience and guidance at ironing out the system integration issues is something I greatly value and I am sure we will soon be able to successfully test the controller on the experimental vehicle.

I would also like to thank the members of my defense committee, Professor John Watts and Professor Mark Cannon for their time and insightful questions.

A pleasant and fun atmosphere in the working group is important for surviving a PhD program and I feel lucky that I got the opportunity to share the lab with a fantastic group of passionate researchers. From collaborating and sharing each other's research via monthly meetings to burger & beer outings, each resulting in a memorable event and a valuable lesson that I will remember and cherish for a long time. I shared my penchant for sporting activities with my friends in the lab; the tennis tutorials with Mathias Metzler and Alessandro Scamarcio, squash sessions with Joao Aguiar and Shayan Taherian were some of my favourite activities outside research that I really looked forward to throughout my years at Surrey. The PhD program is fraught with peaks and troughs and but my labmates were always there to help and I feel grateful of the support and assistance that everyone in the lab extended to their fellow colleagues. A special mention to Arvind Tiwari, Piyush Mohanty, Kaushik Halder, and Ashish Sharma for sharing their delicacies with me and making me look forward to stealing their food.

I was also involved in activities outside university and I was lucky to get an opportunity to play Sunday English cricket with an amazing set of team-mates at the Uplands Cricket Club. The weekends spent playing cricket all over the Surrey countryside were among the highlights of my time as a PhD researcher. I am thankful to all of them for the many enjoyable matches and subsequent discussions reminiscing our exploits on the field and I hope I get to play with them next summer. A big thank you to all my friends from school and previous universities. Most of them are spread all over the globe but were there to support me at all times and I am really thankful for their friendship over the years.

A special shoutout of appreciation and gratitude to my friend Aswin Vairamani, my cousin Rohinee Didi, and my aunt Sudha Bua for their invaluable help in refining the thematic and philosophical aspects of the thesis.

Lastly, I thank my family for all their love, patience, and encouragement. My parents have always supported me in all my pursuits and raised me to be curious about science and technology. My elder brother Ishan, my Anisha Bhabhi, and younger brother Avi have always motivated me to follow all my dreams and I am lucky to have their constant guidance and support. A huge thank you to Sitara for being such a perfect baby and lighting up my phone screen with her antics during all video calls. Thank you.

Abstract

In this thesis, we design and develop controllers for trajectory planning and trajectory tracking to tackle autonomous high-speed overtaking for the next generation of autonomous vehicles. Both the controllers are developed for a JLR Range Rover Sport that is capable of autonomous driving functionalities. To assist with controller development, a high-fidelity vehicle model previously developed in IPG Carmaker is utilised that contains all the multi-body interactions and non-linear tyre characteristics.

Trajectory Planning

Autonomous high-speed driving is a safety-critical task and it is imperative that the planned trajectory of the vehicle can ensure safety (collision-avoidance) while computing smooth and feasible trajectories. We propose a trajectory planning framework that utilises information of the traffic vehicles to identify safe driving zones on the road using potential field functions and a robust model predictive controller for generating feasible trajectories that ensure the vehicle remains within the safe zones while performing the overtaking manoeuvre. The closed-loop performance of this controller is validated in a high-fidelity co-simulation environment.

Trajectory Tracking

The trajectory tracking controller is designed to ensure that the vehicle tracks the trajectory as closely as possible and preserves the lateral-yaw stability at all times. In this thesis, an Enhanced Model Reference Adaptive Control algorithm is used to design a generic lateral tracking controller for an autonomous vehicle. The control algorithm is applied to a vehicle path tracking problem and its tracking performance is investigated when subjected to external disturbances such as crosswind, road surface changes, modelling errors, and parameter miss-matches in a high-fidelity co-simulation environment.

Combined Planning & Control

Finally, the design of a combined motion planning & control scheme is carried out. The lateral tracking controller is augmented to include the dynamics of the steering actuator system and the updated tracking controller is combined with the RMPC based sophisticated path-planning framework to present a hierarchical closed-loop control architecture for autonomous overtaking. This architecture is implemented on the IPG CarMaker/Simulink environment and validated with different overtaking manoeuvring scenarios.

Table of contents

List of figures	xvii
List of tables	xxi
Nomenclature	xxiii
1 Introduction	1
1.1 Motivation	1
1.2 Objectives	3
1.3 Outline & Contributions	4
2 Background & Literature Review	7
2.1 Introduction	8
2.2 System Architecture	12
2.3 Trajectory Planning	13
2.4 Trajectory Tracking	19
2.4.1 Tracking Controllers	21
2.5 Summary	25
3 Trajectory Planning	27
3.1 Introduction	27
3.2 Mathematical Notations and Definitions	31
3.3 Control Oriented Vehicle Model	32
3.4 Control Formulation	35
3.4.1 MPC with Terminal Set Constraints	35
3.4.2 Robust MPC with Terminal Set Constraints	37
3.5 Local Risk Map	40
3.5.1 Lane Velocity Potential	41

Table of contents

3.5.2	Road Potential	41
3.5.3	Lane Potential	42
3.5.4	Car Potential	42
3.6	Selection of the Target Point	43
3.7	Trajectory Generation	45
3.7.1	Nominal MPC	45
3.7.2	Robust MPC	46
3.7.3	Collision Avoidance Constraints	47
3.8	Numerical Results	50
3.8.1	Robust positive invariant set and MPC implementation	53
3.8.2	Simulation Results	54
3.9	Summary	60
4	Trajectory Tracking	63
4.1	Introduction	63
4.2	Mathematical Notations and Definitions	67
4.3	Control Formulation	70
4.4	Path Tracking	76
4.5	Numerical Validation	80
4.5.1	Manoeuvre I: Navigating a hypothetical highway section	81
4.5.2	Manoeuvre II: Driving in crosswind	86
4.5.3	Manoeuvre III: Lane change in low friction conditions with additional passengers	87
4.6	Summary	93
5	Combined Motion Planning & Control	95
5.1	Introduction	95
5.2	Steering Actuator Dynamics	100
5.2.1	Model Augmentation	101
5.3	Control Law	103
5.4	Test Track	103
5.4.1	Local Reference Curvature Generation	104
5.4.2	Numerical Validation	106
5.5	High-Speed Overtaking	113
5.5.1	Local Reference Trajectory	114
5.5.2	Numerical Validation	115
5.6	Summary	124

Table of contents

6 Conclusions & Recommendations	127
6.1 Conclusions	127
6.2 Recommendations	131
6.3 Closing Remarks	132
References	135
Appendix A List of Parameters for Initialisation	151
Appendix B Development of a Prediction Model	155
Appendix C Derivation of Cost Function: Nominal MPC	159
Appendix D Derivation of Cost Function: Robust MPC	161
Appendix E Frequency Response: Vehicle Lateral-Yaw Dynamics	163
Appendix F Determination of Look-Ahead Distance	165
F.1 Medium-speed driving	166
F.2 High-speed driving	167
Appendix G Design of Controllers for Reference Model	169
G.1 Design of Reference Feedforward Controller: K_R^*	169
G.2 Design of Reference Feedback Controller: K_X^*	170
G.3 Closed-loop Dynamics	171

List of figures

2.1	Basic schematic of an overtaking manoeuvre. Note: Different sub-manoeuvres are (i) lane-change; (ii) pass lead vehicle; (iii.a) merge back into original lane; (iii.b) continue in faster lane to pass traffic	10
2.2	Visibility of an autonomous vehicle. Note: SV: Subject Vehicle, TV: Traffic Vehicle. Sensor performance specifications are based on [39]	11
2.3	Overview of an autonomous driving system	13
2.4	General control architecture for an autonomous vehicle [43, 48, 54–56]. (V2X block with dot-dash boundary: optional functionality)	14
2.5	Trajectory planning via (a) Potential Fields [48]; (b) RRT [68]; (c) Virtual Reference Tracking [10]; (d) Model Predictive Control [52]	17
3.1	Road setup: coordinate frames and range of local risk map	32
3.2	Kinematic bicycle model	33
3.3	Schematic to explain identification of collision avoidance zone. Note: SV – blue rectangle, LV and surrounding unsafe region – red polygon, target coordinate – magenta cross, safe zone – green polygon	47
3.4	Closed-loop framework for trajectory planning. Note: LV denotes lead vehicle	50
3.5	Error polyhedron and resulting tightened input set obtained by changing magnitude of eigenvalue	55
3.6	Snapshot of simulation (simulation time $t = 14\text{ s}$); (a) Cumulative potential field U_r from road, lane, and obstacle vehicle; (b) Contour plot of the potential field along with the reachable set (yellow) and reference target on the road (magenta cross). Note: Blue rectangle depicts the subject vehicle and the rectangle in red depicts the lead vehicle	57

List of figures

3.7	Snapshot of simulation demonstrating: reference targets (\times) for different configurations of subject vehicle (\square) and lead vehicle (\diamond) while driving on a highway. Note: solid lines (—) are the road boundaries and dashed line (---) is the lane marking	58
3.8	Simulation results: SV and LV trajectories, longitudinal velocity, heading angle, longitudinal acceleration, and steering angle for a high-speed overtaking manoeuvre. Note: (---) are the system constraints .	59
3.9	Simulation results: trajectory of the subject vehicle (SV) during an overtaking manoeuvre in the lead vehicle (LV) frame of reference (ξ_0, η_0)	60
4.1	EMRAC control scheme [140]	66
4.2	Overview of path-tracking model. Note: Reference path (black-dashed)	78
4.3	Reference road curvature and longitudinal velocity for hypothetical highway driving scenario (Manoeuvre I)	81
4.4	Evolution of K_X , K_R , and K_I for hypothetical highway driving scenario (Manoeuvre I)	82
4.5	Evolution of $ \phi $ and $ \phi_N $ for hypothetical highway driving scenario (Manoeuvre I). Note: Unbounded switching action (Red), gain of the switching action bounded by σ -modification (Blue-dashed) . .	83
4.6	Dynamics of system for hypothetical highway driving scenario (Manoeuvre I). Note: Unbounded switching action (Red), gain of the switching action bounded by σ -modification (Blue dashed), reference model (solid black)	84
4.7	Evolution of state errors for hypothetical highway driving scenario (Manoeuvre I). Note: Unbounded switching action (Red), gain of the switching action bounded by σ -modification (Blue-dashed), reference model (Solid black)	85
4.8	Net control action for hypothetical highway driving scenario (Manoeuvre I). Note: Unbounded switching action (Red), gain of the switching action bounded by σ -modification (Blue-dashed)	86
4.9	Dynamics of system for driving in crosswinds (Manoeuvre II). Note: Uncontrolled (Grey), Switching action bounded by σ -modification (Blue-dashed)	88
4.10	Evolution of $ \phi_N $ and control input for driving in crosswinds (Manoeuvre II)	89
4.11	Reference road curvature for lane changes in low friction (Manoeuvre III)	89

4.12	Dynamics of system for lane changes in low friction (Manoeuvre III). Note: Nominal conditions (Grey-dashed), low-friction and extra passengers (Blue)	91
4.13	Evolution of state errors for lane changes in low friction (Manoeuvre III). Note: Nominal conditions (Grey-dashed), low-friction and extra passengers (Blue)	92
4.14	Evolution of $\ \phi_N\ $ and control input for lane changes in low friction (Manoeuvre III). Note: Nominal conditions (Grey-dashed), low-friction and extra passengers (Blue)	93
5.1	Schematic of a steering actuator system illustrating the input and output interfaces	101
5.2	Frequency-domain response of steering dynamics with exact and approximated delays.	102
5.3	Desired lateral and longitudinal signals for Gaydon test-track; (a) path curvature κ_{des} ; (b) longitudinal velocity v_{des}	105
5.4	Geometric representation of reference curvature generation from given desired path (grey)	105
5.5	Closed-loop control structure: combined local path planning & tracking	107
5.6	Evolution of the EMRAC states and errors for driving on test-track. Note: reference model (red), system states (blue), error between reference model and system (orange)	109
5.7	Simulation results; (a) path coordinates p ; (b) curvature κ as a function of distance travelled along path; (c) longitudinal velocity v over time	110
5.8	Simulation results for tracking desired path; (a) front wheel steering angle δ_f ; (b) norm of switching action $\ \phi_N\ $	111
5.9	Comparison of simulation results for tracking desired coordinates with variation in delay of steering actuator system $\bar{\tau}_{sa}$; (a) front wheel steering angle δ_f ; (b) cross track error η_{xt}	113
5.10	Geometric representation of reference curvature generation from RMPC optimal trajectory. Note: Green dots represent the reference coordinates $p_{ra}^* = (\xi_{ra}^*, \eta_{ra}^*)$ for the rear-axle of the SV	114
5.11	Proposed closed-loop control architecture for autonomous overtaking: combined trajectory planning & tracking	115
5.12	Simulation Results: SV and LV trajectories, longitudinal velocity v , heading angle ψ , longitudinal acceleration a_x , and steering angle δ_f for a high-speed overtaking manoeuvre. Note: (- -) are the system constraints	118

List of figures

5.13 Simulation Results: comparison of reference curvature κ_{ref} and SV's estimated curvature $\kappa \approx r_z/v$ during the overtaking manoeuvre	119
5.14 Simulation results, evolution of the internal states of the EMRAC controller during the overtaking manoeuvre; (a) lateral velocity v_y ; (b) yaw-rate r_z ; (c) lateral error η_e ; (d) heading angle error ψ_e	121
5.15 Simulation results: trajectory of the subject vehicle (SV) during an overtaking manoeuvre in the lead vehicle (LV) frame of reference (ξ_0, η_0)	122
5.16 Simulation results: evolution of the lateral acceleration a_y of the subject vehicle (SV) during an overtaking manoeuvre.	123
5.17 Simulation results, comparison while overtaking in nominal and low-friction conditions; (a) control action δ_f ; (b) norm of gain for continuous part of control action $ \phi $; (c) norm of gain for switching action $ \phi_N $	125
B.1 Schematic of a prediction model	155
E.1 Frequency Response Function: steering angle δ_f to lateral velocity v_y	163
E.2 Frequency Response Function: steering angle δ_f to yaw-rate r_z	164
F.1 Look-ahead distance ξ_{la} and lateral error $\eta_{e,\text{la}}$ at look-ahead point . .	165
F.2 Poles and Zeros of the system $G_{yu}(s)$ with $v_{x,\text{nom}} = 15.27 \text{ m s}^{-1}$ for different look-ahead distances	166
F.3 Poles and Zeros of the system $G_{yu}(s)$ with $v_{x,\text{nom}} = 29.18 \text{ m s}^{-1}$ for different look-ahead distances	167

List of tables

1.1	SAE J3016™: Levels of driving automation [4]	2
2.1	Summary of techniques for trajectory planning to avoid a moving obstacle	19
2.2	Summary of control strategies for vehicle trajectory tracking [79, 82, 86, 87, 89]	24
A.1	Design Parameters: Environment and Situational Awareness	151
A.2	Design Parameters: Robust MPC for Trajectory Planning	152
A.3	Design Parameters: EMRAC for lateral tracking	152
A.4	Design Parameters: EMRAC for lateral tracking: Test-track	153
A.5	Design Parameters: EMRAC for lateral tracking: Overtaking Manoeuvre	154

Nomenclature

Roman Symbols

\hat{x}	Target state vector	
$\mathcal{B}(\cdot, \cdot)$	set representing an open ball with given centre and radius	
\mathcal{G}	set of safe coordinates around subject vehicle	
\mathcal{R}	finite time reachability set of a system	
\mathcal{S}	set of Lebesgue measure zero	
\mathcal{U}	closed set representing the input constraints	
\mathcal{W}	closed set representing bounded disturbance	
\mathcal{X}	closed set representing the state constraints	
\mathcal{Z}	closed set representing error bounds	
\mathfrak{s}	discontinuous vector field	
A	system matrix of a state-space system	
$a(\cdot)$	coefficient of x in the general form of equation of a line	
A_m	system matrix of EMRAC reference model	
a_x	longitudinal acceleration	$[\text{m s}^{-1}]$
B	input matrix of a state-space system	
$b(\cdot)$	coefficient of y in the general form of equation of a line	
B_m	input matrix of EMRAC reference model	
C	output matrix of a state-space system	
$C(\cdot)$	equivalent lateral stiffness of axle	$[\text{N rad}^{-1}]$
$c(\cdot)$	coefficient in the general form of equation of a line	
D	feed-through matrix of a state-space system	

Nomenclature

d	bounded disturbance signal	
$d_{(\cdot)}$	distance from the centre of rear-axle along the longitudinal axis of the vehicle [m]	
e	error vector	
f	vector space map	
I_z	moment of inertia around z -axis	[kg m ²]
K_Ω	nominal controller for terminal set	
K_{FB}^*	feedback control gain of EMRAC reference model	
K_{FF}^*	feedforward control gain of EMRAC reference model	
K_I	integral control gain	
K_N	switching control gain	
K_R	feedforward control gain	
K_X	feedback control gain	
$l_{(\cdot)}$	distance of axle from center of gravity	[m]
M	mass of vehicle	[kg]
N	Prediction Horizon	
N_c	Control Horizon	
P	solution of Lyapunov equation	
p	point in a two dimensional coordinate space	
Q	weighting matrix for state cost	
R	weighting matrix for input cost	
r	reference signal	
$R_{(\cdot)}$	radius of curvature of path	[m]
r_z	yaw-rate	[rad s ⁻¹]
T	weighting matrix for terminal state cost	
t	time vector	
t_s	sampling time	
u	input vector	
U_i	stack of control inputs	
U_r	net potential in road frame of reference	
U_{car}	obstacle potential	

U_{lane}	lane potential	
U_{road}	road potential	
U_{vel}	lane velocity potential	
V	Lyapunov Function	
v	velocity	$[\text{m s}^{-1}]$
V_N	Performance Index/Cost Function	
v_y	lateral velocity	$[\text{m s}^{-1}]$
w	bounded process-disturbance vector	
w_{lane}	width of a lane	$[\text{m}]$
x	state vector	
X_i	stack of predicted states	
y	output vector	
y_e	output error	

Greek Symbols

$\alpha(\cdot)$	weight for the integral part of the adaptive gain	
$\bar{\tau}_{\text{sa}}$	time delay of nominal steering actuator system	$[\text{s}]$
β	vehicle side-slip angle	$[\text{rad}]$
$\beta(\cdot)$	weight for the proportional part of the adaptive gain	
δ	steering angle	$[\text{rad}]$
η	lateral position	$[\text{m}]$
η_{xt}	cross-track error	$[\text{m}]$
$\eta_{e,\text{la}}$	lateral error between desired path and vehicle's longitudinal axis at look-ahead point	$[\text{m}]$
η_e	lateral position error	$[\text{m}]$
κ	path curvature	
λ	eigenvalue	
$\mu_{\text{road,ref}}$	reference friction coefficient of road surface	
μ_{road}	friction coefficient of road surface	
Φ	prediction matrix for state propagation	
$\phi(\cdot)$	integral part of adaptive gain	

Nomenclature

Ψ	prediction matrix for input propagation	
ψ	heading angle	[rad]
ψ_e	heading angle error	[rad]
ρ	combined vector space of states and inputs	
τ	torque	[N]
τ_{sa}	time delay of steering actuator system	[s]
θ	sub-space of steady-states and inputs	
ξ	longitudinal position	[m]

Subscripts

0	initial value
max	maximum limits
min	minimum limits
des	desired value
f	front
r	rear
a	augmented
ca	collision avoidance
c	in continuous-time domain
d	in discrete-time domain
path	pertaining to path tracking model
ss	steady-state
t	related to terminal set/state
x	along longitudinal axis
y	along lateral axis
la	look ahead
ref	reference signal
sa	steering actuator
xt	cross-track

Acronyms / Abbreviations

qp	quadratic programming
------	-----------------------

Nomenclature

ABS	Anti-lock Braking System
ACC	Adaptive Cruise Control
ADAS	Advanced Driver-Assistance Systems
AEB	Automated Emergency Braking
AFS	Active Front Steering
C.G	Center of Gravity
CACC	Cooperative Adaptive Cruise Control
DARPA	Defense Advanced Research Projects Agency
DLC	Discretionary Lane Change
dof	degree of freedom
dv	decision variable
dv	decision variable
ECU	Electronic Control Unit
EMRAC	Enhanced Model Reference Adaptive Control
GNC	Guidance and Navigation Control
I&I	Inversion & Immersion
LDM	Local Dynamic Map
LiDAR	Light Detection And Ranging
LPV	Linear Parameter Varying
LQR	Linear Quadratic Regulator
LTV	Linear Time Varying
LV	Lead Vehicle
MIMO	Multi-input Multi-output
MLC	Mandatory Lane Change
MPC	Model Predictive Control
MRAC	Model Reference Adaptive Control
par	parameter
par	parameter
PID	Proportional Integral Derivative
PID	Proportional Integral Derivative

Nomenclature

Radar	Radio Detection And Ranging
RMPC	Robust Model Predictive Control
RRT	Rapidly-exploring Random Tree
SCMPC	Scenario-based Model Predictive Control
SIMO	Single-input Multi-output
SMC	Sliding Mode Control
SV	Subject Vehicle
TTC	Time-to-Collision
TV	Traffic Vehicle
V2X	Vehicle-to-Everything

Introduction

अक्रमेणानुपायेन कर्मारम्भो न सिद्धति ॥२६॥

— तत्त्वोपाख्यानम्

A work begun with no order and means does not succeed.

— *Tantrapākhyāna* 26

1.1 Motivation

The confluence of personal passion towards cars and a desire to better current and future vehicles through meaningful contributions in vehicle dynamics & control is the motivation behind this thesis.

With substantial improvements being made across the board in sensors capabilities, computing performance, communication systems, advanced control techniques, etc. the first two decades of the 21st century have given a great boost to the development of intelligent vehicles. The rate of progress in the field of intelligent transportation systems has been rapid and quickly jumped from providing only assistance during certain times (e.g., ABS, traction control, etc.) to more advanced capabilities such as lane-keeping, automated parking, assisted lane changing, emergency braking, reading road signs, etc. Moreover, many of the premium series production vehicles provide self-driving capabilities under certain scenarios such as driving in slow moving traffic up to 60 km h^{-1} , park and summon from parking lots, advanced highway cruising capabilities, etc. making SAE level 2 of autonomy already available to the customer and deployed in real world scenarios, see Table 1.1. These features primarily rely on a vehicle's on-board sensor suite (e.g., RADAR, vision, LiDAR, and ultrasound) to gain awareness of its environment and use this information as input to advanced algorithms to continuously monitor and update steering, acceleration, and braking levels for performing the semi-autonomous capabilities mentioned above. As is natural for any technological endeavour, the next steps for engineers and researchers alike is to unlock level 3 and 4 of automation

Introduction

keeping in mind the eventual goal of full autonomy i.e., SAE level 5. Moreover, it is important to be cognizant of the fact that the solutions and systems proposed to achieve any kind of autonomy should be scalable from prototype vehicles to millions of vehicles plying on public roads. Therefore, the safety and reliability of autonomous vehicles needs to be proactively illustrated. To achieve comparable failure rates as the aircraft industry, then the safety goal for autonomous vehicles is to have a mean time between catastrophic failures of 10^9 h [1]. The ISO 26262 standard provide a standardised and widely accepted practice that provides a methodical verification and validation procedure to ensure automotive safety [2]. However, the ISO 26262 standard does not cover all aspects for mapping the various aspects of an autonomous vehicle within its verification and validation framework. A comprehensive review of the unique challenges for verification and validation of autonomous vehicles and the mapping of the technical aspects to the ISO 26262 standard are provided in [3].

Table 1.1 SAE J3016TM: Levels of driving automation [4]

SAE Automation Levels	Description
0 – No Automation	The full-time performance by the human driver of all aspects of the dynamic driving task, even when enhanced by warning or intervention systems.
1 – Driving Assistance	The driving mode-specific execution by a driver assistance system of either steering or acceleration/deceleration using information about the driving environment and with the expectation that the human driver perform all remaining aspects of the dynamic driving task.
2 – Partial Automation	The driving mode-specific execution by one or more driver assistance systems of both steering or acceleration/deceleration using information about the driving environment and with the expectation that the human driver perform all remaining aspects of the driving task.
3 – Conditional Automation	The driving mode-specific performance by an automated driving system of all aspects of the dynamic driving task with the expectation that the human driver will respond appropriately to a request to intervene.
4 – High Automation	The driving mode-specific performance by an automated driving system of all aspects of the dynamic driving task, even if a human driver does not respond appropriately to a request to intervene.
5 – Full Automation	The full-time performance by an automated driving system of all aspects of the dynamic driving task under all roadway and environmental conditions that can be managed by a human driver.

The next set of self-driving capabilities that need to be achieved involve manoeuvres at higher vehicle speeds, greater interaction with other participating traffic

members, increased operating range, all weather capability, etc. However, manoeuvres with higher speeds and increased traffic interaction are inherently complex and thus require a renewed focus on safety of all road participants and requirements such as all weather capabilities highlighting the need for feasibility of the system at all times. It is also noteworthy that gaining the ability to operate safely in diverse environments is highly beneficial as it provides self-driving capabilities to a larger set of users to operate the vehicles in varied operating conditions.

Overtaking slower moving traffic vehicles in high-speed environments such as highways is one such manoeuvre that requires precise control of the lateral and longitudinal motion of the vehicle at high-speeds while ensuring all safety considerations are met and occupant comfort is not sacrificed. Furthermore, gaining the ability to overtake autonomously will not only allow a vehicle to travel further down the road without the need of human intervention but also pave way for performing other tasks such as merging and leaving a highway, collision avoidance, etc.

1.2 Objectives

The aim of this thesis is to improve the autonomous driving capabilities of a vehicle in high-speed environments. The objective is to understand how to design controllers for motion control of a vehicle to perform high-speed manoeuvres autonomously. This leads to the main objective of this research.

Design & develop a closed-loop control architecture that enables a vehicle to perform overtaking manoeuvres at high-speeds in a safe and acceptable manner.

Since, planning and controlling the combined lateral and longitudinal motion of a vehicle is a complex and safety critical task, the approach taken is to tackle it in a sequential manner. The first aspect is to study the immediate surrounding of the vehicle and generate collision-free and feasible trajectories to perform an overtaking manoeuvre. This leads to the following objective

Develop a trajectory planning framework to generate collision-free and feasible trajectories for high-speed overtaking.

Controlling the steering angle of a vehicle to follow a given path is a complex challenge due to the myriad interactions between road, environment, and vehicle systems. This results in the following objective for control of steering angle to track a given path

Introduction

Design a generic steering controller for trajectory tracking to perform typical highway driving manoeuvres.

Finally, the trajectory planning and trajectory tracking controller need to be combined seamlessly to achieve an integrated solution that allows a vehicle to plan and track trajectories to perform an overtaking manoeuvre. This integration should be such that the individual performance characteristics of the controllers are not compromised. Thus, this leads to the following objective

Combine the planning and tracking controller to formulate an integrated motion control architecture with the capability of performing a high-speed overtaking manoeuvre autonomously.

1.3 Outline & Contributions

This section provides a brief outline of the thesis. Additionally, the aim of the work in each chapter and relevant contributions to the field are summarised.

Key takeaways from relevant research work pertaining to the topic of trajectory planning, trajectory tracking for high-speed autonomous vehicles is discussed in Chapter 2. The review helped in comparing the different approaches for trajectory planning & control based on aspects such as feasibility, design approach, performance, etc. Moreover, the review highlighted the need for an autonomous overtaking system that provided safe, dependable, and robust operation by considering vehicle dynamics, environmental conditions, etc. This chapter is based on:

- **Dixit, S.**, Fallah, S., Montanaro, U., Dianati, M., Stevens, A., McCullough, F. and Mouzakitis, A. Trajectory planning and tracking for autonomous overtaking: State-of-the-art and future prospects. *Annual Reviews in Control*, 45 (2018), pp.76-86.

In Chapter 3, the design of a modular framework for trajectory planning to perform high-speed overtaking is discussed. The framework consists of an artificial potential field based situational awareness functionality to identify safe driving zones coupled to a model predictive control approach for generating feasible trajectories to steer the vehicle through the safe zones. Simulation studies are performed to demonstrate the ability of the proposed closed-loop framework to generate feasible and safe trajectories for autonomous overtaking even when the velocity of the subject vehicle is not constant. This chapter is based on:

- **Dixit, S.**, Montanaro, U., Dianati, M., Oxtoby, D., Mizutani, T., Mouzakitis, A. and Fallah, S. Trajectory Planning for Autonomous High-Speed Overtaking in

1.3 Outline & Contributions

Structured Environments Using Robust MPC. *IEEE Transactions on Intelligent Transportation Systems* (2019).

- **Dixit, S.**, Montanaro, U., Fallah, S., Dianati, M., Oxtoby, D., Mizutani, T. and Mouzakitis, A. Trajectory Planning for Autonomous High-Speed Overtaking using MPC with Terminal Set Constraints. In *2018 21st International Conference on Intelligent Transportation Systems (ITSC)* (pp. 1061-1068). IEEE.
- Trajectory planning framework is subject to patent under UKIPO GB1801968.7 (under review)

Chapter 4 is based on the design of a generic lateral tracking controller to follow reference curvatures at high-speeds. The enhanced model reference adaptive control has been utilised and the issue of the unbounded gain for the switching action has been systematically tackled with a σ -modification strategy. The closed-loop system has been proven to be ultimate bounded through the use of an extended Lyapunov theory for discontinuous systems with the aim of ensuring the closed-loop dynamics of the vehicle follow a given reference model despite model miss-matches, uncertainties, and disturbances acting on the system. The proposed controller is numerically validated in a high-fidelity simulation environment to demonstrate its ability to accurately track reference curvatures that are typical for highway driving. This chapter is based on:

- **Dixit, S.**, Montanaro, U., Fallah, S., Dianati, M. and Mouzakitis, A. Integral MRAC with Bounded Switching Gain for Autonomous Vehicle Lateral Tracking. *IEEE Transactions on Control Systems Technology*. (undergoing revisions).

In Chapter 5, the trajectory planning & tracking controllers are combined to realise a hierarchical closed-loop architecture for autonomous high-speed overtaking. Moreover, the steering actuator dynamics are also included within the design of the tracking controller to compute more realistic control signals. The resultant closed-loop architecture is numerically validated by simulation studies and it shown to be an effective method for performing overtaking manoeuvres even in severe weather conditions. This chapter forms the basis for an academic paper that is in preparation to be submitted for publication in a peer-reviewed journal.

The conclusions of the work and recommendations for future research directions are presented in Chapter 6.

In addition to the contributions presented above, close collaboration with research colleagues also resulted in the following publications.

Introduction

- Taherian, S., Montanaro, U., **Dixit, S.** and Fallah, S. Integrated Trajectory Planning and Torque Vectoring for Autonomous Emergency Collision Avoidance. In *2019 22nd International Conference on Intelligent Transportation Systems (ITSC)* (pp. 2714-2721). IEEE.
- Montanaro, U., **Dixit, S.**, Fallah S. Adaptive Control and Robust MPC for Linearising Longitudinal Vehicle Dynamics for Platooning Applications. In *2019 26th IAVSD Symposium on Dynamics of Vehicles on Roads and Tracks (IAVSD)*.
- Montanaro, U., **Dixit, S.**, Fallah, S., Dianati, M., Stevens, A., Oxtoby, D. and Mouzakitis, A. Towards connected autonomous driving: review of use-cases. *Vehicle System Dynamics* (2019), 57(6), pp.779-814.

Chapter 2

Background & Literature Review

यस्तु संचरते देशान् यस्तु सेवेत पण्डितान् ।
तस्य विस्तारिता वृद्धिस्तैलविन्दुरिवाम्भसि ॥ ११:८९ ॥

— सुभाषित मंजरी

The intelligence of a person who travels in different countries and associates with scholars expands, just as a drop of oil expands in water.

— *Subhāṣita Māñjari* 11:89

Trajectory planning and trajectory tracking constitute two important functions of an autonomous overtaking system and a variety of strategies have been proposed in the literature for both functionalities. However, uncertainties in environment perception using the current generation of sensors has resulted in most proposed methods being applicable only during low-speed overtaking. In this chapter, trajectory planning and trajectory tracking approaches for autonomous overtaking systems are reviewed. The trajectory planning techniques are compared based on aspects such as real-time implementation, computational requirements, and feasibility in real-world scenarios. This review shows that two important aspects of trajectory planning for high-speed overtaking are: (i) inclusion of vehicle dynamics and environmental constraints and (ii) accurate knowledge of the environment and surrounding obstacles. The review of trajectory tracking controllers for high-speed driving is based on different categories of control algorithms where their respective advantages and disadvantages are analysed. This study shows that while advanced control methods improve tracking performance, in most cases the results are valid only within well-regulated conditions. Therefore, existing autonomous overtaking solutions assume precise knowledge of surrounding environment which is not representative of real-world driving. The chapter also discusses how in a connected driving environment, vehicles can access additional information that can expand their perception. Hence, the potential of cooperative information sharing for aiding autonomous high-speed overtaking manoeuvre is identified as a possible solution.

2.1 Introduction

ODERN cars are equipped with various sensors and electronic systems to reduce the workload of a driver by providing emergency assistance (e.g., ABS, traction control, stability control, etc.), ADAS (e.g., cruise control, lane keeping, crosswind assistance, blind spot detection, etc.), and navigational assistance (e.g., trip planning, route selection, regular traffic update, etc.). However, the next generation of intelligent vehicles are expected to have increased capabilities which allow automated manoeuvring in various driving scenarios [6, 7]. Overtaking is one of the most common driving manoeuvre and any vehicle capable of end-to-end autonomy must have the ability to determine if, when, and how to perform this driving task.

Overtaking is a complex driving task as it involves both lateral and longitudinal motions of an overtaking vehicle (subject vehicle) while avoiding collisions with a slower moving vehicle (lead vehicle) [8]. Additional complexity arises due to different environmental conditions (e.g., road legislations, visibility, weather, etc.) and diversity of road-users (e.g., small cars, buses, trucks, etc.) [9]. Typically, an overtaking manoeuvre is considered successful on proper completion of three sub-manoeuvres namely, (i) lane change to overtaking lane, (ii) pass lead vehicle(s), and (iii) lane change back to original lane [10]. The lane change sub-manoeuvre which indicates the start and the end of an overtake can be classified under two categories; (i) Discretionary Lane Change (DLC) and (ii) Mandatory Lane Change (MLC) [11]. A DLC sub-manoeuvre is performed when the immediate traffic situation in the faster lane is deemed to be better than the current lane and thus, the lane change is performed in anticipation of an improvement in the immediate driving conditions. On the other hand, an MLC sub-manoeuvre is performed due to compulsion arising from traffic rules (e.g., stalled vehicle, need to follow desired route, etc.). Moreover, the lane change to return back to the original lane can also be either DLC or MLC based on traffic conditions in each lane, legislation, etc. thus, transforming an overtaking manoeuvre into a complex task of dynamically choosing the best driving lane based on (i) legislation, (ii) driving intentions, and (iii) instantaneous traffic situation. This inference that the choice of lane is affected by both; (i) driving intention, and (ii) neighbourhood traffic conditions was verified in [12] using an integrated model (combining MLC and DLC) for lane changing behaviour based on gap acceptance (lead and lag gap). Therefore, it is noted that due to the dynamic nature of driving environments (i.e., traffic conditions in original and fast lane, speed limits, road conditions, etc.) overtaking is not standardised manoeuvre and thus, each over-

This chapter is based on [5]

taking manoeuvre in real-world scenarios is unique. This uniqueness arises from variations in number of overtaken vehicles, duration of overtake, relative velocity between concerned vehicles, distance between concerned vehicles, etc. [13–20]. For an autonomous vehicle, feasibility of an overtaking manoeuvre is evaluated on the basis of safety based on subject vehicle’s states as well as surrounding information leading to a discrete outcome for making tactical decisions (i.e., either perform lane-change or do not perform lane change) which form a part of planning and decision making process. A variety of techniques for decision making are available in literature with (i) multi-level decision trees [21], (ii) probabilistic weighted comparison of concurrent goals [22], and (iii) higher award seeking Markovian Decision Process algorithms [23] being among the prominent methods.

A schematic representation of an overtaking manoeuvre is shown in Figure 2.1 with each sub-manoeuvre labelled with roman numerals. As discussed above, the lane change back to the original lane depends on the traffic conditions and thus both possibilities are depicted in the schematic. Despite the innumerable variations present due to the factors discussed above, overtaking manoeuvres can be classified under the four categories listed below [15]:

- **Normal:** The subject vehicle approaches the lead vehicle and waits for a suitable opportunity to perform the manoeuvre
- **Flying:** The subject vehicle does not adjust its longitudinal velocity and is directly able to overtake the lead vehicle
- **Piggy backing:** The subject vehicle follows a preceding vehicle as they both overtake the lead vehicle
- **2⁺:** The subject vehicle overtakes two or more lead vehicles in a single manoeuvre

For the aforementioned scenarios, the duration of a completed overtake has been found to be in the range of 5.4 s to 12.5 s (subject to dynamic nature of the surrounding traffic and environment) using records of the trajectories of vehicles on typical European highways [8, 19, 24–28]. Performing an autonomous overtaking manoeuvre based on any of the scenarios mentioned above within a given time range requires accurate information of surrounding environment, traffic, and weather conditions along with sophisticated sensing and perception, planning, and control systems [29]. The surrounding environment of a vehicle is populated by different features; (i) permanent (road and lane limits), (ii) slowly changing (e.g., temporary speed limits, road works, traffic density, etc.), and (iii) fast changing (surrounding

Background & Literature Review

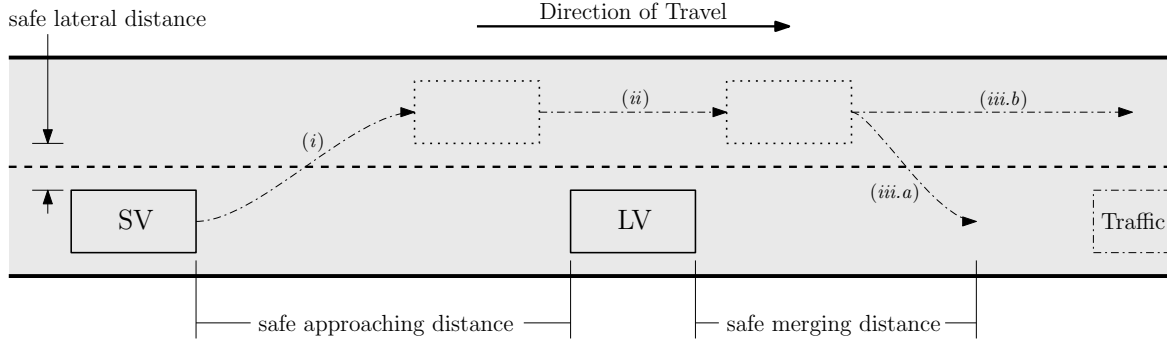


Figure 2.1 Basic schematic of an overtaking manoeuvre. **Note:** Different sub-manoeuvres are (i) lane-change; (ii) pass lead vehicle; (iii.a) merge back into original lane; (iii.b) continue in faster lane to pass traffic

vehicle velocity, position, heading, etc.). A modern day vehicle uses a host of on-board sensors to discern the environment and the placement of an on-board sensor suite used to perform this task can be seen in Figure 2.2. The information from these sensors is combined and used for tasks such as; (i) classify objects, (ii) track stationary and moving obstacles, (iii) identify safe driving zones, etc. Currently, there are some production vehicles that utilise vehicle-to-everything (V2X) information to provide updates on permanent (e.g., road and lane limits, road inclination, etc.) or slowly changing features (e.g., temporary speed limits, road works, traffic updates, etc.) of surrounding environment via a combination of cellular data and Local Dynamic Map (LDM) updates. However, despite an elaborate sensor suite and first generation V2X communication systems the capabilities of the contemporary autonomous vehicles is limited to low-speed overtaking. This is due to limitations such as; (i) range of sensors, (ii) blind spots , (iii) small time-scales for predicting motion of traffic participants, (iv) sensor imperfections, and (v) possible V2X network outages. The combination of one or more of these limitations result in significant uncertainty while planning complex highway manoeuvres (e.g., overtaking) which span several seconds at high-speeds [30, 31]. Moreover, unless all the traffic participants are connected and autonomous the uncertainty arising from predicting the motion of traffic vehicles cannot be brought down to negligible levels even with the advent of perfect on-board sensors and/or V2X communication network. Thus, predicting the motion of traffic participants for risk assessment forms a vital part of manoeuvre planning and this domain has witnessed a lot of research and a large number of techniques are present in literature. The different methods for motion planning for intelligent autonomous vehicles based on abstraction levels of traffic motion are classified as; (i) physics-based [32–34], (ii) manoeuvre-based [35], and (iii) interaction-aware [36, 37]. A comprehensive survey discussing the advantages and limitations

2.1 Introduction

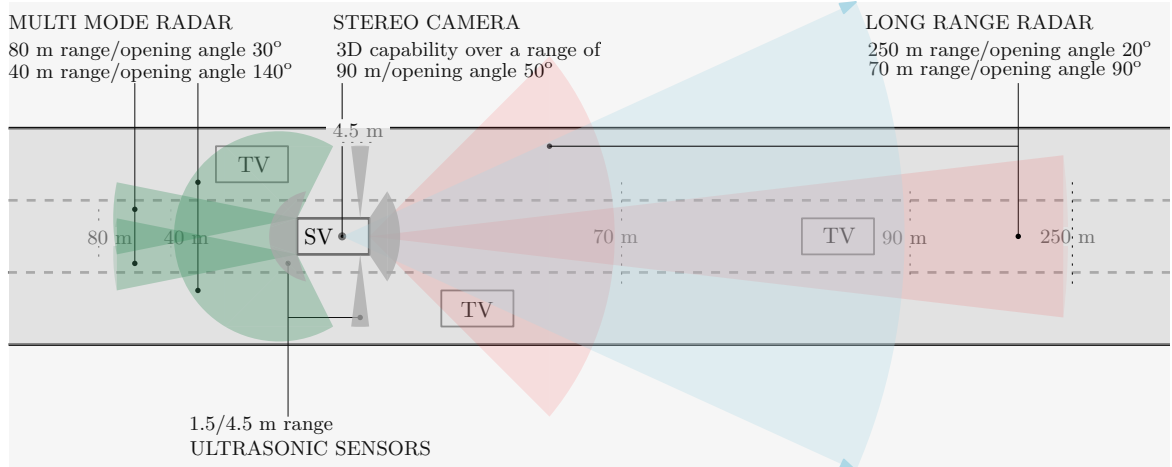


Figure 2.2 Visibility of an autonomous vehicle. **Note:** SV: Subject Vehicle, TV: Traffic Vehicle. Sensor performance specifications are based on [39]

of each of these techniques is presented in [38] and an interested reader is directed towards it.

Recent research has highlighted the potential use of off-board information via V2X communications in expanding the sensory and perception horizon of a vehicle through the communication systems [40–42]. In the context of autonomous overtaking, initial research has been largely focused on the integration of V2X information to: (i) manoeuvre feasibility check, and (ii) decision making stages [14, 15, 40]. However, the potential enhancements that can be achieved in trajectory planning and trajectory tracking of an overtaking manoeuvre by exploiting V2X information are yet to be studied. In this chapter, a review of various techniques for trajectory planning and trajectory tracking for autonomous overtaking systems is presented. The aim is twofold: (i) to gain insight on techniques suitable for autonomous overtaking systems, and (ii) to investigate how V2X information can enhance both trajectory planning and tracking techniques of an autonomous overtaking system.

The chapter is structured as follows: Section 2.2 introduces the system overview of an autonomous driving system and discusses how a two-tier control architecture can be used to perform autonomous overtaking. In Section 2.3, an extensive literature review of trajectory planning methods used for generating overtaking trajectories is presented. Comparison of key aspects pertaining to vehicle models and a review of different control strategies for trajectory tracking applications is performed in Section 2.4. Finally, the findings from the chapter are summarised in Section 2.5.

2.2 System Architecture

An autonomous overtaking manoeuvre requires consideration of a variety of factors such as subject vehicle states and constraints, lead vehicle states, environment limits, safety, and comfort. An overview of an intelligent autonomous driving system capable of performing autonomous overtaking is shown in Figure 2.3. For an autonomous vehicle to successfully perform different tasks (e.g., lane change, pass lead vehicle, and merge) pertaining to overtaking, it is expected that the vehicle can carry out each sub-task within the sensing and perception, planning, and control blocks. Sensing and perception includes gathering information about the driving conditions to determine if and when the conditions are favourable to perform the overtaking [25]. An autonomous vehicle utilises information from on-board sensors (Radar, LiDAR, camera, etc.) and/or off-board information via V2X communications to generate a real-time environmental representation [43], see Figure 2.3. The main objectives of the sensing and perception system are combining (fusing) data from different sensors, lane-level localisation, neighbouring vehicle detection, static obstacle/constraint detection and safe drivable area representation [43].

The planning module utilises the perception information along with the subject vehicle states and dynamic constraints to compute safe collision free local trajectory for the subject vehicle at each time instant [44]. To plan an overtaking manoeuvre the vehicle uses perception data (position and velocity estimates of neighbouring vehicles, infrastructure limits, road geometry, headway time) and subject vehicle data (current state, lateral and longitudinal dynamics) to check feasibility of the manoeuvre and design a collision free and safe local reference trajectory for an overtaking manoeuvre [8, 20, 45–49].

The local trajectory generated via the planning module is used as a reference trajectory to be tracked while performing an overtake (e.g., lane change, pass lead vehicle, lane-merge), and a closed-loop control system is designed to track it by controlled manipulation of steering, throttle and/or brake [8, 10, 20, 45, 46, 48, 50–53].

To preserve the modular nature of the architecture presented in the section above, the different driving tasks can be translated to a control architecture for an autonomous vehicle as shown in Figure 2.4, i.e. trajectory planning controller and trajectory tracking controller [43, 48, 54–56]. The objective of the trajectory planning controller is to perceive the environment, monitor vehicle states (longitudinal and lateral positions, longitudinal and lateral velocities, longitudinal and lateral accelerations, heading, and yaw-rate) and compute safe trajectories for the vehicle to track [47]. The trajectory tracking controller then computes, via feedback algorithms based on the tracking error, the necessary torque (τ_{ref}) and steering inputs (δ_{ref}) required

2.3 Trajectory Planning

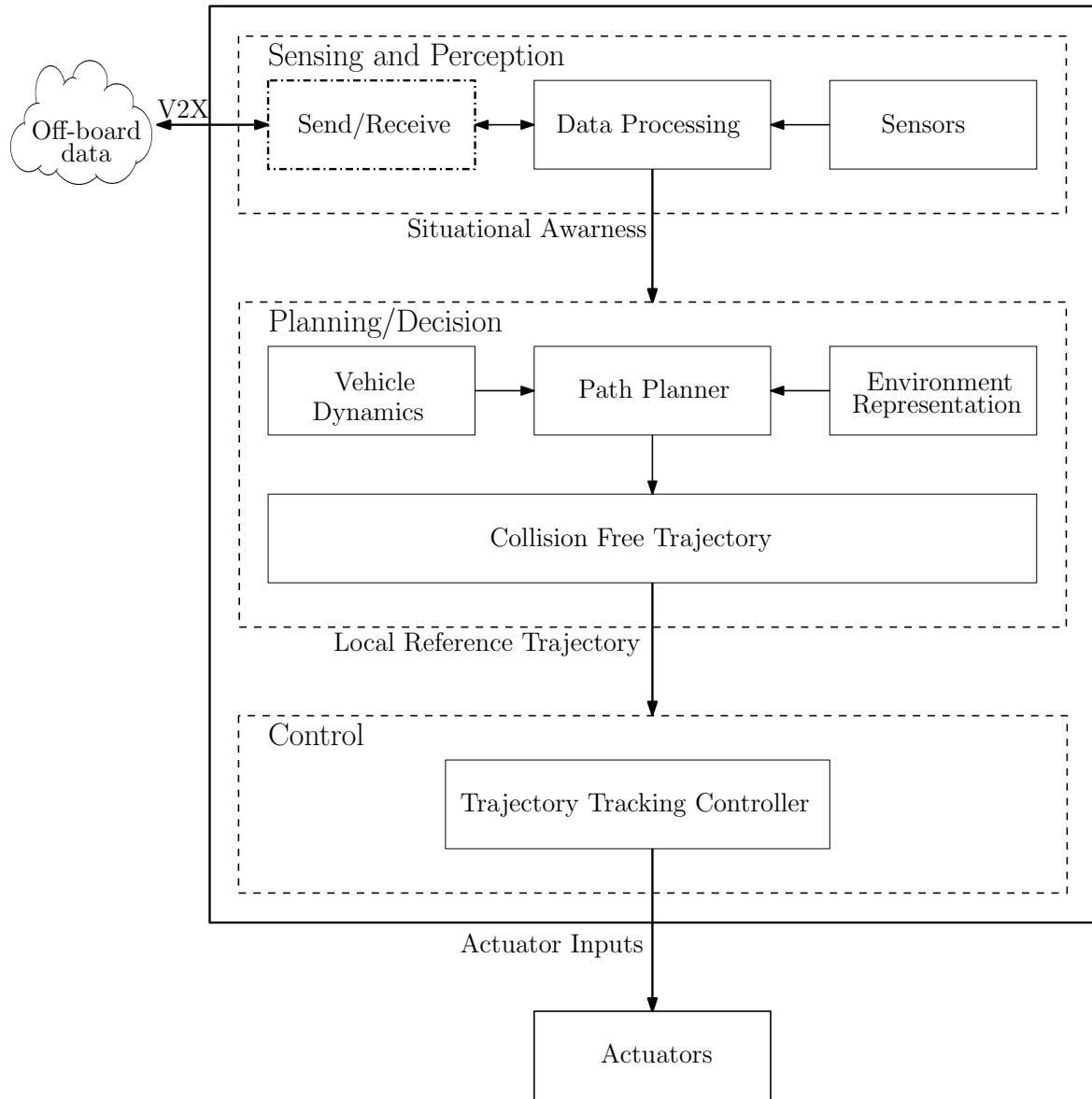


Figure 2.3 Overview of an autonomous driving system

to track the reference, despite possible measurement noise, un-modelled dynamics, parametric uncertainties which may or may not be accounted for by the trajectory planning controller.

2.3 Trajectory Planning

An autonomous vehicle relies on real-time vehicle state and environment information (e.g., surrounding vehicles, road conditions) to derive a local trajectory that

Background & Literature Review

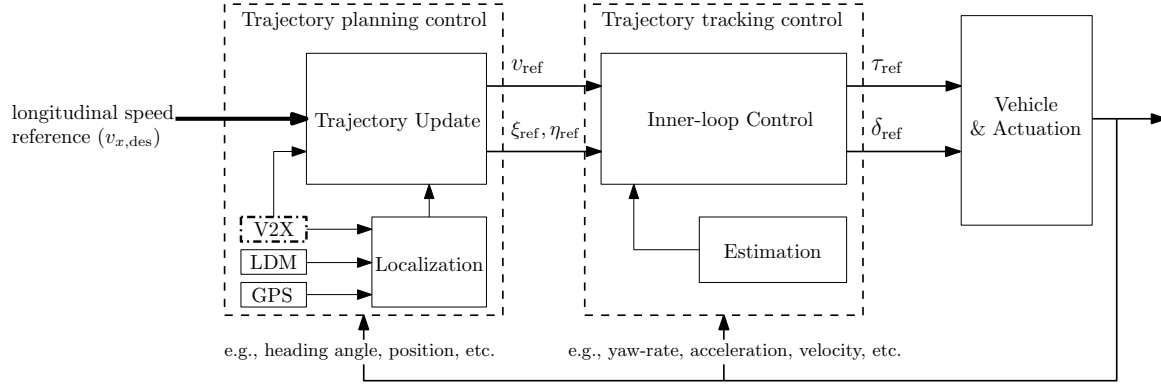


Figure 2.4 General control architecture for an autonomous vehicle [43, 48, 54–56]. (V2X block with dot-dash boundary: optional functionality)

ensures a safe passage while minimising the deviation from the overall journey trajectory (global trajectory). Local trajectory planning can be defined as – *real-time planning of the vehicle’s transition from one feasible state to the next while satisfying the vehicle’s kinematic limits based on vehicle dynamics and constrained by occupant comfort, lane boundaries and traffic rules, while, at the same time, avoiding obstacles* [44]. Technical literature shows that the vast majority of trajectory planning methods for an overtaking application employ one of the four well known techniques i.e., potential fields, cell decomposition, interdisciplinary methods and optimal control. In this section, these techniques are reviewed to gain insight into their performance for different specifications such as computational requirements, safety, feasibility in high-speed overtaking and real-time implementation.

Potential field algorithms assign repulsive fields to obstacles and attractive fields to safe zones of the vehicle and then use an algorithm to compute trajectories along the steepest potential gradient in the resulting field [47, 48], see Figure 2.5(a). The computed path is guaranteed to follow the lowest potential (i.e., find collision free trajectory) in a given space but its safety and accuracy depends heavily on the accuracy of the generated potential field (i.e., definite knowledge of position of stationary and moving obstacles). However, due to the high computation costs and need for very accurate surrounding environment information, the method has only been experimentally verified for low speed (i.e., urban) manoeuvres [48]. Additionally, since potential field based algorithms optimise for a collision-free path without considering the system dynamics and kinematic constraints, the generated trajectories might be unfeasible which results in safety concerns for high-speed driving scenarios [47, 57].

Cell decomposition algorithms such as Rapidly-exploring Random Tree (RRT) is a method used for collision free path planning [58, 59], see Figure 2.5(b). In this

algorithm, a tree is incrementally constructed from a given initial configuration (source cell) by creating connections to neighbouring cells which lie outside of an obstacle. The search ends when the goal (target cell) is reached and parsing this tree to obtain the shortest path from the source cell to the target cell provides a collision-free reference trajectory for an autonomous vehicle to follow. These algorithms can be modified to incorporate the vehicle constraints but they also suffer from computational and memory costs [47, 58, 59]. The computational complexity of such algorithms increases with increasing traffic density and frequency of road curvature thus jeopardizing the on-board computation of an autonomous vehicle on busy roads [58]. Furthermore, the paths created by RRT's are jerky and tracking such a trajectory will have an adverse effect on the comfort of the occupants [44].

Inter-disciplinary techniques inspired by robotics and missile guidance systems [10, 60, 61] for vehicle path-planning are also reported in literature. One of the novel approaches proposed was to use motion primitives (combination of steady-state equilibrium trajectories and pre-specified manoeuvres) [62]. The experimental results demonstrated that collision free and feasible trajectories can be generated in real-time using this approach [62]. Ghumman et al. designed a trajectory planning method based on Rendezvous Guidance technique (passing vehicle is guided in real-time to match the position and velocity of a shadow target during an overtaking manoeuvre) inspired from missile guidance systems [60, 61], see Figure 2.5(c). Similarly, an approach for overtaking manoeuvre consisting of consecutive tracking of virtual reference points positioned a priori at known distances from the lead vehicle is proposed in [10]. Simulation results of both these approaches demonstrated acceptable real-time capabilities for generating feasible trajectories but tracking performance was validated using low order models in computer simulations. Thus, in the absence of experimental validation it is difficult to form conclusions on the efficacy of such approaches.

Optimal control methods minimise a performance index (e.g., change in kinetic energy [20], jerk [29, 57], lateral acceleration [57]) under a set of constraints (e.g., vehicle lateral and longitudinal limits, environment constraints, neighbouring vehicles) to obtain a trajectory for a safe overtaking manoeuvre. The results from literature demonstrate that the method is successful in generating collision free trajectories without high computational requirements [20, 29, 57]. The autonomous vehicle JUNIOR developed by Stanford University has successfully demonstrated the effectiveness of optimal control based trajectory planning techniques at the DARPA Urban Challenge [63]. In this control framework, the researchers design two sets of trajectories, one for lateral motion and another for longitudinal motion each optimised for safety and occupant comfort. A set of combined lateral and longitudinal motion is obtained by combining these two sets. The final trajectory that is provided

Background & Literature Review

to the trajectory tracking controller is computed by following the steps; (*i*) filter out trajectories that breach safety and comfort limits to create a subset of applicable trajectories, (*ii*) use this subset of applicable trajectories to identify an ideal trajectory that minimises deviation from the road centre. However, most of these techniques do not take into account the non-linearities in the vehicle and tire dynamics resulting in unfeasible trajectories under high-speeds and/or low road friction conditions which pose a safety risk for autonomous vehicles [55]. Additionally, trajectories obtained by such open-loop single stage optimisation do not account for uncertainties in a dynamic environment and therefore these trajectory planning methods have limited potential unless used in either extremely controlled or structured environments.

Recently, Model Predictive Control (MPC) methodology has also been used by researchers for local trajectory planning, due to its ability to better handle system constraints and nonlinearities, see Figure 2.5(d). The approach involves solving a constrained finite-time optimal control problem to determine a sequence of control inputs that minimise a performance index (cost function) and applying the optimal inputs (e.g., steering wheel angle, throttle, and brake) using a receding horizon principle [52]. However, the presence of (*i*) nonlinear vehicle dynamics, and (*ii*) time-varying state and input constraints while navigating in a dynamic environment, leads to a non-trivial control problem thus presenting a computational burden to solve the optimisation problem in real-time [52]. Researchers have attempted to reduce the computational complexity arising due to the nonlinear vehicle dynamics by using (*i*) point mass vehicle model [43, 51, 56], (*ii*) linear kinematic bicycle vehicle model [50, 53, 55] and (*iii*) iterative linearisation of nonlinear vehicle model [52], in the prediction model. It is noted that the collision avoidance constraints are non-convex in nature which means that the feasibility and uniqueness of the optimisation cannot be guaranteed. Researchers have proposed different techniques (translating problem from time-dependent system to position-dependent system [43, 51, 55, 64], relaxing collision avoidance constraints [56], approximate linearisation [52] to guarantee uniqueness of solution and reduce the computing and memory requirements of the controller. The experimental results demonstrate the ability of these approaches to generate safe collision free trajectories around static or moving obstacles (i.e. overtaking manoeuvre) but it should be noted that these path-planner methods required exact knowledge of the states, of the obstacles (stationary, moving) and/or a high performance computing platform (desktop class computer) to calculate safe collision free trajectories [43, 50–53, 55, 56]. It is noteworthy that recent publications have demonstrated that computational restrictions may soon become an issue of the past as highly efficient algorithms for implementing MPC controllers on real-time prototyping systems and vehicle electronic control units have been developed and a few successful implementations are discussed in [65–67]. Among the

2.3 Trajectory Planning

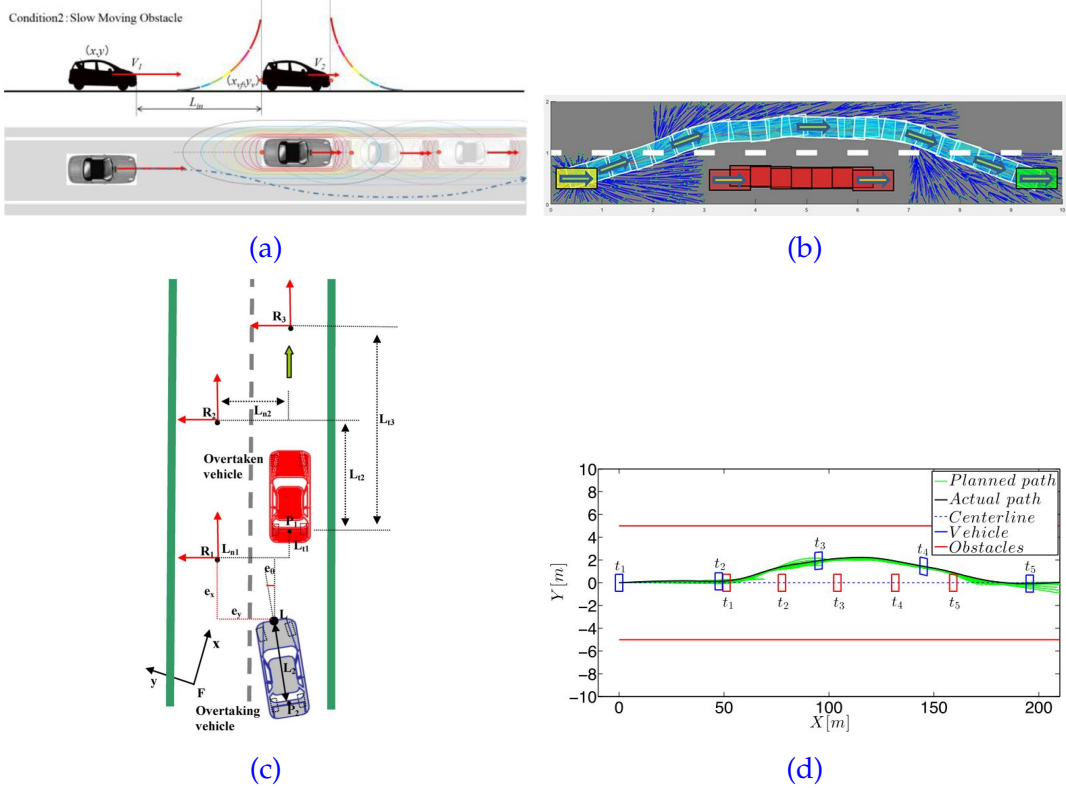


Figure 2.5 Trajectory planning via (a) Potential Fields [48]; (b) RRT [68]; (c) Virtual Reference Tracking [10]; (d) Model Predictive Control [52]

reviewed approaches, MPC provides a promising approach for trajectory planning due to its ability to: (i) include system dynamics and constraints, and (ii) perform receding horizon control which allows it to (re)plan feasible trajectories over a larger operating range.

It is noteworthy that all methods discussed above operate under the assumption that accurate knowledge of the environment and lead vehicle states are available on-demand to the trajectory planning system. The advantages and disadvantages of the various trajectory planning methods discussed above are summarised in Table 2.1. However, due to limitations of on-board sensing systems, the following situations may arise. First, the measurements of the lead vehicle states (e.g., position, velocity, and heading) might have errors, missing information, low accuracy, etc. resulting in inaccurate environmental representation. Second, variations in external conditions (e.g., road legislation, road surface condition, road width, weather, etc.) which are not captured might impact the subject vehicle dynamic limits (e.g., lateral acceleration, longitudinal speed, lateral acceleration, etc.). Trajectory planning methods that are not robust to environmental variations and sensor inaccuracies might lead to unfeasible and/or unsafe reference trajectories, posing a major safety

Background & Literature Review

risk especially during high-speed driving. The various trajectory planning techniques discussed above propose different ways for dealing with the uncertainty in current environment perception and limited future prediction capabilities. Potential field and cell decomposition based methods assign additional buffer zones (based on headway time, instantaneous relative velocity, etc.) around each obstacle and thus the search for feasible trajectories is performed in a constrained search space [69]. Similarly, the trajectory planning techniques in [10, 60, 61] also compute virtual target points conservatively by expanding the margins of the virtual reference points in accordance with the relative velocities of the subject and lead vehicle. On the other hand, a type of MPC control technique known as Scenario-Based MPC (SCMPC) has been proposed in literature to mitigate the uncertainty arising due to traffic interactions in a systematic manner [50, 65, 70, 71]. In this approach either an interaction-aware traffic prediction model [50] or manoeuvre based traffic prediction model [65] is incorporated within the MPC framework to simulate traffic scenarios as a probability distribution and a finite horizon optimal control problem is solved to generate a trajectory that is safe, feasible, and admissible under a selected set of traffic scenarios. The efficacy of the SCMPC trajectory planning technique for generating safe lane change manoeuvres has been demonstrated numerically and its real-time capability has been experimentally validated [50, 65, 70, 71]. However, the effectiveness of this method has a dependence on the accuracy of the modelled traffic scenarios which makes obtaining large quantity of actual traffic data a necessity. Recently, it has been proposed by researchers that a V2X communication system can augment a vehicle's sensing and perception capabilities to potentially mitigate the issues discussed above [14, 15, 40, 50, 72, 73]. Initial studies for trajectory planning using the information obtained through V2X systems, suggest that the safety and feasibility of a manoeuvre can be enhanced by incorporating off-board information [74–76]. Nonetheless, tangible benefits of using off-board information (e.g., lead vehicle states, road conditions, etc.) in trajectory planning methods are not very clearly understood and thus such studies are open to further research. Nonetheless, how a V2X system capable of providing accurate surrounding (e.g., lead vehicle states, road conditions, etc.) information in real-time can improve trajectory planning methods needs to be understood and is a question open to further research. Moreover, a wireless information sharing system induces additional dynamics related to communication delays, packet losses, and connection drop-outs which adds to the complexity of a control system [77]. Additionally, a V2X system with network infrastructure owners, service providers, application developers, and consumers introduces challenges related to network security, data ownership, privacy, malicious cyber attacks, etc. Due to the nature of the application (i.e., autonomous vehicles transporting human occupants at high-speeds) any breakdown or breach in the

2.4 Trajectory Tracking

system can result in harmful consequences such as incorrect environment information leading to unsafe trajectory planning, personal data of private users falling in the hands of malevolent parties, service failure leading to loss of operation, etc. Therefore, meticulous studies are required to ensure that the autonomous driving functionalities enabled via V2X based systems are robust and fault-tolerant against network imperfections and external attacks [78].

Table 2.1 Summary of techniques for trajectory planning to avoid a moving obstacle

Control Strategy	Strength(s)	Weakness
Potential fields	<ul style="list-style-type: none"> Optimality of searched path guaranteed Collision free path guaranteed 	<ul style="list-style-type: none"> High computation cost Inability to handle system constraints No systematic procedure to consider environmental uncertainties
Cell Decomposition	<ul style="list-style-type: none"> Guaranteed collision free trajectories 	<ul style="list-style-type: none"> Computation requirements sensitive to traffic density Computed paths are jerky No systematic procedure to consider environmental uncertainties
Interdisciplinary Techniques	<ul style="list-style-type: none"> Reduced complexity of collision avoidance as trajectory planning converted to reference tracking problem Real-time capable 	<ul style="list-style-type: none"> Experimentally unproven No systematic design procedure Do not consider uncertainties in environment perception while generating reference points
Optimal Control	<ul style="list-style-type: none"> Generate collision free trajectories Ability to include kinematic constraints 	<ul style="list-style-type: none"> Unsuitable for high-speed driving manoeuvres with large angles of tire slip Inability to consider tire dynamics
Model Predictive Control (MPC)	<ul style="list-style-type: none"> Include vehicle and tire dynamics Systematic handling of constraints and traffic uncertainties Computational requirements independent of environment 	<ul style="list-style-type: none"> Optimisation sensitive to number of constraints Computation complexity scales quickly with high-order system models, non-linearity, and non-convexity of constraints

2.4 Trajectory Tracking

Vehicle trajectory tracking (lateral-longitudinal control) is a mature scientific field with a plethora of control methodologies available in literature dating all the way back to the middle of the 20th century. Some useful properties for assessing tracking controllers for autonomous vehicle applications are listed below [79].

Background & Literature Review

- Real-time capability: The control law needs to be implementable on a vehicle's Electronic Control Unit (ECU) and function within the calculation time
- Robustness: The designed controller should be robust against system nonlinearities, model parameter variations, and external disturbances
- Operating Range: The tracking controller should ideally work across the entire range of vehicle speeds ($0 - 120 \text{ km h}^{-1}$)
- Controller parameter tuning: A systematic tuning procedure for the controller parameters allows for a structured controller design procedure

The performance of closed-loop tracking controllers depends on the accuracy of the modelled system dynamics. Vehicle models used for capturing the dynamics should provide a trade-off between model accuracy and fidelity. In literature a variety of vehicle models (ranging from low dimension point mass-models to high-fidelity multi-body models) are presented. Different vehicle models that have been developed over the years to capture the longitudinal, lateral and yaw dynamics of a vehicle have been documented in [80]. Out of the wide variety of vehicle models available in literature a kinematic bicycle model and dynamic bicycle model have been found to provide a good compromise between model complexity and accuracy for controller design related to highway driving applications [66, 81]. A comprehensive review of trajectory tracking control on the aspects of choice of vehicle model, control strategies, and controller performance criteria has been performed in [82]. While going around a corner, a vehicle's wheels on the outside and inside of the curve, trace circles of different radii. Consequently, to prevent the wheels from slipping sideways (laterally) while going along a curved path, vehicles have steering geometries linkages such that each wheel turns around its own pivot (with steering arms that are not parallel) [83]. This, is done such that while going around a curved path the lines perpendicular to each of the vehicle's wheel intersect at a common point corresponding to the centre of the vehicle's cornering arc of radius R_{curve} . The geometric single-track vehicle model are developed based on the Ackermann steering configuration for the front and rear tire and assume no lateral-slip in the tires. Since, this assumption is based solely on the pose of the vehicle and not it's velocity and/or acceleration it does not hold true for high-speed driving scenarios. Consequently, the review demonstrated that geometric models based on Ackermann steering are not suitable for high-speed trajectory tracking due to their inability to include vehicle dynamics (e.g., acceleration and velocity). Additionally, it is highlighted that kinematic models (bicycle, four-wheel) are also unsuitable for high-speed trajectory tracking as they are inaccurate in regions of tire force saturation. Both linear and non-linear dynamic vehicle models (full vehicle model, half vehicle

model, and bicycle model) were found to mitigate these limitations and furthermore providing a more accurate representation of a vehicle during high-speed driving [82]. However, it was also shown that a dynamic bicycle model (linear) was suitable for driving tasks (lane-change manoeuvre, overtaking manoeuvre, highway driving) with small lateral acceleration ($\leq 0.5g$) and low vehicle side-slip angle (5°) [82, 84]. Most of the papers in literature have used a single-track vehicle model (bicycle model) for developing a tracking controller for performing overtaking manoeuvres since an overtaking manoeuvre is performed well within the dynamic limits of the vehicle (i.e., lateral acceleration, vehicle side-slip, and yaw-rate) where both the vehicle as well as tire dynamics can be approximated by linear models. However, at high-speeds and/or under low road friction overtaking scenarios, it is quite possible that the system (i.e., vehicle, and tires) may exhibit significant non-linear behaviour and therefore for appropriate scenarios either nonlinear models, linear parameter varying (LPV) models or multiple models can be used to capture the relevant dynamic behaviour of the system [84, 85]. For a detailed review of different vehicle models the reader is directed towards the work by [82, 86–88].

2.4.1 Tracking Controllers

A comparison of different tracking controllers for autonomous vehicles was performed in [82, 86–88]. Some relevant observations of these comparisons along with other examples of tracking controllers for autonomous overtaking are discussed below.

Geometric controllers are designed using geometric vehicle models [82, 86–88]. Pure-pursuit and ‘Stanley’ method are two prevalent geometric controllers [82, 86–88]. Pure-pursuit is a technique where the vehicle is in constant pursuit of a virtual moving point in front of the vehicle and ‘Stanley’ controller is based on non-linear geometric controller which considers heading and lateral error to compute steering angle corrections [82]. These type of controllers (pure pursuit, Stanley, etc.) are easy to implement but are suitable only for applications that do not need to consider vehicle dynamics. Furthermore, since this approach does not follow a systematic control parameter tuning method, it is difficult to achieve a trade-off between stability and tracking performance [86–88]. It is observed that over-tuning of both pure-pursuit and Stanley controllers leads to poor tracking performance during cornering [86]. Kinematic controllers are alternative control techniques for trajectory tracking. They are feedback controllers which are designed considering the vehicle kinematics (e.g., longitudinal velocity, lateral velocity, yaw-rate, etc.). Kinematic controllers have been shown to improve the tracking performance provided by geometric controllers but the gains over a geometric controllers are not high enough

Background & Literature Review

to justify the additional effort involved in designing and tuning the controller [82, 86, 87]. Moreover, since these methods ignore vehicle dynamics, their applicability in critical driving environments (e.g., high-speed driving, extreme path curvature, etc.) cannot be assured.

Examples of classical control algorithms (e.g., PID, sliding mode controller) are also found in literature. Tracking controllers using classical techniques (PID) are shown to have good tracking performance but tuning of the parameters was found to be major challenge due to the presence of vehicle and tire non-linearities. Sliding Mode Control (SMC), a well-established classical non-linear state-feedback controller has also been used to design vehicle trajectory tracking controllers and shows good tracking accuracy due to the non-linear control law [82, 89]. However, it suffers from a few drawbacks namely: (i) performance is sensitive to the sampling rate of the controller (ii) chattering problems, (iii) robustness only on the sliding surface, and (iv) needs prior knowledge of disturbance and uncertainty bounds [82, 88, 89].

Dynamic state feedback (linear and nonlinear) based control methods demonstrate better performance than geometric and kinematic controllers as they consider the dynamics of the vehicle and tires while computing the control law. Linear Quadratic Regulator (LQR) based control law is easy to design but while tracking trajectories with varying curvature feedforward control is required to achieve error-free tracking. However, adding feedforward control makes the tracking controller sensitive to discontinuities in the reference trajectory which requires additional tuning to attenuate [86]. On the other hand, optimal control based methods can provide accurate trajectory tracking even at high-speeds but this is achieved only when certain assumptions (e.g., velocity of the subject vehicle remains constant during the optimisation horizon) are fulfilled. Recently, nonlinear adaptive control techniques such as Inversion & Immersion (I&I) have also been used for vehicle trajectory tracking controllers. Initial studies demonstrate that this method provides robust closed-loop tracking performance but the controller is sensitive to parameter uncertainties [89]. In the same body of work, an adaptive Proportional-Integral (PI) with non-linear gains controller for trajectory tracking was also proposed. [89]. Simulation results indicate that the controller provides tracking performance at par with an SMC and I&I controller with added advantage in the form of insensitivity to parameter uncertainties. However, in presence of large curvature variations or when operated in non-linear region of vehicle dynamics, the controller gains have a tendency to become high which may have a detrimental effect on the actuators.

There are also examples of advanced model based control techniques such as MPC being used for vehicle trajectory tracking [43, 51–53, 55, 56, 62]. Nonlinear MPC was found to provide very accurate tracking performance but at the same time suffer due to computational requirements of online optimisation [90]. To reduce the

computational burden researchers use a linear vehicle model but such controllers are applicable only in linear region of vehicle and tire behaviour [50, 53]. Designing a MPC framework based on iterative linearisation of a non-linear model has been proposed as a way to expand the working range of linear MPC controllers for trajectory tracking and has been experimentally validated [52]. This approach helps in meeting the compromise between computational requirements and modelling errors.

Neural network and fuzzy logic based approaches have also been proposed in literature and demonstrate tracking performance similar to LQR controllers. However, in the absence of formal stability proofs and exception handling, such approaches cannot be suggested for real-world implementation [87, 91]. The advantages and disadvantages of the different controllers discussed above are summarised in Table 2.2. Since, an overtaking manoeuvre is not standardised and every researcher demonstrates their tracking controller under a unique setting, it is difficult to perform a direct comparison between the different controllers proposed in literature. However, in [88], five different trajectory tracking controllers (Stanley, LQR, SMC, Fuzzy, and MPC) were designed to simulate an overtaking manoeuvre performed at 120 km h^{-1} . This setup provides a basis for direct comparison of different control algorithms since they were applied on an identical system. The tracking performance was assessed by comparing lateral errors and angular errors. Additionally, the actuation effort was compared using steering angle induced during the manoeuvre. The results from this preliminary comparison (i.e., trajectory tracking, and actuation) demonstrated that MPC resulted in the smallest tracking errors (i.e., lateral position and heading angle) with smooth actuation of the steering angle.

All the controllers discussed above are validated in well controlled environments where parameter variations (e.g., vehicle mass, moment of inertia, road friction, etc.) and environmental uncertainties (e.g., headwind, tailwind, etc.) are kept to a minimum. While such practices allow researchers to benchmark different controllers, most of the proposed controllers are operational in a narrow operating window which is not a realistic representation of real-world driving. The operating window of a controller subject to large variations in system dynamics can be increased in the following three ways: (i) control robustness against all uncertainties, (ii) design a ‘bank’ of controllers to cover possible different operational regimes, or (iii) update parameters in real-time to prevent performance drop-off. However, the order of a controller rises with the number robustness criteria that are incorporated and the number of controllers in a ‘bank’ scales exponentially with the number of varying parameters making both these approaches unviable for practical application [82]. On the other hand using a V2X system to update required parameters based on the surrounding conditions can potentially provide a practical solution. Some at-

Background & Literature Review

tempts to use V2X to update control parameters for improving tracking performance have been presented in literature. For instance, in [24], an automated emergency braking (AEB) system that exploits V2X communication to update the road friction co-efficient parameter in the control system model has been proposed. This allows for modification in real-time key constraints such as minimum braking distance and time-to-collision (TTC) making the system suitable for use under a wider range of conditions. Using a similar strategy, a communication system that updates the vehicle model parameters (e.g., road-friction [92], mass, etc.) and system constraints (e.g., road width, speed limit, cross-wind, traffic state and future trajectory) can enhance the usability of model based tracking controller in diverse driving conditions. Hence, V2X communication systems can update relevant parameters of a controller with accurate and real-time information thus preventing the applicability of a designed tracking controller to be limited to certain pre-set conditions and scenarios. However, the range of benefits (e.g., tracking performance, safety improvements, etc.) that can be gained by such a system needs further investigation resulting in an open research question.

Table 2.2 Summary of control strategies for vehicle trajectory tracking [79, 82, 86, 87, 89]

Control Strategy	Strength(s)	Weakness
Geomteric & Kinematic	<ul style="list-style-type: none">• Adequate performance (experimentally validated) in conditions without disturbances (e.g., wind, road banking)• Good tracking performance and robustness at moderate speeds (e.g., kinematic)	<ul style="list-style-type: none">• Do not consider vehicle dynamics• Steady-state error increases for high-speed driving (e.g., geometric)• Unsuitable for high-speed driving as dynamics are neglected (e.g., kinematic)• Requires smooth and continuous reference trajectories
Classical	<ul style="list-style-type: none">• Established method with good performance for non-linear systems• Robust closed-loop performance against uncertainties and noise (e.g., SMC)	<ul style="list-style-type: none">• Tuning of controller parameters is tricky (e.g., PID)• Robust performance only in limited scenarios (e.g., SMC)• Control law is sensitive to path curvature variations (e.g., SMC)

Dynamic state feedback	<ul style="list-style-type: none"> • Consider vehicle dynamics in calculating control law • Optimisation shifted offline resulting in simple implementation of control law 	<ul style="list-style-type: none"> • Obtaining vehicle states (e.g., wheel forces, slip angles, torques etc.) is non-trivial • Control law is sensitive to path curvature variations (e.g., LQR) • Availability of state measurements (e.g., vehicle side-slip angle) for computing control input is not trivial
Neural Network	<ul style="list-style-type: none"> • Sufficient training can make the behaviour very human-like to make the automated car feel natural 	<ul style="list-style-type: none"> • Controller tuning requires simulation with large amounts of real world (training) data • No failure explanations possible
Fuzzy Logic	<ul style="list-style-type: none"> • Closed-loop system acts similar to a human-driver (because of human-like rules) 	<ul style="list-style-type: none"> • Controller tuning is not systematic with no formal stability analysis • Rules can become unmanageable if number of variables is large
Model Predictive Control (MPC)	<ul style="list-style-type: none"> • Systematic design procedure • Ability to include system and actuator constraints in design procedure • Inclusion of vehicle and tire dynamics in control problem 	<ul style="list-style-type: none"> • Non-linear MPCs with have high computing requirements making them unsuitable for high-speed driving environments • The tracking performance is sensitive to the accuracy of prediction model • Larger tuning parameter set compared to industry standard PID

2.5 Summary

This chapter reviewed different approaches towards trajectory planning tracking for autonomous overtaking. The review of trajectory planning methods brings forth the following important aspects. First, vehicle dynamics, constraints and surrounding environment information needs to be considered while designing a trajectory for an overtaking manoeuvre and methods that incorporate these requirements within their framework are suitable candidates for real-world applications. Second, the trajectory planning techniques depend on accurate surrounding environment information, and off-board information via V2X communication can aid in expanding the accuracy and perception horizon thereby reducing safety concerns that might arise due to diverse driving conditions. For tracking controllers, the review showed that: (i) control algorithms that considered vehicle and tire dynamics over large speed ranges provided accurate tracking even at high-speeds and/or large trajectory variations,

Background & Literature Review

and (*ii*) the effectiveness of such controllers hinges on the accuracy of the modelled system dynamics which has difficulty in capturing the large variations encountered typically in daily driving with one low order system. Examples from literature showed that off-board information via V2X systems can be used to update controller parameters in real-time which can prevent drop-off in tracking performance when operated in conditions with variations in system dynamics. However, integration of off-board information into a multi-tier control architecture needs to be seamless as well as capable of graceful degradation on occasions of wireless communication failure. This added complexity in control design can pose significant challenges that will need to be addressed to develop a safe, dependable, and robust control system.

It is noteworthy that the study of potential benefits that can be achieved by leveraging off-board information via V2X communication systems for autonomous trajectory planning and tracking is in a nascent stage and marks a new chapter of study in the field of autonomous vehicles.

Chapter 3

Trajectory Planning

चरन्मार्गान्विजानाति नक्षत्रैविन्दते दिशः ।
आत्मना चात्मनः पञ्च पीड्यन्नानुपीड्यते ॥ १३३:२३ ॥

— महाभारत, आदि पर्व

A wanderer will eventually discover the path, even the constellations will lead to the right direction.

One who keeps the senses under control cannot be harmed by external foes.

— *Mahābhārata, Ādi Parva 133:23*

Automated vehicles are increasingly getting main-streamed and this has pushed development of systems for autonomous manoeuvring (e.g., lane-change, merge, overtake, etc.) to the forefront. A novel framework for situational awareness and trajectory planning to perform autonomous overtaking in high-speed structured environments (e.g., highway, motorway) is presented in this chapter. A combination of a potential field like function and reachability sets of a vehicle are used to identify safe zones on a road that the vehicle can navigate towards. These safe zones are provided as a reference to generate collision-free trajectories using two different control approaches, (*i*) model predictive controller (MPC) which neglects effect of longitudinal velocity on lateral-yaw dynamics and (*ii*) tube-based robust model predictive controller (RMPC) which considers the coupling between lateral and longitudinal motion of a vehicle. The ability of the two frameworks to plan feasible trajectories for high-speed overtaking is validated and compared in a high-fidelity IPG CarMaker/Simulink co-simulink environment. The strengths of the proposed framework are: (*i*) it is free from non-convex collision avoidance constraints, (*ii*) it is real-time implementable, and (*iii*) it ensures feasibility of trajectory even if decelerating or accelerating while performing lateral motion (valid only for RMPC based framework).

3.1 Introduction



HE initial waves of autonomous driving cars are plying on public roads and successfully providing features such as lane-keeping, distance maintenance, lane departure, cruising, etc. Such systems have helped in im-

This chapter is based on [93] and [94]

Trajectory Planning

proving safety on highways, occupant comfort while reducing driver workload simultaneously [6]. However, human intervention or input is still required while performing more challenging, but equally common manoeuvres (e.g., lane-change, merge, overtake etc.). Overtaking represents a template for such complex manoeuvres as it (*i*) combines lateral and longitudinal motion of an overtaking vehicle (subject vehicle) while avoiding collisions with a slower moving obstacle vehicle (lead vehicle), and (*ii*) includes sub-manoeuvres i.e., lane-change, lane-keeping, and another lane change back to the original lane in a sequential manner [10] (see Figure 2.1). Hence, the development of autonomous overtaking systems is under great focus since it unlocks the potential to perform a host of different manoeuvres and pushes the capabilities of autonomous vehicle further towards the overall goal of complete end-to-end autonomy.

The inherently intricate structure of overtaking stems from its dependence on a large number of factors such as road condition, weather, traffic condition, type of overtaking vehicle, type of overtaken vehicle, relative velocity, legislation, culture, etc. [9]. Furthermore, each overtaking manoeuvre is unique in terms of duration of the manoeuvre, relative velocity between vehicles, distance travelled, etc. [13, 15, 16, 19, 20] thus making classification and standardisation difficult. Moreover, safely performing an overtaking manoeuvre requires accurate information of road and lane availability, lead vehicle trajectory, lead vehicle driving intentions, road conditions, etc.

There are a variety of diverse ways proposed in literature for planning safe trajectories to perform an autonomous overtaking manoeuvre by treating it as a moving-obstacle avoidance problem. Incremental search based algorithms and sampling based trajectory planning methods such as ‘Rapidly exploring Random Trees’ (RRT) have been proposed for planning safe trajectories for autonomous overtaking [47, 58, 59, 63, 68]. Even though algorithms incorporating basic vehicle kinematics within a RRT search algorithm have been proposed, the planned trajectories can be jerky which could lead to reduced occupant comfort. If accurate knowledge of road and surrounding obstacles is available, potential field based techniques are shown to be successful at generating collision free trajectories for avoiding stationary or moving obstacles [47, 48]. However, while guaranteeing collision free trajectories, potential field based methods do not incorporate vehicle dynamics and hence cannot ensure feasibility of the planned trajectory [44, 57, 95]. Model Predictive Control (MPC) helps address these shortcomings with its ability to formulate vehicle dynamics and collision avoidance constraints as a finite-horizon constrained optimisation problem. However, collision avoidance constraints for trajectory planning are generally non-convex which limits the feasibility and uniqueness of the solution of the optimisation problem. Researchers rely on techniques such as *convexification* [96],

change of reference frame [51, 55, 64], create approximate linear collision avoidance constraints [56, 97], and shared control [98, 99] to address the issue. In [62] the concept of motion primitives is included within an MPC framework to plan collision avoidance trajectories. However, since these motion primitives were computed offline and accessed via a look-up table, only a subset of all feasible trajectories were considered for motion planning. In [10] overtaking trajectories were generated by directing the vehicle along virtual target points located at safe distances around the lead vehicle thus reformulating trajectory planning into a navigation problem. A similar approach inspired from missile guidance systems called *Rendezvous Guidance* was used to plan a trajectory for an overtaking manoeuvre [60, 61]. However, in all these techniques the subject vehicle (SV) has been modelled as a point mass with no dynamics and hence these methods are unsuitable for high-speed trajectory planning of autonomous vehicles. For the brevity of the chapter, interested readers are directed towards [5] and Chapter 2 for more details related to trajectory planning for autonomous overtaking.

In this chapter, extracting the relevant benefits of each approach described in the literature, we propose a mathematical framework of potential field like functions and MPC for performing an autonomous high-speed overtaking manoeuvre. The framework is composed by three components (*i*) an artificial potential field, (*ii*) a target generation block, and (*iii*) a trajectory generation block. The potential field is used to map the surrounding region of the subject vehicle. Contrary to typical potential field approaches where an obstacle's position has been used to identify high-risk zones, the method in this chapter combines an obstacle's position, orientation and relative velocity to create a map of safe zones surrounding the subject vehicle. At every sampling instant, the target generation block identifies the safest point of the road which is compatible with the dynamics of the subject vehicle and computes the reference state set point (e.g., velocity, lateral position, and heading angle) to be tracked. To achieve this aim of reaching the reference, the target generation block combines the safe zones in the potential field with the vehicle dynamics capability of the subject vehicle which are captured through the reachable set of the subject vehicle from its current state. Finally, the trajectory generation block uses a MPC strategy to generate feasible trajectories and steer the vehicle to the required reference (target) states. Two different MPC approaches, (*i*) nominal MPC in [100] and (*ii*) robust MPC approach in [101, 102] are developed for generating feasible trajectories and steering the vehicle to the required reference (target) states. The dynamics of the lateral and yaw motion of a vehicle have a nonlinear relation with the longitudinal velocity. It has been highlighted in Section 2.1 that an overtaking manoeuvre might require an overtaking vehicle to accelerate while performing the lane-change and thus changing the lateral-yaw dynamics compared to a nominal

Trajectory Planning

linear model. The robust tube based MPC formulation allows this nonlinearity (longitudinal velocity and lateral-yaw dynamics) to be modelled as an additive disturbance which allows the controller to plan feasible lateral motion (lane-change) trajectories over a large range of longitudinal velocities. Consequently, a comparison is performed between the two MPC approaches mentioned above to gain insight on the benefits of using a robust MPC based technique for trajectory planning in environments where the longitudinal velocity of the subject vehicle is not constant. Moreover, the robust MPC method proposed in [101, 102] guarantees (*i*) closed-loop stability, and (*ii*) persistent feasibility of the optimisation problem which is desirable for any model predictive control formulation [103]. Additionally, a novel technique of designing collision avoidance constraints as a function of the longitudinal velocity and lateral position of the vehicle is presented. This technique differs from the ones in literature since the constraint design does not depend on the longitudinal position thus allowing the designers the possibility of reducing the state dimension of the system. This is beneficial as removing a state from the system model helps in reducing the dimension of the parameters space which helps in bringing down the memory and computational requirements for solving the constrained optimisation problem. Hence, this chapter represents practical use of the theory on MPC for tracking piecewise references presented in [100] and robust MPC presented in [101, 102] to design admissible, safe, and collision free trajectories for autonomous vehicles. The effectiveness of the entire framework for high speed autonomous overtaking is validated in a co-simulation platform where high-fidelity vehicle dynamics are simulated in IPG-CarMaker while the trajectory planning method with the MPC is implemented in MATLAB/Simulink.

The chapter is structured as follows: Section 3.2 introduces the basic symbols and mathematical definitions used in the chapter. The mathematical formulation of relevant vehicle dynamics and vehicle model structure to be used for controller design is discussed in Section 3.3. In Section 3.4, the two different MPC approaches are briefly overviewed to give to the reader the fundamental details of the algorithm(s) which have been used for trajectory planning. In Section 3.5, the situation awareness system for the vehicle using potential field like functions is presented, while Section 3.6 is dedicated to the design of the target generation block. The design of trajectory planning based on the two different MPC methods along with the design of the collision avoidance constraints is covered in Section 3.7. The effectiveness of the framework to support high speed overtaking is numerically shown in Section 3.8. Finally, the concluding remarks are presented in Section 3.9.

3.2 Mathematical Notations and Definitions

For a symmetric matrix M and vector x , $\|x\|_M$ denotes the weighted norm given by $\|x\|_M = \sqrt{x^T M x}$. Given two sets \mathcal{U} and \mathcal{V} , such that $\mathcal{U} \subseteq \mathbb{R}^n$ and $\mathcal{V} \subseteq \mathbb{R}^n$, the Minkowski sum is defined by $\mathcal{U} \oplus \mathcal{V} \triangleq \{u + v | u \in \mathcal{U}, v \in \mathcal{V}\}$ and the Pontryagin set-difference is $\mathcal{U} \ominus \mathcal{V} \triangleq \{w \in \mathbb{R}^n | w + v \in \mathcal{U}, v \in \mathcal{V}\}$. The matrix $\mathcal{O}_{n,m} \in \mathbb{R}^{n \times m}$ denotes a matrix of zeros, and matrix $\mathcal{I}_n \in \mathbb{R}^{n \times n}$ denotes the identity matrix. For vectors $a \in \mathbb{R}^n$, $b \in \mathbb{R}^m$, vector (a, b) denotes $[a^T, b^T]^T$. For a given set $\Gamma \subset \mathbb{R}^{n_a+n_b}$, the projection operation is defined as $\mathcal{A} = \text{Proj}_a(\Gamma) = \{a \in \mathbb{R}^{n_a} : \exists b \in \mathbb{R}^{n_b}, (a, b) \in \Gamma\}$. For a system with states $x \in \mathcal{X} \subseteq \mathbb{R}^{n_x}$ and inputs $u \in \mathcal{U} \subseteq \mathbb{R}^{n_u}$, whose dynamics are:

$$\dot{x} = f(x, u) \quad (3.1)$$

where $f(\cdot, \cdot)$ is the state function (linear or non-linear), $\mathcal{R}(t_*; x_0)$ denotes the reachable set at the time instant t_* when the initial state is $x(0) = x_0$ and it is defined as

$$\mathcal{R}(t_*; x_0) = \bigcup_{u(t), t \in [0, t_*]} x(t_*; x_0, u(\cdot)) \quad (3.2)$$

with $u(\cdot) \in \mathcal{U}$ being an admissible input in the time range $[0, t_*]$ and $x(t_*; x_0, u(\cdot))$ is the solution of (4.1) with initial condition x_0 and input $u(\cdot)$ [104].

For solving the overtaking problem through the combined use of MPC and potential field, in addition to a coordinate inertial-frame (I-frame), three additional coordinate frames are exploited, i.e., vehicle-frame (V-Frame), obstacle-frame (O-frame), and road-frame (R-frame). The V-frame is located in the centre of gravity of the subject vehicle and follows the Roll-Pitch-Yaw (RPY) convention [105]. Similarly, the O-frame is located at the centre of gravity of the lead vehicle and follows the RPY convention while the R-frame is a moving coordinate frame located at the projection of the origin of V-frame onto the innermost (rightmost) edge of the road with x-axis in the direction of the travel. A generic point on the road is denoted as $p = (\xi, \eta)$, $p_r = (\xi_r, \eta_r)$, $p_v = (\xi_v, \eta_v)$, or $p_o = (\xi_o, \eta_o)$ when expressed in the inertial, road, vehicle, or obstacle frame, respectively. The coordinate frames are depicted in Figure 3.1 where $w_{\text{lane}} [\text{m}]$ is the width of the lane while shadow area denotes a rectangle moving along the road-frame with vertices $V = \{V_1, V_2, V_3, V_4\}$. The potential field is computed online within this region for situational awareness and thus the values of $\{V_1, V_2, V_3, V_4\}$ are chosen in a range relevant for high-speed overtaking [5, 15, 8]. Finally, T_j^i with $i, j \in \{\text{I}, \text{V}, \text{R}, \text{O}\}$, denotes the linear transformation from i -frame to the j -frame. Notice that, this transformation can be applied to either individual vectors or sets. When applied to a generic set $\Delta \subset \mathbb{R}^2$, $T_j^i(\Delta)$ denotes the following set $T_j^i(\Delta) \triangleq \{T_j^i(z)\}_{z \in \Delta}$.

Trajectory Planning

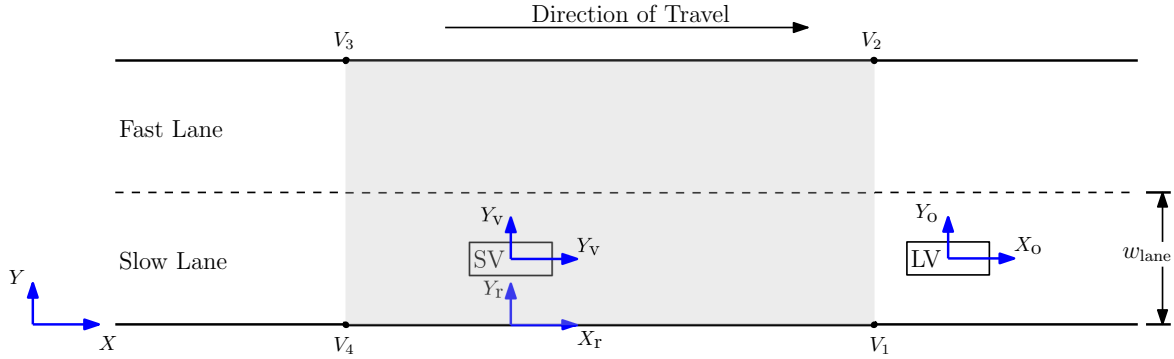


Figure 3.1 Road setup: coordinate frames and range of local risk map

3.3 Control Oriented Vehicle Model

A wide variety of vehicle models have been developed by researchers to study the dynamics of a vehicle and controller design for various applications [106]. A comprehensive survey of vehicle model for trajectory planning in [44] list out the relevant vehicle models for this task. Moreover, the review paper for trajectory planning for autonomous high speed overtaking demonstrates that compared to point mass vehicle models, single track vehicle models (i.e., bicycle models) provide a suitable compromise between model order and model accuracy [5]. A nonlinear kinematic vehicle model assumes no slip between tyre and road is found to be suitable for trajectory planning for highway driving when lateral acceleration is within bounds ($|a_y| \leq 0.4 g$) [66, 107] (see Figure 3.2). Furthermore, since normal driving on the highway involves small steering inputs, small angles approximation for the side-slip angle and steering angle are often assumed [108, 109]. Under this assumption of small angles approximation the vehicle bicycle model is:

$$\dot{\zeta} = v \quad (3.3a)$$

$$\dot{\eta} = v\psi + \frac{l_r}{l_f + l_r}v\delta_f \quad (3.3b)$$

$$\dot{\psi} = \frac{1}{l_f + l_r}v\delta_f \quad (3.3c)$$

$$\dot{v} = a_x \quad (3.3d)$$

where ζ and η are the longitudinal and lateral displacement of the centre of gravity in the I-frame, ψ is the inertial heading angle, v is the velocity of the vehicle, l_f is the distance of front axle from centre of gravity, and l_r is the distance of the rear axle from the centre of gravity. The control inputs are longitudinal acceleration

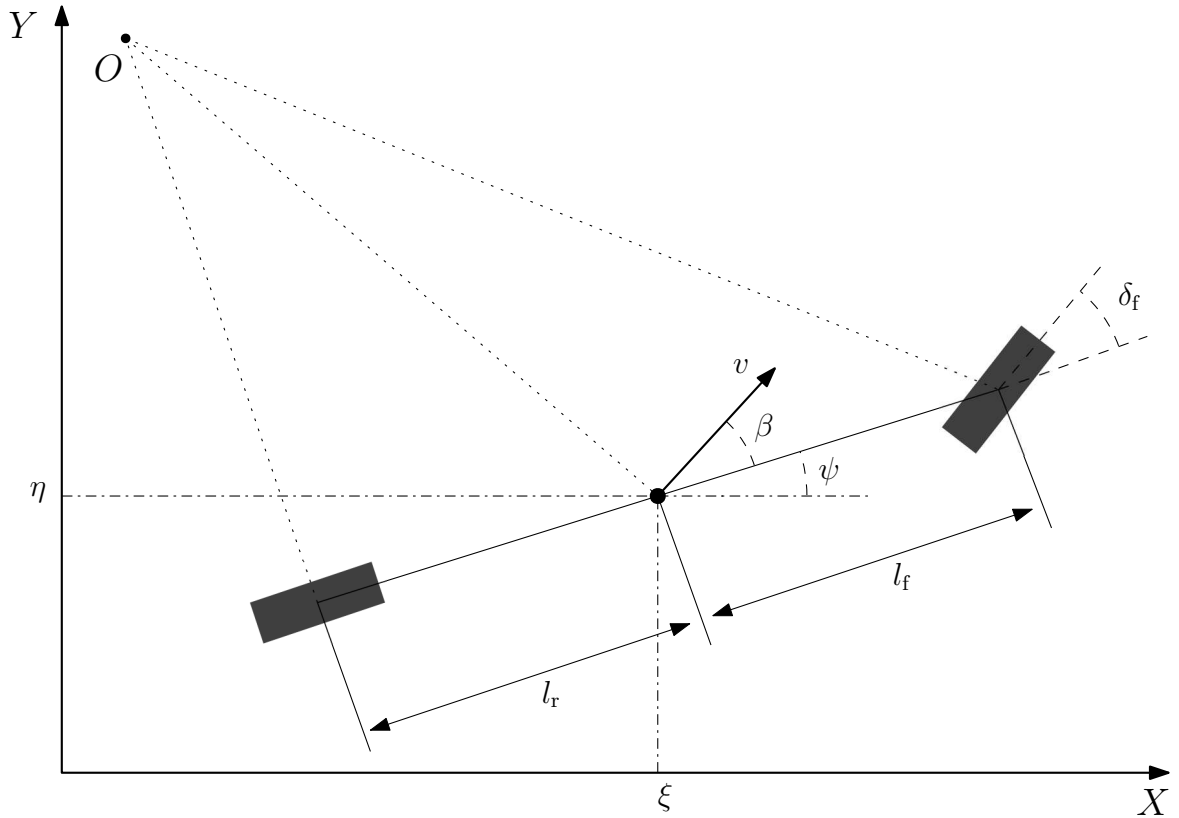


Figure 3.2 Kinematic bicycle model

a_x and front steering angle δ_f . The two aspects that stand-out based on the system dynamics in (3.3) are: (i) nonlinearity in the system, and (ii) close dependence of longitudinal velocity on the lateral and yaw dynamics of the vehicle. To simplify the design of path planning, system in (3.3) might be linearised around a nominal longitudinal speed. However, the resulting lateral and yaw predictions of such linear system are valid only when the longitudinal speed does not deviate with respect to the nominal one. Hence, as a vehicle is expected to accelerate (and possibly decelerate) while performing the lane change and passing sub-manoeuvres of the overtaking manoeuvre, linearising this system around a nominal velocity might lead to inaccuracies in lateral and yaw predictions leading to unfeasible and/or unsafe trajectory generation. To tackle nonlinear vehicle dynamics systematically, authors have proposed (i) maintain constant vehicle longitudinal velocity during the lane change [10], (ii) design non-linear controllers [10], and (iii) successive linearisation [52]. In this chapter, model (3.3) is used for computing the reachability sets of a vehicle to identify safe driving zones, while for the generation of the vehicle trajectory toward a target point, model (3.3) is rewritten as a linear time invariant (LTI) system subjected to an additive bounded disturbance. This is achieved by

Trajectory Planning

denoting $x_a \triangleq [\xi, \eta, \psi, v]^T \in \mathcal{X}_a \subseteq \mathbb{R}^4$ as the system state and $u \triangleq [a_x, \delta_f]^T \in \mathcal{U} \subseteq \mathbb{R}^2$ the system input with \mathcal{X}_a and \mathcal{U} being state and input convex constraint sets, respectively, system (3.3) can be recast as a linear parameter varying (LPV) system

$$\dot{x}_a = A_c(v)x_a + B_c u \quad (3.4)$$

$$A_c(v) = \begin{bmatrix} 0 & 0 & 0 & 1 \\ 0 & 0 & v & 0 \\ 0 & 0 & 0 & 0 \\ 0 & 0 & 0 & 0 \end{bmatrix}, \quad B_c(v) = \begin{bmatrix} 0 & 0 \\ 0 & \frac{v \cdot l_f}{l_f + l_r} \\ 0 & \frac{v}{l_f + l_r} \\ 1 & 0 \end{bmatrix} \quad (3.5)$$

where $v \in \text{Proj}_v(\mathcal{X}_a)$. System (3.4) is discretised as a zero-order hold (zoh) equivalent with a specified sampling time t_s to obtain the linear parameter varying discrete system shown below.

$$x_a(k+1) = A_d(v)x_a(k) + B_d(v)u(k) \quad (3.6)$$

The pair $(A_d(v), B_d(v))$ is the discretised version of the pair $(A_c(v), B_c(v))$ where

$$A_d(v) = e^{A_c(v)t_s}, \quad B_d(v) = \int_0^{t_s} e^{A_c(v)\tau} B_c(v) d\tau \quad (3.7)$$

For a given parameter (here $v \in \text{Proj}_v(\mathcal{X}_a)$), $(A_d(v), B_d(v))$ can take values from the convex set \mathcal{P} defined as

$$\mathcal{P} = \text{co}\{(A_{d,j}(v_j), B_{d,j}(v_j)) \mid j \in \mathcal{J}\} \quad (3.8)$$

with $\mathcal{J} \in \{1, 2, \dots, J\}$, see [110] (chapter 3). Accordingly the dynamics of the LPV system (3.6) can be rewritten as a nominal LTI system subjected to an additive disturbance, i.e.,

$$x_a(k+1) = A_{dm}x_a(k) + B_{dm}u(k) + w_a \quad (3.9)$$

where the pair (A_{dm}, B_{dm}) is obtained by the expression below [110].

$$A_{dm} = \left(\frac{1}{J}\right) \sum_{j=1}^J A_{d,j}(v_j), \quad B_{dm} = \left(\frac{1}{J}\right) \sum_{j=1}^J B_{d,j}(v_j) \quad (3.10)$$

Moreover, the disturbance w_a is defined as

$$w_a = (A_d(v) - A_{dm})x_a(k) + (B_d(v) - B_{dm})u(k) \quad (3.11)$$

and thus is bound by the set \mathcal{W} defined as

$$\begin{aligned} \mathcal{W} = & \{(A_d(v) - A_{dm})x_a + (B_d(v) - B_{dm})u \mid \\ & (A_d(v), B_d(v)) \in \mathcal{P}, (x_a, u) \in \mathcal{X}_a \times \mathcal{U}\} \end{aligned} \quad (3.12)$$

The set \mathcal{W} is defined from the discrete-time matrices which are an approximate of the continuous-time matrices described in (3.5) and hence it is an estimate of the actual disturbance due to the varying parameter v . It is noted that the structure of model (3.9) enables the use the robust tube-based MPC which is briefly revised in the following section.

3.4 Control Formulation

3.4.1 MPC with Terminal Set Constraints

This section provides an overview of the MPC approach proposed in [100]. Compared to the classical MPC formulation [103], the advantage of the control method in [100] is its ability to steer the state of a constrained system towards any set-point (i.e. desired target steady state) whether it belongs to the terminal set or not. The method guarantees the asymptotic convergence of the system state to any admissible target steady state. Furthermore, if the target steady state is not admissible, the control strategy in [100] steers the system to the closest admissible steady state. In the rest of the section, details for implementing this MPC control method are reported.

Given a discrete time LTI system with states $x \in \mathcal{X} \subseteq \mathbb{R}^{n_x}$, inputs $u \in \mathcal{U} \subseteq \mathbb{R}^{n_u}$, and outputs $y \in \mathcal{Y} \subseteq \mathbb{R}^{n_y}$, a discrete time state-space system is given by

$$x(k+1) = Ax(k) + Bu(k) \quad (3.13)$$

$$y(k) = Cx(k) + Du(k) \quad (3.14)$$

where the matrices A , B , C , and D are constant and the pair (A, B) is controllable. The subspace of steady-states and inputs of the system (3.13) are represented in the linear mapping of the form

$$\rho_{ss} = M_\theta \theta \quad (3.15)$$

where $\theta \in \mathbb{R}^{n_\theta}$ is a parameter vector that characterises the subspace of steady-states and inputs and M_θ is a matrix of suitable dimensions (see [100] for further details). At any time instant k , given a target steady state $\hat{x} \in \mathbb{R}^{n_x}$ and prediction horizon N , the control action $u(k)$ is generated by solving a constrained optimisation problem to steer system (3.21) to an admissible steady-state $\rho_{ss} = (x_{ss}, u_{ss}) \in \mathcal{X} \times \mathcal{U}$, such that

Trajectory Planning

x_{ss} is as close as possible to \hat{x} . The constrained optimisation problem is parametrised in $x_p = x(k)$ and \hat{x} and is given as

$$\begin{aligned} & \min_{U_i, \theta} V_N(U_i, \theta; x_p, \hat{x}) \\ & \text{subject to} \\ & x(0) = x_p \\ & x(i+1) = Ax(i) + Bu(i), \quad i = 0, 1, \dots, N \\ & (x_{ss}, u_{ss}) = M_\theta \theta \\ & x(i) \in \mathcal{X} \\ & u(i) \in \mathcal{U} \\ & (x(N), \theta) \in \mathcal{X}_t \end{aligned} \tag{3.16}$$

where $U_i = \{u(0), u(1), \dots, u(N-1)\}$ is the vector of stacked inputs, (x_{ss}, u_{ss}) is the stack of the steady-state solution of (3.13), and the terminal set \mathcal{X}_t is chosen as

$$\mathcal{X}_t = \{(x, \theta) \in \mathbb{R}^{n_x+n_\theta} : (x, K_\Omega x + L\theta) \in \mathcal{X} \times \mathcal{U}, M_\theta \theta \in \mathcal{X} \times \mathcal{U}, (A + BK_\Omega)x + BL\theta \in \mathcal{X}\} \tag{3.17}$$

with $K_\Omega \in \mathbb{R}^{n_u \times n_x}$ being a constant matrices such that the eigenvalues of $A + BK_\Omega$ lie within the unit circle, $L = [K_\Omega, I_{n_u}] M_\theta$, and the cost function $V_N(U_i, \theta; x_p, \hat{x})$ is

$$\begin{aligned} V_N(U_i, \theta; x_p, \hat{x}) = & \sum_{i=0}^N \left[\|x(i) - x_{ss}\|_Q^2 + \|u(i) - u_{ss}\|_R^2 \right] \\ & + \|x(N) - x_{ss}\|_P^2 + \|x_{ss} - \hat{x}\|_T^2 \end{aligned} \tag{3.18}$$

where the matrices $Q \in \mathbb{R}^{n_x \times n_x}$, $R \in \mathbb{R}^{n_u \times n_u}$, $T \in \mathbb{R}^{n_x \times n_x}$ are positive definite, and $P \in \mathbb{R}^{n_x \times n_x}$ is a positive definite matrix solving the Lyapunov equation

$$(A + BK_\Omega)^T P (A + BK_\Omega) - P = - \left(Q + K_\Omega^T R K_\Omega \right) \tag{3.19}$$

Remarks

- U_i and θ are the decision variables of the optimisation problem in (3.16), while x and \hat{x} are its parameters. Furthermore, the optimal control action is applied using a receding horizon strategy $u(k) = u^*(0)$, with $u^*(0)$ being the first element of the optimal control sequence U_i^*

- The optimisation problem can be recast as a quadratic programming problem which can be solved using any of the commonly available solver. The main steps taken to express (3.16) as *qp*-problem are outlined in Appendix C
- The last term of the performance index in (3.18) represents the tracking error cost. The weighting matrix T can be used to achieve a balance between tracking the target state \hat{x} and the virtual steady-state x_{ss}
- Closed loop asymptotic stability and feasibility of the proposed controller are proven in [100]
- For the remainder of this chapter, the control design methodology discussed above will be referred to as nominal MPC

3.4.2 Robust MPC with Terminal Set Constraints

This section provides an over view of the robust MPC approach proposed in [101, 102]. This MPC formulation extends the MPC with terminal set constraints discussion in Section 3.4.1 by using tube-based robust MPC design technique to maintain tracking performance even on systems subjected to bounded disturbances. Given a discrete linear time-invariant system with states $x \in \mathcal{X} \subseteq \mathbb{R}^{n_x}$, inputs $u \in \mathcal{U} \subseteq \mathbb{R}^{n_u}$, outputs $y \in \mathcal{Y} \subseteq \mathbb{R}^{n_y}$, and bounded process disturbance $w \in \mathcal{W} \subseteq \mathbb{R}^{n_x}$, where \mathcal{X}, \mathcal{U} and \mathcal{W} are known bounded convex sets, a discrete time state-space system is given by

$$x(k+1) = Ax(k) + Bu(k) + w \quad (3.20a)$$

$$y(k) = Cx(k) + Du(k) \quad (3.20b)$$

where the matrices A, B, C , and D are constant and it is assumed that the pair (A, B) is controllable. The control objective is to stabilize system (3.20) and steer it in the neighbourhood of a reference set-point despite the disturbance while keeping the system state and control input within the required set constraints (i.e., \mathcal{X} and \mathcal{U} , respectively) The solution proposed in [101, 102] leverages a nominal system of the plant in (3.20) defined as

$$\bar{x}(k+1) = A\bar{x}(k) + B\bar{u}(k) \quad (3.21a)$$

$$\bar{y}(k) = C\bar{x}(k) + D\bar{u}(k) \quad (3.21b)$$

where \bar{x} , \bar{u} , and \bar{y} are the state, input and output of the nominal model, respectively. The idea in [101, 102] to solve the constrained control problem for the uncertain

Trajectory Planning

system (3.20) is to use an MPC approach to steer the nominal model (3.21) towards the desired set point but with modified state and input set constraints, denoted as $\bar{\mathcal{X}}$, and $\bar{\mathcal{U}}$, respectively. The set constraints for the nominal model are selected such that if the closed-loop solution of the nominal system satisfies $(\bar{x}(k), \bar{u}(k)) \in \bar{\mathcal{X}} \times \bar{\mathcal{U}}, \forall k$, then $(x(k), u(k)) \in \mathcal{X} \times \mathcal{U}$. These tightened set constraints for the nominal system are computed as

$$\bar{\mathcal{X}} = \mathcal{X} \ominus \mathcal{Z}, \bar{\mathcal{U}} = \mathcal{U} \ominus K\mathcal{Z} \quad (3.22)$$

where $K \in \mathbb{R}^{n_x \times n_u}$ so that $A_K = A + BK$ is Hurwitz, and \mathcal{Z} is a robust positively invariant set [111] for the system $e(k+1) = A_K e(k) + w$, with $e \triangleq (x - \bar{x})$, such that

$$A_K \mathcal{Z} \oplus \mathcal{W} \subseteq \mathcal{Z} \quad (3.23)$$

In [101, 102] it was proven that if $\bar{\mathcal{X}}$ and $\bar{\mathcal{U}}$ are non-empty sets and they contain the steady state set-points and control inputs ($\subseteq \mathcal{X}_{ss} \times \mathcal{U}_{ss}$) then the set of steady-states and inputs can be robustly imposed to system (3.20) when $e(0) = x(0) - \bar{x}(0) \in \mathcal{Z}$, under the control action

$$u = \bar{u} + Ke, \bar{u} \in \bar{\mathcal{U}} \quad (3.24)$$

It is noted that, given a target steady state $\hat{x} \in \mathbb{R}^{n_x}$, the control action \bar{u} is generated by using a receding horizon technique to steer system (3.21) to an admissible steady-state $\rho_{ss} = (\bar{x}_{ss}, \bar{u}_{ss}) \in \bar{\mathcal{X}} \times \bar{\mathcal{U}}$, such that \bar{x}_{ss} is as close as possible to \hat{x} . Moreover, the subspace of steady-states and inputs of system (3.21) have a linear representation of the form

$$\rho_{ss} = M_\theta \theta \quad (3.25)$$

where $\theta \in \mathbb{R}^{n_\theta}$ is a parameter vector that characterises the subspace of steady-states and inputs and M_θ is a matrix of suitable dimensions (see [101, 102] for further details). Furthermore, by denoting N as the prediction horizon, the control action \bar{u} at the time instant k is computed by solving the following optimisation problem parametrised in $x_p = x(k)$ and \hat{x} [112, 113].

$$\begin{aligned} & \min_{\bar{U}_i, \theta, \bar{x}} V_N(\bar{x}, \bar{u}_i, \theta; x_p, \hat{x}) \\ & \text{subject to} \\ & \bar{x} \in x_p \oplus (-\mathcal{Z}) \\ & \bar{x}(i) \in \bar{\mathcal{X}} \\ & \bar{u}(i) \in \bar{\mathcal{U}} \\ & \bar{X}_i = \Phi \bar{x} + \Psi \bar{U}_i, i = 0, 1, \dots, N \\ & (\bar{x}_{ss}, \bar{u}_{ss}) = M_\theta \theta \\ & (\bar{x}(N), \theta) \in \mathcal{X}_t \end{aligned} \quad (3.26)$$

where $\bar{U}_i = \{\bar{u}(0), \bar{u}(1), \dots, \bar{u}(N-1)\}$ is the vector of stacked inputs, the vector of stacked predicted states is given by $\bar{X}_i = \{\bar{x}(1), \bar{x}(2), \dots, \bar{x}(N)\}$, and Φ and Ψ are the prediction matrices of appropriate dimensions constructed based on the nominal system dynamics described in (3.21) resulting in a prediction model (derived in Appendix B)

$$\bar{X}_i = \Phi \bar{x} + \Psi \bar{U}_i, i = 0, 1, \dots, N \quad (3.27)$$

and the terminal set \mathcal{X}_t is chosen as

$$\begin{aligned} \mathcal{X}_t = \{(\bar{x}, \theta) \in \mathbb{R}^{n_x+n_\theta} : & (\bar{x}, K_\Omega \bar{x} + L\theta) \in \bar{\mathcal{X}} \times \bar{\mathcal{U}}, \\ & M_\theta \theta \in \bar{\mathcal{X}} \times \bar{\mathcal{U}}, (A + BK_\Omega) \bar{x} + BL\theta \in \bar{\mathcal{X}}\} \end{aligned} \quad (3.28)$$

with $K_\Omega \in \mathbb{R}^{n_x+n_\theta}$ being a constant matrix such that the eigenvalues of $A + BK_\Omega$ lie within the unit circle, $L = [K_\Omega, \mathcal{I}_{n_u}] M_\theta$, and the cost function $V_N(\bar{x}, \bar{u}_i, \theta; x_p, \hat{x})$ is

$$\begin{aligned} V_N(\bar{x}, \bar{u}_i, \theta; x_p, \hat{x}) = \sum_{i=0}^N & \left[||\bar{x}(i) - \bar{x}_{ss}||_Q^2 + ||\bar{u}(i) - \bar{u}_{ss}||_R^2 \right] \\ & + ||\bar{x}(N) - \bar{x}_{ss}||_P^2 + ||\bar{x}_{ss} - \hat{x}||_T^2 \end{aligned} \quad (3.29)$$

where the matrices $Q \in \mathbb{R}^{n_x \times n_x}$, $R \in \mathbb{R}^{n_u \times n_u}$, $T \in \mathbb{R}^{n_x \times n_x}$ are positive definite, and $P \in \mathbb{R}^{n_x \times n_x}$ is a positive definite matrix solving the Lyapunov equation

$$(A + BK_\Omega)^T P (A + BK_\Omega) - P = - \left(Q + K_\Omega^T R K_\Omega \right) \quad (3.30)$$

It is noteworthy that in the optimisation problem (3.26), the initial state of the nominal system $\bar{x}(0) = \bar{x}$ is also a decision variable selected such that $x_p - \bar{x} \in \mathcal{Z}$, which guarantees the evolution of the system (3.20) in $\mathcal{X} \times \mathcal{U}$ for any $w \in \mathcal{W}$ (see [101, 102] for further details). Therefore, the solution of the optimisation problem (3.26) yields an optimal initial state $\bar{x}^*(x_p, \hat{x})$ and an optimal input sequence $\bar{U}_i^* = \{\bar{u}^*(0, x_p, \hat{x}), \bar{u}^*(1, x_p, \hat{x}), \dots, \bar{u}^*(N-1, x_p, \hat{x})\}$ along with a parametrised steady-state $\theta^*(x_p, \hat{x})$. The net control action applied on the plant is given as

$$u(k) = \bar{u}^*(0, x_p, \hat{x}) + K(x_p - \bar{x}^*(x_p, \hat{x})) \quad (3.31)$$

Remarks

- \bar{x} , \bar{u}_i , and θ are the decision variables of the optimisation problem (3.26), while x_p and \hat{x} are its parameters

- The terms of the cost function under the summation represent the penalty for deviating from the steady-state and input, the second term penalises the deviation of the terminal state from the steady-state, and the final term penalises the deviation of the artificial state from the reference state
- As the optimisation problem (3.26) can be expressed as a quadratic programming problem (see Appendix D for further details), it can be converted to an explicit MPC form to reduce online computations [90]
- System constraint handling capabilities and closed loop asymptotic stability and feasibility of the proposed controller are proven in [101]
- The minimal robust invariant set \mathcal{Z} can be computed offline using the recursive algorithm proposed in [111]. The MPC approach discussed above is a *right tube* MPC strategy which is known to be conservative even in \mathcal{Z} is minimal [114]
- If the additive disturbance caused by the parameter uncertainty tends towards a steady-state value then the closed-loop system reaches a steady-state different from \bar{x}_{ss} . This can be mitigated by modifying the desired set-point \hat{x} and removing the offset by estimating the steady-state disturbance as described in [101]
- The robust MPC with terminal set constraints discussed above is referred as robust MPC for the remaining portion of this chapter

3.5 Local Risk Map

In this chapter, it is assumed that the vehicles (subject vehicles and other traffic vehicles) are travelling on a one-way straight road of infinite length. At highway speeds, in addition to maintaining approximately a lane-width's distance with each vehicle in the lateral direction, vehicles also maintain safety distances of ≈ 50 m to the vehicle in front and behind [15]. Therefore, an overtaking manoeuvre is expected to maintain these distances while performing the lane-change manoeuvres that mark the start and end of an overtaking manoeuvre resulting in the need for a subject vehicle to have accurate situational awareness of the surrounding obstacles in this range to plan safe trajectories. The authors in [115, 116] mentioned that embedding driving rules and collision avoidance constraints within a multi-objective optimisation problem results in a control law with large computation requirements. On the other hand, a potential field like function for environmental

risk detection can be shaped in such a way that it guides towards desired driving behaviour. In this chapter the surrounding environment is described through the use of a potential field where several road elements (i.e., road limits, road markers, and other road users) are considered for shaping the potential function so as to include driving rules and guide the subject vehicle through safe road regions. The net potential function is generated by combining several potential functions where the design of each function is intended to incorporate one or more driving rule(s). The road potential function (U_{road}) is designed to keep the subject vehicle away from the road limits, the lane potential function (U_{lane}) is used for lane-keeping, the lane velocity potential function (U_{vel}) is designed such that the subject vehicle occupies the innermost (slowest) lane when more than one lane is available, and the car potential function (U_{car}) is designed such that a subject vehicle either maintains a safe distance to the lead vehicle or if the other lane is available, moves to a faster lane. Similar to the approach presented in [69], a net potential function (U_r) is generated by superimposing these individual potential functions to create local risk maps that can be used for autonomous overtaking in a human-like manner. The construction of the individual potential functions is discussed below.

3.5.1 Lane Velocity Potential

Different lanes on a road have an implicit velocity associated with them, i.e., the velocity progressively increases from inner (right-most) to outer (left-most) lane. Thus, if one assumes that higher-speeds represent higher-risk, each lane of the road can be appropriated a certain potential to describe its risk. This is achieved by a simple gain-based function as shown below.

$$U_{\text{vel},i}(p_r) = \gamma [v_{\text{lane},i}(p_r) - v_{\text{lane},1}(p_r)] \quad (3.32)$$

where γ is a gain factor, $v_{\text{lane},i}$ is the nominal velocity of the i^{th} lane, and $U_{\text{vel},i}$ is the potential due to lane-velocity of the i^{th} lane.

3.5.2 Road Potential

The road potential [69] is designed such that the boundaries of the road have the highest (∞) potential and the centre of the road has the lowest potential. A function often used in robotics for perception is used here to describe the road potential and is given below.

$$U_{\text{road}}(p_r) = \frac{1}{2} \zeta \sum_{b=1}^2 \left(\frac{1}{\eta_r - \eta_{r,b}} \right)^2 \quad (3.33)$$

Trajectory Planning

where ζ is a scaling factor and $\eta_{r,b}$ is the y-coordinate of the b^{th} road edge, $b \in \{1, 2\}$.

3.5.3 Lane Potential

A lane potential function [69] creates a virtual barrier between lanes to direct the subject vehicle towards the lane centre. A Gaussian function shown below is used to achieve this desired behaviour.

$$U_{\text{lane},i}(p_r) = A_{\text{lane}} \exp\left(\frac{-(\eta_r - \eta_{l,i})^2}{2\epsilon^2}\right) \quad (3.34)$$

Where $\eta_{l,i}$ is the y-coordinate of the i^{th} lane division, ϵ and A_{lane} are scaling factors, and $U_{\text{lane},i}$ is the potential due to lane boundary of the i^{th} lane.

3.5.4 Car Potential

A technique inspired by [69] is used to embed lead vehicle position, orientation, and velocity within the potential function as an obstacle vehicle. By modelling the lead vehicle as a rectangular area, virtual triangular wedges, also denoted as buffer zones, are appended to the front and rear of the lead vehicle which act as safety margins. The location (x, y coordinate) of triangle's vertex behind the lead-vehicle is calculated based on the velocity of the subject vehicle and the headway time h_t while the location of the triangle's vertex in front of the lead-vehicle is calculated based on the velocity of the lead vehicle and the headway time h_t . By denoting Γ_{lv} as the set of coordinates in the R-frame containing the obstacle vehicle and the two triangular wedges, a Yukawa function is used to describe the potential due to an obstacle vehicle as given below.

$$U_{\text{car}}(p_r) = A_{\text{car}} \left(\frac{e^{-\alpha K_d}}{K_d} \right) \quad (3.35)$$

where α is a Yukawa scaling factor, A_{car} is the Yukawa amplitude [117], and K_d is the Euclidean distance to the nearest coordinate of the obstacle given as

$$K_d = \min_{b_0 \in \Gamma_{\text{lv}}} \|b_0 - p_r\| \quad (3.36)$$

where b_0 represents the set of points lying within the obstacle. These individual potentials are superimposed to obtain an overall risk map in the surrounding of the

vehicle given by the expression below.

$$U_r(p_r) = U_{\text{vel}} + U_{\text{road}} + U_{\text{lane}} + U_{\text{car}} \quad (3.37)$$

Where $U_{\text{lane}} = \sum_{i=1}^{N_{\text{lanes}}} U_{\text{lane},i}$ and $U_{\text{vel}} = \sum_{i=1}^{N_{\text{lanes}}} U_{\text{vel},i}$ with N_{lanes} being the number of lanes. To facilitate trajectory planning the potential field is studied in the inertial frame through the use of the function $U(p) \triangleq U_r(T_R^I(p))$. By assigning a threshold limit U_{safe} , the safe regions of the road surrounding the subject vehicle are expressed in the inertial frame using the set

$$\mathcal{G} = \{p \in T_R^I(\Gamma_{\text{lv}}) : U(p) \leq U_{\text{safe}}\} \quad (3.38)$$

Thus, equation (3.38) provides a set of safe regions and the subject vehicle needs to plan trajectories that keep it within this region set thereby reducing risk. Moreover, since the net potential field depends on the states of the subject vehicle (longitudinal position, lateral position, and longitudinal velocity) and the lead vehicle (longitudinal position, lateral position, and longitudinal velocity), it updates at each time instant to provide an accurate environmental representation for a subject vehicle. It is worth noting that the risk map computed in this section is based on heuristics and the absolute value of the potential in isolation at any given point does not provide an insight on the risk associated with it. However, this framework can be easily augmented with more sophisticated models based on uncertainties in surrounding traffic movement, interaction-aware probabilistic risk assessment, data-driven surrounding traffic motion prediction, etc. that can enhance the qualitative information of the potential fields and risk analysis. Moreover, the set (3.38) does not consider vehicle dynamics of the subject vehicle, thus some regions of the road with satisfactory potential may not be reachable in practice. The method designed for selecting reference points in the set of safe regions which are compatible with the dynamics of the subject vehicle is detailed in the next section.

3.6 Selection of the Target Point

In this section, the method designed for selecting reference points in the set of safe regions which are compatible with the dynamics of the subject vehicle is detailed. In ideal highway cruising conditions, a vehicle is expected to traverse along at a constant desired longitudinal velocity v_{des} while maintaining its lane position. While travelling on a straight road, these dynamics of the system from (3.3) can be described by $\dot{x}_a = [v_{\text{des}}, 0, 0, 0]^T$. However, in real world scenarios, a vehicle is

Trajectory Planning

unable to maintain constant longitudinal velocity and lane position (due to traffic, route, etc.) and has to perform different manoeuvres such as lane-change, merge, etc. These manoeuvres can be thought of as transitions from one set of states to another set of states within the set $\mathcal{X}_{\text{ac}} = \{x \in \mathcal{X}_a : \psi = 0\}$. In such ideal scenarios the objective of the subject vehicle is to adjust its trajectory to avoid obstacles while ensuring that the vehicle's speed is maintained within the range $v \in \text{Proj}_v(\mathcal{X}_a)$. Starting from an initial position $p_0 = (\xi_0, \eta_0)$ and travelling at v_{des} , using admissible control actions from the set $\{(a_x, \delta_f) : a_x \leq 0, (a_x, \delta_f) \in \mathcal{U}\}$, the set $\mathcal{R}_{\text{total}} \subset \mathbb{R}^4$ of the vehicle configurations (states) reachable without exceeding the desired velocity v_{des} in the time interval $[0, t_*]$ of the system can be computed using (3.2) and the vehicle model (3.3). The set of points on the road that are reachable $\mathcal{R} \subset \mathbb{R}^2$ form a subset of $\mathcal{R}_{\text{total}}$ and is expressed as

$$\mathcal{R} = \text{Proj}_p(\mathcal{R}_{\text{total}}) \quad (3.39)$$

Remarks

- The velocity v_{des} corresponds to the maximum velocity of the SV as desired by the occupants and it is upper-bounded by the legal speed-limit of the road.
- Thus, from a given initial position p_0 , the subject vehicle can theoretically reach all points lying within the set \mathcal{R} without exceeding the maximum desired velocity v_{des} . It is noteworthy that the set of admissible control actions mentioned above is a subset of \mathcal{U} and is used only for computing the reachable set, the trajectory planning algorithm will have the entire set \mathcal{U} at its disposal for generating feasible trajectories.

From (3.38), (3.39) the safe zones surrounding the subject vehicle which are reachable with respect to the current vehicle state and vehicle dynamics is

$$\mathcal{R}_{\text{safe}} \triangleq \mathcal{G} \cap \mathcal{R} \quad (3.40)$$

Then, the reference target coordinates $\hat{p} = (\hat{\xi}, \hat{\eta})$ are chosen from $\mathcal{R}_{\text{safe}}$ with the aim to maximise the distance travelled by the subject vehicle in the time interval $[0, t_*]$, i.e.

$$\hat{p} = \arg \max_{p \in \mathcal{R}_{\text{safe}}} \|p - p_0\| \quad (3.41)$$

The longitudinal distance from ξ_0 to $\hat{\xi}$ can be traversed by the SV by travelling with a uniform longitudinal velocity calculated using the equation below.

$$\hat{v} = \frac{||\hat{\xi} - \xi_0||}{t_*} \quad (3.42)$$

A vehicle with the ability to closely match or follow the reference velocity computed above will enhance its ability of get closer to the reference position \hat{p} . Thus, if the initial velocity v_0 of the vehicle is not equal to the target velocity \hat{v} , the trajectory planner should come up with a suitable acceleration profile to accelerate/decelerate the vehicle to achieve the target velocity \hat{v} . Moreover, since the subject vehicle is assumed to be travelling on a straight road, the target heading angle of the subject vehicle remains

$$\hat{\psi} = 0 \quad (3.43)$$

It is noteworthy that in case the subject vehicle is travelling on a curved road, target heading angle $\hat{\psi}$ can be obtained from the road orientation at the given coordinate $(\hat{\xi}, \hat{\eta})$ stored in the vehicle's mapping functionality. Thus, stacking the reference targets for each state the target state vector $\hat{x}_a = [\hat{\xi}, \hat{\eta}, \hat{\psi}, \hat{v}]^T$ for the system is obtained. It is noted that, the set of reachable lateral and longitudinal coordinates for subject vehicle in the vehicle frame is

$$\mathcal{R}_V = T_V^I(\mathcal{R}) \quad (3.44)$$

3.7 Trajectory Generation

The target states \hat{x}_a which are generated using the approach in Section 3.6 at each time step result in piecewise references (e.g., if a lane-change is required, $\hat{\eta}$ will change from the centre of one lane to another). The MPC approaches overviewed in Sections 3.4.1 and 3.4.2 are used in the proposed framework to plan trajectories for directing the vehicle from its current state $x_a(0) = [\xi_0, \eta_0, \psi_0, v_0]^T$ to a (safe) target state $\hat{x}_a = [\hat{\xi}, \hat{\eta}, \hat{\psi}, \hat{v}]^T$ in an admissible way (i.e. by considering vehicle dynamics, state constraints, and input constraints).

3.7.1 Nominal MPC

As the dynamics of the state $\hat{\xi}$ of system in (3.4) depends only on v , it is possible to further simplify the system for the trajectory generation, thus reducing the computational time for its generation. The reduced order system for trajectory generation is

$$x(k+1) = Ax(k) + Bu(k), \quad y(k) = x(k) \quad (3.45)$$

Trajectory Planning

where $x = [\eta, \psi, v]^T$ is the system state, $u = [a_x, \delta_f]^T$ is the input, and the system and input matrices A and B are obtained by extracting the appropriate rows and columns of A_{dm} and B_{dm} in (3.9), respectively. The state and input constraints polyhedrons \mathcal{X} and \mathcal{U} are

$$\mathcal{X} = \{x \in \mathbb{R}^3 : x_{\min} \leq x \leq x_{\max}\} \quad (3.46a)$$

$$\mathcal{U} = \{u \in \mathbb{R}^2 : u_{\min} \leq u \leq u_{\max}\} \quad (3.46b)$$

where $x_{\min}, x_{\max} \in \mathbb{R}^3$ and $u_{\min}, u_{\max} \in \mathbb{R}^2$ are constant vectors representing the minimum and maximum limits of the states and inputs respectively. From (3.45) and (3.46), it follows that the vehicle dynamics of interest for the overtaking manoeuvre match the hypothesis required for the application of the robust MPC in Section 4.3, which is therefore used for the generation of a feasible path to steer the vehicle toward $\hat{x} = [\hat{\eta}, \hat{\psi}, \hat{v}]^T$ belonging to the safe reachable set (3.40), where $\hat{\eta}$, $\hat{\psi}$ and \hat{v} are defined in the previous section.

3.7.2 Robust MPC

The approach for trajectory planning using robust MPC is analogous to the technique using nominal MPC discussed in the section above. The difference lies in considering the parameter varying system description from (3.9). The reduced order model from (3.45) is further augmented with the additive disturbance term to arrive at system dynamics for trajectory generation given below.

$$x(k+1) = Ax(k) + Bu(k) + w, \quad y(k) = x(k) \quad (3.47)$$

where $x = [\eta, \psi, v]^T$ is the system state, $u = [a_x, \delta_f]^T$ is the input, w is the disturbance vector composed by the last three entries of the w_a -term in (3.11), and the system and input matrices A and B are obtained by extracting the appropriate rows and columns of A_{dm} and B_{dm} in (3.9), respectively. The state and input constraints polyhedrons \mathcal{X} and \mathcal{U} are in (3.46). It is noted that the boundedness of \mathcal{X} and \mathcal{U} and the structure of the w_a -term in (3.11) imply that the w -term in (3.9) belongs to a bounded polyhedral set denoted as \mathcal{W} [110]. From (3.47) and (3.46), it follows that the vehicle dynamics of interest for the overtaking manoeuvre match the hypothesis required for the application of the robust MPC in Section 4.3, which is therefore used for the generation of a feasible path to steer the vehicle toward $\hat{x} = [\hat{\eta}, \hat{\psi}, \hat{v}]^T$ belonging to the safe reachable set (3.40), where $\hat{\eta}$, $\hat{\psi}$ and \hat{v} are defined in Section 3.6.

3.7.3 Collision Avoidance Constraints

The basic tools that are used to construct the potential field for situational awarness can also be used to obtain collision avoidance constraints that can be added to the optimisation problem in (3.16) or (3.26). An example demonstrating how the collision avoidance constraints can be designed while approaching a lead vehicle is explained using Figure 3.3 as an exemplar. While designing the potential field in Section 3.5.4, the equation $a_{ca}\xi + b_{ca}\eta + c_{ca} = 0$ is one of the hyperplanes that is used to construct the bounds of the unsafe region around the lead vehicle (Γ_{lv}). However, the utility of this hyperplane is expanded by using it to divide the given road segment into two zones; (i) safe zone represented by $a_{ca}\xi + b_{ca}\eta + c_{ca} > 0$, and (ii) unsafe zone represented by $a_{ca}\xi + b_{ca}\eta + c_{ca} < 0$, see Figure 3.3. Thus, for a subject vehicle located at (ξ_0, η_0) , an MPC based trajectory planner can ensure collision-free motion if constraints are designed that limits all planned trajectories to stay within the safe zone. This is the crux of the various collision avoidance constraints that are described in literature [118, 51]. However, as discussed in the section above, in this chapter a reduced order system that does not have longitudinal position ξ as one of its states is used by the MPC for planning trajectories. This gives rise to the need of expressing the collision avoidance constraints using the states from the reduced order system i.e., η and v . The formulation of the necessary collision-avoidance constraints for both the nominal and the robust MPC framework are presented below.

Constraint I

If (ξ_0, η_0) represent the current location of the SV in global coordinates and in the context of MPC are known values then the satisfaction of the following constraint equation guarantees that initially the subject vehicle is within the safe zone. The linear inequality representing this constraint can be included into the nominal and

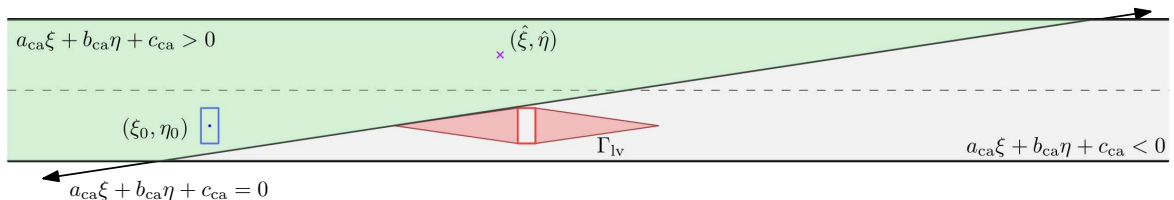


Figure 3.3 Schematic to explain identification of collision avoidance zone. **Note:** SV – blue rectangle, LV and surrounding unsafe region – red polygon, target coordinate – magenta cross, safe zone – green polygon

Trajectory Planning

the robust MPC using the equation below.

$$\text{nominal/robust MPC: } a_{\text{ca}}\xi_0 + b_{\text{ca}}\eta_0 + c_{\text{ca}} > 0 \quad (3.48)$$

Constraint II

The nominal initial state $\bar{x}(0) = (\bar{\eta}, \bar{\psi}, \bar{v})$ is part of the decision variable of the problem (3.26) which lies within the robust MPC framework and not the nominal MPC framework. Therefore, the equation given is applicable only for trajectory planning using robust MPC and ensures that the nominal initial position of the SV is also within the safe zone.

$$\text{robust MPC: } a_{\text{ca}}\xi_0 + b_{\text{ca}}\bar{\eta} + c_{\text{ca}} > 0 \quad (3.49)$$

Constraint III

Finally, it is important to ensure that the trajectory obtained by solving the optimisation problem in (3.16) or (3.26) guarantees that the SV stays within the safe zone throughout the prediction horizon. From (3.3a), (3.4) it is evident that the evolution of the longitudinal position ξ is a function of the longitudinal velocity of a vehicle v . Thus, along a given prediction horizon N , the predicted nominal longitudinal position $\xi(\cdot)$ (or $\bar{\xi}(\cdot)$) can be estimated using the initial longitudinal position ξ_0 and the predicted nominal velocity $v(\cdot)$ (or $\bar{v}(\cdot)$) for the nominal MPC (or robust MPC) using the equations below.

$$\text{nominal MPC: } \xi(j) = \left[\xi_0 + \sum_{i=1}^j (v(i) \cdot t_s) \right]; j = 1, 2, \dots, N \quad (3.50a)$$

$$\text{robust MPC: } \bar{\xi}(j) = \left[\xi_0 + \sum_{i=1}^j (\bar{v}(i) \cdot t_s) \right]; j = 1, 2, \dots, N \quad (3.50b)$$

The expression above is utilized to create N different constraints that fulfil the collision avoidance criterion along the entire prediction horizon. The generalized constraint equation that is used to create the N different constraint equations is given

below.

$$\text{nominal MPC: } a_{\text{ca}} \left[\xi_0 + \sum_{i=1}^j (v(i) \cdot t_s) \right] + b_{\text{ca}} \eta(j) + c_{\text{ca}} > 0; j = 1, 2, \dots, N \quad (3.51\text{a})$$

$$\text{robust MPC: } a_{\text{ca}} \left[\xi_0 + \sum_{i=1}^j (\bar{v}(i) \cdot t_s) \right] + b_{\text{ca}} \bar{\eta}(j) + c_{\text{ca}} > 0; j = 1, 2, \dots, N \quad (3.51\text{b})$$

where the predicted velocity $v(i)$ and the predicted lateral position $\eta(i)$ can be obtained from the evolution of states in (3.13) for the nominal MPC. Similarly, the predicted nominal velocity $\bar{v}(i)$ and predicted lateral position $\bar{\eta}(i)$ for the robust MPC can be obtained from the prediction model in (3.27). Therefore, the set of $(N + 2)$ equations obtained from (3.48), (3.49) and from different values of j in (3.51) represent collision avoidance constraints that are expressed solely as a function of two states namely lateral position and longitudinal velocity. These inequalities representing the collision avoidance constraints can be supplemented to the constraints of the optimisation problem in (3.16) or (3.26) to ensure that the planned trajectory is collision free along the entire prediction horizon. It is noteworthy that the technique for design of the collision avoidance constraints described above can be easily adapted to situations where (i) the SV needs to perform the lane-change while completing an overtaking manoeuvre and/or (ii) when there are multiple hyperplanes representing collision-avoidance constraints for more than one traffic member.

At each discrete time instant k , problem in (3.16) with additional constraints (3.48), (3.49), and (3.51) is solved by setting the target state and the initial state as $\hat{x} = [\hat{\eta}, \hat{\psi}, \hat{v}]^T$ and $x_p = x(k)$ respectively. The optimal trajectory $x^* = [\xi^*, \eta^*, \psi^*, v^*]^T$ is generated by simulating the vehicle model (3.3) with the optimal inputs $u^* = [a_x^*, \delta_f^*]^T$ from the solution of MPC problem (3.16) and then passed to a trajectory tracking controller as reference signals. The generic closed-loop structure for trajectory planning that is valid for both the MPC planners is depicted in Figure 3.4 and a skeleton of this algorithm that is used for performing a safe overtaking manoeuvre using the nominal MPC framework for trajectory generation is depicted in Algorithm 3.1.

Likewise, at each discrete time instant k , the problem in (3.26) with the collision avoidance constraints from (3.48), (3.49), and (3.51) is solved by setting the target state and the initial state as \hat{x} and x_p respectively. The optimal trajectory $x^* = [\xi^*, \eta^*, \psi^*, v^*]^T$ is generated by simulating the vehicle model (3.3) with the net control

Trajectory Planning

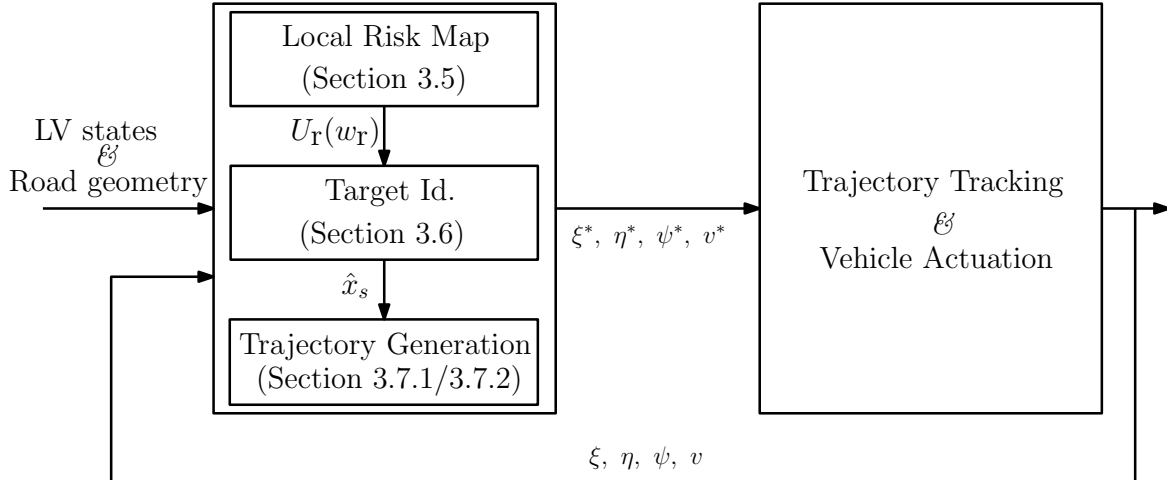


Figure 3.4 Closed-loop framework for trajectory planning. **Note:** LV denotes lead vehicle

action based on (3.31) obtained from the solution of MPC problem (3.26) and then passed to a trajectory tracking controller as reference signals. As mentioned above, the closed-loop control structure depicted in Figure 3.4 is applicable also for the RMPC based trajectory planning approach and the important steps are highlighted in Algorithm 3.2.

3.8 Numerical Results

In this section, results obtained from a closed-loop simulations are used to evaluate the ability of the proposed framework for planning trajectories for a high-speed overtaking manoeuvre. The scenario used is as follows: both the subject vehicle and the lead vehicle are travelling on a two-lane one-way road of infinite length at longitudinal velocity v and v_{LV} , respectively. The dimensions of the road, lane-limits and lead vehicle's states are available to the subject vehicle on-demand through for example a V2X communication link. Each lane of the highway is assumed to have a nominal desired velocity which is provided to the subject vehicle by the route planner while the decision to perform an overtaking manoeuvre and availability of the faster lane is verified by the decision making block of the SV [23, 119]. The design parameters, state, and input set constraints in Tables A.1 and A.2 used to set up the scenario and controller within an integrated Simulink and IPG CarMaker co-simulation platform. It is noteworthy that, the constraints for the inputs were designed by considering the steering and longitudinal acceleration applied by an inbuilt IPG CarMaker controller for several smooth high-speed overtaking

Algorithm 3.1 Trajectory Planning using nominal MPC

```

1: initialize:
2:  $\mathcal{R}_V \leftarrow$  bank of reachable sets in V-frame
3:  $U_{\text{safe}} \leftarrow$  upper bound of risk potential
4: procedure GENERATETRAJECTORY
5: top:
6:    $v_{\text{des}} \leftarrow$  desired longitudinal velocity from user
7:    $\mathcal{R}_{\text{total}} \leftarrow$  reachable set for given  $v_{\text{des}}$  as (3.2)
8:    $\mathcal{R} \leftarrow$  projection of  $\mathcal{R}_{\text{total}}$  in I-frame as (3.39)
9: loop:
10:    $U_r \leftarrow$  net potential field in R-frame as (3.37)
11:    $U \leftarrow$  net potential field in I-frame
12:    $\mathcal{G} \leftarrow$  safe regions of the road as (3.38)
13:    $\mathcal{R}_{\text{safe}} \leftarrow \mathcal{G} \cap \mathcal{R}$  as (3.40)
14:    $\hat{x}_a \leftarrow \text{generateTargetStates}(\mathcal{R}_{\text{safe}})$  as (3.41)-(3.43)
15:    $x_a \leftarrow \text{getCurrentStateVector}(\cdot)$ 
16:    $\text{getCollisionAvoidanceConstraints}(\cdot)$  as (3.48)-(3.51)
17:    $u^* \leftarrow \text{solveMPC}(x, \hat{x})$  as (3.16)
18:    $x^* \leftarrow \text{applyOptimalInput}(u(k))$  as (3.3)
19:   if user request change in  $v_{\text{des}}$  then
20:     goto top.
21:   else
22:     goto loop.

```

manoeuvres in CarMaker. Furthermore, the control weights were chosen so as to ensure that the generated trajectory was similar to the one obtained via IPG CarMaker's default lane-change trajectory. Alternatively, other techniques can be used to tune the control weights and a comprehensive review of such techniques is available in [120, 121].

Remarks

- The region around the SV contained within the vertices $V = V_1, V_2, V_3, V_4$ is divided in a uniform two-dimensional grid. For every point on this grid the individual potential field due to each road feature and traffic member is calculated using (3.32)-(3.37). The set \mathcal{G} in (3.38) is then computed by performing a search over all grid point and selecting the points which have a potential lower than the threshold.
- The trivial choice for the transformation matrix M_θ to characterise the subspace of steady-states and inputs is the identity matrix $\mathcal{I}_{n_x+n_u}$ which results in $n_\theta =$

Trajectory Planning

Algorithm 3.2 Trajectory Planning using Robust MPC

```

1: initialize:
2:  $\mathcal{R}_V \leftarrow$  bank of reachable sets in V-frame
3:  $U_{\text{safe}} \leftarrow$  upper bound of risk potential
4: procedure GENERATETRAJECTORY
5: top:
6:    $v_{\text{des}} \leftarrow$  desired longitudinal velocity from user
7:    $\mathcal{R}_{\text{total}} \leftarrow$  reachable set for given  $v_{\text{des}}$  as (3.2)
8:    $\mathcal{R} \leftarrow$  projection of  $\mathcal{R}_{\text{total}}$  in I-frame as (3.39)
9: loop:
10:   $U_r \leftarrow$  net potential field in R-frame as (3.37)
11:   $U \leftarrow$  net potential field in I-frame
12:   $\mathcal{G} \leftarrow$  safe regions of the road as (3.38)
13:   $\mathcal{R}_{\text{safe}} \leftarrow \mathcal{G} \cap \mathcal{R}$  as (3.40)
14:   $\hat{x}_a \leftarrow \text{generateTargetStates}(\mathcal{R}_{\text{safe}})$  as (3.41)-(3.43)
15:   $x_a \leftarrow \text{getCurrentStateVector}(\cdot)$ 
16:   $\text{getCollisionAvoidanceConstraints}(\cdot)$  as (3.48)-(3.51)
17:   $u^* \leftarrow \text{solveRobustMPC}(x, \hat{x})$  as (3.31)
18:   $x^* \leftarrow \text{applyOptimalInput}(u(k))$  as (3.3)
19:  if user request change in  $v_{\text{des}}$  then
20:    goto top.
21:  else
22:    goto loop.

```

$n_x + n_u$. For the scenario being discussed in this section, the values of steady-state heading angle ψ_{ss} , steady-state acceleration $a_{x,ss}$, and steady-state steering angle $\delta_{f,ss}$ are 0. Hence, the dimension of the parameter vector can be reduced and hence linear mapping matrix M_θ characterising the subspace of steady-states and inputs in (3.15) and (3.25) is given as

$$M_\theta = \begin{bmatrix} 1 & 0 & 0 \\ 0 & 1 & 0 \\ 0 & 0 & 1 \\ 0 & 1 & 0 \\ 0 & 1 & 0 \end{bmatrix} \quad (3.52)$$

- As discussed in the section above, the optimal trajectory generated by the trajectory planner acts as reference signal for a lower level trajectory tracking controller, see Figure 3.4. The trajectory tracking controller is responsible for actuating the steering, accelerator brakes to follow the reference trajectory as closely as possible while handling system non-linearities and disturbances. In

this chapter, the optimal velocity v^* obtained from the robust MPC is passed on to a longitudinal tracking controller as a reference signal. The longitudinal tracking controller is sensitive to the powertrain delays and factors them in while computing an appropriate longitudinal acceleration signal for the SV. On the other hand, the lateral tracking is performed by an adaptive controller that uses x^* as its reference to compute appropriate steering action [122]. In addition to tracking the reference trajectory as closely as possible, these lower level controllers can handle system delays, tire nonlinearities, road surface variations, etc. However, the task of longitudinal and lateral tracking can also be performed by the multitude of techniques available in literature but is beyond the scope of this chapter (the reader is referred to [5, 82, 86–88] for possible alternative techniques).

- The entire co-simulation was run on a laptop machine with an Intel i7-6820HQ processor, 16GB RAM running Microsoft Windows 7 64-bit, and MATLAB 2012b 32-bit. The average time required at each time step for the optimisation routine was 0.0077 s with a standard deviation of 0.0011 s.

3.8.1 Robust positive invariant set and MPC implementation

The robust positive invariant set \mathcal{Z} for the error dynamics and the nominal control law in (3.23), (3.24) is calculated using the algorithm in [111]. The algorithm in [111] provides an iterative technique based on the supporting function of polytopic sets to calculate the outer approximation of a minimal robust positively invariant set for a discrete-time linear time-invariant system. Equation (3.23) suggests that the structure of the set \mathcal{Z} has a dependence on (i) size of set \mathcal{W} , and (ii) the matrix A_K . Since, the set \mathcal{W} is fixed by the vehicle geometric constraints and chosen longitudinal velocity range (see Table A.1), the only degree of freedom available for designing the set \mathcal{Z} is via the design of a Hurwitz matrix A_K by choosing an appropriate controller K to ensure stable error dynamics. The tradeoff for the design of the nominal controller with fixed gain K (or equivalently the design of the matrix) are twofold; (i) to constrain the error set \mathcal{Z} to a reasonable size such that the deviation between nominal system and actual system is reduced and (ii) to ensure that the input set $\bar{\mathcal{U}}$ for the MPC is as large as possible, thus enlarging the decision space for the MPC to compute smooth control inputs. Furthermore, it was noted that A_K -matrices with eigenvalues close to the origin of the complex plane might result in an empty $\bar{\mathcal{U}}$, while if the eigenvalues of A_K are close to the unit circle, the set \mathcal{Z} might become so large that $\bar{\mathcal{X}}$ is an empty set, thus both extreme cases make the MPC problem in (3.26) ill-posed. For this application, this trade-off was met by

selecting the dominant eigenvalue λ of A_K for the lateral and yaw dynamics such that \mathcal{Z} is a bounded set and $\bar{\mathcal{U}}$ is as large as possible. Figure 3.5 provides a visual representation for this behaviour where the plot on the left depicts the disturbance set \mathcal{W} and the robust positively invariant set \mathcal{Z} for a given controller, whereas the plot on the right depicts the net input set \mathcal{U} and the constrained input set $\bar{\mathcal{U}}$. It is noteworthy that only a projection of the disturbance and error sets onto the lateral and yaw dimension of the system is plotted since the disturbance for the system exists only along these dimensions (the variation in dynamics in the LPV system in (3.6), (3.6) exists only on two states namely lateral position η and heading angle ψ), see (3.11). Furthermore, by increasing the dominant eigenvalue beyond $\lambda = 0.72$ results in a large \mathcal{Z} that renders $\bar{\mathcal{X}} = \phi$. Likewise, the plots show that the error set grows along the lateral position dimension as the eigenvalue changes whereas the absolute limits along the heading angle dimension are close to constant. However, even for the error set \mathcal{Z} obtained with the larger eigenvalue, the magnitude of the error limits in lateral position is a small fraction of the actual limits in lateral position while allowing a large $\bar{\mathcal{U}}$ making it a suitable choice for being used to solve the MPC problem in (3.26).

3.8.2 Simulation Results

A simulation environment is initialised with the subject vehicle behind the lead vehicle and the initialisation parameters given in Tables A.1 and A.2. The simulation is then allowed to run and the proposed framework performs three primary tasks; (i) surrounding risk zone detection, (ii) safe target identification, and (iii) trajectory generation at each sampling time. Some details for each task output as well as overall simulation results are discussed below. Figures 3.6(a) and 3.6(b) show the snapshot of the output of the local risk map and target point selection at the time instant $t = 14$ s during the overtaking when the subject vehicle has detected the lead vehicle as it is performing the first lane change of the overtaking manoeuvre. Figure 3.6(a) provides a 3D-view of the entire potential function computed as in (3.37) and the local minima at the centre of each lane for guiding a subject vehicle can be seen along with the trapezoidal field created by a lead vehicle (it is noted that in Figures 3.6(a) and 3.6(b) large values of the potential field are truncated for the sake of readability of the figure). Significantly, the potential field approach can be expanded to accommodate more lanes, additional traffic members, and/or more complex road geometries. Furthermore, the computation of potential fields is based on simple mathematical operations and hence addition of traffic participants, more lanes, etc. will not result in any significant computation overhead. Similarly, the design of collision avoidance constraints relies of basic mathematical operations

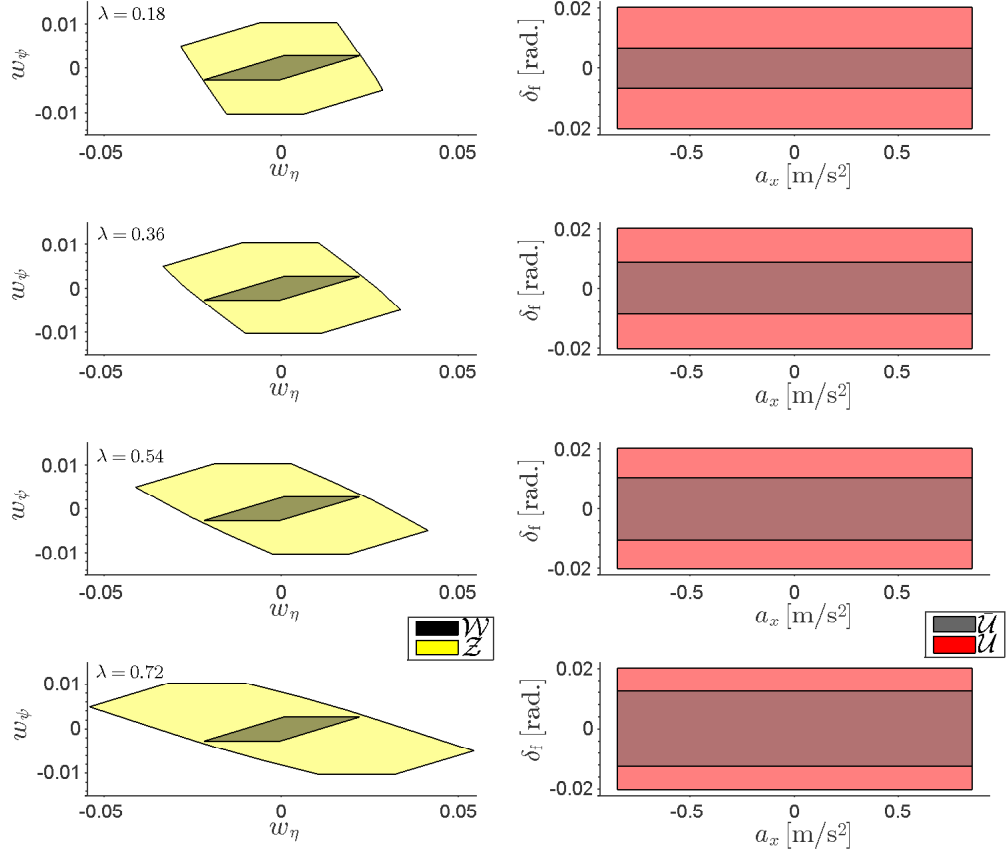


Figure 3.5 Error polyhedron and resulting tightened input set obtained by changing magnitude of eigenvalue

and thus collision avoidance constraints for each traffic participant can be generated without any major computation overhead. However, the design of potential fields for different road types is not the primary focus of this body of work and hence not discussed in greater detail. Figure 3.6(b) depicts the level curves of the potential field for the same time instant in the R-frame along with the reachable set of the subject vehicle and identified target on the road computed as in (3.41), which also represents the output of the block Target Id. In Figure 3.6(b), the lead vehicle is depicted as red rectangle and the buffer zones (as triangular appendages), where the potential field rapidly increases to prevent the subject vehicle from getting too close to the lead vehicle during the different phases of an overtaking manoeuvre, can be easily observed. As the region Γ_{lv} (unsafe region) surrounding the lead vehicle moves in the R-frame with speed $v_{\text{LV}} - v$, at each time step the local risk map of the

Trajectory Planning

safe reachable region and the reference targets change accordingly. Figure 3.7 shows some of the target references selected by the subject vehicle for safely overtaking.

The reference points, dynamically generated, are used by the Trajectory Generation block in Figure 3.4 as described in Section 3.7. The results from the entire simulation are depicted in Figure 3.8. The trajectories of the subject and lead vehicles as well as the relevant states and inputs of the subject vehicle are shown in the inertial frame in Figure 3.8. Moreover, Gaussian noise is added to the lead vehicle's velocity in an attempt to (i) introduce sensor imperfections, (ii) wireless network packet loss, and (iii) lack of accurate knowledge of lead-vehicle states. Introducing this noisy signal in the potential field calculation in (3.35) will help in understanding if the proposed technique is robust against the random variations in lead-vehicle states. The top plot shows the actual path followed by the subject and lead vehicles and the trajectory of the overtaking manoeuvre for the subject vehicle can be observed. Moreover, since the subject vehicle is travelling with a higher longitudinal velocity, it covers a larger portion of the road segment in the given time. The bottom four plots of Figure 3.8 show the states and input of the subject vehicle evolving over time. The key aspect about the overtaking manoeuvre is that the overtaking manoeuvre is initiated close to 10 s and one can observe the longitudinal velocity of the vehicle increasing while the first lane change manoeuvre is being performed. The reverse behaviour (i.e., decreasing velocity while performing the lane change) is visible after 20 s. This is reminiscent of a real-world overtaking manoeuvre where a vehicle may accelerate or decelerate while performing the lane change manoeuvre(s) thus demonstrating the efficacy of the proposed controller. The noisy data from the lead vehicle's velocity also does not have any impact on the trajectory planning process as both the states and input signals are devoid of high-frequency oscillation. Another key aspect is that the two states of SV, (i) longitudinal velocity and (ii) heading-angle show smooth evolution without any high-frequency oscillation during either of the lane-changes. The longitudinal acceleration profile is obtained via the tracking controller discussed above and it also does not demonstrate any high-frequency oscillations. However, it is designed using basic frequency-based techniques and is not tuned to minimize the jerk but if required this controller can be swapped with any preferred control technique available in literature. Similarly, the steering action for the lateral motion demonstrates smooth evolution with no high-frequency oscillation. Moreover, just as in the case of the longitudinal tracking controller, if necessary another controller for the steering action can be utilized with the proposed trajectory planning framework. Also, as expected the MPC controller respects all the system and input constraints which is evident from the plots in Figure 3.8.

To show the need of the robust MPC to tackle variations of the longitudinal vehicle speed while performing the overtaking manoeuvre, we compare the performance

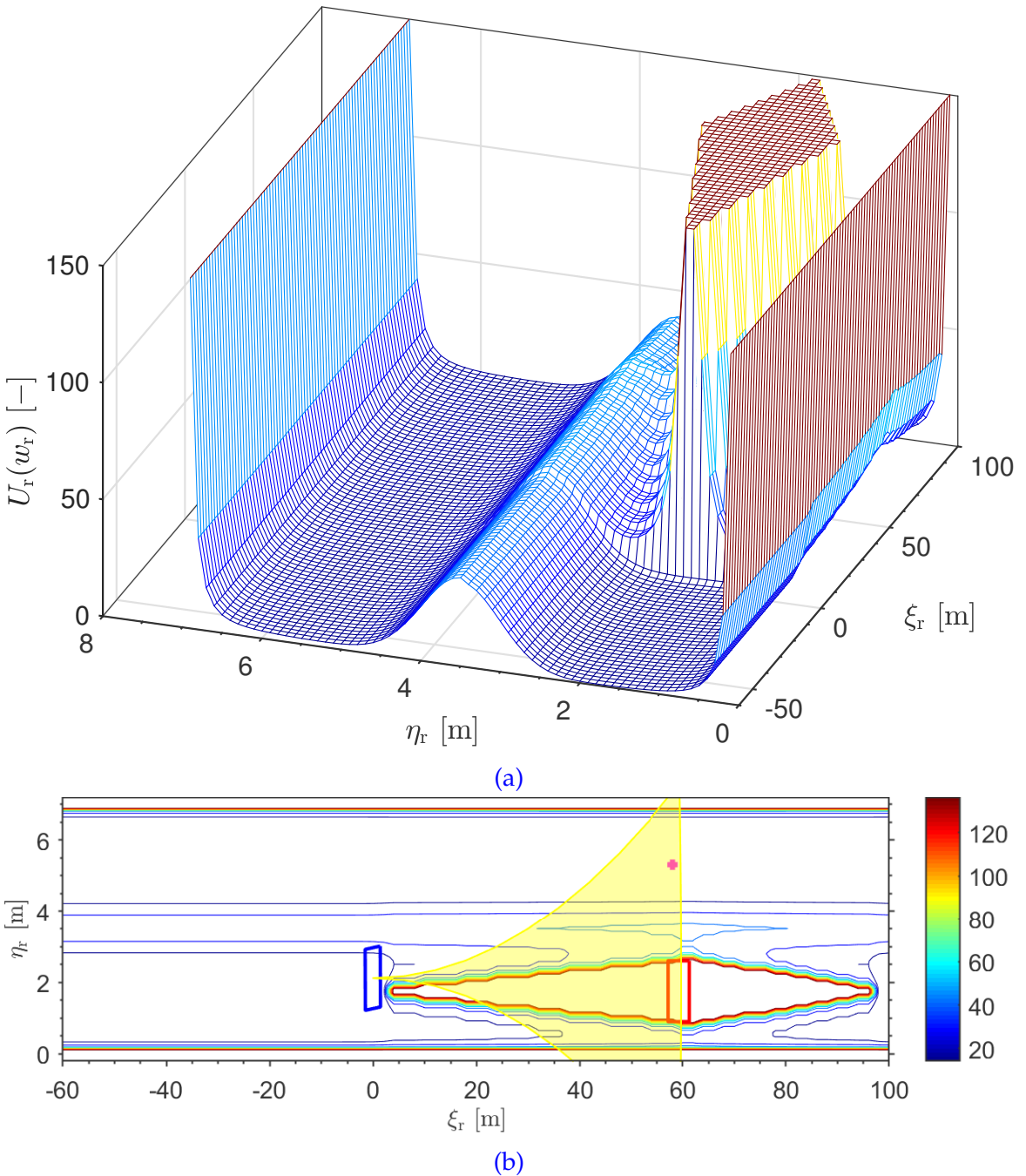


Figure 3.6 Snapshot of simulation (simulation time $t = 14$ s); (a) Cumulative potential field U_r from road, lane, and obstacle vehicle; (b) Contour plot of the potential field along with the reachable set (yellow) and reference target on the road (magenta cross). **Note:** Blue rectangle depicts the subject vehicle and the rectangle in red depicts the lead vehicle

of the proposed framework when the robust MPC in the Trajectory Generation Block

Trajectory Planning

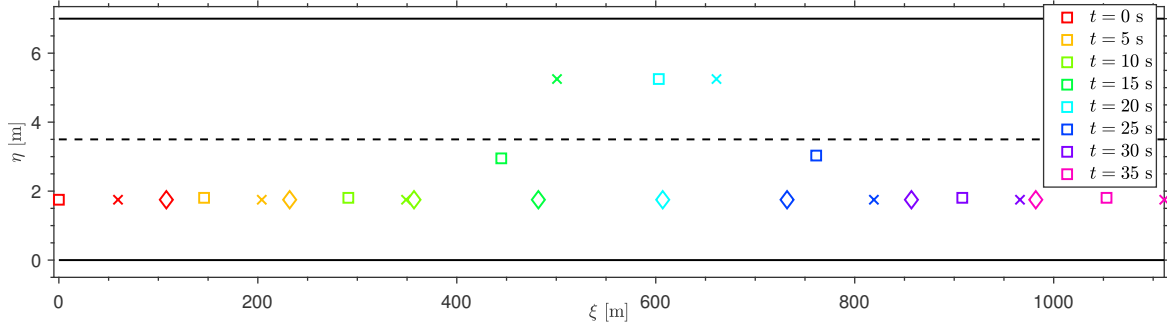


Figure 3.7 Snapshot of simulation demonstrating: reference targets (\times) for different configurations of subject vehicle (\square) and lead vehicle (\diamond) while driving on a highway. Note: solid lines (–) are the road boundaries and dashed line (- -) is the lane marking

in Figure 3.4 is replaced by the MPC strategy for disturbance free LTI systems proposed in Section 3.4.1 (i.e. nominal MPC). The LTI vehicle model for the design of the nominal MPC is obtained from system (3.21) based on (3.10), while the remaining vehicle parameters for the control tuning are set to those listed in Table A.2. It is noted that, despite the fact that nominal MPC is effective for overtaking with fixed speed (see [93] for further details), its performance to generate feasible trajectories reduces when the longitudinal speed change during the overtaking manoeuvre. This is confirmed in Figure 3.9 where the reference and actual vehicle trajectories of the subject vehicle in the O-frame of reference are depicted both for the nominal and robust MPC. These results demonstrate the nominal MPC struggles to generate suitable trajectories for the overtaking manoeuvre with varying longitudinal velocity. The trajectories suffer from overshoot and also takes the subject vehicle very close to the lead vehicle during the initial lane change. Both these factors make the nominal MPC based technique unsuitable for planning overtaking trajectories with variable velocity. On the other hand, the robust MPC based trajectory generates very little overshoot and also maintain the safety margins to the lead vehicle during all three sub-manoeuvres. Furthermore, due to its ability to generate consistent and uniform trajectories for lane change while accelerating and decelerating, the controller proposed in this chapter appeals to a wider application set (lane-change, merging into traffic, etc.). It is noted that in the proposed approach, the parameters of the MPC strategy (i.e., Q , R , P , T , and N) can be tuned for adjusting the aggressiveness of a manoeuvre. Additionally, at each time step the optimisation problem underlying the robust MPC techniques is always feasible according to *Theorem 2* in [101].

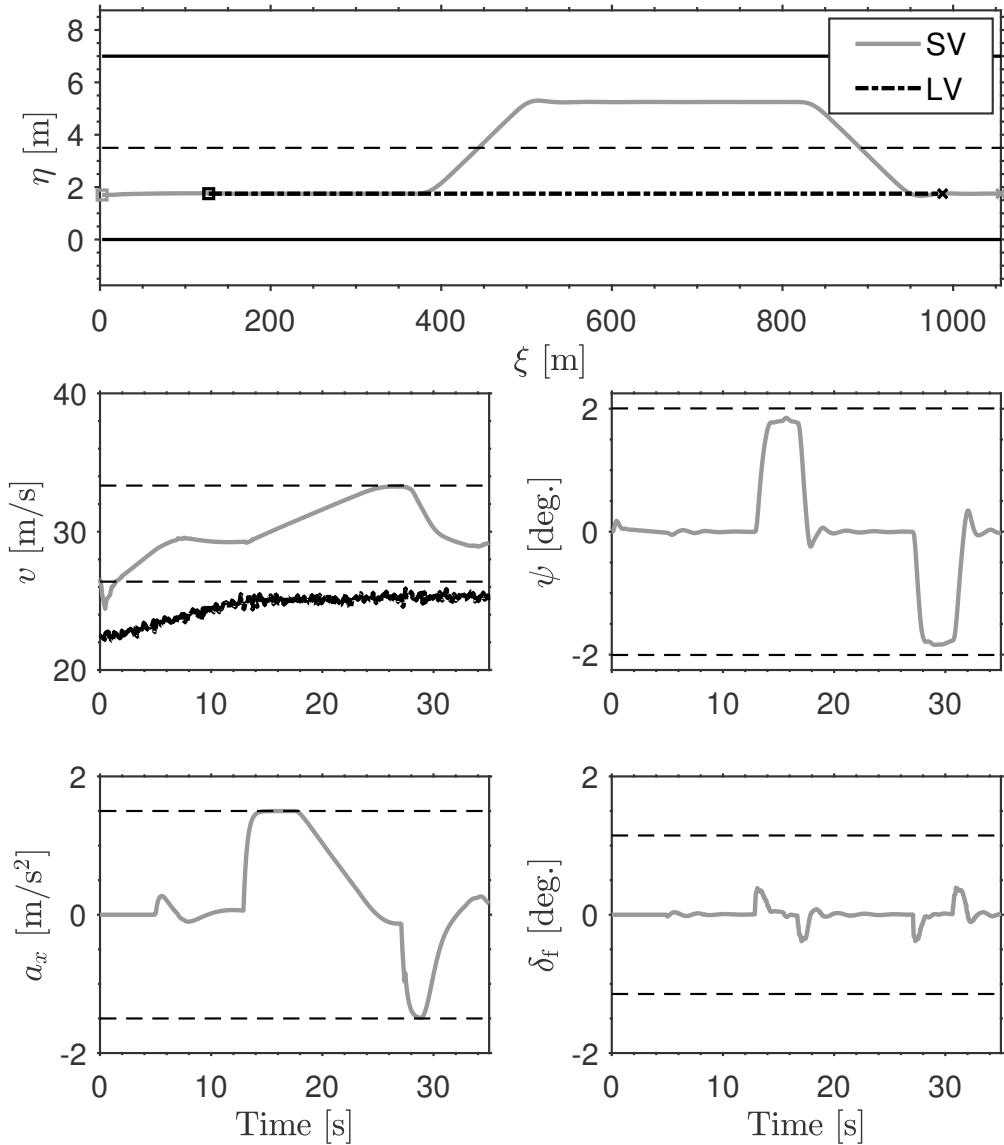


Figure 3.8 Simulation results: SV and LV trajectories, longitudinal velocity, heading angle, longitudinal acceleration, and steering angle for a high-speed overtaking manoeuvre. **Note:** (--) are the system constraints

Trajectory Planning

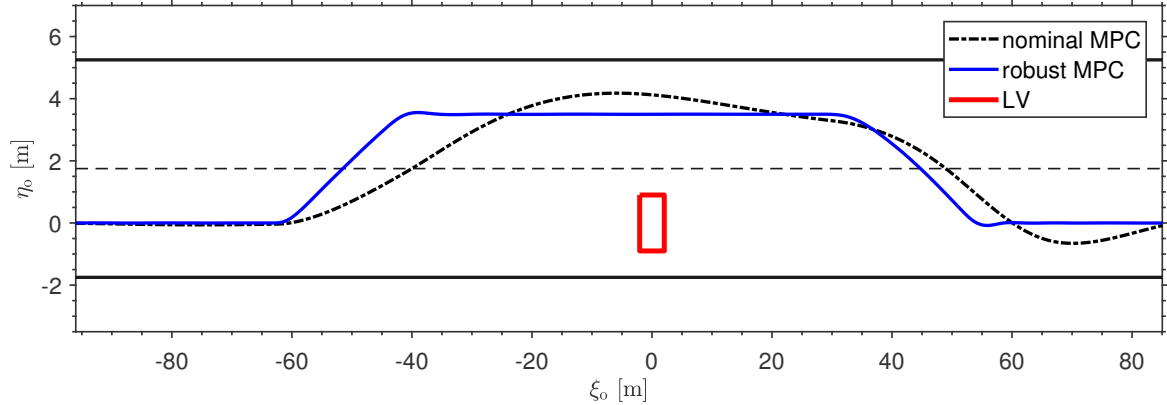


Figure 3.9 Simulation results: trajectory of the subject vehicle (SV) during an overtaking manoeuvre in the lead vehicle (LV) frame of reference (ξ_o, η_o).

3.9 Summary

In this chapter, a modular control framework for autonomous high-speed overtaking was presented with (i) local risk map generation, (ii) safe target identification, and (iii) trajectory planning being the different modules of the system. In this framework the onus of situational awareness lies with the local risk map and safe zone identification sub-systems and the onus of feasible and collision-free trajectory generation lies with the MPC controller. This modular design allows the framework to avoid non-convex constraints allowing for an MPC formulation that can be solved using commonly available optimisation solvers. Moreover, two different trajectory planners (i) nominal MPC which does not consider coupling of longitudinal and lateral dynamics and (ii) robust MPC which models this non-linear coupling between longitudinal and lateral dynamics as additive disturbance are presented. Additionally, a novel technique for designing collision avoidance constraints based only on lateral position and longitudinal velocity of the subject vehicle was presented. This allows the trajectory planning controller to generate feasible and safe trajectories with admissible inputs even while performing lateral manoeuvres with changing longitudinal velocity. Numerical results in a Simulink/IPG CarMaker co-simulation environment demonstrated that the algorithm is able to fulfil the safety considerations for high speed overtaking manoeuvre and generate trajectories which are also compatible with the vehicle dynamics and safety considerations. Furthermore, comparing the results of the nominal MPC and the robust MPC demonstrated the added benefits of the robust based approach at generating feasible trajectories despite variations in longitudinal velocity of the subject vehicle. As future work the proposed framework will be extended to (i) more challenging overtaking scenarios with multiple traffic

3.9 Summary

participants, external disturbances, etc. and (ii) other manoeuvres under different road geometries.

Trajectory Tracking

यतो यतो निश्चरति मनश्चलमस्थिरम् ।
ततस्तो नियम्यैतदात्मन्येव वशं नयेत् ॥ ६:२६ ॥

— श्रीमद् भगवद्गीता

From whatever cause the restless and unsteady mind wanders away, from that let him restrain it and bring it under the control of the Self alone.

— *Śrīmad Bhagavadgītā* 6:26

In this chapter, an Enhanced Model Reference Adaptive Control (EMRAC) algorithm is used to design a generic lateral tracking controller for an autonomous vehicle. This EMRAC is different from the EMRAC in the literature as it adopts a σ -modification approach to bind the adaptive gains of the switching action of the controller. Moreover, an extended Lyapunov theory for discontinuous systems is used to analytically prove the ultimate boundedness of the proposed closed-loop control system when the adaptive gain of the switching action is bounded with a σ -modification strategy. The control algorithm is applied to a vehicle path tracking problem and its tracking performance is investigated under conditions of (i) external disturbances such as crosswind, (ii) road surface changes, (iii) modelling errors, and (iv) parameter miss-matches in a high fidelity co-simulation environment based on IPG Carmaker/MATLAB. The simulation studies show that the controller is effective at tracking a given reference path for performing different autonomous highway driving manoeuvres while ensuring the boundedness of all closed-loop signals even when the system is subjected to the conditions mentioned above.

4.1 Introduction



HE recent push towards autonomous driving has resulted in an ever increased focus of researchers to propose improvements and devise enhancements for the three architectural layers that are typically present in every self-driving platform [5]:

- *Scanning and perception:* responsible for gathering information about the driving conditions in the neighbourhood of the autonomous vehicle

This chapter is based on [122]

Trajectory Tracking

- *Planning:* utilize input from the perception layer to compute a safe and feasible driving trajectory for the vehicle
- *Control:* use the planned trajectory from the planning layer and a reference and compute steering, acceleration, and brake input to make the autonomous vehicle follow the reference trajectory as closely as possible while ensuring the safety and comfort of the occupants

While the top two layers are relative newcomers to the field of automotive engineering, the control layer which mainly involving steering (i.e., lateral/path-tracking control) and throttle/brake control (i.e., longitudinal control) of a vehicle has been a topic of intense research over the past three to four decades [123]. Whereas the initial attempts at lateral controllers were focussed on driver assistance systems (lane-departure warning, lane keeping assistance, etc.), the emphasis in recent years has expanded to a multitude of autonomous driving use-cases ranging from performing complex manoeuvres on public roads (rural, urban, and highways), off-road driving, etc. to motorsport events for autonomous vehicles. There is a vast amount of technical literature available on the different control methods for vehicle lateral control and comprehensive reviews of different controllers are available [82, 87]. These reviews demonstrate that control of lateral dynamics of a vehicle poses a formidable challenge for control engineering due to a combination of reasons such as: (i) significant dependence of lateral dynamics on the longitudinal velocity of a vehicle, (ii) non-linear tire dynamics, (iii) difficulties in estimation of system parameters such as road surface coefficient, vehicle mass distribution, (iv) non-linearities of road/path curvature, etc. The typical control techniques for path-tracking in technical literature are aimed at reducing the lateral position error of the vehicle with respect to the path while ensuring lateral and yaw stability. Researchers have proposed a variety of control techniques to achieve desirable path-tracking performance for an autonomous vehicle [5, 82, 87]. There are control strategies based on geometric constraints such as (i) follow the carrot [82], (ii) Stanley controller [124], and (iii) pure pursuit [82] which have demonstrated their effectiveness in various experimental tests [31, 86, 87, 125]. Although these control techniques are relatively easy to implement on real-time hardware and provide desired tracking performance around the nominal operational condition, their performance rapidly declines when they operate in different driving conditions [88]. Consequently, other control strategies such as PID, LQR, and sliding mode controllers with feedforward action have been proposed as alternate schemes for lateral control of a vehicle [89, 126]. In these controllers, the feedback controller is designed to reduce the tracking error whereas the feedforward action is developed to counter path curvature. However, it is noted that the LQR controllers have zero gain margin against model uncertainties,

sliding-mode controllers suffer from chattering phenomenon, and tuning of PID controllers is not a trivial task making these control strategies difficult to apply over a wide range of path tracking situations [5, 82, 86, 87]. With an increase in available computational resources and development of efficient optimisation solvers, advanced model based control techniques (e.g., Model Predictive Control (MPC)) are also employed for lateral control of a vehicle [127–130]. MPC controllers ranging from standard linear MPC, Linear time-varying (LTV) MPC, and highly complex controllers based on non-linear vehicle and tire models are available in literature [131–133]. These advanced control techniques improve tracking performance but their tracking performance is highly sensitive to the accuracy of the system model and hence makes them unsuitable in all driving conditions. The issue of model error is mitigated by nonlinear MPC's but these controllers require large computing resources which makes them impractical for most of the automotive platforms. Recently, active research to augment the abovementioned control techniques with advancements such as neural network, fuzzy logic, etc. to further enhance their applicability and performance has gained great momentum [54, 134–137]. However, these techniques rely heavily on readily available training data which is not easily obtainable in the automotive industry. Nevertheless, the difficulties in estimation of system parameters and presence of rapidly changing dynamics due to nonlinearities such as tire dynamics, longitudinal velocity, external disturbances, etc. make vehicle lateral control very challenging problem.

The theoretical framework for adaptive control was formulated over seven decades ago and since then it has been a topic of active research especially for systems that have large dynamic variations and parameter uncertainties [138]. Model Reference Adaptive control (MRAC) is a well-known adaptive control design method and is based on the objective of ensuring that the controlled variables of a plant track a given reference model. This control technique is backed by an established theoretical framework and has proven to be a viable model based control technique especially for systems where real time model parameters are unknown [138]. To improve the tracking of the reference model despite un-modelled system dynamics, system nonlinearities and rapid varying disturbances, in [139] an adaptive integral control action and an adaptive switching control action were added to the standard feedback and feedforward MRAC strategy. The augmented MRAC, also known in the literature as Enhanced MRAC (EMRAC) [140] (see Figure 4.1 for a representation of closed-loop control scheme) has shown to be effective at imposing dynamics of the reference model to plants of engineering interest affected by model uncertainties and disturbances such as electronic throttle body [139], common rail systems [141], thermo-hygrometric control [142]. Nevertheless, despite the additional benefits obtained by the auxiliary control action, the concern of unbounded drift of the

Trajectory Tracking

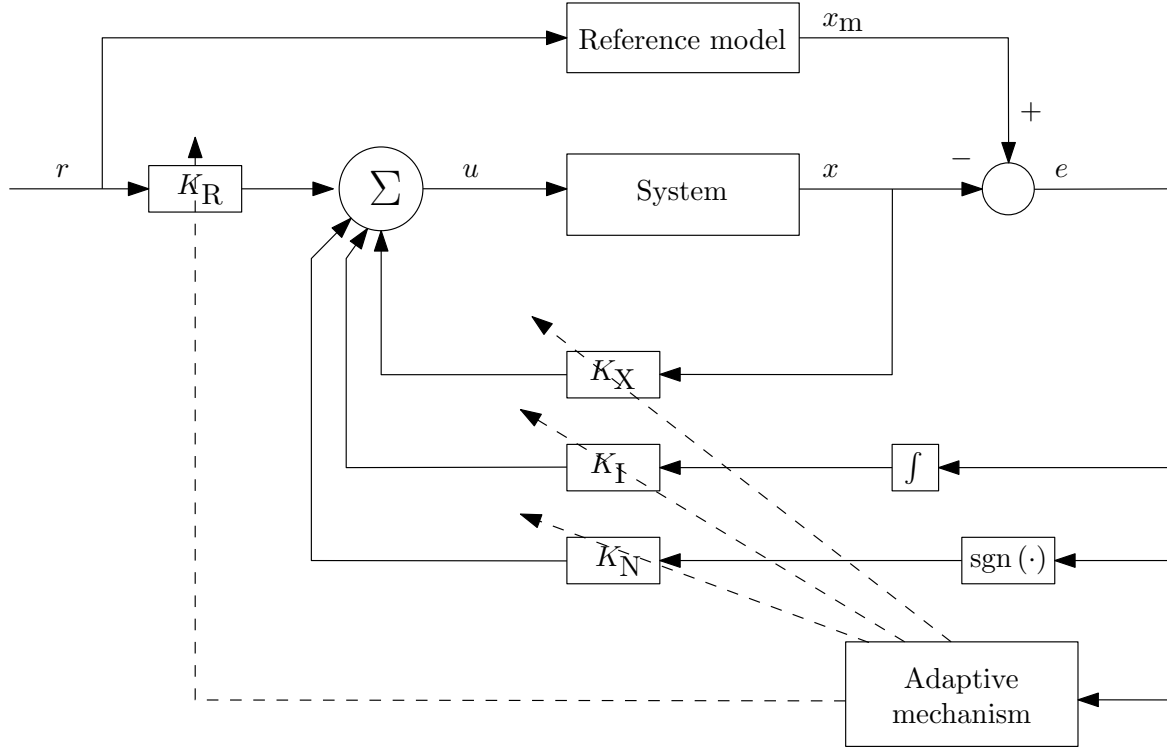


Figure 4.1 EMRAC control scheme [140]

adaptive control gains leading to degraded tracking performance and/or loss of closed-loop stability has been point of concern for these control schemes. In [143], two different methods namely: (i) parameter-projection and (ii) σ -modification were suggested to prevent unbounded drift of the feedback, feedforward, and integral control gains for systems. The parameter-projection based scheme demonstrated its capability to provide asymptotic zero tracking error and boundedness of adaptive gains even when subjected to transient disturbances. Moreover, when the system is subjected to time-bounded disturbances, the σ -modification scheme guarantees ultimate boundedness of the closed-loop system when subjected to persistent disturbances. However, only heuristic solutions (saturation) have been suggested to bind the adaptive gain of the switching action [144].

Notwithstanding its ability to handle parameter variations and system nonlinearities and general control flexibility, MRAC schemes for lateral control of a vehicle are marginally studied in literature [145–147]. One of the reasons is the concern of unbounded drift of the controller gains leading to instability [148]. A possible approach is to prevent the unbounded drift of the control gains is to saturate the gains. However, this may have a negative impact on the closed-loop performance the saturation will prevent the controller gains from adapting to values beyond the limit counter sudden transients. A more elegant approach would be to allow

controller gains to increase (if required) to counter any large transients but have an inbuilt mechanism that allows the gains to fall back to smaller values once the need for large control action is over and σ -modification technique provides this mechanism by the addition of damping to an ideal adaptive law. In this chapter, the σ -modification framework to guarantee bounds on the adaptive control gains discussed above is extended to bind systematically the possible drift in the adaptive switching action gain of the EMRAC. The closed-loop signals system is a piecewise smooth system and the uniform ultimate boundedness of all the closed loop signals including adaptive gains is proven using the extended Lyapunov theory for non-smooth systems [149]. Moreover, the conditions for the ultimate bound are computed using the above mentioned extended Lyapunov theory [150, 151]. Finally, the adaptive control design is applied to the vehicle path-tracking/lateral control problem. The closed-loop system is implemented on an IPG Carmaker-Simulink co-simulation environment and its behaviour in different driving conditions is investigated. The reference model for the lateral-tracking problem is based on a path-tracking bicycle model from literature [106, 152]. The states of this system capture the dynamics of both, lateral-yaw motion of the vehicle as well as the path deviation errors. A stable reference model is obtained by designing a feedback controller using pole placement for stability along with a feedforward action based on required steady-state cornering behaviour of the vehicle to counter the reference path curvature. This reference model describes the preferred dynamical behaviour of the system for achieving stable cornering while accurately tracking any given reference path curvature that the vehicle might encounter during normal highway driving scenarios.

This chapter is structured as follows. Section 4.2 introduces the basic symbols and mathematical definitions used in the chapter. Section 4.3 lays out the mathematical control formulation for the adaptive control scheme together with the analytical proof of the ultimate boundedness of the closed-loop system. The path following system model for the vehicle is discussed in Section 4.4. In Section 4.5, the numerical validation of the closed-loop system is carried out in a MATLAB-IPG CarMaker co-simulation environment. Finally, the concluding remarks and future research directions are laid out in Section 4.6.

4.2 Mathematical Notations and Definitions

The signum function of a real number x is defined as $\text{sgn}(x) = (d/dx)|x|$, $x \neq 0$. For a symmetric matrix M and vector x , $\|x\|_M$ denotes the weighted norm given by $\|x\|_M = \sqrt{x^T M x}$, $\|x\|$ denotes the 2-norm of a vector, and $\lambda_{\min}(M)$ and $\lambda_{\max}(M)$

Trajectory Tracking

are the minimum and maximum eigenvalue of M , respectively. The matrix $\mathcal{O}_{n,m} \in \mathbb{R}^{n \times m}$ denotes a matrix of zeros, and matrix $\mathcal{I}_n \in \mathbb{R}^{n \times n}$ denotes the identity matrix. For a given vector x , $\text{diag}(x)$ represents a diagonal matrix with x as its diagonal. For vectors $x \in \mathbb{R}^n$, $y \in \mathbb{R}^m$, vector (x, y) denotes $[x^T, y^T]^T$. L_∞ is the set of bounded scalar functions. Given a non-smooth time-varying system of the form

$$\dot{\tilde{x}} = \mathbf{f}(t, \tilde{x}) \quad (4.1)$$

where $\tilde{x} \in \mathbb{R}^n$ is the state of system and $\mathbf{f} : \mathbb{R} \times \mathbb{R}^n \rightarrow \mathbb{R}^n$ is the discontinuous vector field. Filippov solutions and the concept of differential inclusions allows solutions to be defined at points of discontinuities in the vector field $\mathbf{f}(t, \tilde{x})$. According to [149, 153] vector function $\tilde{x}(\cdot)$ in $t \in [t_0, t_1]$ is a Filippov solution of the system (4.1) if: (i) $\tilde{x}(\cdot)$ is an absolutely continuous solution and (ii) for almost all $t \in [t_0, t_1]$

$$\dot{\tilde{x}} \in \mathbf{K}[\mathbf{f}](t, \tilde{x}) \quad (4.2)$$

with $\mathbf{K}[\mathbf{f}](t, \tilde{x})$ being the Filippov set valued map defined as

$$\mathbf{K}[\mathbf{f}](\tilde{x}) \triangleq \bigcap_{v>0} \bigcap_{\pi(\mathcal{S})=0} \overline{\text{co}} \{ \mathbf{f}(\mathcal{B}(\tilde{x}, v) \setminus \mathcal{S}) \}, \quad \tilde{x} \in \mathbb{R}^n \quad (4.3)$$

where $\bigcap_{\pi(\mathcal{S})=0}$ denotes the intersection of all sets \mathcal{S} of Lebesgue measure zero, $\mathcal{B}(\tilde{x}, v)$ is the open ball centered at \tilde{x} with radius $v > 0$, and $\overline{\text{co}}$ denotes the convex closure. Moreover, systems of type (4.1) with discontinuous right-hand sides also result in non-smooth Lyapunov functions which hinders the use of standard stability theory proofs [149]. Clarke's generalised gradient presented in detail in [154] is a powerful tool that can be used to streamline proofs for non-smooth analysis. For a globally Lipschitz function $V : \mathbb{R}^n \times \mathbb{R} \rightarrow \mathbb{R}$, the generalised gradient of V at (\tilde{x}, t) is given by

$$\partial V(\tilde{x}, t) = \overline{\text{co}} \{ \lim \nabla V(\tilde{x}, t) | (\tilde{x}_i, t_i) \rightarrow (\tilde{x}, t), (\tilde{x}_i, t_i) \notin \Xi_V \} \quad (4.4)$$

where Ξ_V is the set of measure zero where the gradient of V is not defined [149]. It is noteworthy that Lipschitz means Lipschitz in (\tilde{x}, t) and discontinuities in t are not allowed. Furthermore, if $V(\tilde{x}, t)$ has no explicit dependence on t , the last component of ∂V can be dropped as it is zero. The generalised directional derivative of V is defined in [149] as

$$V^\circ(\tilde{x}; v) = \lim_{\tilde{y} \rightarrow \tilde{x}, t \downarrow 0} \sup \frac{V(\tilde{y} + tv) - V(\tilde{y})}{t} \quad (4.5)$$

4.2 Mathematical Notations and Definitions

and if V is Lipschitz near \tilde{x} , then

$$V^\circ(\tilde{x}; \nu) = \max\{\langle \varphi, \nu \rangle \mid \varphi \in \partial V(\tilde{x})\} \quad (4.6)$$

Thus, by using the definitions in (4.5) and (4.6), a function V is called a regular function if the following two conditions are fulfilled [149]

- $\forall \nu$, the one-sided directional derivative $V'(\tilde{x}; \nu)$ exists,
- $\forall \nu$, $V'(\tilde{x}; \nu) = V^\circ(\tilde{x}; \nu)$.

According to Theorem 2.2 in [149] if $\tilde{x}(\cdot)$ is a solution to (4.1) and $V(\tilde{x}, t)$ is a regular function, then $(d/dt)V(\tilde{x}, t)$ exists almost everywhere and it can be computed as

$$\frac{d}{dt}V(\tilde{x}, t) \in^{\text{a.e.}} \dot{V}(\tilde{x}, t) \quad (4.7)$$

where

$$\dot{V} = \bigcap_{\varphi \in \partial V(\tilde{x}, t)} \varphi^T \begin{pmatrix} \mathbf{K}[f](t, \tilde{x}) \\ 1 \end{pmatrix} \quad (4.8)$$

The solutions of the system in the form (4.1) are said to be uniformly ultimately bounded [155] if; there exists a time interval T (dependent on $\tilde{x}(t_0)$) and a \mathcal{KL} -class function $\Psi : \mathbb{R}^+ \times \mathbb{R}^+ \rightarrow \mathbb{R}^+$ such that

$$||\tilde{x}(t)|| \leq \Psi(||\tilde{x}(t_0)||, t - t_0) \quad \forall t \in [t_0, t_0 + T] \quad (4.9a)$$

and:

$$||x(\tilde{t})|| \leq \epsilon \quad \forall t \in [t_0, t_0 + T] \text{ and } \epsilon > 0 \quad (4.9b)$$

The aforementioned definitions and theorems have been recently used in [156] to formulate the conditions that guarantee the ultimate boundedness of the discontinuous system described in (4.1) and the main theorem is reported below.

Theorem 4.2.1. Assume that for any initial conditions, the differential inclusion (4.2) for system (4.1) is well-posed in the sense of Filippov solutions and there exists a positive globally Lipschitz continuous function $V : \mathbb{R}^n \times \mathbb{R} \rightarrow \mathbb{R}$, two positive functions $W_1, W_2 \in \mathcal{K}_\infty$, and $W_3 \in \mathcal{K}$ such that

$$W_1(\tilde{x}) \leq V(\tilde{x}, t) \leq W_2(\tilde{x}) \quad (4.10a)$$

$\exists \mu > 0$, such that

$$\dot{V}(\tilde{x}, t) \leq -W_3(\tilde{x}), \text{ when } ||\tilde{x}|| \geq \mu \quad (4.10b)$$

Trajectory Tracking

with $\dot{\tilde{V}}(\tilde{x}, t)$ being the generalised gradient of V , then the non-smooth system in (4.1) is globally uniformly ultimately bounded. It is noteworthy that Theorem 4.2.1 is a special case of Theorem 3.1 in [156] by assuming (i) zero the time delays, (ii) the solution of the differential inclusion (4.2) exists for any initial condition, and (iii) $V(\tilde{x}, t)$ is defined for all $\tilde{x} \in \mathbb{R}^n$.

4.3 Control Formulation

Consider a plant modelled in the form

$$\dot{x} = Ax + B_1u + B_2r + B_1d \quad (4.11)$$

where $x \in \mathbb{R}^n$, $u \in \mathbb{R}$, $r \in \mathbb{R}$, and $d \in \mathbb{R}$ are the state, actuated input, un-actuated input, and the disturbance of the system, respectively. The disturbance acting on the plant is assumed to belong to L_∞ , thus there exists Δ_∞ such that $|d| < \Delta_\infty$. The structure of the system matrices $A \in \mathbb{R}^{n \times n}$, $B_1 \in \mathbb{R}^n$, and $B_2 \in \mathbb{R}^n$ are assumed to be known and constructed from the nominal parameters of the given system. The control objective is to steer the dynamics of the system (4.11) towards those of an asymptotically stable LTI reference system of the form

$$\dot{x}_m = A_m x_m + B_m r \quad (4.12)$$

where $x_m \in \mathbb{R}^n$ is the reference model state, and $A_m \in \mathbb{R}^{n \times n}$, $B_m \in \mathbb{R}^n$ are the reference model system matrices with A_m being Hurwitz. By assuming that there exist two constant matrices K_X^* and K_R^* such that the following matching conditions are satisfied

$$A_m = A + B_1 K_X^* \quad (4.13a)$$

$$B_m = B_1 K_R^* + B_2 \quad (4.13b)$$

The aforementioned model reference control problem is solved by the EMRAC control action

$$u(t) = K_X(t)x(t) + K_R(t)r(t) + K_I(t)e_I(t) + K_N(t)\text{sgn}(y_e(t)) \quad (4.14)$$

where the state tracking error is defined as

$$e = x_m - x \quad (4.15)$$

4.3 Control Formulation

and e_I is the integral of the state tracking error e . The output error y_e is defined as

$$y_e = C_e e, \text{ with } C_e = B_1^T P \text{ and } PA_m + A_m^T P = -Q \quad (4.16)$$

with Q being a positive definite matrix and the solution P of the Lyapunov equation in (4.16) exists as A_m is Hurwitz. The output error y_e is a projection of the state-tracking error and it is based on the selection of an output matrix C_e that makes part of the feedback loop passive. Further details on the output error and the associated passivity theorems are provided in [139]. The adaptive control gains K_X , K_R , and K_I are computed as in [143]. Differing from the solutions available in literature, in this work K_N is bounded by including the σ -modification strategy into the adaptive law of K_N , thus avoiding the use of heuristic solutions (saturations of the gain). Hence, K_N is adapted as

$$K_N = \phi_N \text{ and } \dot{\phi}_N = \alpha_N |y_e| + f_N \quad (4.17)$$

where α_N is a positive constant and f_N is the σ -modification term defined as:

$$f_N = -\rho_N \cdot \sigma_{\phi_N} (||\phi_N||) \cdot \phi_N \quad (4.18a)$$

$$\sigma_{\phi_N} (||\phi_N||) = \begin{cases} 0 & \text{if } ||\phi_N|| \leq \hat{M}_{\phi_N} \\ \eta_{\phi_N} \left(\frac{||\phi_N||}{\hat{M}_{\phi_N}} - 1 \right) & \text{if } \hat{M}_{\phi_N} < ||\phi_N|| \leq 2\hat{M}_{\phi_N} \\ \eta_{\phi_N} & \text{if } ||\phi_N|| > 2\hat{M}_{\phi_N} \end{cases} \quad (4.18b)$$

where \hat{M}_{ϕ_N} , η_{ϕ_N} , and ρ_N are positive constants and

$$\eta_{\phi_N} > \frac{3}{4} \cdot \alpha_N^{-1} \cdot \rho_N \cdot \lambda_{\min}(Q) \quad (4.19)$$

Theorem 4.3.1. Consider system (4.11) with $r, d \in L_\infty$ and the reference model (4.12). Let the adaptive control action be given by (4.14), with the adaptive gain for the discontinuous action computed as in (4.17). Then all resultant closed-loop signals are bounded and the state of the closed-loop system is globally uniformly ultimately bounded.

Before providing the proof for Theorem 4.3.1, the following lemma is given.

Trajectory Tracking

Lemma 4.3.2. Similar to Lemma 2 from [143], an additional set of guarantees given below can be derived:

$$\phi_{Ne}\alpha_N^{-1}f_N \geq 0, \quad \forall \phi_N \in \mathbb{R} \quad (4.20a)$$

$$\phi_{Ne}\alpha_N^{-1}f_N > 0, \quad \forall \phi_N : ||\phi_N|| \geq \hat{\mathcal{M}}_{\phi_N} \quad (4.20b)$$

$$\phi_{Ne}\alpha_N^{-1}f_N > \frac{\eta_{\phi_N}}{2} \phi_{Ne}^T \alpha_N^{-1} \rho_N \phi_{Ne}, \quad \forall \phi_N : ||\phi_N|| > 2\hat{\mathcal{M}}_{\phi_N} \quad (4.20c)$$

Proof of Lemma 4.3.2:

From (4.18a) one can state the following

$$\phi_{Ne}\alpha_N^{-1}f_N = \phi_{Ne}\alpha_N^{-1}[-\rho_N \cdot \sigma_{\phi_N}(||\phi_N||) \cdot \phi_N] \quad (4.21a)$$

$$= -\rho_N \cdot \sigma_{\phi_N}(||\phi_N||) \cdot \phi_{Ne} \cdot \alpha_N^{-1} \cdot \phi_N \quad (4.21b)$$

The definition of σ_{ϕ_N} in (4.18b) shows that $\sigma_{\phi_N} = 0$ for $||\phi_N|| < \hat{\mathcal{M}}_{\phi_N}$ and thus the Lemma is satisfied. Furthermore, since $K_N^* = \phi_N^* = 0$ and $\phi_{Ne} = (\phi_N^* - \phi_N)$ the equation above can be expressed as

$$\phi_{Ne}\alpha_N^{-1}f_N = \rho_N \cdot \sigma_{\phi_N}(||\phi_N||) \cdot \phi_N \cdot \alpha_{Ne}^{-1} \cdot \phi_{Ne} \quad (4.22)$$

where once again the definition of σ_{ϕ_N} in (4.18b) shows that when $||\phi_N|| \geq \hat{\mathcal{M}}_{\phi_N}$

$$\phi_{Ne}\alpha_N^{-1}f_N = \rho_N \cdot \eta_{\phi_N} \left(\frac{||\phi_N||}{\hat{\mathcal{M}}_{\phi_N}} - 1 \right) \phi_{Ne} \cdot \alpha_N^{-1} \cdot \phi_{Ne} > 0 \quad (4.23)$$

when $||\phi_N|| > 2\hat{\mathcal{M}}_{\phi_N}$

$$\phi_{Ne}\alpha_N^{-1}f_N = \rho_N \eta_{\phi_N} \phi_{Ne} \alpha_N^{-1} \phi_{Ne} > \frac{\eta_{\phi_N}}{2} \phi_{Ne}^T \alpha_N^{-1} \rho_N \phi_{Ne} \quad (4.24)$$

and hence (4.20) is verified.

Proof of Theorem 4.3.1:

The proof of the theorem above is based on two steps, i.e., (i) recast the closed-loop system as a Filippov system and (ii) prove the existence of a positive definite function V that satisfies Theorem 4.2.1.

Closed-loop dynamics

By considering the plant in (4.11), the reference model in (4.12), the control action in (4.14), and the matching condition in (5.8) and performing some algebraic manipulations, the equations of the closed-loop dynamics can be expressed as

$$\dot{e} = A_m e + B_1 [\phi_e^T w - y_e w^T \Gamma_\beta w + \phi_{Ne} \operatorname{sgn}(y_e) - d] \quad (4.25a)$$

$$\dot{\phi}_e = -y_e \Gamma_\alpha w - f \quad (4.25b)$$

$$\dot{\phi}_{Ne} = -\alpha_N |y_e| + f_N \quad (4.25c)$$

$$\text{with } w^T = [x^T, r, e_I^T], \quad w \in \mathbb{R}^{2n+1}$$

and ϕ_e being the vector collecting the mis-matches between the plant parameters and the integral parts of the adaptive gains K_X , K_R , and K_I (see [143] for its mathematical definition), Γ_α and $\Gamma_\beta \in \mathbb{R}^{(2n+1) \times (2n+1)}$ are the positive matrices representing the adaptive weights for the integral part and the proportional part of K_X , K_R , and K_I respectively, and f is the σ -modification limiting the evolution of their integral part (see [143] for its mathematical definition). It is noteworthy that due to the discontinuities arising from the switching action of the controller, the vector field in (4.25) expressed as $\mathfrak{f} : \mathbb{R} \times \mathbb{R}^{3n+2} \rightarrow \mathbb{R}^{3n+2}$ is a piecewise-defined system. Thus, using the mathematical formulation in (4.1) and (4.2), the closed-loop system in (4.25) can be described by the differential inclusion

$$\dot{\tilde{x}} \in \mathbf{K}[\mathfrak{f}](\tilde{x}) \quad (4.26)$$

where $\mathbf{K}[\mathfrak{f}](\tilde{x})$ represents the Filippov set-valued map of the piecewise system and $\tilde{x}^T = [e^T, \phi_e^T, \phi_{Ne}]$.

Existence of Candidate Lyapunov Function

The candidate Lyapunov function is

$$V(\tilde{x}) = \tilde{x}^T \tilde{P} \tilde{x} \quad (4.27)$$

where $\tilde{P} = \operatorname{diag}(P, \Gamma_\alpha^{-1}, \alpha_N^{-1})$, with P being the solution of the Lyapunov equation in (4.16). It is noteworthy that (4.27) can be bounded as [143, 155]

$$W_1(\tilde{x}) \leq V(\tilde{x}) \leq W_2(\tilde{x}) \quad (4.28)$$

where $W_1(\tilde{x}) = \lambda_{\min}(\tilde{P}) \|\tilde{x}\|^2$ and $W_2(\tilde{x}) = \lambda_{\max}(\tilde{P}) \|\tilde{x}\|^2$. As V is a smooth function and by extension a regular function [149, 155, 156], $(d/dt)V(\tilde{x})$ exists and can be

Trajectory Tracking

computed as in (4.7). Therefore, by using (4.26) the derivative of (4.27) along the closed-loop trajectories (4.25) can be expressed as

$$\frac{d}{dt}V(\tilde{x}) \in^{\text{a.e}} \dot{V}(\tilde{x}) = \bigcap_{\varphi \in \partial V(\tilde{x})} \varphi^T \mathbf{K}[\mathbf{f}] (\tilde{x}) \quad (4.29)$$

According to [149], since $V(\tilde{x})$ is a smooth function

$$\dot{V}(\tilde{x}) = \nabla V^T \cdot \mathbf{K}[\mathbf{f}] (\tilde{x}) \quad (4.30)$$

$$\dot{V}(\tilde{x}) \subset 2 \begin{bmatrix} e \\ \phi_e \\ \phi_{Ne} \end{bmatrix}^T \tilde{P} \cdot \mathbf{K}[\mathbf{f}] (\tilde{x}) \quad (4.31)$$

The differential inclusion $\mathbf{K}[\mathbf{f}](\tilde{x})$ in (4.26) can be expanded as

$$\mathbf{K}[\mathbf{f}] = \mathbf{K} \begin{bmatrix} A_m e + B_1 [\phi_e^T w - y_e w^T \Gamma_\beta w + \phi_{Ne} \text{sgn}(y_e) - d] \\ -y_e \Gamma_\alpha w - f \\ -\alpha_N |y_e| - f_N \end{bmatrix} \quad (4.32a)$$

$$= \begin{bmatrix} A_m e + B_1 [\phi_e^T w - y_e w^T \Gamma_\beta w + \phi_{Ne} \mathbf{K}[\text{sgn}(y_e)] - d] \\ -y_e \Gamma_\alpha w - f \\ -\alpha_N |y_e| - f_N \end{bmatrix} \quad (4.32b)$$

After some algebraic manipulations, using the Lyapunov equation in (4.16) and the differential inclusion in (4.32), the right hand side of (4.31) is

$$\begin{aligned} \dot{V}(\tilde{x}) &= -e^T Q e - 2y_e^2 w^T \Gamma_\beta w + 2y_e \phi_{Ne} \mathbf{K}[\text{sgn}(y_e)] - \\ &\quad 2y_e d - 2\phi_e^T \Gamma_\alpha^{-1} f - 2\phi_{Ne} \alpha_N^{-1} f_N \end{aligned} \quad (4.33)$$

Note that $\mathbf{K}[\text{sgn}(y_e)]$ is a set-valued map that is computed as

$$\mathbf{K}[\text{sgn}(y_e)] = \begin{cases} -1 & , y_e < 0 \\ [-1, 1] & , y_e = 0 \\ 1 & , y_e > 0 \end{cases} \quad (4.34)$$

Thus, after further simplification (4.33) can be upper bounded as

$$\dot{V}(\tilde{x}) \leq -e^T Q e - 2y_e d - 2\phi_e^T \Gamma_\alpha^{-1} f - 2\phi_{Ne} \alpha_N^{-1} f_N \quad (4.35)$$

4.3 Control Formulation

It is noted that, to obtain (4.35), the term $2y_e\phi_{Ne}\mathbf{K}[\text{sgn}(y_e)]$ is cancelled by $-2\phi_{Ne}|y_e|$ when $y_e \neq 0$ and both terms are zero when $y_e = 0$. The first three terms on the right hand side of (4.35) have been considered in [143] and the equation above can be further manipulated as in the proof of Theorem 2 in [143] by using the same steps. Thus, $\dot{\tilde{V}}$ can be further upper-bounded as:

$$\dot{\tilde{V}}(\tilde{x}) \leq -\frac{3}{4}\lambda_{\min}(Q)||e||^2 + 4\frac{||B_1^T P||^2}{\lambda_{\min}(Q)}|d|^2 - 2\phi_e^T \Gamma_\alpha^{-1} f - 2\phi_{Ne} \alpha_N^{-1} f_N \quad (4.36)$$

By defining

$$\tilde{\Gamma}_\alpha^{-1} = \text{diag}(\Gamma_\alpha^{-1}, \alpha_N^{-1}) \quad (4.37a)$$

$$\tilde{f} = \begin{bmatrix} f \\ f_N \end{bmatrix} \quad (4.37b)$$

$$\tilde{\phi}_e = \begin{bmatrix} \phi_e \\ \phi_{Ne} \end{bmatrix} \quad (4.37c)$$

the expression in (4.36) becomes the following.

$$\dot{\tilde{V}}(\tilde{x}) \leq -\frac{3}{4}\lambda_{\min}(Q)||e||^2 + 4\frac{||B_1^T P||^2}{\lambda_{\min}(Q)}|d|^2 - 2\tilde{\phi}_e^T \tilde{\Gamma}_\alpha^{-1} \tilde{f} \quad (4.38)$$

It is noted that $\dot{\tilde{V}}$ is then upper-bounded as in the proof of Theorem 2 in [143], thus it can be further manipulated by using the same steps in [143], thus

$$\dot{\tilde{V}}(\tilde{x}) \leq -W_3(\tilde{x}), \text{ where } ||\tilde{x}|| \geq \mu \quad (4.39)$$

where $W_3(\tilde{x})$ is defined as

$$W_3(\tilde{x}) = \theta\alpha||\tilde{x}||^2, \text{ where } ||\tilde{x}|| \geq \mu; \alpha, \theta \in (0, 1) \quad (4.40a)$$

$$\mu = \sqrt{\frac{\mu_2}{\mu_1(1-\theta)}} \quad (4.40b)$$

$$\mu_1 = \frac{3}{4}\lambda_{\min}(Q) \quad (4.40c)$$

$$\mu_2 = 3\frac{||B_1^T P||^2}{\mu_1}\Delta_\infty^2 + \mu_1(2\hat{\mathcal{M}}_\phi + ||\phi^*|| + 2\hat{\mathcal{M}}_{\phi_N})^2 \quad (4.40d)$$

and $\hat{\mathcal{M}}_\phi$ and ϕ^* are the threshold and the ideal control gains defined in [143], respectively. Consequently, by considering (4.28) and (4.39), the closed-loop dynamics (4.25) satisfy all the conditions in Theorem 4.2.1. Thus, the closed-loop system is

ultimately bounded with the ultimate bound given below.

$$W_1^{-1}(W_2(\mu)) = \sqrt{\frac{\lambda_{\max}(\tilde{P})}{\lambda_{\min}(\tilde{P})}}\mu \quad (4.41)$$

4.4 Path Tracking

The primary objective of a path tracking controller is to accurately follow the reference path under a wide range of operating conditions. Path tracking for autonomous vehicles is a particularly challenging task as the dynamics of a vehicle change significantly with changes in longitudinal velocity, road surface, external disturbances such as wind, challenging manoeuvres etc. The initial generation of path tracking controllers were based on geometric controllers (e.g., Stanley, follow the carrot, etc.) and were shown to provide suitable performance under nominal conditions both in simulation and real world experiments. However, their performance suffers when the system deviates far from nominal conditions and thus prompted researchers to develop more advanced control algorithms (e.g., sliding mode control, robust control, adaptive control, MPC, etc.) that were suitable for the complex nature of the problem. In this section, the path-following system model is presented and the application of the control law in (4.14) to an autonomous vehicle's lateral control problem is discussed. In order to apply the control law in (4.14), the relevant vehicle and error states of the system need to be expressed in the format given in (4.11). To capture the relevant lateral and yaw dynamics of the autonomous vehicle, the single-track dynamic bicycle model of the vehicle is utilized, (see Figure 4.2). The vehicle's lateral velocity v_y and yaw rate r_z are used to get a representation of the vehicle's dynamics. Additional states that are augmented to this model are, (i) the lateral position error defined as the lateral distance error from the Centre of Gravity (C.G.) of the vehicle from the desired path η_e , measured perpendicularly to the vehicle's orientation and (ii) the heading angle error ψ_e , defined as the difference between the orientation of the vehicle and the desired yaw angle. The equations that describe the evolution of the four states have been described in [80, 152] and have also been used by researchers to develop their lateral-yaw tracking controller

for autonomous vehicles [152].

$$\begin{bmatrix} \dot{v}_y \\ \dot{r}_z \\ \dot{\eta}_e \\ \dot{\psi}_e \end{bmatrix} = \begin{bmatrix} \frac{C_f + C_r}{Mv_x} & \frac{l_f C_f + l_r C_r}{Mv_x} - Mv_x & 0 & 0 \\ \frac{l_f C_f - l_r C_r}{MI_z} & \frac{l_f^2 C_f + l_r^2 C_r}{v_x I_z} & 0 & 0 \\ -1 & 0 & 0 & v_x \\ 0 & -1 & 0 & 0 \end{bmatrix} \begin{bmatrix} v_y \\ r_z \\ \eta_e \\ \psi_e \end{bmatrix} + \begin{bmatrix} -\frac{C_f}{M} \\ -\frac{l_f C_f}{I_z} \\ 0 \\ 0 \end{bmatrix} \delta_f + \begin{bmatrix} 0 \\ 0 \\ 0 \\ v_x \end{bmatrix} \kappa \quad (4.42)$$

where $x_{\text{path}}^T = [v_y, r_z, \eta_e, \psi_e]$ are the states of the system, the front wheel steering angle $u = \delta_f$ is the actuated input, and the desired path curvature $r = \kappa$ is the un-actuated input to the system. The parameters C_f, C_r are the equivalent lateral-stiffness of the front and rear axle respectively, M is the mass of the vehicle, I_z is the moment of inertia of the vehicle along the vertical z -axis, and l_f, l_r are the distance of the front and rear axle from the centre of gravity of the vehicle. Moreover, by defining the system matrices as

$$A_{\text{path}} = \begin{bmatrix} \frac{C_f + C_r}{Mv_x} & \frac{l_f C_f + l_r C_r}{Mv_x} - Mv_x & 0 & 0 \\ \frac{l_f C_f - l_r C_r}{MI_z} & \frac{l_f^2 C_f + l_r^2 C_r}{v_x I_z} & 0 & 0 \\ -1 & 0 & 0 & v_x \\ 0 & -1 & 0 & 0 \end{bmatrix} \quad (4.43a)$$

$$B_{1,\text{path}}^T = \begin{bmatrix} -\frac{C_f}{M} & -\frac{l_f C_f}{I_z} & 0 & 0 \end{bmatrix} \quad (4.43b)$$

$$B_{2,\text{path}}^T = \begin{bmatrix} 0 & 0 & 0 & v_x \end{bmatrix} \quad (4.43c)$$

the system in (4.42) can be expressed in the compact form given below.

$$\dot{x} = Ax + B_1 u + B_2 \kappa \quad (4.44)$$

where $x = x_{\text{path}}$, $A = A_{\text{path}}$, $B_1 = B_{1,\text{path}}$, and $B_2 = B_{2,\text{path}}$. For normal road-going vehicle, the system matrix A in (4.44) has two poles in the negative half plane (stable lateral dynamics of understeered vehicle) and two poles on the origin (from the error states), resulting in an unstable system. It is noteworthy that the matrices

Trajectory Tracking

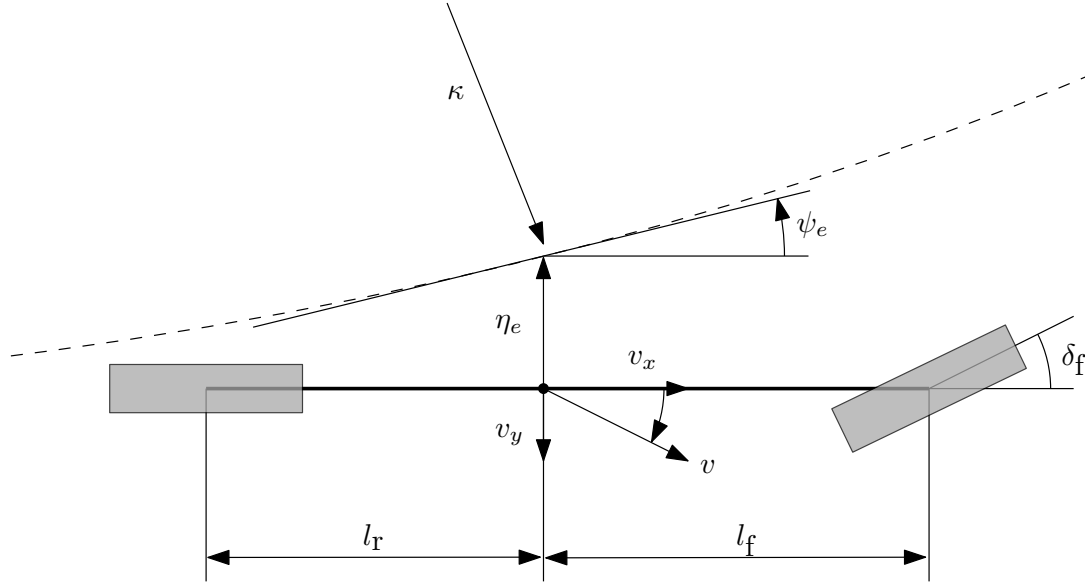


Figure 4.2 Overview of path-tracking model. Note: Reference path (black-dashed)

A and B_1 are dependent on the vehicle parameters (mass, weight distribution, moment of inertia, tire cornering stiffness, etc.) and generally nominal values of these parameters are used to create the system model. However, the entries of the matrices of the plant are not precisely known because of plant parameter uncertainties and variation of the longitudinal speed, thus opening the need of adaptive solutions. In general, a combination of feedback and feedforward control law is designed to obtain accurate path tracking of the autonomous vehicle. The feedback control is used to stabilise the system and achieve desired path-tracking performance. However, if the unactuated control input i.e., κ is very large (representing tight highway turns/curves), a feedback control can lead to large lateral position errors and thus, an appropriate feedforward controller is utilized to counter the road curvature input and theoretically achieve zero steady-state lateral position error. A typical control law implementation involves designing a control law of the form [152]:

$$u = K_{FB}(v_x)x + K_{FF}(v_x, \kappa)\kappa \quad (4.45)$$

The application of the control law from (4.45) for a given set of nominal vehicle parameters and a given longitudinal speed results in the following closed-loop dynamics of the system in (4.44)

$$\dot{x} = (A + B_1 K_{FB}^*)x + (B_1 K_{FF}^* + B_2)\kappa \quad (4.46)$$

where K_{FB}^* and K_{FF}^* represent the nominal feedback and feedforward controller based on default vehicle parameters. Successful implementation of the resultant closed-loop control scheme law in experimental tests have demonstrated their ability at tracking the curvature of tight highway corners under medium to high-speed driving ($70 - 120 \text{ km h}^{-1}$) scenarios. However, due to the controlled nature of the testing environments, it is yet to be seen how they cope with variations such as rapidly changing road friction, wind gusts, vehicle parameter variations, etc. which are possible scenarios an autonomous vehicle will face during its operation beyond controlled test environments. It is noteworthy, that from an occupant acceptance point of view, it will be advantageous to have a system that can provide uniformity in its behaviour despite changes in system parameters or external perturbation i.e., the vehicle should perform the same manoeuvre in a uniform manner under different internal and/or external perturbations. To this effect, the system dynamics are modelled as

$$\dot{x} = Ax + B_1u + B_2\kappa + B_1d \quad (4.47)$$

where $d \in \mathbb{R}$ is a bounded disturbance acting upon the system and contains the deviation between a nominal system model and the actual system due to modeling miss-match, parameter variation, external disturbances, degradation, etc. A control law that steers the dynamics of the system in (4.47) to the reference system in (4.46) where the system matrices in (4.12) are selected as $A_m = A + B_1K_{FB}^*$ and $B_m = B_1K_{FF}^* + B_2$, while fulfilling three requirements of: (i) ensuring lateral stability of system, (ii) providing accurate path tracking, and (iii) assuring that the cornering dynamics and lateral tracking performance of the vehicle remains consistent over the entire operating range can be a viable option for real world usage and user acceptance. Subsequently, an MRAC based control formulation presented in Section 4.3 can be a viable framework to achieve the three requirements mentioned above. Moreover, ensuring boundedness of all the adaptive gains using the σ -modification technique means that the inputs and states will not need to be artificially saturated like previous implementations of MRAC in autonomous vehicles [145–147]. Thus, the control law in (4.14)–(4.18) is designed for a system model in (4.47). The resultant controller is then implemented in a MATLAB-IPG CarMaker co-simulation (closed-loop) structure with the CarMaker environment providing the high-fidelity plant dynamics. In the following section, this implementation is explained in further detail and the efficacy of the proposed control law for steering control of an autonomous vehicle is shown using a number of simulation studies.

4.5 Numerical Validation

As mentioned in the section above, the ability of the control law in (4.14)-(4.18) to impose the desired vehicle path is tested in a MATLAB-IPG CarMaker co-simulation environment. The simplified system model in (4.42) is created using the nominal vehicle parameters obtained from the IPG vehicle model. A reference model of the form (4.46) is created in two steps namely: (i) the feedback controller is designed using the pole placement method by introducing two stable poles for the error states while keeping the stable poles of v_y, r_z intact, and (ii) computing a reference feedforward based on the equations from [80]. The MRAC is then designed using the techniques discussed in Section 4.3 and the resultant control law is connected in closed-loop with the high-fidelity vehicle and system model from IPG CarMaker. This results in a closed-loop structure as illustrated in Figure 4.1. It is noteworthy that the task of longitudinal control is assigned to the default Adaptive Cruise Controller (ACC) provided by the IPG CarMaker platform. The closed-loop simulation is performed for different manoeuvres to mimic typical driving conditions that an autonomous vehicle might encounter in a highway environment. These simulations are designed to numerically evaluate the performance of the proposed controller when it encounters a combination of typical issues such as: (i) modelling errors, (ii) disturbances, (iii) rapidly changing disturbances, etc. The design parameters used for the simulation platform are provided in Tables A.1 and A.3.

Remarks

- The presence of the discontinuous switching action in (4.14) can introduce chattering action (high-frequency switching of the control action). To mitigate this undesirable behaviour, the discontinuous control action u_N is smoothed as [139]

$$u_N(t) = K_N(t) \frac{y_e(t)}{|y_e(t)| + \epsilon} \quad (4.48)$$

where ϵ is a sufficiently small positive constant that can be chosen appropriately

- $\hat{\mathcal{M}}_\phi$ and $\hat{\mathcal{M}}_{\phi_N}$ are positive constants that are chosen to achieve a suitable compromise between tracking performance and controller aggressiveness when the norms of the control action $\|\phi\|$ and $\|\phi_N\|$ are within the locking region that activates the σ -modification

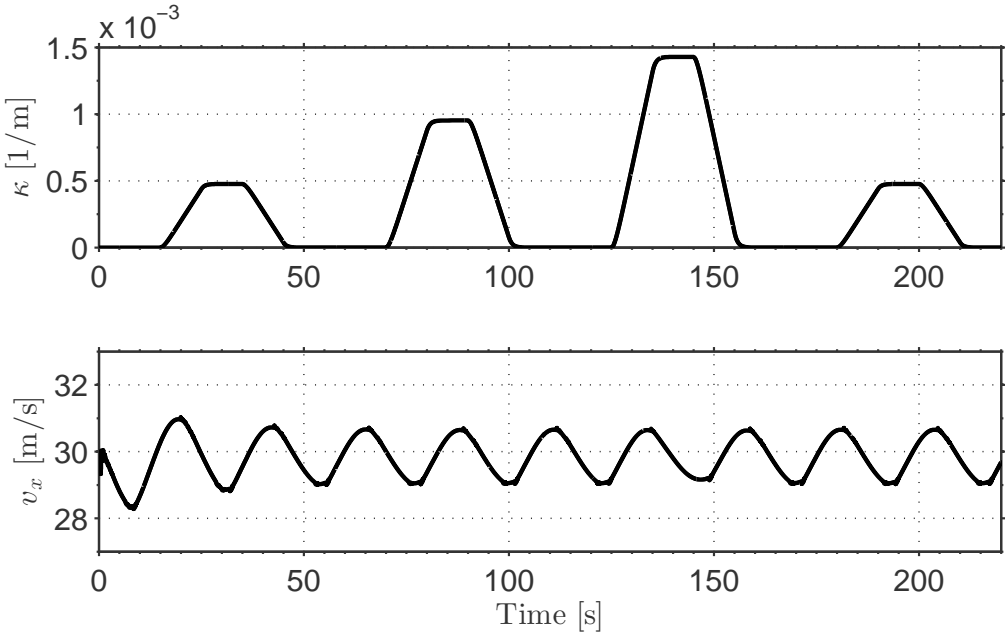


Figure 4.3 Reference road curvature and longitudinal velocity for hypothetical highway driving scenario (Manoeuvre I)

4.5.1 Manoeuvre I: Navigating a hypothetical highway section

In this section, the controller's ability to track a reference vehicle model over a large highway road segment while ensuring boundedness of control inputs is demonstrated. The hypothetical highway segment consists of straight driving sections interspersed with four corners of different radii, see Figure 4.3 (top). The tightest of these corners corresponds to a curve of radius which is approximately equal to the tightest corner allowed on highways [152]. During the simulation the proposed tracking controller will control the steering of the vehicle to track the road curvature whereas as mentioned above, the standard ACC from IPG will be used to maintain the desired vehicle velocity (i.e., 107 km h^{-1}). On performing the simulation, it was observed that the ACC is unable to keep very tight control over the longitudinal velocity of the vehicle and as a result the longitudinal velocity of the vehicle is not maintained constant during the entirety of the manoeuvre, Figure 4.3 (bottom). Furthermore, the manoeuvre is also simulated without locking the evolution (preventing unbounded evolution) of the adaptive gain of the switching control action (referred henceforth as ctrl0). Thus, this simulation test can be used to gain insight on three important aspects namely: (i) behaviour of closed-loop system, (ii) evolution of adaptive control gains, and (iii) ability of controller to counter variations in parameters of system/plant. The evolution of the adaptive gains K_X , K_R , and K_I when the adaptive switching action is bounded using σ -modification over the entire

Trajectory Tracking

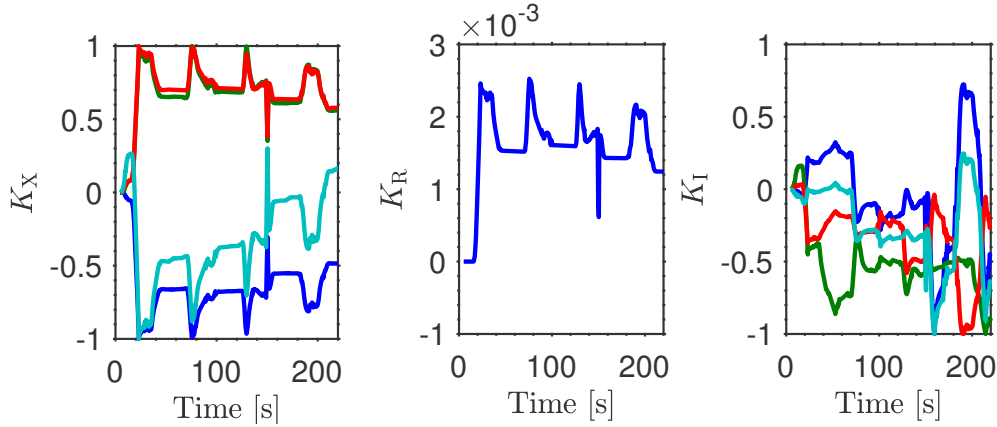


Figure 4.4 Evolution of K_X , K_R , and K_I for hypothetical highway driving scenario (Manoeuvre I)

simulation can be observed in Figure 4.4 which confirm their bounded evolution. Figure 4.5 depicts the evolution of $\|\phi_N\|$ and the evolution of the magnitude of the integral part of the gains K_X , K_R , and K_I denoted as $\|\phi\|$. As shown in the top plot of Figure 4.5, the evolution of $\|\phi\|$ does not remarkably change when the σ -modification strategy for $\|\phi_N\|$ is activated. However, the evolution of $\|\phi_N\|$ in bottom plot of Figure 4.5 clearly exhibits one of the main contributions of this chapter. When there is no locking strategy the control gain for the switching action is unbounded and keeps on increasing. On the other hand, preventing the unbounded evolution of $\|\phi_N\|$ using a σ -modification strategy is also illustrated.

The closed-loop dynamics of the system and the evolution of the system states are presented in Figure 4.6. According to the plots, the closed-loop performance obtained with and without bounding the $\|\phi_N\|$ are very similar if not identical. Both, the states representing vehicle lateral-yaw dynamics (i.e., v_y and r_z) and the error states (i.e., η_e and ψ_e) closely match the reference closed-loop dynamics during the entire manoeuvre. However, close inspection (of especially v_y and r_z) towards the end of the simulation shows that the behaviour of the two controllers seems to be diverging. Further insight on this behaviour can be gained by observing the evolution of the state error (4.15) is plotted in Figure 4.7. The absolute magnitude of the error helps in confirming that both controllers achieve accurate tracking of the reference model. However, while negotiating the final curve of the manoeuvre which is identical to the first curve, the performance of the controller with unbounded evolution of $\|\phi_N\|$ visibly deteriorates. Moreover, due to the time-scale of the plot it appears as if the discontinuous (switching) action present in both controller is leading to oscillatory behaviour in the system. However, this is not entire the case and the plot insets show that the error for the first two states (and by extension the states v_y and r_z) for

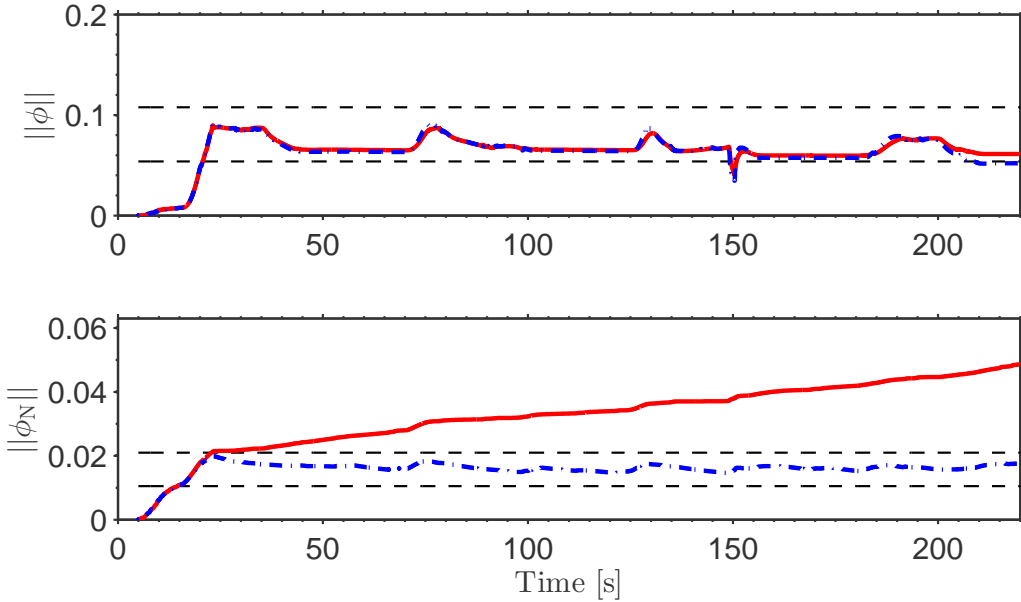


Figure 4.5 Evolution of $\|\phi\|$ and $\|\phi_N\|$ for hypothetical highway driving scenario (Manoeuvre I). **Note:** Unbounded switching action (Red), gain of the switching action bounded by σ -modification (Blue-dashed)

ctrl0 have oscillatory behaviour akin to chattering whose amplitude and frequency appears to be increasing with time. This oscillatory behaviour in the lateral-yaw dynamics of the system has a negative impact not only on the stability of the system but also on the comfort of the occupants. On the contrary, when evolution of $\|\phi_N\|$ is bounded controller exhibits no such degradation and there is no introduction of chattering like behaviour in the state or error dynamics. Since, both controllers have very similar evolution of $\|\phi\|$, the consistency in the performance of the proposed controller (Figures 4.6 and 4.7) and its advantages can be traced to the successful implementation of a locking strategy for $\|\phi_N\|$ (see both plots in Figure 4.5).

The applied control action with and without bounding the gain $\|\phi_N\|$ is shown in Figure 4.8. While the general control action applied by both the controllers is very similar, the larger spikes that get introduced in the control action for ctrl0 after 50 s are easily observable. As seen from the plots above, this more aggressive control action does not bring any tangible benefits to the closed-loop performance and after approximately 150 s this aggressive control action damages the closed-loop performance giving rise to high-frequency oscillations. Furthermore, the plot inset in Figure 4.8 illustrates that while the proposed controller does not suffer from any chattering like problem, the same cannot be said for ctrl0. Interestingly, the deviation in the control action of the two controllers can be traced back to the time when the

Trajectory Tracking

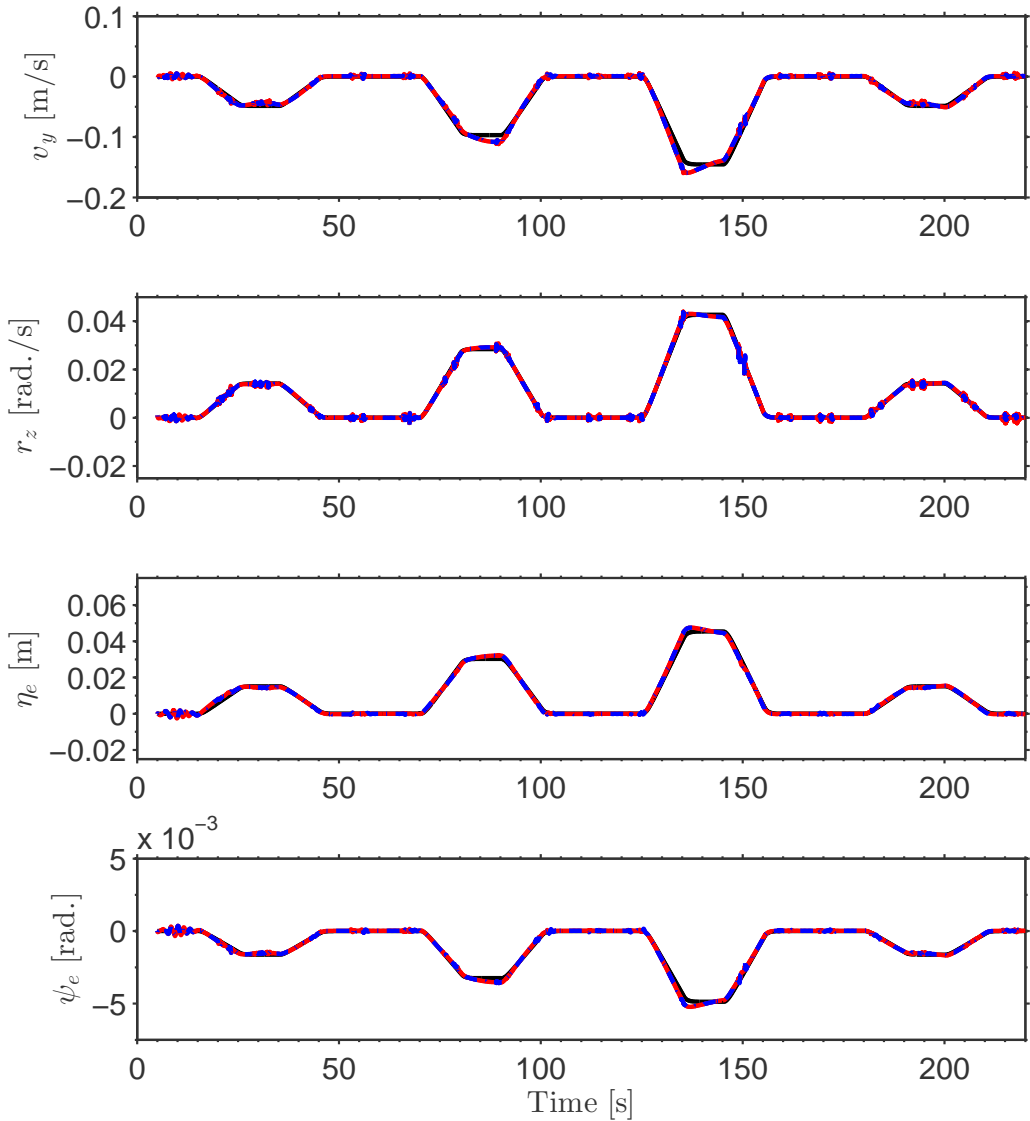


Figure 4.6 Dynamics of system for hypothetical highway driving scenario (Manoeuvre I). **Note:** Unbounded switching action (Red), gain of the switching action bounded by σ -modification (Blue dashed), reference model (solid black)

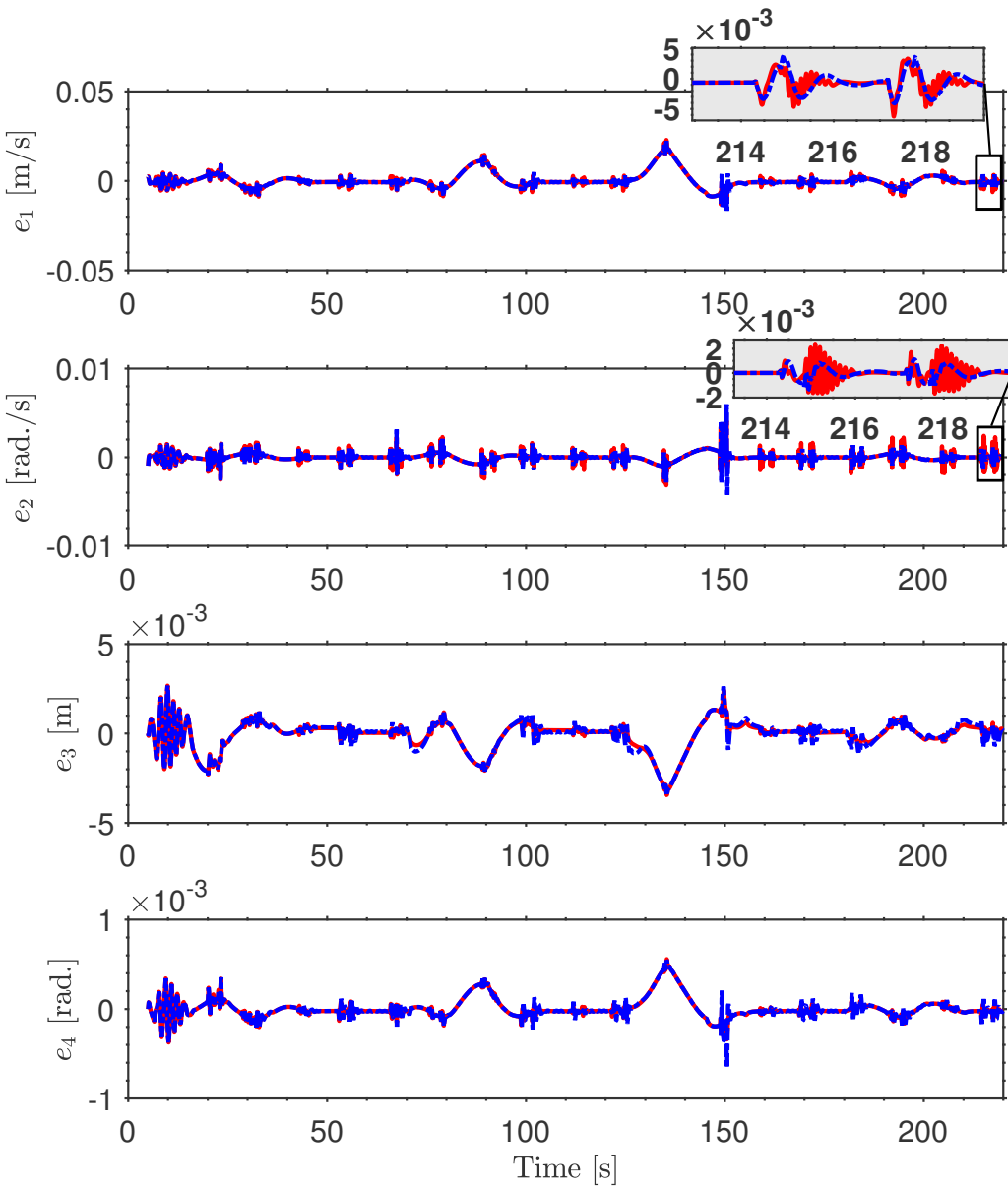


Figure 4.7 Evolution of state errors for hypothetical highway driving scenario (Manoeuvre I). **Note:** Unbounded switching action (Red), gain of the switching action bounded by σ -modification (Blue-dashed), reference model (Solid black)

Trajectory Tracking

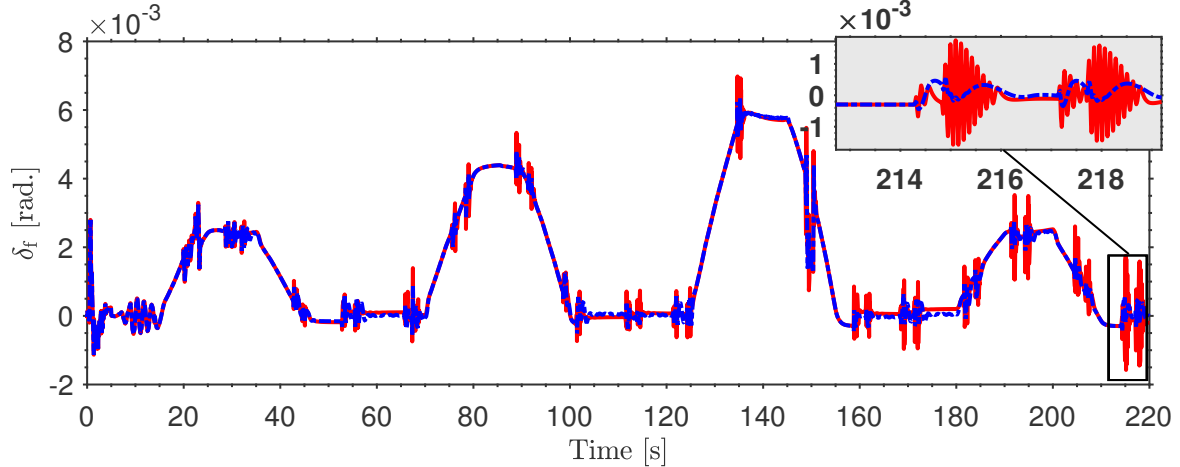


Figure 4.8 Net control action for hypothetical highway driving scenario (Manoeuvre I). **Note:** Unbounded switching action (Red), gain of the switching action bounded by σ -modification (Blue-dashed)

$||\phi_N||$ uncontrollably increased beyond the bounds around 50 s as clearly seen in Figure 4.5. Thus, successfully utilising the σ -modification strategy to lock the gain of the switching action of the control law allows the resultant closed-loop system to maintain its performance even with un-modelled non-linearities of the plant.

4.5.2 Manoeuvre II: Driving in crosswind

A common source of disturbance while traveling on highways is crosswinds. Crosswinds that are blowing across the vehicle's path are especially dangerous if not actively countered as they tend to veer a vehicle off its intended path/lane and can lead to extremely dangerous consequences (e.g., roll over, collisions with other vehicles, leaving built road, etc.). Moreover, the location and magnitude of crosswinds is difficult to measure/estimate and thus successfully rejecting their effects forms an important challenge for any trajectory tracking controller. In this section, the controller's capability to reject sudden large gust of crosswind is assessed. The scenario is as explained: the autonomous vehicle is driving on a straight road while maintaining the desired velocity (i.e., 107 km h^{-1}) and at about 3.45 s the vehicle encounters crosswind blowing at 110 km h^{-1} perpendicular to the path of the vehicle for a duration of 3.55 s. The scenario explained above is simulated twice. Once with no active steering control and the second time with the proposed controller. The main results of the simulation test are as follows.

The system dynamics of the vehicle are presented in Figure 4.9 where both, the uncontrolled vehicle and the vehicle controlled with the proposed controller are

shown. It is noteworthy that the dynamics of the reference model are not plotted here for the clarity and readability of plots but the reader is reminded that since the vehicle is assumed to be travelling on a straight piece of road, the reference states are constant (i.e., $x_m^T = [0, 0, 0, 0]$). Moreover, the duration of the simulation when the vehicle is subjected to the crosswind is marked with the yellow rectangle. The third and the fourth plot in Figure 4.9 show that the uncontrolled vehicle gets blown off the road as soon as it encounters the wind gust thus re-emphasising the need for closed-loop control techniques in autonomous vehicles to actively counter such environmental disturbances. On the other hand, on encountering the wind gust, the vehicle with active control recovers quickly to regulate the lateral velocity v_y , and yaw-rate r_z of the vehicle. This limits the increase in the lateral error η_e and heading angle error ψ_e which means that the vehicle follows the reference states (and by extension reference path/lane) as accurately as possible. A zoomed in plot of the evolution of the lateral error state is shown in the third plot of Figure 4.9. The plot demonstrates that while there is a peak deviation of approximately $|\eta_{e,\max}| \approx 0.05$ m due to crosswind, the controller is able to prevent its further rise. Furthermore, the magnitude of the error is very small compared to a typical lane width (i.e., 3.5 m) which means that no safety violations occur and the entire vehicle safely remains within its lane limits.

In general, the switching action of the controller is added to continuous control action to reject the effect of such large and sudden external disturbances. The evolution of the switching action gain is shown in top plot of Figure 4.10. The plot shows that the switching gain increases rapidly on the onset of the disturbance but the σ -modification technique helps in limiting its unbounded rise for the remaining manoeuvre. The control action that is applied is illustrated in the bottom plot of Figure 4.10. The advantage of having a switching action within the control law assists the initial phase of large actuation as soon as the wind gust is encountered. Furthermore, the locking strategy ensures that the switching action does not become dominant.

4.5.3 Manoeuvre III: Lane change in low friction conditions with additional passengers

In this section, the closed-loop performance of the system when there is a large mismatch between the reference model and the actual plant is evaluated. This scenario is created by: (i) changing the friction coefficient of road from its nominal value ($\mu_{\text{road,ref}} = 0.8$) to a hypothetical road covered with snow/ice ($\mu_{\text{road}} = 0.4$) and (ii) two additional passengers weighing 75 kg are added on the rear-seat of the vehicle. This has the combined effect of changing the plant parameters (e.g.,

Trajectory Tracking

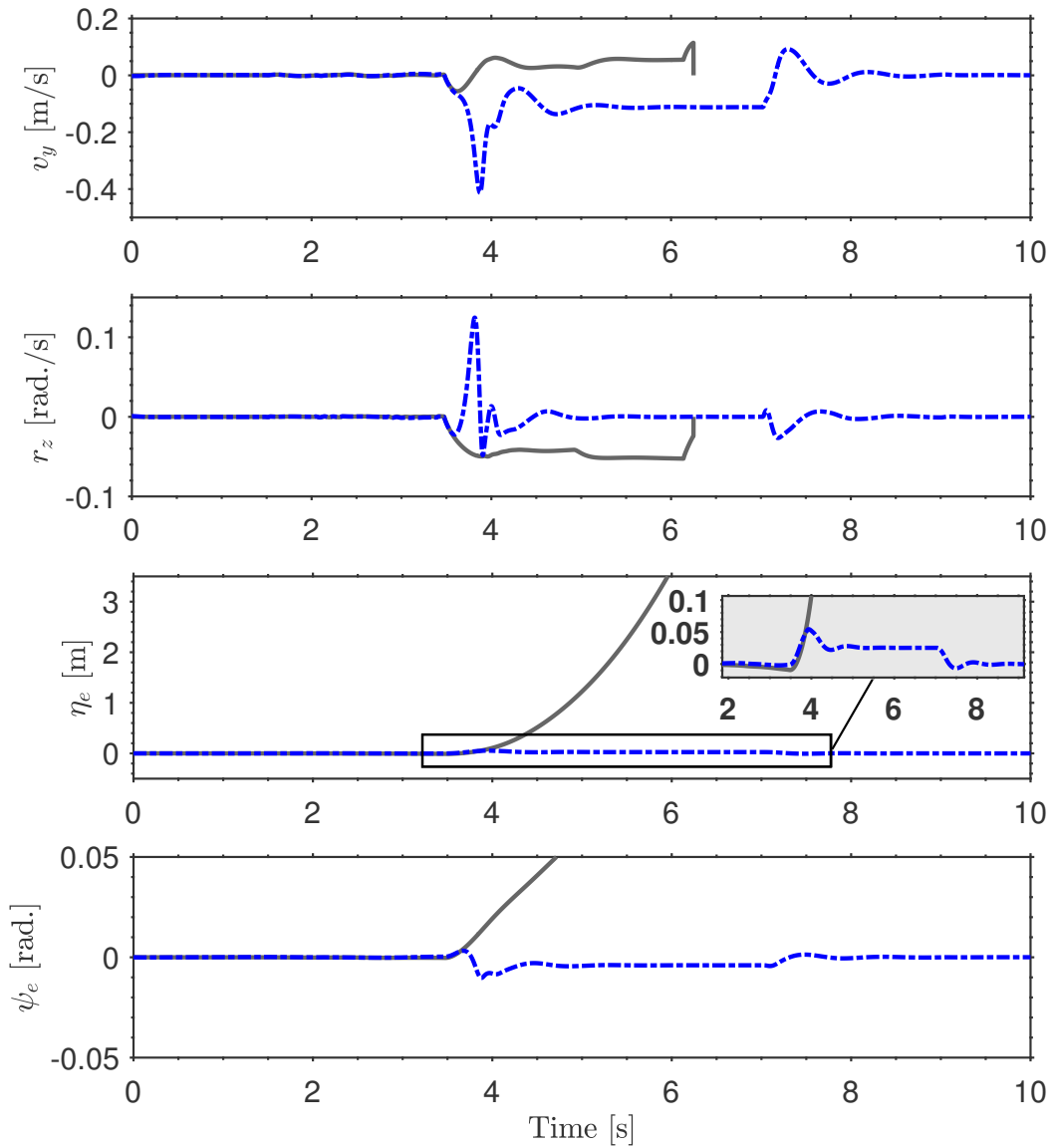


Figure 4.9 Dynamics of system for driving in crosswinds (Manoeuvre II). **Note:** Uncontrolled (Grey), Switching action bounded by σ -modification (Blue-dashed)

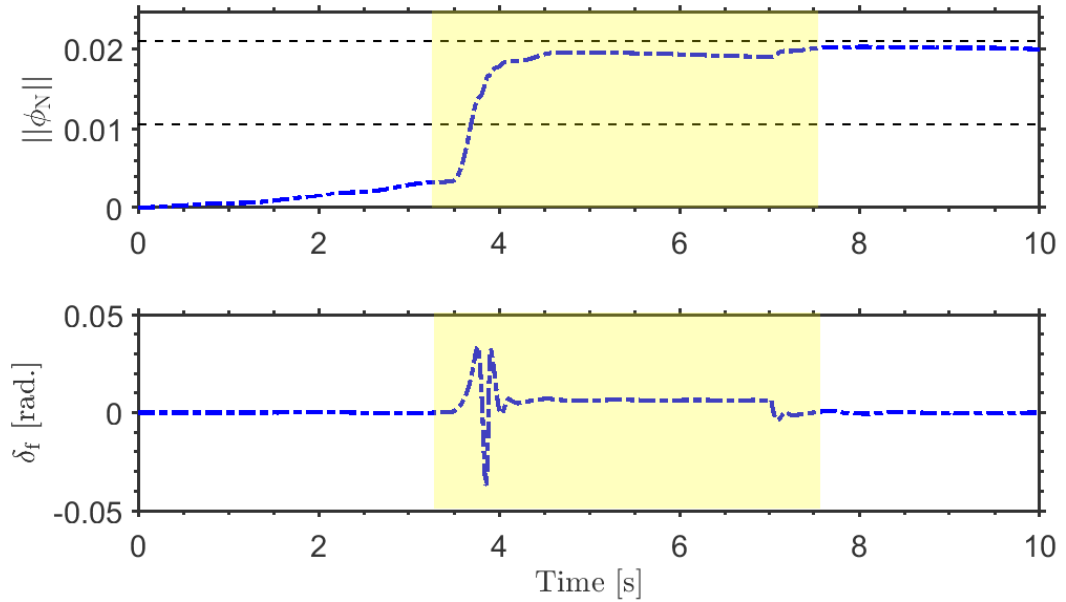


Figure 4.10 Evolution of $\|\phi_N\|$ and control input for driving in crosswinds (Manoeuvre II)

$M, I_z, C_f, C_r, l_f, l_r$) such that the dynamics of the plant are different from the nominal model used for control design. This closed-loop system is then simulated on the given icy road segment and the vehicle is subjected to three lane-change manoeuvres (see Figure 4.11) and the ability of the trajectory tracking controller to counter this large model miss-match while performing these manoeuvres is investigated. It is noteworthy that such deviations of the actual system from nominal plant dynamics are very common for autonomous vehicles as they are operated in a diverse range of conditions all across the parameter range. Thus, it is important for a tracking controller to be truly roadworthy, it needs to ensure uniform closed-loop dynamics for the vehicle across such diverse conditions.

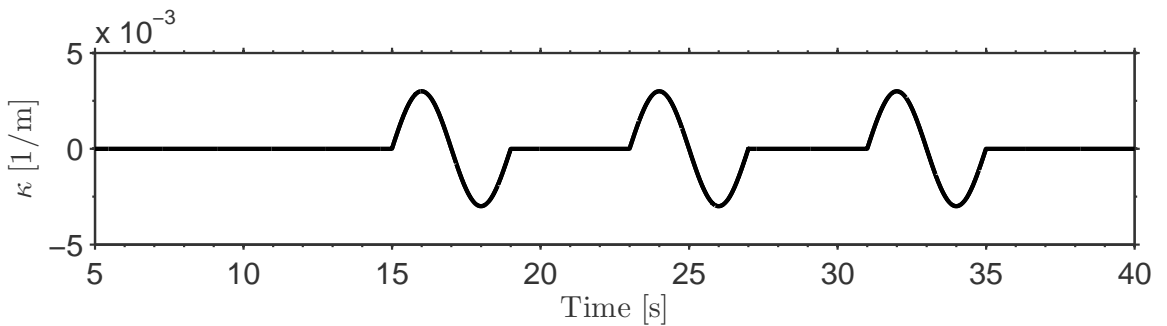


Figure 4.11 Reference road curvature for lane changes in low friction (Manoeuvre III)

Trajectory Tracking

The closed-loop dynamics of the system is presented in Figure 4.12 and the corresponding error dynamics are shown in Figure 4.13. The closed-loop dynamics of the system under the same manoeuvre but with the plant also under nominal conditions is also plotted to gain better insight on the controller's behaviour. The first two plots in Figure 4.12 demonstrate that the initial vehicle response when subjected to the first lane change differs in amplitude from the nominal vehicle (and the reference vehicle). The direct consequence of this is greater deviation from the reference path as observed from the error states in the bottom two plots of Figure 4.12. However, safety of the manoeuvre is never compromised since the controller adapts to the model miss-match and pushes the system dynamics towards the reference (and nominal) system dynamics. By the time the vehicle is subjected to the third lane-change manoeuvre, the closed-loop system appears to have adapted and the trajectories of all the states almost converge with the reference (and nominal) model. Some of these insights can also be obtained by observing the error plots in Figure 4.13. These plots illustrate how the magnitude of error gets smaller with each subsequent lane change manoeuvre thus showing that the controller adapts to the changes quickly and helps in ensuring that the system maintains its fundamental closed-loop behaviour even when subjected to large variations in plant parameters.

The evolution of the switching action is presented in the top plot of Figure 4.14. The differences in the initial evolution of the gain up to 15 s are clearly visible. However, in the locking region of the controller, the evolution of $\|\phi_N\|$ is very similar and the σ -modification strategy is able to successfully ensure that the locking policy works effectively. The net control action applied by the controller is shown in the bottom plot of Figure 4.14. It is worth noting that the controller gains are reset (i.e., $\|\phi\| = 0$ and $\phi_N = 0$) at the start of the simulation. Consequently, there is an initial transient in the control action (i.e., at 15 s) which is largely due to the activation of the control action but the oscillation quickly attenuates as the controller adapts to the environmental conditions. As a result, the subsequent control action for the remaining portion of the simulation is smooth without any high-frequency content which highlights the benefits of preventing unbounded increase in the gain of switching control action. This test highlights that the control law can quickly adapt to distinct environmental disturbances and uncertainties even when it has no prior chance to adapt to the situation and ensure the closed-loop performance. In a real world scenario it is more likely that the controller gains will not be reset and hence such oscillation due to rapid build-up of controller gains is not very likely.

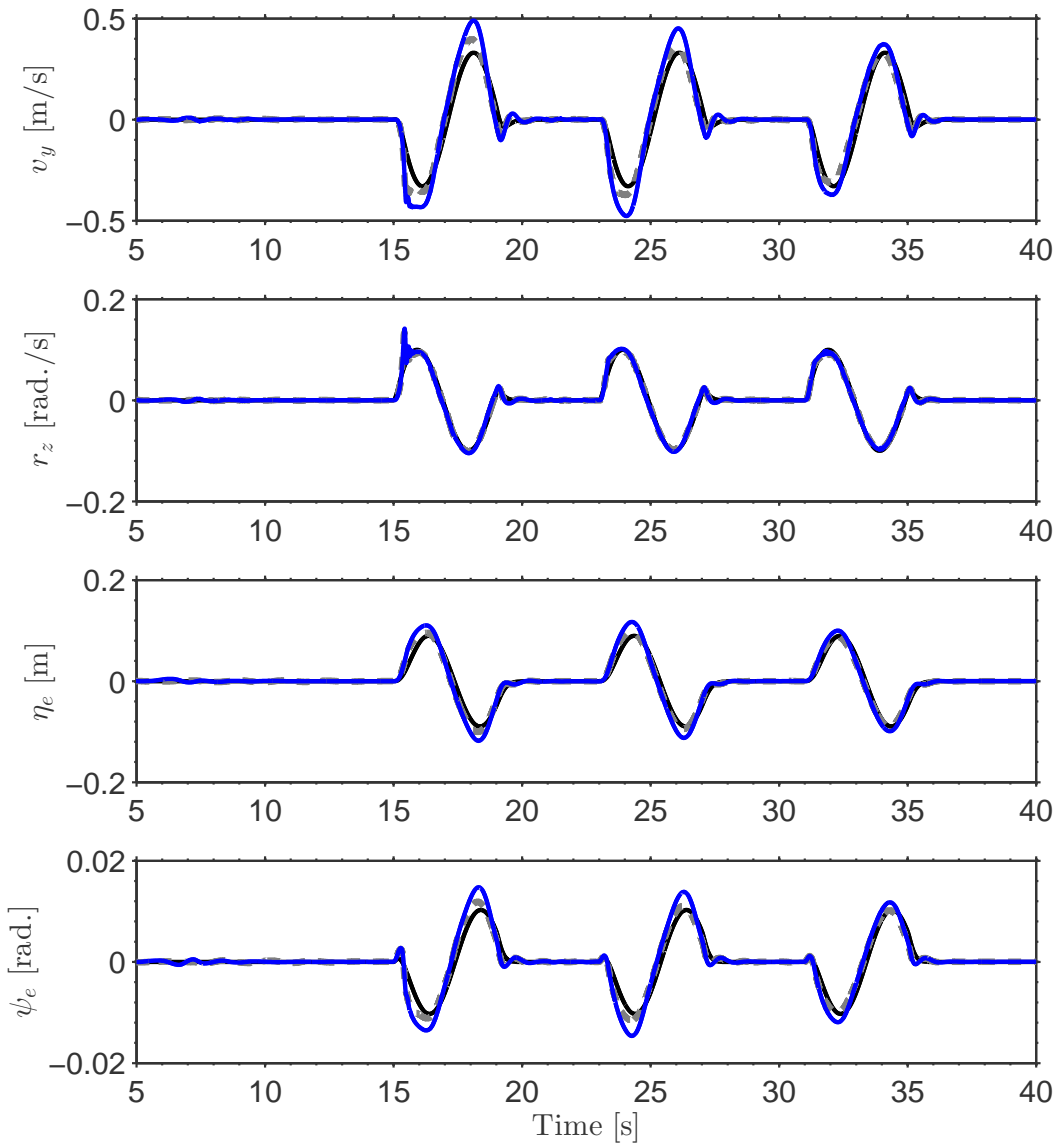


Figure 4.12 Dynamics of system for lane changes in low friction (Manoeuvre III).
Note: Nominal conditions (Grey-dashed), low-friction and extra passengers (Blue)

Trajectory Tracking

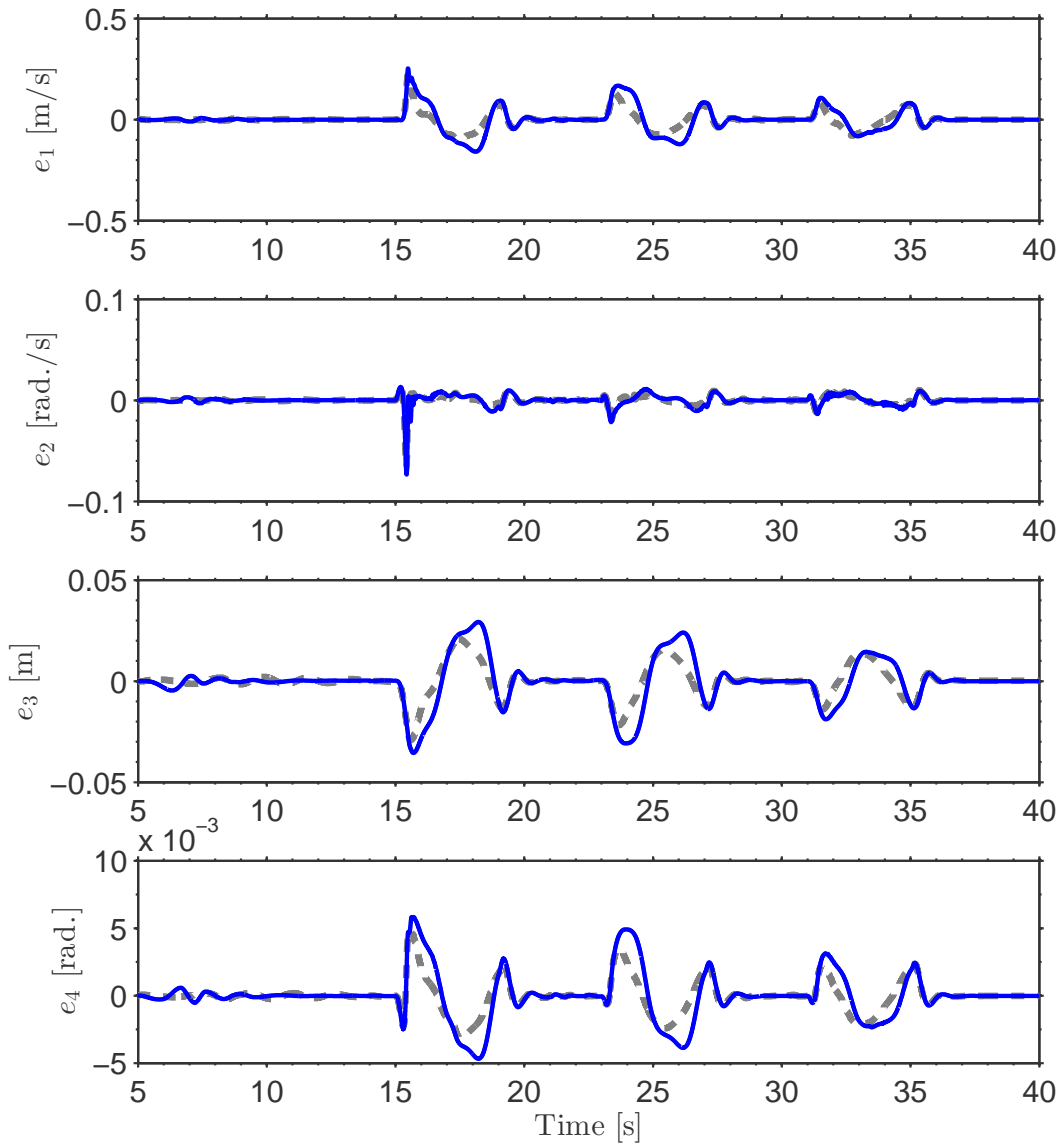


Figure 4.13 Evolution of state errors for lane changes in low friction (Manoeuvre III).
Note: Nominal conditions (Grey-dashed), low-friction and extra passengers (Blue)

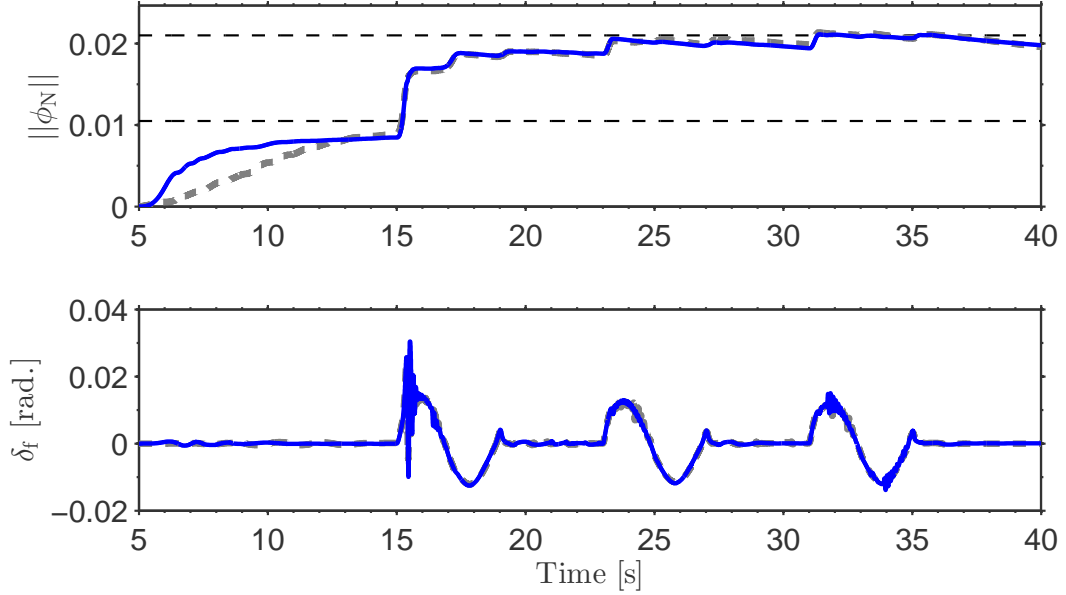


Figure 4.14 Evolution of $\|\phi_N\|$ and control input for lane changes in low friction (Manoeuvre III). **Note:** Nominal conditions (Grey-dashed), low-friction and extra passengers (Blue)

4.6 Summary

Lateral tracking of an autonomous vehicle for following a given reference path is a challenging task due to inherent aspects of the system such as external disturbances, system nonlinearities, rapidly changing dynamics, etc. arising due to tire dynamics, wind gusts, road surface changes, modelling miss-matches, etc. In this chapter, a generic lateral tracking controller has been designed using an Enhanced Model Reference Adaptive Control (EMRAC) strategy due to its ability to maintain closed-loop performance even for systems that are affected by the phenomenon mentioned above. Furthermore, a systematic technique of binding the gain of the switching control action of the EMRAC controller using σ -modification strategy has been presented. The ultimate boundedness of the resulting closed-loop system is proven using an extended Lyapunov theory for discontinuous systems. The effectiveness of the EMRAC control framework with bounded adaptive gains is numerically evaluated by designing a lateral controller for a vehicle and investigating the closed-loop performance under different scenarios in an IPG CarMaker-Simulink co-simulation environment. The evaluation performed over three representative examples showed that the proposed controller can achieve effective closed-loop performance even when the system is subjected to large external disturbances, modelling errors, etc.

Trajectory Tracking

while ensuring bounded evolution of adaptive control gain of the switching control action thus providing numeric validation of the proposed method to confine its dynamics.

Chapter 5

Combined Motion Planning & Control

अल्पानामपि वस्तुनां संहतिः कार्यसाधिका तृणैर्गुणत्वमापन्नैर् वध्यन्ते मत्तदन्तिनः ॥ २०१ ॥

— संस्कृत सुभाषित

Even insignificant things, when put together, can do great work. A rope made up of hay sticks can control a powerful elephant. Unity is power.

— *Samskṛta Subhāṣita 201*

In this chapter, a hierarchical trajectory planning and trajectory tracking structure to realise a combined motion control architecture for performing autonomous high-speed overtaking is developed. This control architecture is developed in three steps by building on the previous work where the development of the trajectory planner and the lateral tracking controller was performed in isolation. First, the EMRAC lateral tracking controller is augmented with steering actuator dynamics which are approximated using Padé approximations. Secondly, this updated steering controller is coupled with a basic geometry based local path planner and the successful implementation of the hierarchical control structure is demonstrated using simulation results of driving around a test-track in an IPG CarMaker/MATLAB co-simulation environment. Moreover, the robustness of the proposed controller to variations in steering actuator system's dynamics is also numerically shown. Finally, this updated lateral tracking controller is combined with the more sophisticated RMPC based trajectory planner to develop the hierarchical motion control architecture for autonomous high-speed overtaking. The effectiveness of this proposed framework for performing manoeuvres and its robustness to constant and sudden environmental disturbances is illustrated using simulation studies in a high fidelity IPG CarMaker/MATLAB co-simulation environment.

5.1 Introduction

COMPLETE end-to-end autonomy of a vehicle in real world driving scenarios has been an elusive goal that engineers and researchers all over the world are chasing since the past four decades. Worldwide competitions such as DARPA Urban Challenge and DARPA Grand Challenge have been very successful at achieving significant strides at autonomous driving but at the same

time also helped in identifying the remaining challenges that need to be tackled before delivering a completely roadworthy fully autonomous vehicle [124, 157, 158]. Additionally, away from the DARPA-like competitions, collaborations between research groups and automotive manufacturers have also provided crucial solutions and insights to challenges faced in achieving real world autonomy [31, 159].

Safe and feasible trajectory planning and accurate trajectory tracking for vehicle motion control form two very important links in this endeavour of developing fully autonomous intelligent vehicles. Furthermore, in addition to the stand-alone performance characteristics of a planning controller or a tracking controller, it is also important that their performance does not deteriorate when they are integrated within the overall self-driving architecture of an autonomous vehicle. The variety of approaches taken by researchers and engineers for trajectory planning and trajectory tracking have been discussed in detail in Chapter 2. Trajectory planning and trajectory tracking functionalities are usually slotted in a hierarchical or cascaded scheme within the overall self-driving architecture, see Figure 2.3. However, often while discussing the performance of a trajectory planner it is assumed that the vehicle tracks the planned trajectory perfectly and similarly while discussing trajectory tracking a offline generated trajectory is utilised with the assumption that replanning is not necessary. Contrarily, what is also important is to obtain a synergy when coupling two or more of such systems together within the overall autonomous driving architecture of the vehicle [119, 160]. As a result, recently there have been many more studies that discuss the aspects related to coupling of trajectory planning and trajectory tracking controllers and their resultant characteristics at performing various autonomous driving manoeuvres.

Although there are plenty of stand-alone techniques in literature for motion planning and motion tracking, there is not an abundance of literature on methods and frameworks that provide insight on the overall system performance when motion planning and motion tracking systems are coupled within an autonomous driving framework. In [161], a two layer control architecture consisting of a path planning level and a path following level is proposed where the authors designed two different MPC controllers for performing each task. The higher level controller (path planner) uses a point mass model of the vehicle in combination with a potential field function of the obstacle within its optimisation routine to compute a collision free path. The collision free path (as ξ_{ref} , η_{ref} , v_{ref}) functions as the reference to the lower level controller (path follower) which uses a more accurate bicycle model of the vehicle to track the given reference and compute actuator level signals (a_x , δ_f) for the vehicle. The proposed control architecture is then applied on a closed-loop simulation environment and the results demonstrate its ability to successfully avoid static and moving obstacles in a dynamic environment. Similarly, a hierarchical MPC

framework called Guidance and Navigation Control System (GNC) for autonomous vehicles is presented in [133]. The upper level controller trajectory replanning is designed to generate feasible trajectories to track given road coordinates and reference longitudinal velocity and uses a point mass vehicle model within a nonlinear MPC framework. The optimal trajectory generated by the upper level controller is then converted to desired heading angle ψ_{des} and lateral position η_{ref} which act as reference signals for the lower level Active Front Steering (AFS) controller designed by means of a LTV MPC with a dynamic bicycle model of the vehicle. The authors validated the proposed control architecture by simulating obstacle avoidance manoeuvres in low friction driving conditions. Moreover, the performance of the proposed GNC architecture was compared with the control scheme without the path replanning MPC discussed above (i.e., only AFS controller). The comparison showed that the presence of a high-level path replanner that accounts for a vehicle's stability limits allowed for significant reduction in the complexity of the low level controller by means of (i) lower prediction horizon and (ii) relaxed constraints for tire side-slip angles thus providing an example of how a hierarchical control scheme can be utilised to relax design constraints for different controller without sacrificing closed-loop performance and vehicle stability. Likewise, a two-level MPC for obstacle avoidance is proposed in [55] where a low fidelity spatial bicycle model is used for the upper-level control and a higher fidelity four-wheel vehicle model for the low level control. The interface between the two control layers is designed similar to [133] with the addition being that the authors in [55] validated their scheme on an experimental setup in snowy/slippery conditions and was shown to be successful at avoiding multiple obstacles at high-speeds. The two-level control scheme using MPC for each level is also utilised by the authors in [162] to design a system for emergency collision avoidance in autonomous vehicles. The work differs from the others discussed above primarily as (i) an artificial potential field function for avoiding obstacles is added within the path planning cost function and (ii) the lower level controller design is based on a vehicle with four independently actuated wheels. The authors demonstrate the ability of the proposed control architecture for avoiding obstacles in different emergency situations in a simulation environment. With its ability to handle system constraints and dynamics in a structured framework, MPC is a popular candidate among researchers to develop path planning controllers but there are also other approaches available in literature. The authors in [163] propose a hierarchical architecture consisting of optimal control for reference generation and PID control based path-following for collision avoidance and performing evasive manoeuvres. The reference path of the vehicle is approximated by a fifth-order polynomial and the optimal control technique is used to compute appropriate weights for this fifth order polynomial to avoid obstacles while keeping

Combined Motion Planning & Control

the vehicle within limits of stability. The safe reference path generated by the optimal controller is then converted to desired yaw-rate $r_{z,des}$ and desired lateral velocity $v_{y,des}$ for the tracking controller. The tracking controller is a PID controller with gains scheduled based on vehicle velocity. Additionally, a feedforward action based on steady-state cornering is also used to improve tracking accuracy. Furthermore, the desired steering angle angle $\delta_{f,des}$ is then converted to an appropriate steering-wheel torque τ_{sw} to be requested from the electronic power steering system. The authors validated the proposed cascaded control scheme on an experimental setup for different rear end collision avoidance scenarios thus demonstrating that two different control techniques can be coupled without any loss in individual performance. Likewise, the authors in [57] also proposed a cascaded control architecture that coupled a planning and a tracking controller designed using different methods. The path planner consists of an optimal control framework that replans a vehicle's path parametrised as a 6th-order polynomial subjected to stability and collision avoidance constraints. This path (ξ_{des}, η_{des}) is then tracked using a nonlinear MPC strategy which utilises an eight degree of freedom (dof) model which models the lateral, yaw, and roll dynamics of the vehicle and computes appropriate steering action as well as wheel torque distribution for the vehicle's actuators. The efficacy of the proposed control architecture at safely navigating past static and moving obstacles in medium speed driving is demonstrated in a simulation environment with a high-fidelity vehicle model simulating the plant dynamics. An integrated scheme for local trajectory replanning and control for static obstacle avoidance is proposed in [164]. The authors present motion planning and control hierarchical scheme that can fit within an autonomous diving architecture. The local motion planning is performed using an MPC framework with obstacle and path constraints for generating feasible and collision-free trajectories for the vehicle. This desired path is then converted into a desired path curvature κ_{des} that is provided to a model based controller to compute appropriate steering angle $\delta_{f,des}$ for the vehicle actuators such that the vehicle accurately follows the desired path curvature. The proposed control architecture is validated in a simulation environment where it is shown to successfully re-plan local trajectories for avoiding obstacles on curved roads and accurately track them in medium and high-speed driving conditions.

The review of the literature highlights that there are no prescribed standards for combining trajectory tracking and following control architectures in a hierarchical scheme and metrics available to assess the performance of combined motion planning and control scheme. Moreover, the decision governing the choice for a particular coupling between a trajectory planning scheme and a trajectory tracking scheme appears to be based on availability within the research group rather a choice based on control techniques that provide complementary performance benefits to

a multi-level control architecture. While the different combinations of planning and control techniques have been shown to work well for a whole range of driving conditions, a structured approach to assess the influence of the hierarchical control on the stability and dynamics of the vehicle akin to [7] is missing in literature. Andresson in Chapter 6 of his PhD thesis [160] touches upon the demarcation of tasks of a vehicle's trajectory planner and control functionalities. However, due to the lack of any consensus and best-practices discussed within the research community, a fair comparison between the different approaches for motion planning & control proposed in literature continues to be a challenging task.

The trajectory planning scheme proposed in Chapter 3 provides a framework to compute feasible and collision-free trajectories for performing lane-changes and overtaking manoeuvres. Moreover, the MPC framework allows for systematically tackling the system and actuator constraints over a range of longitudinal velocities. Nevertheless, while the planning controller does provide safe and feasible reference trajectories aspects such as (i) ensuring lateral-yaw stability, (ii) tyre dynamics, (iii) road surface changes, etc. are not considered while planning the trajectory. Consequently, an EMRAC based tracking controller is developed in Chapter 4 that computes appropriate steering action for tracking a given reference path trajectory despite external disturbances, road surface changes, modelling miss-matches, etc. However, in the previous chapter, the reference path trajectories were defined offline whereas in real-world situations local motion replanning of the vehicle is necessitated and thus coupling the EMRAC trajectory tracking with a local trajectory re-planner is required. In this chapter, the design for coupling of the trajectory planning from Chapter 3 and trajectory tracking from Chapter 4 for high-speed autonomous overtaking is undertaken in three steps. First, the steering actuator dynamics are introduced and modifications are made to the tracking controller from Chapter 4 to include the approximate steering actuator dynamics within the control framework. Next, this updated trajectory tracking controller is paired with a local trajectory re-planner and the resultant closed-loop scheme is validated in simulation for medium speed driving on a proving ground test track. Finally, the updated tracking controller is coupled to the RMPC based trajectory planning framework to realise the coupled motion-control hierarchical architecture for autonomous high-speed overtaking. The combined control framework is implemented in simulation environment and its performance is validated in a high-fidelity IPG CarMaker environment.

The structure of this chapter is as follows. The steering actuator system, state-space formulation of its approximated dynamics, and the augmentation of this systems into the path-tracking model is discussed in Section 5.2. Next the design of the EMRAC based steering control law for lateral tracking in the augmented

system is presented in Section 5.3. The lateral tracking controller is coupled to a basic local path planning technique and the validity of the resultant closed-loop system is illustrated using simulation based studies in Section 5.4. The lateral tracking controller is then combined with the RMPC based trajectory planner and the effectiveness of the proposed hierarchical closed-loop control architecture for autonomous high-speed overtaking in different conditions is shown in Section 5.5. Finally, the conclusions and future research directions are discussed in Section 5.6.

5.2 Steering Actuator Dynamics

The results discussed in Chapter 4 have been obtained under the assumption that there are no steering actuator dynamics and the steering angle computed by the EMRAC controller is immediately applied to the vehicle. However, this is not the case in actual hardware systems and there are significant actuator (steering) dynamics that have a detrimental effect on the closed-loop tracking performance. Consequently, it is common to incorporate the actuator dynamics within the design of the tracking controller by approximating them as low order transfer functions (e.g., first/second order low-pass filters) [165].

For the test vehicle used in this thesis, simulation and experimental tests in the past have shown that the dynamics of its steering system can be approximated as a pure delay system expressed using the equation below

$$\delta_f(t) = \delta_{f,des}(t - \tau_{sa}) \quad (5.1)$$

where τ_{sa} is the actuator time-delay and $\delta_{f,des}$ is the desired front steering angle. Moreover, (5.1) can also be expressed as a transfer function from $\delta_{f,des}$ to δ_f given by $G_{sa}(s) = e^{-\tau_{sa}s}$. A schematic representation of such a steering actuator system is given in Figure 5.1. As a result, path tracking controllers which approximated the steering system as low pass filters did not provide adequate tracking performance.

However, augmenting (5.1) into the system (4.44) gives rise to a very challenging problem in terms of controller design and stability analysis [166]. Padé approximations provide a way of modelling a delay with a finite-dimensional rational transfer function that can be used for subsequent controller development [166, 167]. In this chapter, a 1st-order Padé approximation given below

$$G_{sa}(s) \approx \frac{2 - \tau_{sa}s}{2 + \tau_{sa}s} \quad (5.2)$$

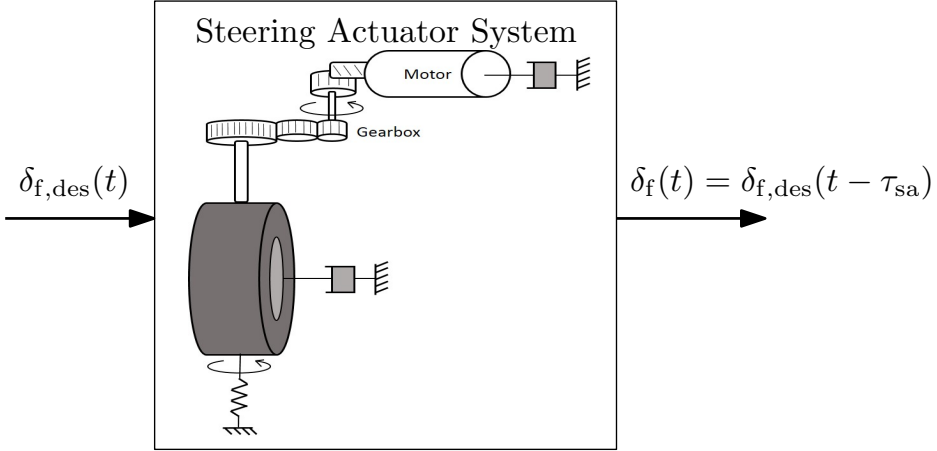


Figure 5.1 Schematic of a steering actuator system illustrating the input and output interfaces

is utilised to approximate the steering actuator dynamics for control design, see Figure 5.2. For a given nominal delay i.e., $\tau_{\text{sa}} = \bar{\tau}_{\text{sa}}$, the transfer function in (5.2) can be represented in a state-space format given as

$$\dot{x}_{\text{sa}} = A_{\text{sa}}x_{\text{sa}} + B_{\text{sa}}u_{\text{sa}} \quad (5.3a)$$

$$y_{\text{sa}} = C_{\text{sa}}x_{\text{sa}} + D_{\text{sa}}u_{\text{sa}} \quad (5.3b)$$

where $x_{\text{sa}} \in \mathbb{R}$ is an internal state for the actuator dynamics, the desired front steering angle $u_{\text{sa}} = \delta_{\text{f},\text{des}} \in \mathbb{R}$ is the input of the system, actual front steering angle $y_{\text{sa}} = \delta_{\text{f}} \in \mathbb{R}$ is the output of the system, and $(A_{\text{sa}}, B_{\text{sa}}, C_{\text{sa}}, D_{\text{sa}})$ are the state-space matrices of appropriate dimensions.

5.2.1 Model Augmentation

The steering actuator model in (5.3) is coupled with the path-tracking model in (4.42) to arrive at the integrated model of the overall system. The integrated model preserves the mathematical structure given in (4.44). A model augmented with the steering actuator dynamics is created by designing system matrices computed using the expressions given below

$$A = \begin{bmatrix} A_{\text{path}} & B_{1,\text{path}} \cdot C_{\text{sa}} \\ \mathcal{O}_{n,1} & A_{\text{sa}} \end{bmatrix} \quad (5.4a)$$

$$B_1^T = \begin{bmatrix} (B_{1,\text{path}} \cdot D_{\text{sa}})^T & B_{\text{sa}} \end{bmatrix} \quad (5.4b)$$

$$B_2^T = \begin{bmatrix} B_{2,\text{path}}^T & \mathcal{O}_{1,1} \end{bmatrix} \quad (5.4c)$$

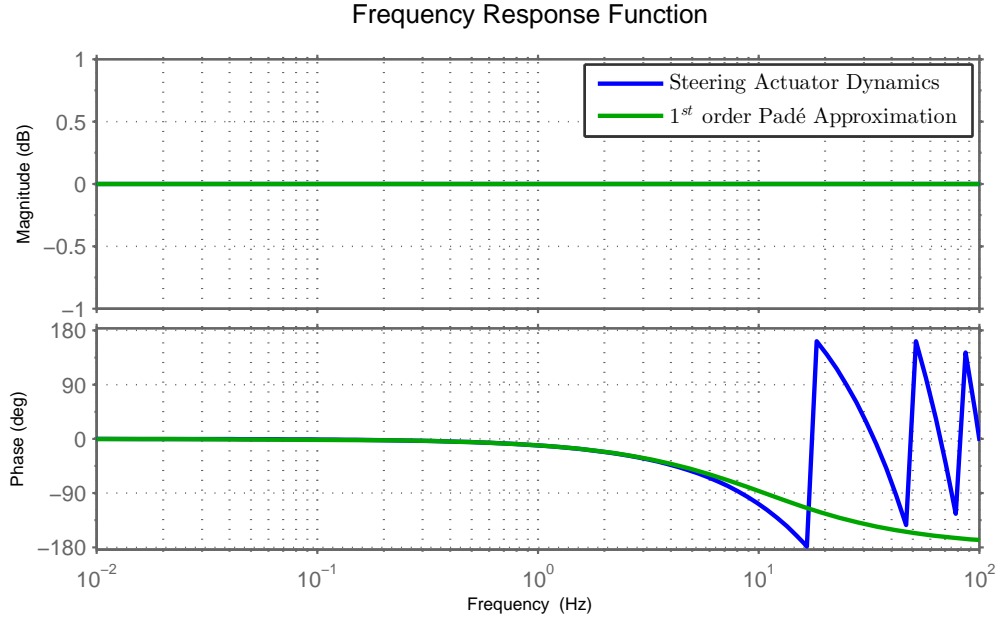


Figure 5.2 Frequency-domain response of steering dynamics with exact and approximated delays.

where $x = (x_{\text{path}}, x_{\text{sa}}) \in \mathbb{R}^5$ represents the state vector of the system, $u = \delta_{f,\text{des}} \in \mathbb{R}$ is the input to the system, the resultant coupled system description can also be represented using the compact notation given below.

$$\dot{x} = Ax + B_1u + B_2\kappa \quad (5.5)$$

Furthermore, as discussed in Section 4.4, the dependence of the system matrices on the plant parameters and vehicle longitudinal velocity still exists and thus the challenges highlighted in Section 4.4 still exist. Moreover, coupling the approximate steering actuator dynamics introduces additional modelling uncertainties to the state-space model. Therefore, the coupled system dynamics are represented more realistically if the description from (4.47) is used, resulting in the model given below

$$\dot{x} = Ax + B_1u + B_2\kappa + B_1d \quad (5.6)$$

where once again $d \in \mathbb{R}$ is a bounded disturbance acting upon the system and contains the deviation between a nominal system model and the actual system due to modelling miss-match, parameter variation, external disturbances, degradation, etc.

5.3 Control Law

Similar to Section 4.3, the control objective here is to steer the system in (5.6) towards an asymptotically stable LTI reference system whose dynamics are described as

$$\dot{x}_m = A_m x_m + B_m r \quad (5.7)$$

where $x_m \in \mathbb{R}^5$ is the reference model state, $r = \kappa \in \mathbb{R}$, and (A_m, B_m) are the reference model system matrices of appropriate dimensions with A_m being Hurwitz. The matching conditions given below

$$A_m = A + B_1 K_X^* \quad (5.8a)$$

$$B_m = B_1 K_R^* + B_2 \quad (5.8b)$$

are satisfied by assuming the existence of two constant matrices K_X^* and K_R^* of appropriate dimensions. By designing adaptive control gains K_X , K_R , K_I , and K_N using the techniques presented in Section 4.3, the aforementioned model reference control problem is solved by the EMRAC control action given below

$$u(t) = K_X(t)x(t) + K_R(t)r(t) + K_I(t)e_I(t) + K_N(t)\text{sgn}(y_e(t)) \quad (5.9)$$

The boundedness of the resultant closed-loop system has been proven in Theorem 4.3.1.

5.4 Test Track

To test the effectiveness of the lateral-tracking controller discussed above, its closed-loop performance is evaluated in a simulation around a lap of a test track. The (x, y) coordinates of the centre of the track are known and act as the reference path for the vehicle to follow. These coordinates can be used to compute the desired path-curvature as a function of distance travelled along path using the equation from [168] given below

$$\kappa = \frac{\xi' \eta'' - \eta' \xi''}{[(\xi')^2 + (\eta')^2]^{\frac{3}{2}}} \quad (5.10)$$

where $(\cdot)'$ represents the derivative with respect to path length s . The resultant desired path-curvature for the test-track obtained using the equation above is shown in Figure 5.3(a). Moreover, the desired velocity profile of the vehicle is known (see Figure 5.3(b)) and provided to the default IPG CarMaker's ACC system mentioned in Chapter 4. A lateral tracking controller is designed using the parameters in

Tables A.1 and A.4 and the resultant control law is connected in closed-loop with the high-fidelity vehicle and system model from IPG CarMaker with the goal of driving along the centre of the track as closely as possible despite variations in the vehicle's velocity and other system uncertainties. It is noteworthy that the nominal controllers for reference model of the EMRAC are designed using the procedure described in Appendices F and G.

Moreover, since the eventual goal is to test and validate the control scheme on an experimental vehicle, the high-fidelity environment is set-up to mimic the sampling times of the Controller Area Network (CAN) bus and the vehicle actuators. As a result the co-simulation environment is discretised at 1000 Hz whereas the EMRAC controller is discretised at 50 Hz. The implementation of the controller designed in continuous-time domain in a discrete-time environment necessitates some retuning of the weighting matrices for the adaptation law and the values in Table A.4 reflect weighting matrices suitable for implementation in a discrete-time environment.

5.4.1 Local Reference Curvature Generation

As presented in the previous chapter, the lateral tracking controller proposed in this thesis does not require reference path coordinates for tracking but rather tries to follow a given reference path curvature. However, the desired path curvature from Figure 5.3(a) is not a suitable choice for the reference to the lateral tracking controller as it is an LTI function (of the desired path coordinates) which is generated offline. Thus, if the vehicle deviates from the desired path, following the desired path curvature will not result in the vehicle rejoining the path. Consequently, an appropriate local trajectory/path (and by extension curvature) needs to be generated which the SV needs to follow to reduce the deviation from the desired path.

A computationally efficient technique for estimating the reference curvature that a vehicle should follow to track a desired path is shown to be effective in experimental tests in [152]. This procedure which is briefly discussed below is utilised to generate the local reference curvature that can act as reference signal for the EMRAC lateral tracking controller. This method relies on two phenomena observed for a vehicle in steady-state cornering conditions at low lateral accelerations namely: (i) in steady-state conditions the lateral motion of a vehicle follows circular arcs and (ii) the centre of rotation of front-wheel steered vehicles using Ackermann geometry lies on a virtual line passing through the rear-axle of the vehicle [106]. Therefore, the lateral error at a look-ahead distance can be reduced to zero if the vehicle travels along a circular arc of a certain radius, see Figure 5.4 for a geometrical interpretation of the concept.

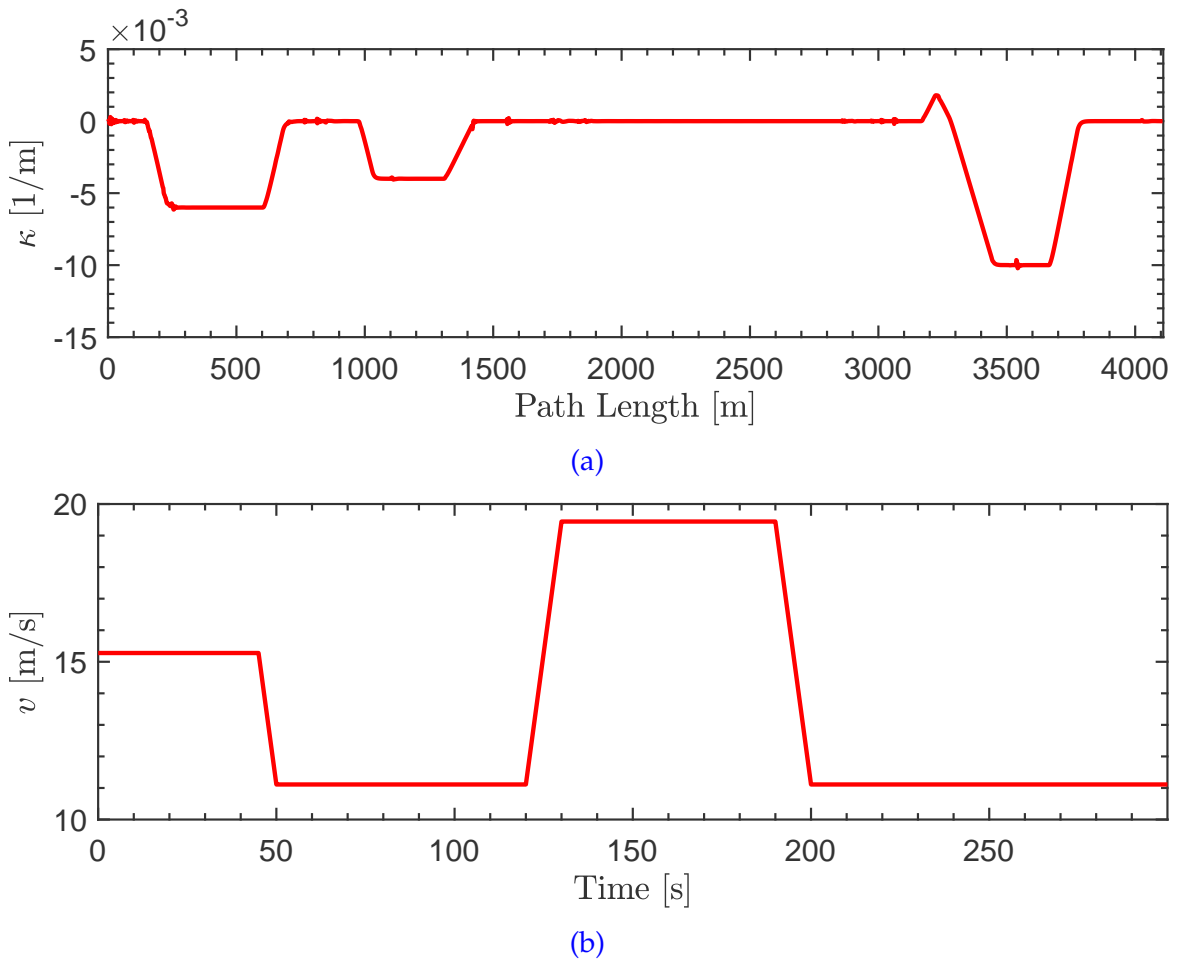


Figure 5.3 Desired lateral and longitudinal signals for Gaydon test-track; (a) path curvature κ_{des} ; (b) longitudinal velocity v_{des}

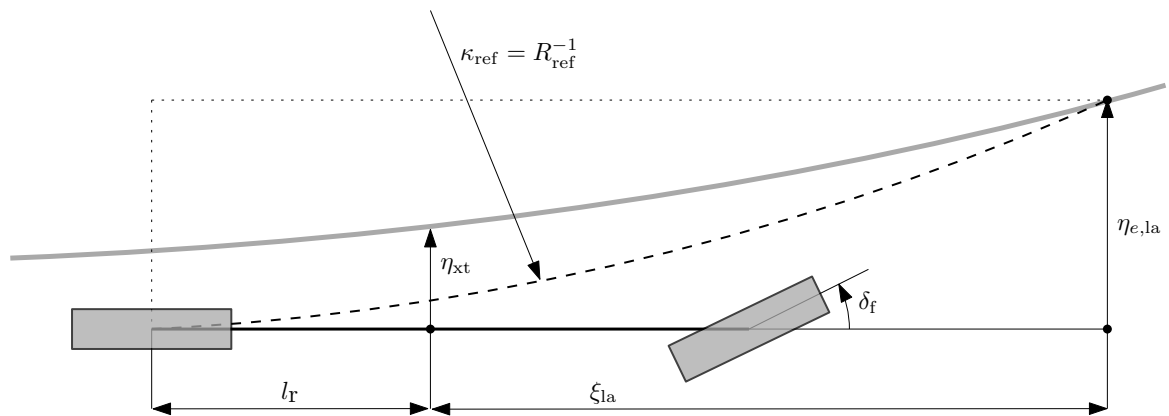


Figure 5.4 Geometric representation of reference curvature generation from given desired path (grey)

By assigning lateral error at the look-ahead point $\eta_{e,la}$ as the sagitta of the circular arc (starting from rear-axle) and utilising the net look-ahead distance from the rear axle as $d_{la} = l_r + \xi_{la}$, the reference curvature of the arc κ_{ref} can be estimated as

$$\kappa_{ref} = \frac{2\eta_{e,la}}{d_{la}^2}, \quad \text{when } \eta_{e,la} \ll R_{ref} \quad (5.11)$$

where R_{ref} is the radius of the circular arc. Thus, the path-following problem is transformed into a curvature following problem which is suitable for the lateral-tracking controller proposed in this thesis.

Remarks

- The cross-track error η_{xt} is defined as the distance of the centre of gravity of the vehicle from the desired path (of the test track). This distance is measured perpendicular to the vehicle's longitudinal axis.
- The lateral position error $\eta_e (\neq \eta_{xt})$ defined in Section 4.4 is the lateral distance error from the Centre of Gravity (C.G) of the vehicle to the reference path and is also measured perpendicular to the vehicle's longitudinal axis.
- Similarly, the instantaneous curvature of the path κ_{des} can be computed based on the path coordinates (ξ_{des}, η_{des}) and differs from the reference curvature κ_{ref} which is computed from the circular arc in Figure 5.4.
- The look-ahead distance $x_{i,la}$ can be designed to be a function of the longitudinal velocity of the vehicle. The design of the function is generally performed based on trade-off between tracking accuracy and vehicle lateral stability and a preliminary study on this aspect is provided in Appendix F

5.4.2 Numerical Validation

In this section, the ability of the proposed architecture (local reference generation and updated tracking controller) in Figure 5.5 to accurately track a desired path/curvature around the test track is discussed. It is evident from Figure 5.3(a) that the test track consists of three corners with different curvatures interlaced with straight driving sections. Moreover, the desired longitudinal velocity v_{des} shown in Figure 5.3(b) is varying which means that the lateral-yaw dynamics of the vehicle are different for each corner thus providing a direct way of observing the closed-loop tracking performance. It is noteworthy, that just like Section 4.5, the task of tracking a desired longitudinal velocity is laid upon IPG's default ACC controller. At each point on the

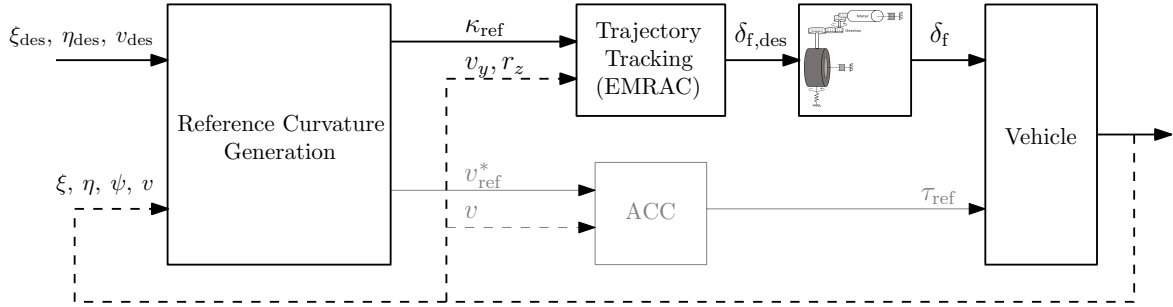


Figure 5.5 Closed-loop control structure: combined local path planning & tracking

track, the reference curvature κ_{ref} is computed based on Section 5.4.1 and provided to the EMRAC lateral-tracking controller which calculates the appropriate front steering angle $\delta_{f,\text{des}}$ for the vehicle. This desired front steer angle is the input for the steering actuator and based on its dynamics, the actual front steering angle δ_f is applied to the vehicle. Moreover, to demonstrate the robustness of the proposed framework to deviation of steering actuator dynamics from nominal conditions, the simulation with the same controller is repeated twice with (i) no steering actuator dynamics i.e., $\delta_{f,\text{des}}$ is applied directly to the vehicle and (ii) the delay of the steering actuator is larger than modelled delay by 25%. The comparison of the simulation results between the nominal case and the two cases mentioned above provide insight on the performance of the proposed controller to variations in steering actuator dynamics.

The evolution of the internal states of the EMRAC controller is shown in Figure 5.6 and some key takeaways are as follows. The plots show that while cornering there is some error between the states of the vehicle and reference model within the MRAC, this error is the largest during the first corner but then as the controller gains adapt it reduces over the rest of the simulation despite the last corner being the tightest. During the first corner, the lateral velocity of the vehicle v_y does not match the reference model completely and this can be traced as the cause for the additional initial lateral error η_e , see Figures 5.6(a) and 5.6(c). However, the plots show that η_e does not grow beyond 0.1 m and also progressively reduces as the simulation goes on. While navigating the first corner, the SV is travelling at very close to the nominal longitudinal velocity (see Figure 5.3(b)) and as a result the yaw-rate of the SV matches the reference model in Figure 5.6(b). For the remaining two corners the longitudinal velocity is lower and as a result the SV's yaw-rate is lower when compared to the reference model. Moreover, Figure 5.6(d) shows that

there exists a constant miss-match between the heading angle error of the SV and the reference model. However, some of these discrepancies can be contributed to the two assumptions made within the path-tracking model namely; (i) the tyres do not generate any lateral-slip and (ii) no side-slip of the vehicle body. From Figure 5.6(e) it is observed that the discrepancy between the reference model and the actual state is the least among all states in case of the internal steering actuator state. This is expected as the steering actuator state is generated using (5.3) which exactly matches the model within the EMRAC controller. The closed-loop tracking performance of the EMRAC states in Figure 5.6 shows that the SV is able to closely follow the reference model of the controller despite the simplifications and assumptions made while modeling path-tracking dynamics as well as the steering actuator dynamics and thus demonstrate that the EMRAC design procedure is flexible and can be used when steering actuator dynamics are incorporated into controller design for lateral-tracking controllers.

The discussion above shows that the EMRAC controller performs satisfactorily after being modified with steering actuator dynamics. Moreover, the overall path tracking performance of the closed-loop architecture from Figure 5.5 (EMRAC controller when coupled with a local path/trajectory re-planning) is illustrated in Figure 5.7. The plot of the coordinates of the path and the centre of gravity of the SV in Figure 5.7(a) shows that the vehicle can follow a given desired path accurately. The plot inset which depicts a closer view of the tightest final corner also illustrates that the coordinates of the path and SV are so close to each other that it is not possible to differentiate between them at these scales. The desired path curvature κ_{des} , the reference curvature κ_{ref} generated as in Section 5.4.1, and the curvature followed by SV ($\kappa \approx r_z/v$) in Figure 5.7(b) shows that the reference curvature generated from circular arcs are a very close match to the desired path curvature. Moreover, the SV is able to track the reference curvature very accurately all along the test track demonstrates the ability of the proposed closed-loop architecture as a capable path-tracking solution. The plot inset provides a closer look at the ability of the closed-loop control system in preventing the SV from deviating far from the desired path. The usage of a look-ahead-point for generating a reference path/curvature also results in a vehicle cutting corners and this phenomenon is also clearly visible in the inset where the reference curvature and SV's curvature signal clearly cut the peak of the reference curvature signal. Finally, the variation of the longitudinal velocity v of the vehicle is depicted in Figure 5.7(c). The tracking performance of the longitudinal velocity controller is sufficient for the purposes of this study and a detailed discussion on it is beyond the scope of this thesis.

The control action $\delta_{f,\text{des}}$ computed using the EMRAC algorithm is given in Figure 5.8(a). The presence of some oscillations can be observed during the first corner

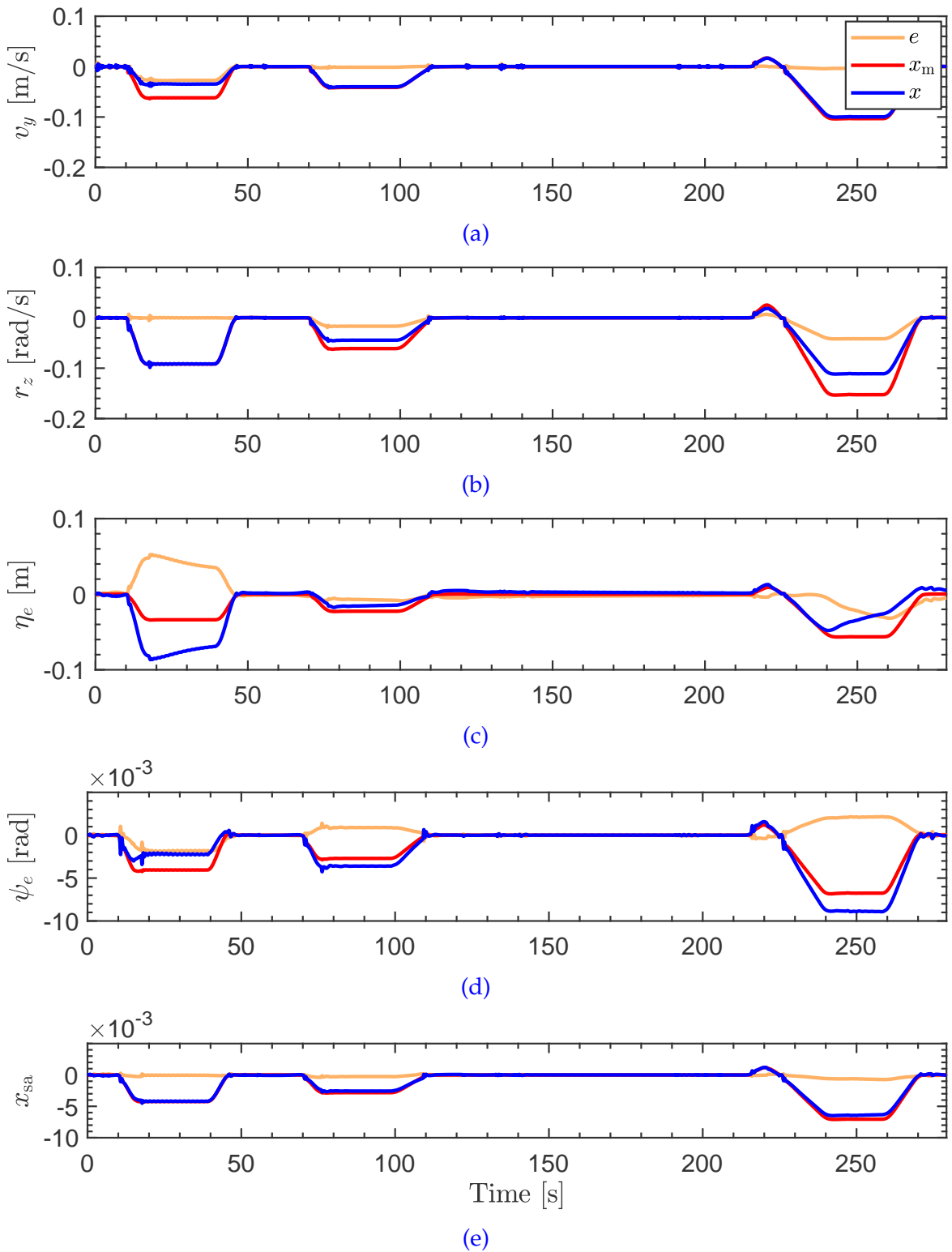


Figure 5.6 Evolution of the EMRAC states and errors for driving on test-track. Note: reference model (red), system states (blue), error between reference model and system (orange)

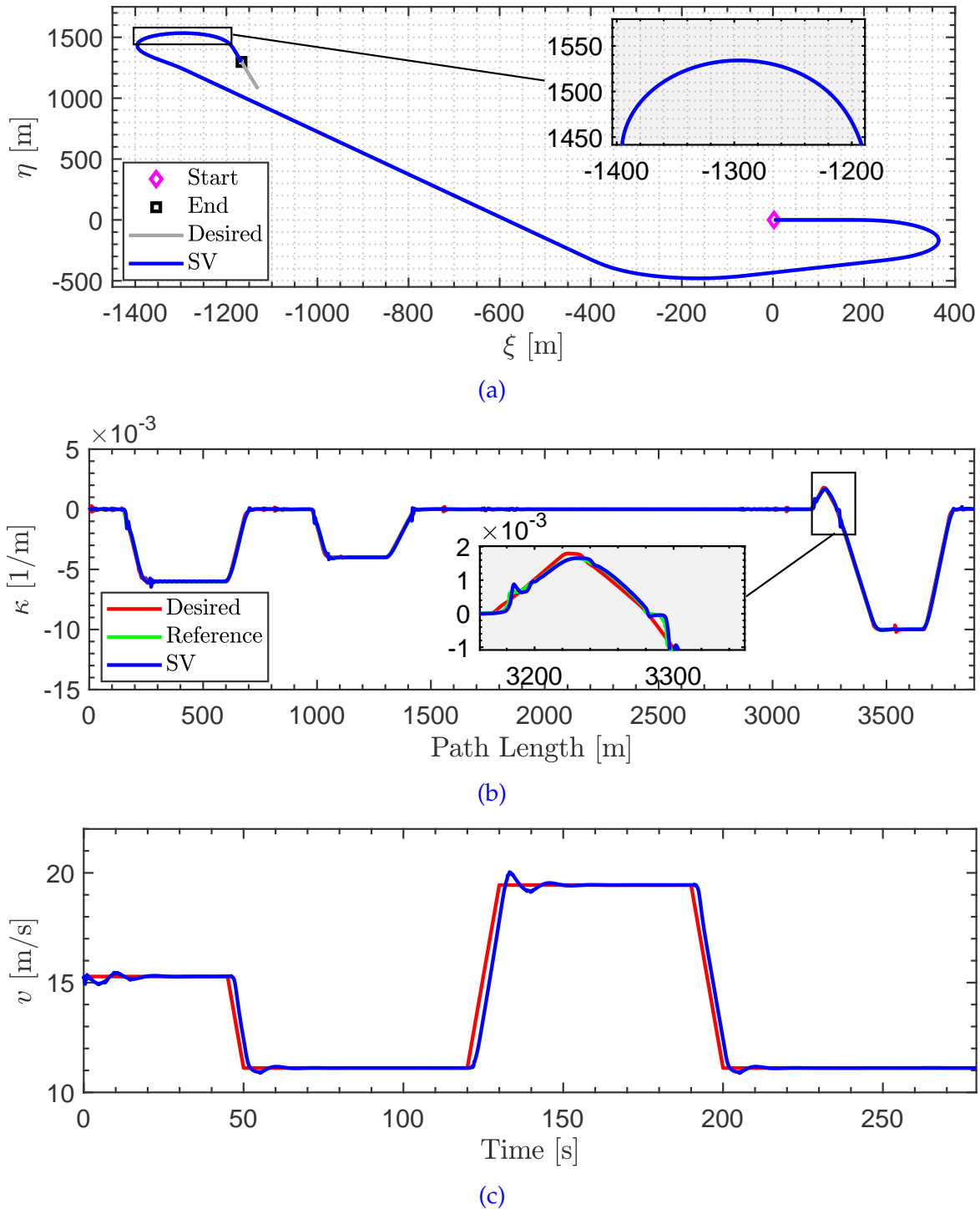


Figure 5.7 Simulation results; (a) path coordinates p ; (b) curvature κ as a function of distance travelled along path; (c) longitudinal velocity v over time

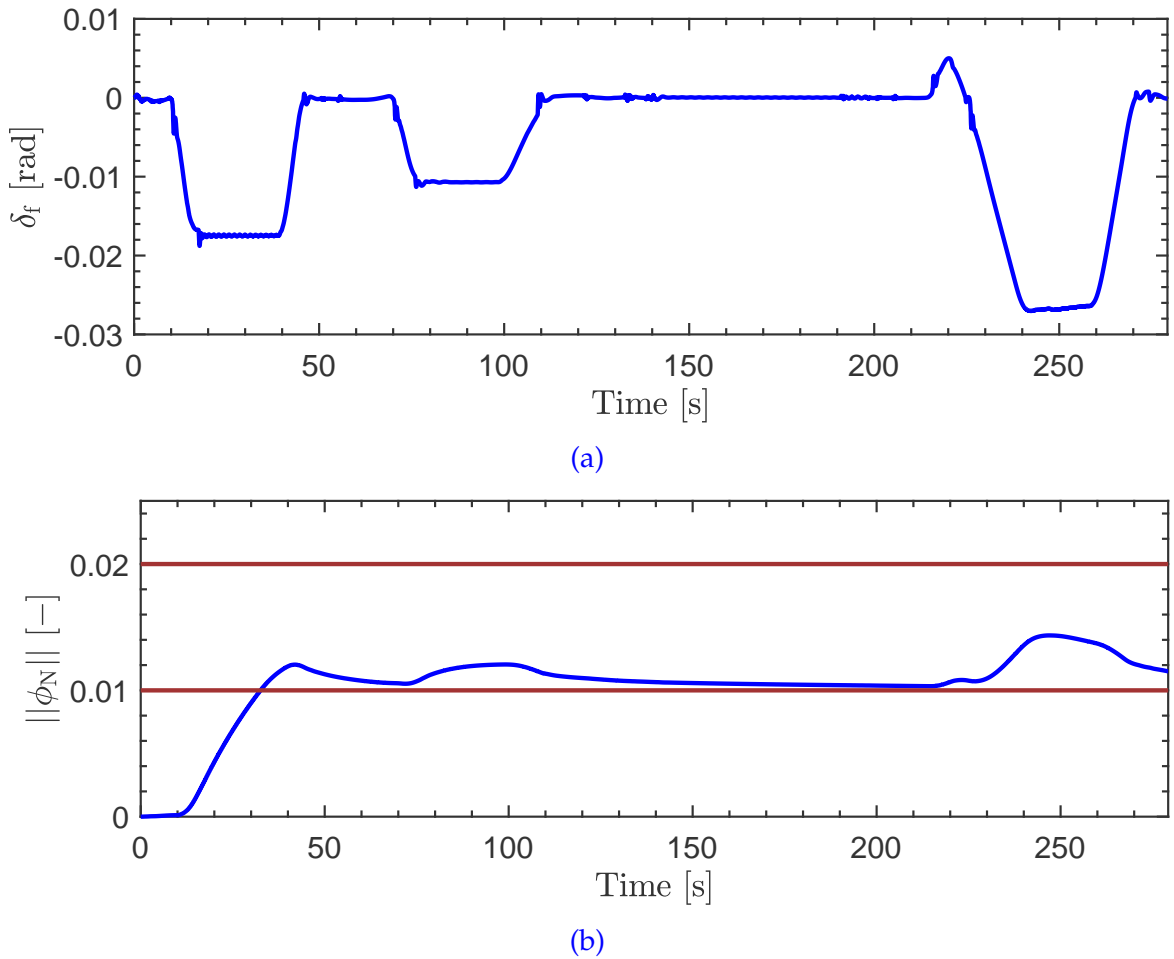


Figure 5.8 Simulation results for tracking desired path; (a) front wheel steering angle δ_f ; (b) norm of switching action $\|\phi_N\|$

but they are quickly attenuated as the gains of the controller adapt. Consequently, the steering action in the remaining part of the simulation is devoid of any high-frequency oscillatory behaviour that would have a detrimental effect on the occupant comfort and lateral-yaw stability of the vehicle. Furthermore, the plot shows that the control action for transiting from straight driving to cornering gets increasingly smoother with each corner despite the reference curvature being the largest (smallest cornering radius) for the final corner. The smooth control action is due to bounded evolution of the control gains and the evolution of the norm of the gain for switching control action is shown in Figure 5.8(b). Once again, the plot demonstrates the ability of the σ -modification technique discussed in Chapter 4 to bind the evolution of the controller gain within the prescribed limits.

The robustness of proposed tracking controller to variations of the path-tracking parameters was already demonstrated in Chapter 4. Likewise, the robustness of

the proposed controller to changes in the steering actuator dynamics is investigated in this section. This is performed by using the controller designed in this section for the nominal time delay $\bar{\tau}_{\text{sa}}$ as it is but the simulation of driving around the test-track is repeated by varying the delay of the steering actuation system between the range given in Tables A.1 and A.4. Particularly, for the purpose of this study, the simulation is repeated twice with the steering actuator system having its internal delay; (i) $\tau_{\text{sa}} = 0$ and (ii) $\tau_{\text{sa}} = 1.25\bar{\tau}_{\text{sa}}$. The plot of the respective cross-track error η_{xt} from each simulation is plotted in Figure 5.9(b) and can be used to compare the closed-loop performance. Firstly, the plot shows that η_{xt} is virtually identical for the three different simulations which shows that the proposed control algorithm is robust to variations in time-delay of the steering actuator system and the magnitude of η_{xt} in all the three simulations is within the acceptable range for path-following techniques for autonomous vehicle. Secondly, the phenomenon of cutting the corners (due to look-ahead point) which was discussed above in Figure 5.7(b) is more clearly evident in the plot of the cross-track error. The cutting of corners is evident at the start and end of each corner (e.g., $t \approx \{10, 40, 70, 100, 120, 220, 270\}$ s) of Figure 5.9(b). As the vehicle is turning right, cutting the corner at the start of the curve results in positive error contribution to η_{xt} and a negative contribution to η_{xt} at the end of the corner. The steering actuation computed by controller for the three simulation runs is illustrated in Figure 5.9(a). The three signals are virtually indistinguishable from each other with the only perceptible difference being at the start of the first corner where the control action for the largest delay in the steering actuator system shows some high-frequency oscillations. However, these oscillations are quickly terminated and the signal demonstrates smooth evolution for the remaining duration of the test. Since the control action is virtually unchanged even when the delay within the steering system varies, it is safe to infer that the other signals such as the states of the EMRAC controller, gains of the controller, etc. also evolve just like the nominal case and are thus not illustrated for brevity. Therefore, these results help in highlighting the robustness of the proposed lateral-tracking controller to variations in the dynamics of the steering actuator system.

The simulation results discussed in this section demonstrate the efficacy of lateral-tracking control architecture illustrated in Figure 5.5. In addition to the closed-loop performance which has already been discussed some additional key takeaways are (i) the EMRAC generic lateral tracking controller proposed in Chapter 4 can be augmented with steering actuator dynamics such that the control law considers these additional dynamics while computing appropriate steering action and (ii) the proposed EMRAC controller can be successfully be coupled with a local trajectory/curvature replanning method and thus can be incorporated within a larger autonomous vehicle driving architecture.

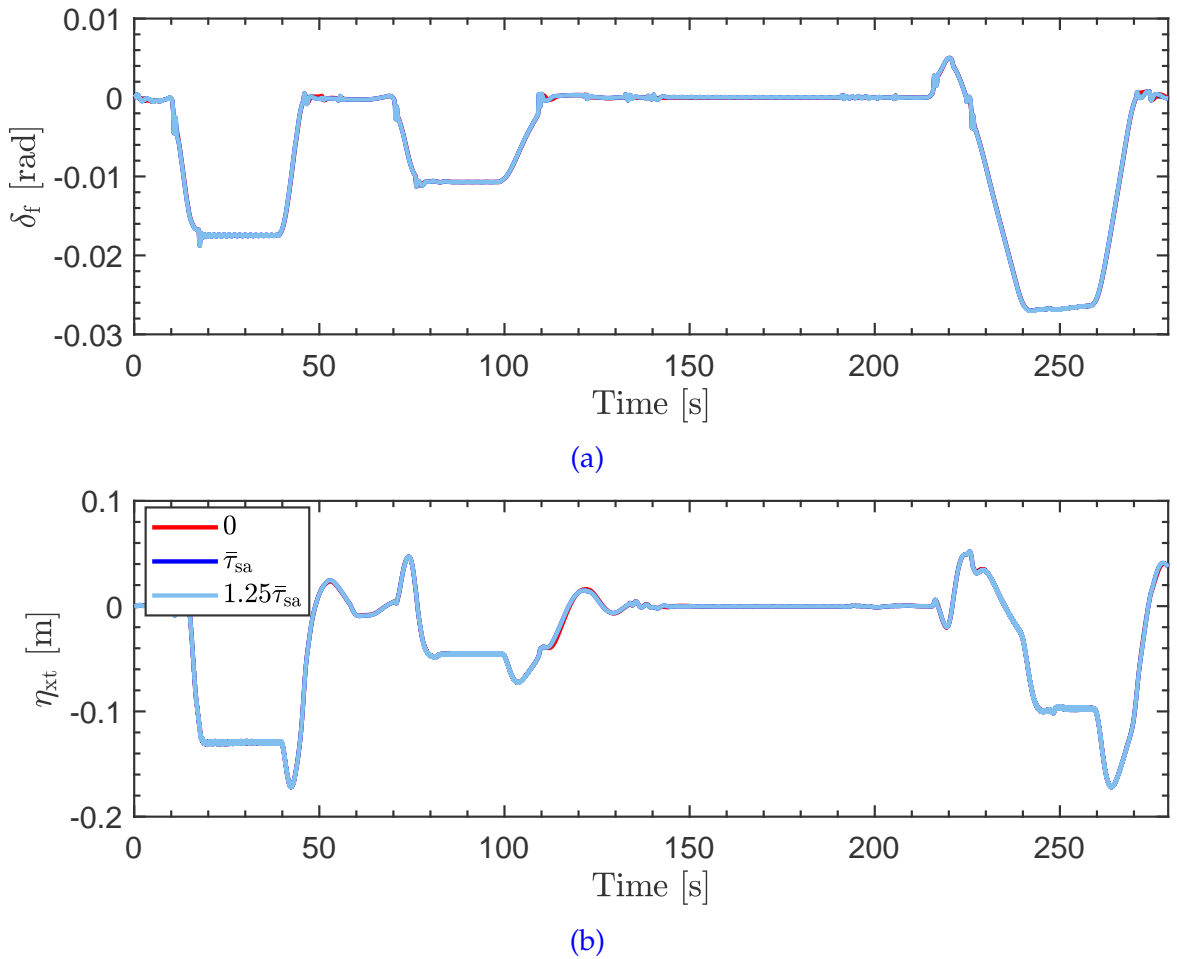


Figure 5.9 Comparison of simulation results for tracking desired coordinates with variation in delay of steering actuator system $\bar{\tau}_{sa}$; (a) front wheel steering angle δ_f ; (b) cross track error η_{xt}

5.5 High-Speed Overtaking

In this section, the coupling of the EMRAC based lateral-tracking controller with a more sophisticated trajectory planning technique (from Chapter 3) for autonomous high-speed overtaking is discussed. The steps that are undertaken to couple the RMPC based trajectory planning controller with the EMRAC lateral-tracking controller was briefly touched upon in Section 3.8 and is discussed in greater detail below.

5.5.1 Local Reference Trajectory

The optimal trajectory $x_{\text{rmpc}}^* = [\xi^*, \eta^*, \psi^*, v^*]^T$ generated using Algorithm 3.2 provides a feasible and collision-free reference local trajectory for the SV's C.G. By assuming a rigid connection between the C.G and rear-axle of the vehicle, the reference pose of the vehicle (ξ^*, η^*, ψ^*) is used to compute the coordinates of the reference path that rear-axle of the vehicle $p_{\text{ra}}^* = (\xi_{\text{ra}}^*, \eta_{\text{ra}}^*)$ needs to follow. It is remarkable that considering the scale of the vehicle velocities and the magnitude of the distances between vehicles it is reasonable to assume that the reference coordinates for the rear-axle also trace a collision-free path.

Generation of Reference Curvature

The reference coordinates for the rear-axle $(\xi_{\text{ra}}^*, \eta_{\text{ra}}^*)$ represents the trajectory that the rear-axle of the SV needs to follow. Consequently, as described in Section 5.4.1, the coordinates of reference path for the rear-axle are used to generate a reference curvature κ_{ref} for a given look-ahead distance d_{la} using (5.11). Thus, at each time instant the re-planned local trajectory from the trajectory planner is used to constantly update κ_{ref} which acts as the reference signal for the lateral-tracking controller. A geometrical interpretation of the procedure used for generating κ_{ref} from the path generated by the trajectory planner is illustrated in Figure 5.10.

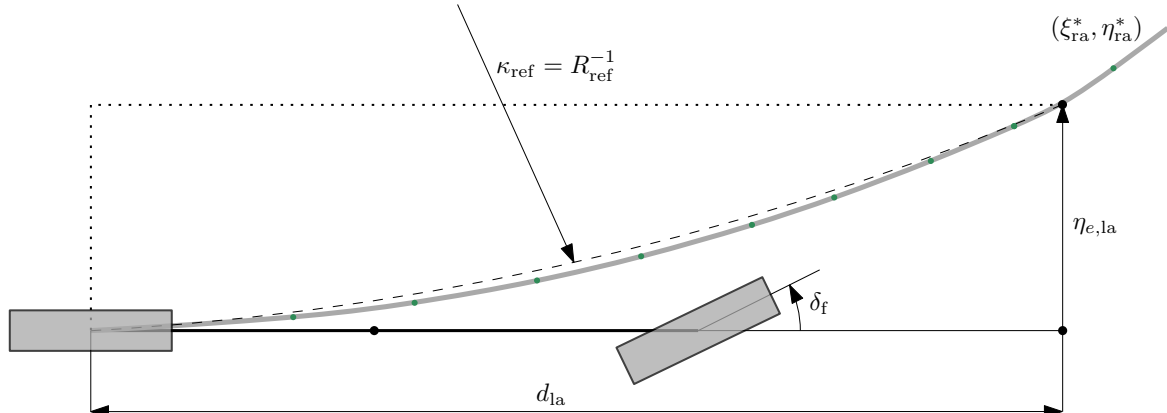


Figure 5.10 Geometric representation of reference curvature generation from RMPC optimal trajectory. **Note:** Green dots represent the reference coordinates $p_{\text{ra}}^* = (\xi_{\text{ra}}^*, \eta_{\text{ra}}^*)$ for the rear-axle of the SV

5.5.2 Numerical Validation

The resultant net closed-loop system obtained by coupling (i) trajectory planning from Chapter 3, (ii) reference curvature generation from Section 5.5.1, and (iii) lateral tracking from Section 5.3 is shown in Figure 5.11. The blocks contained within the grey outline are responsible for the motion-planning and control for an autonomous vehicle and provide an interface between (i) perception and decision making and (ii) actuator level controllers of a typical autonomous driving system architecture illustrated in Figure 2.3. In this section, the ability of this proposed motion control system for autonomous high-speed overtaking is evaluated in a MATLAB-IPG CarMaker co-simulation environment.

The scenario used is similar to the one described in Section 3.8 and re-iterated here for the sake of clarity. Both the subject vehicle and the lead vehicle are travelling on a two-lane one-way road of infinite length at longitudinal velocity v and v_{LV} , respectively. The dimensions of the road, lane-limits and lead vehicle's states are available to the subject vehicle on-demand through for example a V2X communication link. Each lane of the highway is assumed to have a nominal desired velocity which is provided to the subject vehicle by the route planner while the decision to perform an overtaking manoeuvre and availability of the faster lane is verified by the decision making block of the SV [23, 119]. The design of the different blocks within the proposed motion control structure has been discussed in the prior chapters and sections of this thesis and the important steps for coupling them are summarized in Algorithm 5.1. Furthermore, the design parameters used for trajectory planning, curvature generation, and trajectory tracking are provided in Tables A.1, A.2 and A.5. As mentioned in the previous Section 5.4, the nominal controllers for reference model of the EMRAC are designed using the procedure described in Appendices F and G. Moreover, just like Section 5.4 the overtaking simulations are also performed in a

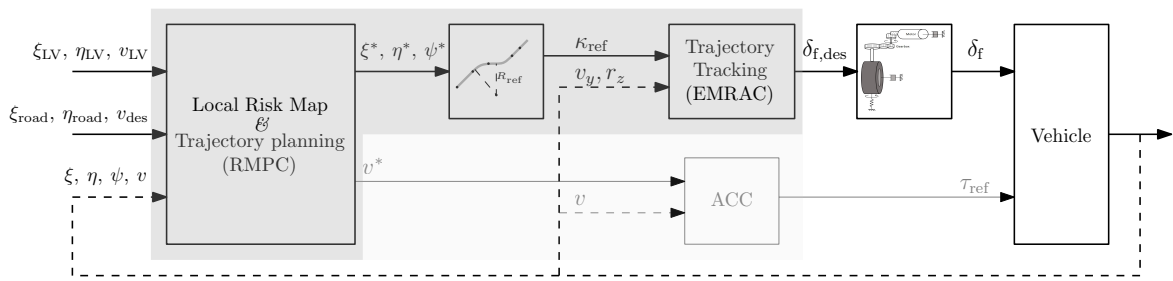


Figure 5.11 Proposed closed-loop control architecture for autonomous overtaking: combined trajectory planning & tracking

Algorithm 5.1 Autonomous Overtaking

```

1: initialize:
2:  $\mathcal{R}_V \leftarrow$  bank of reachable sets in V-frame
3:  $U_{\text{safe}} \leftarrow$  upper bound of risk potential
4: procedure MOTION PLANNING & CONTROL
5: top:
6:    $v_{\text{des}} \leftarrow$  desired longitudinal velocity from user
7:    $\mathcal{R}_{\text{total}} \leftarrow$  reachable set for given  $v_{\text{des}}$  as (3.2)
8:    $\mathcal{R} \leftarrow$  projection of  $\mathcal{R}_{\text{total}}$  in I-frame as (3.39)
9:    $d_{\text{la}} \leftarrow$  look-ahead distance from rear-axle
10: loop:
11:    $(\xi^*, \eta^*, \psi^*, v^*) \leftarrow \text{generateTrajectory}$  as Algorithm 3.2
12:    $p_{\text{ra}}^* \leftarrow$  reference trajectory for rear-axle
13:    $\kappa_{\text{ref}} \leftarrow \text{calculateReferenceCurvature}(p_{\text{ra}}, p_{\text{ra}}^*, d_{\text{la}})$  as (5.11)
14:    $\delta_{\text{f,des}} \leftarrow \text{lateralControl}(\kappa_{\text{ref}})$  as (5.9)
15:   if user request change in  $v_{\text{des}}$  then
16:     goto top.
17:   else
18:     goto loop.

```

discrete-time environment with the same sampling times as mentioned above which once again means that the weighting matrices for the adaptive gains in Table A.5 are for implementing the controller in discrete-time environment sampled at 50 Hz.

The results from the simulation are used to gain insight on the performance of the proposed closed-loop motion control when performing complex high-speed manoeuvres such as overtaking autonomously. The study also provides an opportunity to ascertain that trajectory planner's (tasked with generating safe and feasible trajectories) performance is not hindered by the trajectory tracker (tasked with lateral-yaw tracking and stability) and vice-versa. Furthermore, like the results presented in Section 3.8.2, Gaussian noise is added to the lead vehicle's velocity to simulate noise and imperfections in the different input channels. Moreover, to illustrate the ability of the controller architecture to conserve its performance in unforeseen environmental conditions the simulation is repeated by initialising all the controller parameters as Tables A.2 and A.5 (nominal conditions) while modifying the external world in two ways (*i*) split- μ condition on both lanes with road friction lowered by 25% and (*ii*) cross-winds blowing at 15 m s^{-1} across the road. Since, such situations are not rare for highway driving and these effects are not considered during the design of either controller, it is important to illustrate the robustness of the proposed control architecture to such external disturbances.

The results of the simulation for the overtaking manoeuvre under nominal environmental conditions are illustrated in Figure 5.12. The successful completion of the overtaking manoeuvre can be seen in the top plot which shows the paths traced by the LV and the SV. It is noteworthy that the insights gained about the closed-loop performance of the proposed system have been discussed in Section 3.8.2 and are also applicable here. Additionally, the evolution of the heading angle ψ shows that the SVs transitions from one lane to another is even smoother than Figure 3.8 despite the addition of steering actuator dynamics to the closed-loop framework. An interesting observation which is along expected lines is the slight difference between the evolution of ψ during the first and second lane change. In comparison to the first lane-change, the peak in ψ is sustained for longer and also decays at a slower rate and this is due to reducing velocity of the SV during the second lane-change which results in the need for a higher heading angle to travel identical lateral distance of one lane-width. The control action (i.e., steering angle) is devoid of any high-frequency oscillations that have a detrimental effect on the passenger comfort and actuator. The reader's attention is drawn to fact that this control action is generated by the EMRAC lateral-tracking controller and yet remains well within the system constraints described within the trajectory planning RMPC formulation. The performance of the longitudinal tracking is not discussed here as it has been tackled earlier in Section 3.8.2 and the observations in Figure 5.12 are consistent with Figure 3.8.

The discussion above provides a high-level illustration on the performance of the proposed motion control architecture. The remainder of this section is devoted to understanding interactions of the various inter-connections to gain greater insight of this hierarchical control architecture. As mentioned in the previous sections, the reference curvature generation provides a key interface between the trajectory planner and the trajectory tracking controller by transforming a given reference trajectory (ξ^*, η^*, ψ^*) into a equivalent reference curvature κ_{ref} . The reference path curvature κ_{ref} is generated using the technique presented in Section 5.5.1 and its evolution is depicted in Figure 5.13. The signal shows smooth transition while moving from start of lane-change to end of the lane change for each lane-change event. While the curvature of the path generated depends greatly on the tuning of the RMPC trajectory planner, the choice of the look-ahead distance d_{la} provides a certain degree of freedom to tune the aggressiveness of the resultant κ_{ref} . Thus, the choice of d_{la} is made to achieve a balance between accuracy, safety, and comfort while maintaining lateral-yaw stability (i.e., accurate tracking of safe path while maintaining stability). A transient and dynamic manoeuvre like overtaking (involving changes in longitudinal velocity and curvature) makes it difficult to measure the actual curvature followed by the SV during the manoeuvre. However, at each sampling instant the

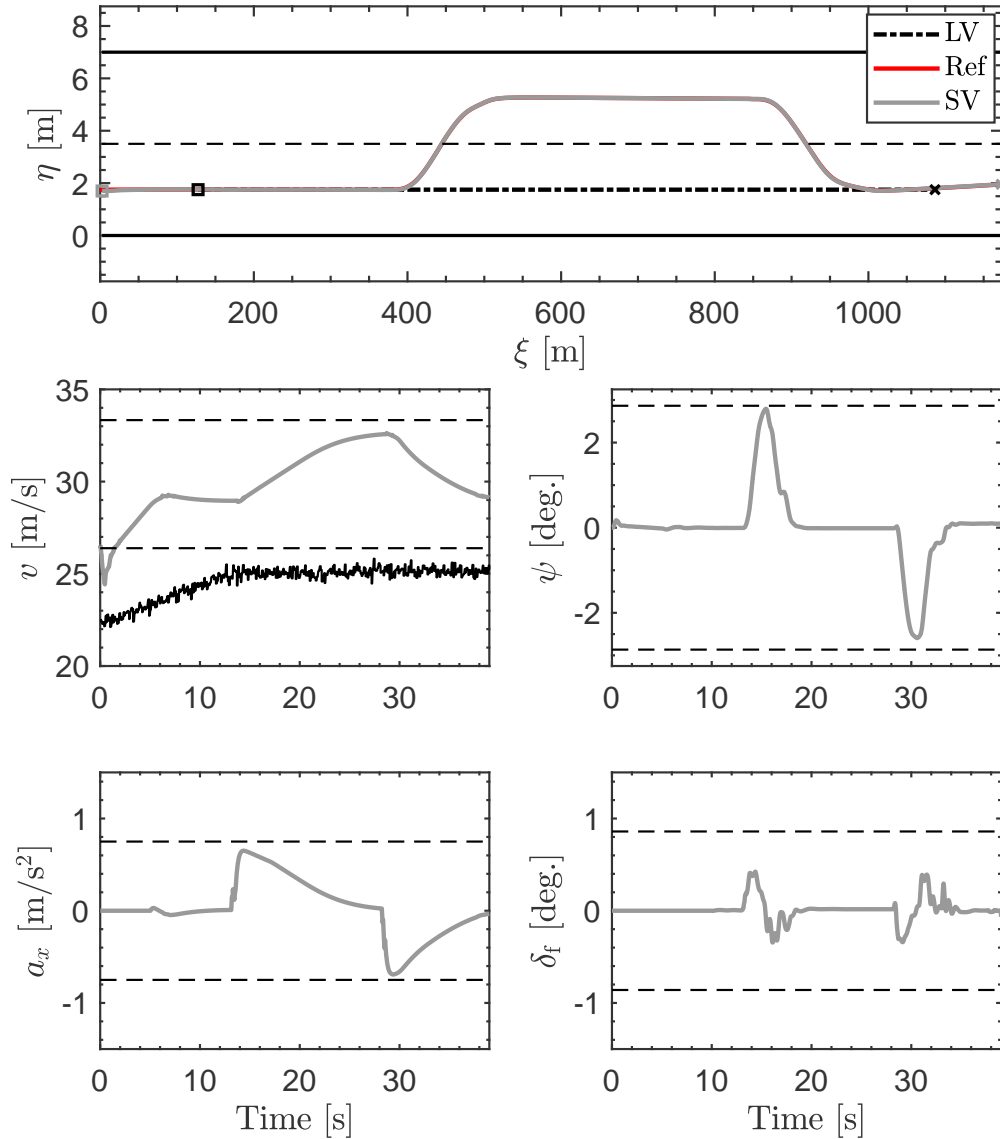


Figure 5.12 Simulation Results: SV and LV trajectories, longitudinal velocity v , heading angle ψ , longitudinal acceleration a_x , and steering angle δ_f for a high-speed overtaking manoeuvre. **Note:** (- -) are the system constraints

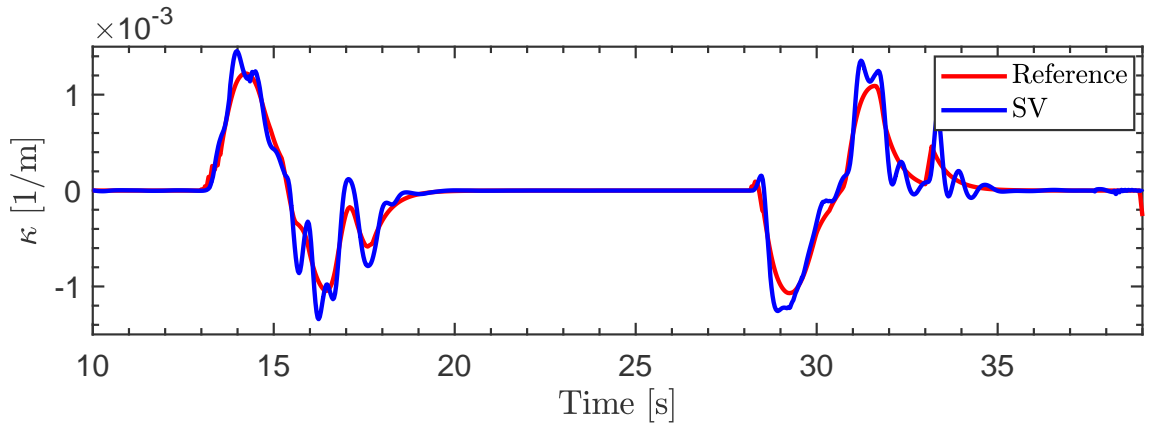


Figure 5.13 Simulation Results: comparison of reference curvature κ_{ref} and SV's estimated curvature $\kappa \approx r_z/v$ during the overtaking manoeuvre

instantaneous curvature being followed by the SV can be approximated by $\kappa \approx r_z/v$ and is also plotted in Figure 5.13. The plots shows that this estimated curvature follows the reference curvature but the tracking accuracy deteriorates whenever there is a transition in the reference signal. The presence of the large(r) peaks in the estimated curvature can be attributed to the change in the yaw-rate r_z of the vehicle as it transitions from lane-following to lane-changing and vice-versa and not to longitudinal velocity v which has much slower dynamics in Figure 5.12. The existence of such peaks in r_z might raise concerns of lowered comfort for the occupants but since the amplitude is a small fraction of the overall magnitude they do not have a negative effect on the evolution of the heading-angle of the vehicle as seen in Figure 5.12.

The curvature signal in Figure 5.13 is the reference for the lateral tracking controller to compute appropriate steering action to track the reference curvature. The closed-loop performance of the path-tracking states of the EMRAC controller is illustrated in Figure 5.14. For the first lane-change manoeuvre which takes place around 15 s the lateral velocity v_y of the SV has an amplitude comparable to the reference model signal but has some oscillations which are not present in the reference model signal, see Figure 5.14(a). On the other hand, for the second lane-change around the 30 s mark the oscillations are missing but the magnitude of error between the SV signal and the reference model is larger. The absence of the oscillations during the latter part of the simulations show that the adaptive controller has successfully adapted the control gains (K_X , K_I , K_R , and K_N) to counter the modelling errors that exist in the path tracking model due to (i) parameter (e.g., tire/axle lateral stiffness coefficients) miss-matches, (ii) un-modelled roll dynamics, etc. Furthermore, the higher longitudinal velocity of the SV (when compared to v_{nom}) at the start of the

second lane-change results in a larger lateral velocity response for steering input (see Figure E.1 in Appendix E) which explains the increased magnitude of error in v_y tracking during the initial phase of the second-lane change. On the other hand, the tracking of the yaw-rate reference model is much better during the entire manoeuvre as illustrated in Figure 5.14(b) which shows that this vehicle state is less sensitive to longitudinal velocity variations, see Figure E.2. Moreover, as expected some oscillations in the SV's r_z signal as predicted from Figure 5.13 plot can be seen but their magnitude is a small fraction of the actual value and thus does not pose any problems for the yaw stability and/or occupants comfort. The plot of the lateral error state η_e in Figure 5.14(c) shows that while the behaviour of the SVs signal and the reference model's signal are largely similar the magnitude of lateral error in the SV's trajectory is substantially greater. This is mainly due to larger v_y of the SV as discussed above which increases the deviation of the vehicle from the reference circular path. However, it is noteworthy that this error does not exceed 5 cm which is below the accuracy of vehicle localisation techniques [169] and considering the scale of distances between the SV and other obstacles (e.g., traffic vehicles, lane/road boundaries) does not pose any safety risk anytime during the entire manoeuvre. Finally, the heading angle error ψ_e tracking can be seen in Figure 5.14(d). The discrepancies in tracking the heading angle error of the reference model can be traced to the reasons discussed for the miss-matches in the v_y and r_z signals in Figures 5.14(a) and 5.14(b). Additionally, ignoring the vehicle and tire side-slip during controller design also contributes towards miss-matches between the SV and the reference model as at such high-speeds even gentle cornering manoeuvres give rise to non-zero vehicle and tire slip angles.

The results discussed in this section so far demonstrate the ability of the proposed control architecture to successfully perform a high-speed overtaking manoeuvre under nominal circumstances. However, in real world scenarios an autonomous vehicle might encounter conditions that have not (or cannot) be considered for controller development. As a result, it is important to study the robustness of the closed-loop system when subjected to un-modelled environmental disturbances. The conditions are modified as follows; (i) both the lanes are assumed to have a wet surface running along its length and extending halfway along the width giving rise to reverse ordered split- μ conditions for each lane and (ii) a wind gust blowing at 16 m s^{-1} from left to right hits the SV (in the fast lane) just as it draws level with the LV (in the slow lane) thus forcing the SV into the path of the LV. Therefore, when the SV is travelling in the slow lane the left tires are under low friction conditions and while travelling on the fast lane the right tires are under low friction conditions. Moreover, the sudden wind gust is a sudden disturbance acting on the system that might cause a safety breach if not countered by the controller(s). The rest of the

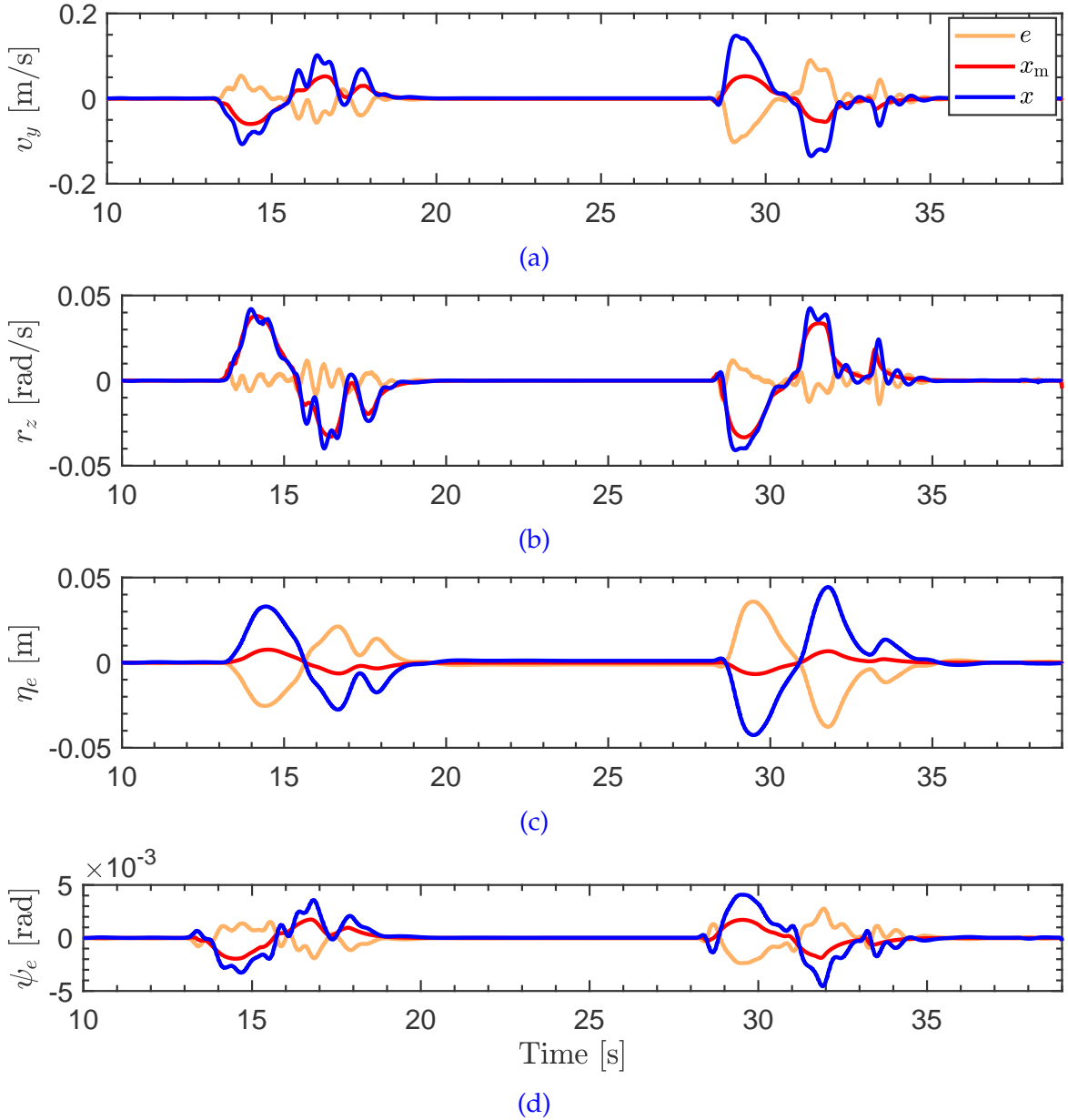


Figure 5.14 Simulation results, evolution of the internal states of the EMRAC controller during the overtaking manoeuvre; (a) lateral velocity v_y ; (b) yaw-rate r_z ; (c) lateral error η_e ; (d) heading angle error ψ_e

scenario is unchanged (including the tuning and initialisation parameters for both the planning and tracking controller) and the results obtained from the closed-loop simulation are presented below.

A plot comparing the trajectory followed by the SV while performing the overtaking manoeuvre under nominal and the split- μ conditions is illustrated in Figure 5.15. These trajectories plotted in the LV frame of reference (O-frame) show that the SV performs very similar manoeuvres for each run. The two lane-changes performed during the split- μ conditions are alike and also match the lane-change manoeuvre from the nominal conditions demonstrating that the closed-loop control structure can cope with variations in road friction changes. Furthermore, the plot shows that the effect of the wind gust is successfully suppressed by the closed-loop controller and the lateral deviation of the SV from the lane centre is marginal and does not cause the SV to drift back into the slow lane which may lead to safety concerns.

The two vehicle models used in Sections 3.3 and 4.4 to describe the dynamics of the vehicle are based on the assumption that the tyres of the vehicle are in the linear region of operation. This simplification was made due to the fact that during normal highway driving a vehicle rarely (if ever) is subjected to limit-handling scenarios which result in the tyre operating in non-linear regimes resulting in saturation of tyre forces. The validity of these assumption can be assessed by observing the lateral acceleration a_y of the subject vehicle during the overtaking manoeuvre in nominal and split- μ conditions shown in Figure 5.16. Since, the tyre remains in the linear operation for low values of lateral acceleration ($|a_y| \leq 0.4 g$ [66, 107]), the plot demonstrate that this assumption (and requirement) is comfortably fulfilled for both conditions. Moreover, the large wind-gust around the 25 s mark is successfully tackled without the subject vehicle developing a large lateral acceleration which

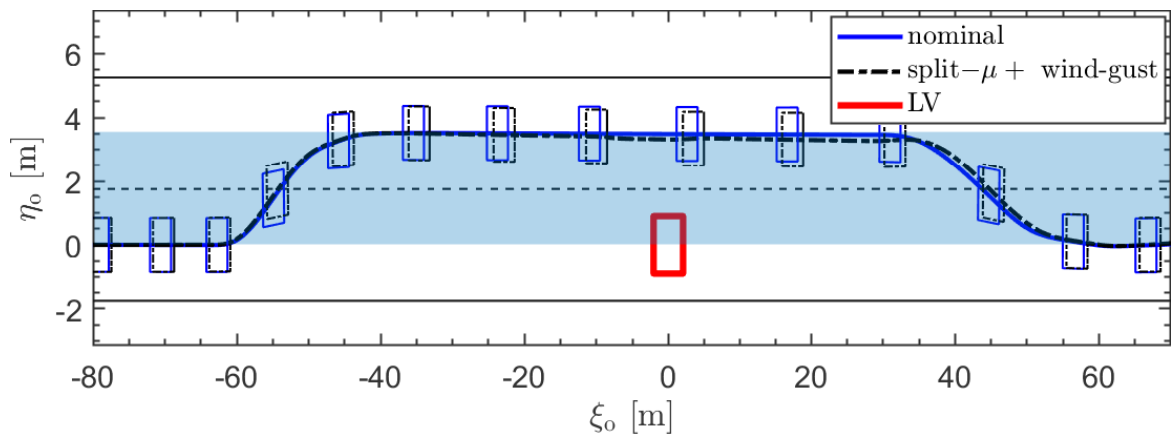


Figure 5.15 Simulation results: trajectory of the subject vehicle (SV) during an overtaking manoeuvre in the lead vehicle (LV) frame of reference (ξ_0, η_0) .

signifies that the tyre remains within the linear region of operation even during sudden disturbance.

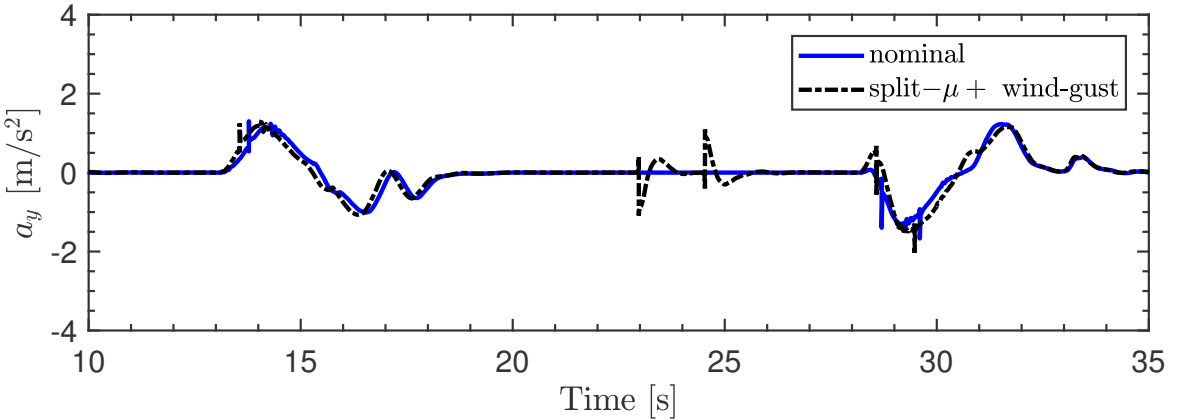


Figure 5.16 Simulation results: evolution of the lateral acceleration a_y of the subject vehicle (SV) during an overtaking manoeuvre.

A comparison of the control action during the two overtaking manoeuvres is shown in Figure 5.17(a). The plot shows that adaptations in the control action that are undertaken to achieve consistent overtaking despite the variations in external environment. The plot shows that primary differences are around the 25 s mark where there is aggressive steering action to counter the effect of the wind-gust. Moreover, towards the end of the simulation there is additional steering action to ensure the SV stays in the centre of the lane.

The magnitude of the integral part of the gains K_X , K_R , and K_I denoted as $\|\phi\|$ is plotted in Figure 5.17(b). This plot shows that the controller gain which is initialised within the σ -modification limits is indistinguishable for the two simulation runs. Moreover, the adaptations in $\|\phi\|$ for the different sub-manoeuvres is not visible in the plot and only the slow decay of the gain towards the lower limit can be observed. Consequently, it can be inferred that the closed-loop tracking performance of the SV in the nominal conditions (with varying velocity) and adverse weather conditions (with additional environmental disturbances) can be attributed to the evolution of the control gain for the switching action $\|\phi_N\|$ in Figure 5.17(c) thus providing another opportunity to verify the (i) benefit of a adaptive switching action for maintaining closed-loop performance and (ii) ability of the σ -modification strategy at preventing unbounded growth of the control gain. The plot illustrates that right from the initiation of the first lane-change before 15 s, the evolution of $\|\phi_N\|$ is slightly different for the split- μ case. The rapid increase in $\|\phi_N\|$ beyond the limits around 25 s corresponds to sudden disturbance that is encountered (i.e., wind-gust) and the gradual decay in the value of $\|\phi_N\|$ shows that the σ -modification strategy

performs as expected in preventing unbounded evolution of the control gain. For the remainder of the simulation the value of $||\phi_N||$ traces a similar shape with the difference being that the gain once again increases beyond the limits for the split- μ condition only to gradually fall back to a value within the designed limits. These results demonstrate the advantage of including the switching control action within the control law to counter sudden un-modelled disturbances that the system (here SV) may encounter.

The numerical results presented in this section demonstrate that the proposed closed-loop hierarchical motion control architecture from Figure 5.11 is applicable for autonomous trajectory planning and trajectory tracking for complex high-speed manoeuvre such as overtaking. These additional results build on top of the capability for trajectory planning shown in Chapter 3 [93, 94] and trajectory tracking shown in Chapter 4 [122]. This coupling of motion planning and control was presented in detail and the results show its capability at achieving autonomous high-speed overtaking not only under nominal situations but also suitable in adverse weather and road conditions.

5.6 Summary

The main objective of this chapter was to validate the combined trajectory planning from Chapter 3 and tracking control from Chapter 4 architecture for autonomous high-speed overtaking. This was achieved by incrementally moving towards a hierarchical closed-loop motion control framework. The first task was the inclusion of steering actuator dynamics within the lateral tracking control framework which was achieved by approximating the pure time-delay dynamics of the actuator system using 1st-order Padé approximation. Next, this updated lateral tracking controller was combined with a geometric local path re-planning strategy to demonstrate its ability to be part of a multi-level control framework. The simulation studies involving autonomously following a desired path around a test track validated the closed-loop control framework. Moreover, further simulations were performed to show the robustness of the lateral tracking controller to variations in the steering actuator dynamics. Eventually, the knowledge acquired over the previous two steps was assimilated and utilised to realise the two-level trajectory planning and trajectory tracking control architecture for autonomous high-speed overtaking. Simulations performed in high-fidelity software platforms successfully present the synergistic coupling of the two controller resulting in generation of safe and feasible trajectories and accurate tracking for performing high-speed overtaking manoeuvres. Additionally, further simulations in environments with low-friction and cross-winds

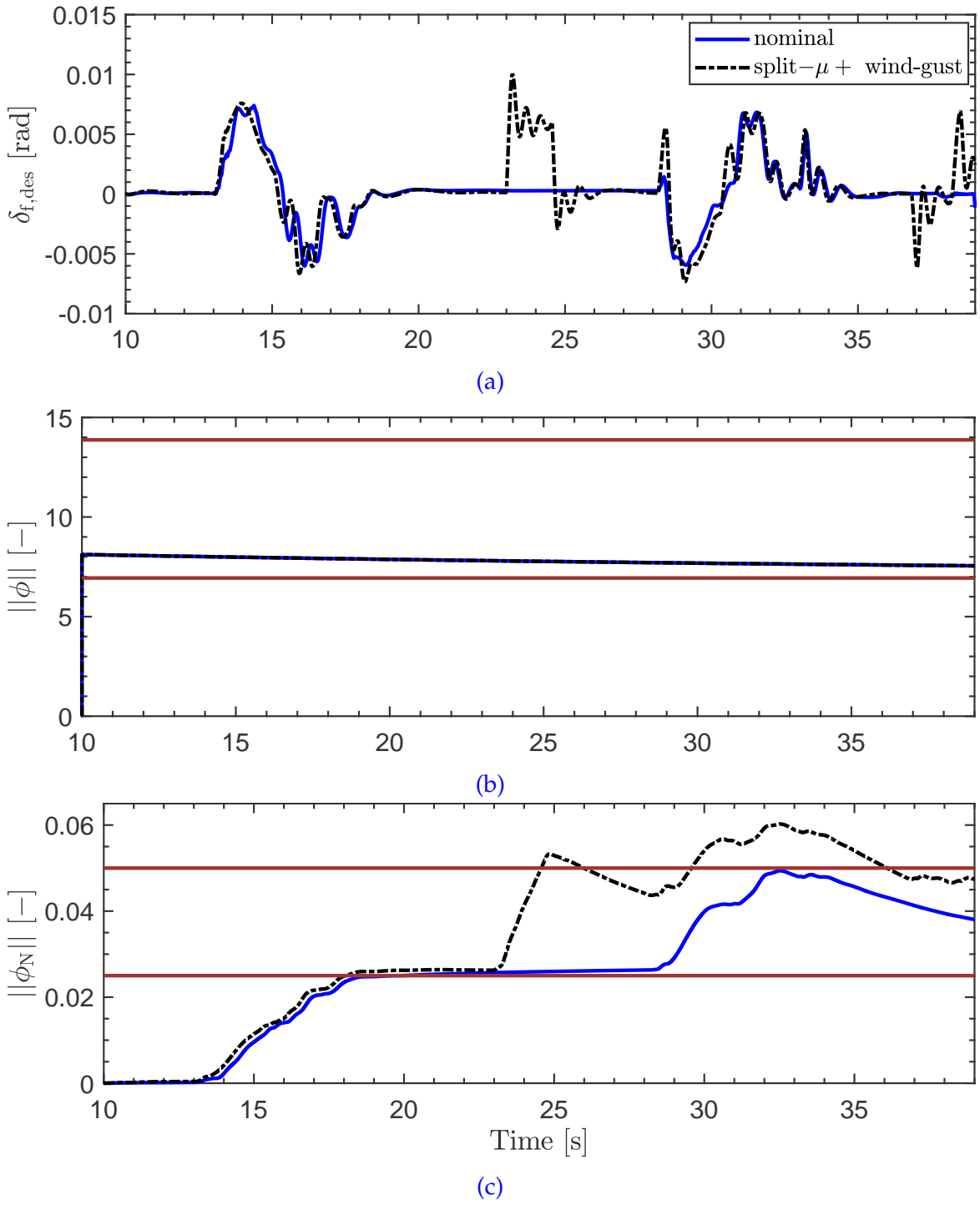


Figure 5.17 Simulation results, comparison while overtaking in nominal and low-friction conditions; (a) control action δ_f ; (b) norm of gain for continuous part of control action $\|\phi\|$; (c) norm of gain for switching action $\|\phi_N\|$

Combined Motion Planning & Control

was performed to assess the robustness of the control architecture to environmental disturbances. The results showed that the proposed framework was able to match the performance obtained during nominal conditions thereby highlighting the ability of the proposed controller to perform suitably even under challenging conditions that might be encountered in real world scenarios.

Conclusions & Recommendations

उत्तिष्ठत जाग्रत प्राप्य वरान् निवोधत ।
क्षुरस्य धारा निशिता दुरत्यया दुर्गं पथस्तत् कवयो वदन्ति ॥ १:३:१४ ॥

— कथा उपनिषद्

Arise, awake; having reached the great, learn; the edge of a razor is sharp and
impassable; that path, the intelligent say, is hard to go by.

— *Kathā Upaniṣad 1:3:14*

6.1 Conclusions

 RECENT advancements in development of intelligent systems have propelled autonomous vehicles towards the forefront of research and development. Incremental improvements made in each aspect of self-driving functionalities makes one believe that fully autonomous vehicles may prove to be veritable choice for future transportation systems. This thesis aims to contribute towards this goal by attempting to tackle the following as the main research problem.

Design & develop a closed-loop control architecture that enables a vehicle to perform overtaking manoeuvres at high-speeds in a safe and acceptable manner.

Since autonomous high-speed manoeuvring is a safety critical functionality with many complexities, the algorithms for generation of a path for overtaking and following the given path are designed separately. This allowed the main research problem to be divided into the following objectives.

- Develop a trajectory planning framework to generate collision-free and feasible trajectories for high-speed overtaking
- Design a generic steering controller for trajectory tracking to perform typical highway driving manoeuvres

Conclusions & Recommendations

- *Combine the planning and tracking controller to formulate an integrated motion control architecture with the capability of performing a high-speed overtaking manoeuvre autonomously*

The 21st century has seen a flurry of development of different functionalities related to autonomous driving architectures. This multi-pronged effort undertaken by engineers, researchers, and automotive manufacturers across the globe has helped in creating a plethora of innovative control strategies for solving the motion planning & control problem of an autonomous vehicle. In Chapter 2, a literature review on the state-of-the-art of two important aspects namely trajectory planning and trajectory tracking for autonomous overtaking was presented. An important finding of the literature review was that an overtaking manoeuvre is governed by factors such as traffic conditions, speed limits, road conditions, vehicle velocities, etc. and due to the innumerable variations present in these factors each instance of this manoeuvre is unique and not easy to standardise. This review illustrated that guaranteeing collision-free paths, respecting safety margins at all times, and incorporation of vehicle dynamics together form the primary requirements for any trajectory planning algorithm particularly in high-speed environments. Additionally, the random nature of real-world driving conditions resulting in environmental uncertainty poses a considerable challenge that can be mitigated by vehicle-to-everything (V2X) communication systems. Furthermore, the review of path tracking control techniques highlighted that maintaining tracking accuracy for manoeuvres performed over a large range of vehicle velocities, robustness against system and external uncertainties, and lateral-yaw stability are pivotal requirements. The review also showed that, trajectory planning and trajectory tracking controllers are combined in a hierarchical manner within an autonomous driving architecture and it is necessary that the resultant complex system can deliver its performance in a safe, dependable, and robust manner under diverse driving conditions.

The insights gained from the review in Chapter 2 were utilised to propose and develop a modular trajectory planning architecture for autonomous overtaking in Chapter 3. The first part is situational awareness of the vehicle which was created using artificial potential field based functions. This potential field function was created using environmental information (e.g., road limits, lane limits, speed limits, etc.) and traffic conditions (e.g., relative velocity with subject vehicle, dimension, traffic vehicle states, etc.) to generate a local risk map for the vehicle which is continuously updated. The risk map which provides information of the high and low risk regions around a subject vehicle was combined with reachability set of a vehicle to identify a safe driving corridor and provide target positions on road for the vehicle to travel on. Additionally, the potential field were also utilised to generate

6.1 Conclusions

collision avoidance constraints that can be used to ensure collision-free behaviour for the generated trajectories. Two different trajectory planners both using a Model Predictive Control (MPC) formulation were created to compute safe and feasible trajectories that steer the vehicle along the generated target points. The two MPC controllers namely nominal MPC and robust MPC utilise the collision avoidance constraints and the target points to generate collision-free trajectories in the form of coordinate position, heading angle, and longitudinal velocity signals for the vehicle. A positive invariant set of steady-state conditions of the vehicle was computed that is used as terminal set constraints for both the MPC formulations to guarantee that the generated trajectory is always kept within safe bounds. Additionally, the robust MPC based planner also considers the close coupling between the lateral-yaw dynamics of the vehicle and its longitudinal velocity by modelling the interaction as an additive disturbance. The modular nature of the trajectory planning architecture was illustrated by pairing the local risk map and target generation functionalities with both the MPC formulations to simulate autonomous high-speed overtaking in highway scenarios. The results of these simulations demonstrated the ability of the proposed architecture to generate safe and collision-free trajectories. The trajectory planning using the RMPc approach was found to be more suitable as it generated feasible trajectories for a larger range of longitudinal velocities.

The design of a lateral controller for manipulating steering inputs to follow a generic trajectory was discussed in Chapter 4. This controller is based on an Enhanced Model Reference Adaptive Control (EMRAC) algorithm to maintain closed-loop performance confined to stable reference dynamics despite system uncertainties, external disturbances, changing longitudinal velocity, etc. Moreover, the concern of unbounded drift in controller gains was tackled by extending the implementation of a σ -modification strategy for limiting evolution of gains to the switching control action as well. The resultant closed-loop architecture utilises an adaptive law to modify the controller gains to manipulate the steering input for following a given reference path curvature with minimum position and heading angle errors while ensuring the lateral-yaw dynamics of the vehicle are stable. Furthermore, the ultimate boundedness of the net closed-loop system (i.e., lateral controller and adaptive law for controller gain) was proven by using the mathematical framework based on an extended Layapunov theory for discontinuous systems. The proposed trajectory tracking controller and the net closed-loop system was numerically validated by performing a number of diverse manoeuvres under in a high-fidelity simulation environment. These studies demonstrated that the proposed controller was successful at maintaining the tracking performance of the vehicle while performing manoeuvres such as lane-keeping, lane-changing, etc. at high-speeds even when subjected to large external disturbances such as wind gusts,

Conclusions & Recommendations

low friction surfaces, additional mass in vehicle, etc. These results showed that the proposed control algorithm and the closed-loop architecture is a feasible candidate for a steering controller for autonomous highway driving applications.

Finally in Chapter 5 the trajectory planner and the trajectory tracker were combined to determine if the combination presents a feasible and robust motion control architecture for performing autonomous overtaking. For this, first the lateral tracking controller from Chapter 4 was extended by augmenting it with steering actuator dynamics. It is noteworthy that while the actuator dynamics are represented as a pure delay system, a Padé approximation was used to estimate these dynamics within the formulation of the EMRAC tracking controller. Next, this updated trajectory tracking controller was combined with a basic geometric path planner to demonstrate the tracking controller can be a part of a larger autonomous driving architecture. Numerical simulations were performed to demonstrate the ability of this control architecture to achieve accurate path tracking even when subjected to variations in the dynamics of the actual steering system. Consequently, the final step was to combine the RMPC based trajectory planning algorithm with the EMRAC lateral tracking controller to achieve a seamless hierarchical closed-loop architecture. This was done by designing an interface that transformed the reference trajectory generated by the RMPC (i.e., coordinate position, heading angle, and velocity) into an equivalent curvature signal to act as the reference for the lateral tracking controller. The efficacy of this closed-loop architecture for performing autonomous high-speed overtaking manoeuvres was demonstrated on a high-fidelity simulation platform. Additionally, the system was also tested by simulating severe weather conditions such as split- μ and wind gusts to assess its behaviour beyond nominal operating conditions. The results illustrated proposed closed-loop architecture ensured (i) feasibility of generated trajectory, (ii) collision free manoeuvring, (iii) smooth control action, and (iv) lateral-yaw stability even when performing a high-speed manoeuvre autonomously even when subjected to sudden and large external disturbances.

In summary, the main research problem of this thesis was to design a hierarchical control architecture for a vehicle to perform autonomous overtaking manoeuvres. The trajectory planning controller is designed using a modular system that uses potential fields to identify the safe driving zones around a vehicle and a robust MPC framework to generate a feasible trajectory that guides the vehicle through the safe zones. Next, a path tracking controller is designed using an EMRAC with bounded gains to accurately follow a reference path using controlled manipulation of the front wheel angle. Finally, the two controllers are combined and the resultant closed-loop systems ability to successfully perform high-speed overtaking manoeuvres in nominal and also severe weather conditions is demonstrated.

6.2 Recommendations

Certain simplifications and assumptions were made during the research to tackle the problems. Moreover, additional challenges were discovered over the course of this work. These simplifications, assumptions, and new challenges are culminated to come up with a list of recommendations for future research directions in this field.

- The vehicle's situational awareness of safe and unsafe zones in its vicinity was computed using potential functions based on the environmental boundaries and states of the obstacles. This information can be made richer ensuring the potential field functions are dynamically updated based on changes in weather, lighting conditions, traffic density, etc.
- The combination of artificial potential field for situational awareness and reachability sets to calculate safe target points provides good results for safe trajectory planning. However, this method is primarily based on heuristics and in future more sophisticated techniques (e.g., based on probabilistic, stochastic, data driven, etc. methods to capture environmental interactions) can be used to couple this functionality with the decision making module of an autonomous vehicle to achieve better coupling with the self-driving software stack.
- Currently, the longitudinal velocity reference signal is computed with the intent of maintaining a uniform velocity over the entire MPC prediction horizon. However, this approach can be augmented with the requirements of vehicle energy optimisation and powertrain efficiency optimisations to compute a reference longitudinal velocity profile that fulfils the safety as well as energy efficiency demands.
- The non-linear relation between the lateral-yaw and longitudinal dynamics of a vehicle were represented using a convex disturbance polyhedron within the RMPC formulation. The size of this polyhedron increases rapidly as a larger range of velocities are considered. Currently, a controller designed using pole-placement techniques was used to limit the increase in the size of this polyhedron. Future work can focus on improving the design of this controller to prevent unbounded increase in the size of the disturbance polyhedron for a larger range of vehicle velocities.
- The uncertainty sets that are used within the RMPC formulation lead to a conservative controller design. The use of data driven techniques to dynamically compute adjustable uncertainty sets can capture the deviation between the nominal dynamics and the actual system in a more realistic manner paving way to design of controllers that are less conservative.

Conclusions & Recommendations

- The reference model for the EMRAC design was obtained using a very basic optimisation routine. There is scope to improve this technique further by shaping the response of each state in the reference model dynamics by considering the desirable closed-loop behaviour of the following; (i) lateral-yaw dynamics, (ii) error tracking, and (iii) steering actuator dynamics.
- The ultimate boundedness of the closed-loop system for the EMRAC controller was proven for a single-input-multi-output (SIMO) system. However, to make the proposed control law more applicable for general multi-input-multi-output (MIMO) systems the mathematical treatment to prove the ultimate boundedness can be expanded to prove its validity for all combinations of input and output dimensions. Generally, for autonomous vehicles, lateral tracking and lateral/yaw stability are handled by separate control loops. However, the development of a MIMO EMRAC scheme provides a possible approach to unite path tracking (i.e., steering control) and lateral/yaw stabilisation (i.e., torque vectoring) within a single closed-loop control framework.
- The overtaking manoeuvres simulated in Chapters 3 and 5 were performed while travelling on straight roads. However, highway roads can also have gentle bends (with tightest radius approximately 750 m) where overtaking is allowed and thus the next logical step is to test and validate the proposed closed-loop architecture on curved roads.
- Finally, the results of individual controller schemes from Chapters 3 and 4 and the overall control architecture from Chapter 5 represent the initial results of the proposed techniques. In future they should be tested under more challenging driving scenarios which eventually lead towards experimental validation of the individual functionalities and the overall hierarchical architecture.

6.3 Closing Remarks

A generic motion planning and control framework for autonomous vehicles can accelerate the shift towards reliable and trustworthy all-time autonomy in transportation systems. Striving towards the development of such a framework results in gradual expansion in the operating range of an autonomous vehicle. The development of closed-loop architecture for autonomous overtaking in this thesis is one such endeavour to expand self-driving capabilities beyond lane-keeping and distance keeping towards performing manoeuvres such as lane-change, exiting/merging,

6.3 Closing Remarks

collision avoidance, which can be derived from the capabilities and insights gained from an overtaking manoeuvre.

References

- [1] Ricky W Butler and George B Finelli. The infeasibility of experimental quantification of life-critical software reliability. 1991.
- [2] Road vehicles — Functional safety. URL <https://www.iso.org/obp/ui/#iso:std:iso:26262:-1:ed-1:v1:en>.
- [3] Philip Koopman and Michael Wagner. Challenges in autonomous vehicle testing and validation. *SAE International Journal of Transportation Safety*, 4(1):15–24, 2016.
- [4] Automated Driving: Levels Of Driving Automation Defined In New SAE International Standard J3016. URL https://www.sae.org/mis/pdfs/automated_driving.pdf.
- [5] Shilp Dixit, Saber Fallah, Umberto Montanaro, Mehrdad Dianati, Alan Stevens, Francis Mccullough, and Alexandros Mouzakitis. Trajectory planning and tracking for autonomous overtaking: State-of-the-art and future prospects. *Annual Reviews in Control*, 45:76–86, 2018. ISSN 1367-5788.
- [6] Azim Eskandarian. *Handbook of Intelligent Vehicles: Vol 2*. Springer, 2012. ISBN 9780857290847.
- [7] T.J. Gordon and M. Lidberg. Automated driving and autonomous functions on road vehicles. *Vehicle System Dynamics*, 53(7):958–994, 2015. ISSN 0042-3114.
- [8] Vicente Milanés, David F. Llorca, Jorge Villagrá, Joshué Pérez, Carlos Fernández, Ignacio Parra, Carlos González, and Miguel A. Sotelo. Intelligent automatic overtaking system using vision for vehicle detection. *Expert Systems with Applications*, 39(3):3362–3373, 2012. ISSN 09574174.
- [9] Benoit Vanholme, Dominique Gruyer, Benoit Lusetti, Sébastien Glaser, and Saïd Mammar. Highly automated driving on highways based on legal safety. *IEEE Transactions on Intelligent Transportation Systems*, 14(1):333–347, 2013. ISSN 15249050.
- [10] P. Petrov and F. Nashashibi. Modeling and Nonlinear Adaptive Control for Autonomous Vehicle Overtaking. *IEEE Transactions on Intelligent Transportation Systems*, 15(4):1643–1656, 2014. ISSN 1524-9050.

References

- [11] Sara Moridpour, Geoff Rose, and Majid Sarvi. Effect of surrounding traffic characteristics on lane changing behavior. *Journal of Transportation Engineering*, 136(11):973–985, 2010. ISSN 0733-947X.
- [12] Tomer Toledo, Haris Koutsopoulos, and Moshe Ben-Akiva. Modeling Integrated Lane-Changing Behavior. *Transportation Research Record: Journal of the Transportation Research Board*, 1857(03):30–38, 2003. ISSN 0361-1981.
- [13] Jonathan Baber, Julian Kolodko, Tony Noel, Michael Parent, and Ljubo Vlacic. Cooperative autonomous driving: intelligent vehicles sharing city roads. *IEEE Robotics & Automation Magazine*, 12(1):44–49, 2005. ISSN 1524-9050.
- [14] Michael Motro, Alice Chu, Junil Choi, Patricia S. Lavieri, Abdul Rawoof Pinjari, Chandra R. Bhat, Joydeep Ghosh, and Robert W. Heath. Vehicular ad-hoc network simulations of overtaking maneuvers on two-lane rural highways. *Transportation Research Part C: Emerging Technologies*, 72:60–76, 2016. ISSN 0968090X.
- [15] Geertje Hegeman, Karel Brookhuis, and Serge Hoogendoorn. Opportunities of advanced driver assistance systems towards overtaking. *EJTIR*, 5(4):281–296, 2005.
- [16] Christian Thiemann, Martin Treiber, and Arne Kesting. Estimating Acceleration and Lane-Changing Dynamics Based on NGSIM Trajectory Data. *Transportation Research Record: Journal of the Transportation Research Board*, 2088: 90–101, 2008. ISSN 0361-1981.
- [17] Arne Kesting, Martin Treiber, and Dirk Helbing. General Lane-Changing Model MOBIL for Car-Following Models. *Transportation Research Record: Journal of Transportation Research Board*, 1999(1):86–94, 2007. ISSN 0361-1981.
- [18] Nathan Alexander Webster, Takahiro Suzuki, Edward Chung, and Masao Kuwahara. Tactical driver lane change model using forward search. In *Transportation Research Board 86th Annual Meeting*, pages 07–0378, 2007.
- [19] Eleni I. Vlahogianni. Modeling duration of overtaking in two lane highways. *Transportation Research Part F: Traffic Psychology and Behaviour*, 20:135–146, 2013. ISSN 13698478.
- [20] Tzila Shamir. How should an autonomous vehicle overtake a slower moving vehicle: Design and analysis of an optimal trajectory. *IEEE Transactions on Automatic Control*, 49(4):607–610, apr 2004. ISSN 00189286.
- [21] Laurene Claussmann, Ashwin Carvalho, and Georg Schildbach. A path planner for autonomous driving on highways using a human mimicry approach with Binary Decision Diagrams. In *2015 European Control Conference, ECC 2015*, pages 2976–2982, 2015. ISBN 9783952426937.
- [22] Michael Ardel, Constantin Coester, and Nico Kaempchen. Highly automated driving on freeways in real traffic using a probabilistic framework. *IEEE Transactions on Intelligent Transportation Systems*, 13(4):1576–1585, 2012. ISSN 15249050.

- [23] Simon Ulbrich and Markus Maurer. Towards tactical lane change behavior planning for automated vehicles. In *2015 IEEE 18th International Conference on Intelligent Transportation Systems (ITSC)*, pages 989–995, 2015. ISBN 9781467365956.
- [24] James J Jong, Hyuk Park, Han-chieh Chao, and Neil Y Yen. *Advanced Multimedia and Ubiquitous Engineering: Future Information Technology*, volume 2. Springer, 2016. ISBN 9783662478943.
- [25] Alexander Kanaris, Elias B. Kosmatopoulos, and Petros A. Ioannou. Strategies and spacing requirements for lane changing and merging in automated highway systems. *IEEE Transactions on Vehicular Technology*, 50(6):1568–1581, 2001. ISSN 00189545.
- [26] Alireza Khodayari, Ali Ghaffari, Sina Ameli, and Jamal Flahatgar. A historical review on lateral and longitudinal control of autonomous vehicle motions. In *ICMET 2010 - 2010 International Conference on Mechanical and Electrical Technology, Proceedings*, pages 421–429, 2010. ISBN 9781424481019.
- [27] Jürgen Valldorf and Wolfgang Gessner. *Advanced Microsystems Automotive Applications*. Springer, 2006. ISBN 9783540334095.
- [28] Liming Wan, Pongsathorn Raksincharoensak, Kozo Maeda, and Masao Nagai. Lane Change Behavior Modeling for Autonomous Vehicles Based on Surroundings Recognition. *International Journal of Automotive Engineering*, 2:7–12, 2011.
- [29] Keonyup Chu, Minchae Lee, and Myoungho Sunwoo. Local Path Planning for Off-Road Autonomous Driving With Avoidance of Static Obstacles. *IEEE Transactions On Intelligent Transportation Systems*, 13(4):1599–1616, 2012.
- [30] Young Seop Son, Wonhee Kim, Seung Hi Lee, and Chung Choo Chung. Robust multirate control scheme with predictive virtual lanes for lane-keeping system of autonomous highway driving. *IEEE Transactions on Vehicular Technology*, 64(8):3378–3391, 2015. ISSN 00189545.
- [31] Michael Aeberhard, Sebastian Rauch, Mohammad Bahram, Georg Tanzmeister, Julian Thomas, Yves Pilat, Florian Homm, Werner Huber, and Nico Kaempchen. Experience, results and lessons learned from automated driving on Germany’s highways. *IEEE Intelligent Transportation Systems Magazine*, 7(1):42–57, 2015. ISSN 1939-1390.
- [32] Robin Schubert, Karsten Schulze, and Gerd Wanielik. Situation assessment for automatic lane-change maneuvers. *IEEE Transactions on Intelligent Transportation Systems*, 11(3):607–616, 2010. ISSN 15249050.
- [33] Robin Schubert, Christian Adam, Marcus Obst, Norman Mattern, Veit Leonhardt, and Gerd Wanielik. Empirical evaluation of vehicular models for ego motion estimation. *IEEE Intelligent Vehicles Symposium, Proceedings*, (IV):534–539, 2011. ISSN 1931-0587.

References

- [34] Robin Schubert, Eric Richter, and Gerd Wanielik. Comparison and evaluation of advanced motion models for vehicle tracking. *Information Fusion, 2008 11th International Conference on*, (1):1–6, 2008.
- [35] Julian Eggert, Stefan Klingelschmitt, and Florian Damerow. The foresighted driver: Future adas based on generalized predictive risk estimation. In *FAST-zero 2015 Symposium*, pages 93–100, 2015.
- [36] Andreas Lawitzky, Daniel Althoff, Christoph F Passenberg, Georg Tanzmeister, Dirk Wollherr, and Martin Buss. Interactive scene prediction for automotive applications. In *2013 IEEE Intelligent Vehicles Symposium (IV)*, pages 1028–1033, 2013. ISBN 9781467327541.
- [37] Mohammad Bahram, Constantin Hubmann, Andreas Lawitzky, Michael Aeberhard, and Dirk Wollherr. A combined model-and learning-based framework for interaction-aware maneuver prediction. *IEEE Transactions on Intelligent Transportation Systems*, 17(6):1538–1550, 2016. ISSN 15249050.
- [38] Stéphanie Lefèvre, Dizan Vasquez, and Christian Laugier. A survey on motion prediction and risk assessment for intelligent vehicles. *ROBOMECH Journal*, 1(1), 2014. ISSN 2197-4225.
- [39] Radar, Stereo Camera, Ultrasound All-round Protection by Networking Sensors. URL http://www.caricos.com/cars/m/mercedes-benz/2018_mercedes-benz_s-class/images/41.html.
- [40] Yugong Luo, Yong Xiang, Kun Cao, and Keqiang Li. A dynamic automated lane change maneuver based on vehicle-to-vehicle communication. *Transportation Research Part C: Emerging Technologies*, 62:87–102, 2016. ISSN 0968090X.
- [41] Scott Andrews. Vehicle-to-Vehicle (V2V) and Vehicle-to- Infrastructure (V2I) Communications and Cooperative Driving. In *Handbook of Intelligent Vehicles*, pages 1121–1144. Springer, 2012. ISBN 9788578110796.
- [42] Lino Guzzella. Automobiles of the future and the role of automatic control in those systems. *Annual Reviews in Control*, 33(1):1–10, 2009. ISSN 13675788.
- [43] Beomjun Kim, Dongwook Kim, Sungyoul Park, Yonghwan Jung, and Kyongsu Yi. Automated Complex Urban Driving based on Enhanced Environment Representation with GPS / map, Radar, Lidar and Vision. *IFAC-PapersOnLine*, 49(11):190–195, 2016. ISSN 24058963.
- [44] Christos Katrakazas, Mohammed Quddus, Wen-Hua Chen, and Lipika Deka. Real-time motion planning methods for autonomous on-road driving: State-of-the-art and future research directions. *Transportation Research Part C: Emerging Technologies*, 60:416–442, 2015.
- [45] Pairoj Saengpredeekorn and Jakkree Srinonchat. A new technique to define the overtake distance using image processing. In *2009 6th International Conference on Electrical Engineering/Electronics, Computer, Telecommunications and Information Technology*, volume 02, pages 1142–1145, 2009. ISBN 978-1-4244-3387-2.

- [46] Rahul Kala and Kevin Warwick. Motion planning of autonomous vehicles in a non-autonomous vehicle environment without speed lanes. *Engineering Applications of Artificial Intelligence*, 26(5-6):1588–1601, 2013. ISSN 09521976.
- [47] Sébastien Glaser, Benoit Vanholme, Saïd Mammar, Dominique Gruyer, and Lydie Nouvelière. Maneuver-based trajectory planning for highly autonomous vehicles on real road with traffic and driver interaction. *IEEE Transactions on Intelligent Transportation Systems*, 11(3):589–606, 2010. ISSN 15249050.
- [48] Shohei Kitazawa and Tetsuya Kaneko. Control Target Algorithm for Direction Control of Autonomous Vehicles in Consideration of Mutual Accordance in Mixed Traffic Conditions. In *International Symposium on Advanced Vehicle Control 2016*, 2016.
- [49] Ashwin Carvalho, Stéphanie Lefévre, Georg Schildbach, Jason Kong, and Francesco Borrelli. Automated driving: The role of forecasts and uncertainty - A control perspective. *European Journal of Control*, 24:14–32, 2015. ISSN 09473580.
- [50] Georg Schildbach and Francesco Borrelli. Scenario model predictive control for lane change assistance on highways. In *2015 IEEE Intelligent Vehicles Symposium*, pages 611–616, 2015. ISBN 9781467372664.
- [51] Nikolce Murgovski and Jonas Sjöberg. Predictive cruise control with autonomous overtaking. In *IEEE 54th Annual Conference on Decision and Control (CDC)*, 2015, pages 644–649, 2015. ISBN 9783902823625.
- [52] Ashwin Carvalho, Yiqi Gao, Andrew Gray, H Eric Tseng, and Francesco Borrelli. Predictive control of an autonomous ground vehicle using an iterative linearization approach. In *16th International IEEE Conference on Intelligent Transportation Systems (ITSC 2013)*, number ITSC, pages 2335–2340, 2013. ISBN 978-1-4799-2914-6.
- [53] Yiqi Gao, Andrew Gray, H Eric Tseng, and Francesco Borrelli. A tube-based robust nonlinear predictive control approach to semiautonomous ground vehicles. *Vehicle System Dynamics*, 52(6):802–823, 2014. ISSN 0042-3114.
- [54] José E. Naranjo, Carlos González, Ricardo García, and Teresa De Pedro. Lane-change fuzzy control in autonomous vehicles for the overtaking maneuver. *IEEE Transactions on Intelligent Transportation Systems*, 9(3):438–450, 2008. ISSN 15249050.
- [55] Yiqi Gao, Andrew Gray, Janick V Frasch, Theresa Lin, Eric Tseng, J Karl Hedrick, and Francesco Borrelli. Spatial Predictive Control for Agile Semi-Autonomous Ground Vehicles. *Proceedings of the 11th International Symposium on Advanced Vehicle Control*, VD11(2):1–6, 2012.
- [56] Julia Nilsson, Yiqi Gao, Ashwin Carvalho, and Francesco Borrelli. Manoeuvre generation and control for automated highway driving. In *IFAC Proceedings Volumes (IFAC-PapersOnline)*, volume 19, pages 6301–6306. IFAC, 2014. ISBN 9783902823625.

References

- [57] Taehyun Shim, Ganesh Adireddy, and Hongliang Yuan. Autonomous vehicle collision avoidance system using path planning and model-predictive-control-based active front steering and wheel torque control. *Proceedings of the Institution of Mechanical Engineers, Part D: Journal of Automobile Engineering*, 226(6):767–778, 2012. ISSN 0954-4070.
- [58] Liang Ma, Jianru Xue, Kuniaki Kawabata, Jihua Zhu, Chao Ma, and Nanning Zheng. A fast RRT algorithm for motion planning of autonomous road vehicles. In *2014 17th IEEE International Conference on Intelligent Transportation Systems, ITSC 2014*, pages 1033–1038, 2014. ISBN 9781479960781.
- [59] Yoshiaki Kuwata, Gaston A. Fiore, Justin Teo, Emilio Frazzoli, and Jonathan P. How. Motion planning for urban driving using RRT. In *2008 IEEE/RSJ International Conference on Intelligent Robots and Systems, IROS*, pages 1681–1686, 2008. ISBN 9781424420582.
- [60] Ghumman Usman and Faraz Kunwar. Autonomous vehicle overtaking - An online solution. In *Proceedings of the 2009 IEEE International Conference on Automation and Logistics, ICAL 2009*, number August, pages 596–601, 2009. ISBN 9781424447954.
- [61] Usman Ghumman, Faraz Kunwar, and Beno Benhabib. Guidance-Based On-Line Motion Planning For Autonomous Highway Overtaking. *International Journal On Smart Sensing And Intelligent Systems*, 1(2):549–571, 2008.
- [62] Andrew Gray, Yiqi Gao, Theresa Lin, J Karl Hedrick, H Eric Tseng, and Francesco Borrelli. Predictive Control for Agile Semi-Autonomous Ground Vehicles using Motion Primitives. In *2012 American Control Conference (ACC)*, pages 4239–4244, Berkeley, 2012. ISBN 9781457710964.
- [63] Moritz Werling, Julius Ziegler, Sören Kammler, and Sebastian Thrun. Optimal trajectory generation for dynamic street scenarios in a frenét frame. In *2010 IEEE International Conference on Robotics and Automation (ICRA)*, pages 987–993, 2010. ISBN 9781424450381.
- [64] Johan Karlsson, Nikolce Murgovski, and Jonas Sjöberg. Temporal vs. spatial formulation of autonomous overtaking algorithms. In *2016 IEEE 19th International Conference on Intelligent Transportation Systems (ITSC)*, pages 1029–1034, 2016. ISBN 9781509018895.
- [65] Gianluca Cesari, Georg Schildbach, Ashwin Carvalho, and Francesco Borrelli. Scenario Model Predictive Control for Lane Change Assistance and Autonomous Driving on Highways. *IEEE Intelligent Transportation Systems Magazine*, 9(3):23–35, 2017.
- [66] Jason Kong, Mark Pfeiffer, Georg Schildbach, and Francesco Borrelli. Kinematic and Dynamic Vehicle Models for Autonomous Driving Control Design. In *Intelligent Vehicles Symposium (IV), 2015 IEEE*, pages 1094–1099, 2015.
- [67] Georg Schildbach and Elektronische Fahrwerksysteme GmbH. A New Non-linear Model Predictive Control Algorithm for Vehicle Path Tracking. In *International Symposium on Advanced Vehicle Control 2016*, 2016.

- [68] Weria Khaksar, Khairul Salleh Mohamed Sahari, and Tang Sai Hong. Application of Sampling-Based Motion Planning Algorithms in Autonomous Vehicle Navigation. *Autonomous Vehicle*, 2016.
- [69] Michael T. Wolf and Joel W. Burdick. Artificial potential functions for highway driving with collision avoidance. In *Proceedings - IEEE International Conference on Robotics and Automation*, pages 3731–3736, 2008. ISBN 9781424416479.
- [70] Georg Schildbach, Lorenzo Fagiano, Christoph Frei, and Manfred Morari. The scenario approach for Stochastic Model Predictive Control with bounds on closed-loop constraint violations. *Automatica*, 50(12):3009–3018, 2014. ISSN 00051098.
- [71] Ashwin Carvalho, Yiqi Gao, Stephanie Lefevre, and Francesco Borrelli. Stochastic predictive control of autonomous vehicles in uncertain environments. In *Proc. 12th International Symposium on Advanced Vehicle Control*, number November 2016, 2014.
- [72] Florian Damerow, Benedict Flade, and Julian Eggert. Extensions for the Foresighted Driver Model: Tactical lane change, overtaking and continuous lateral control. In *2016 IEEE Intelligent Vehicles Symposium (IV)*, pages 186–193, 2016. ISBN 9781509018215.
- [73] Niall Ohara, Marco Slot, Julien Monteil, Vinny Cahill, and Melanie Bouroche. Towards Evaluating the Benefits of Inter-vehicle Coordination. In *IEEE Conference on Intelligent Transportation Systems, Proceedings, ITSC*, pages 2444–2450, 2015. ISBN 9781467365956.
- [74] Joshué Pérez, Vicente Milanés, Enrique Onieva, Jorge Godoy, and Javier Alonso. Longitudinal fuzzy control for autonomous overtaking. In *2011 IEEE International Conference on Mechatronics, ICM 2011 - Proceedings*, pages 188–193, 2011. ISBN 9781612849836.
- [75] Feng You, Ronghui Zhang, Guo Lie, Haiwei Wang, Huiyin Wen, and Jianmin Xu. Trajectory planning and tracking control for autonomous lane change maneuver based on the cooperative vehicle infrastructure system. *Expert Systems with Applications*, 42(14):5932–5946, 2015. ISSN 09574174.
- [76] Zichao Huang, Qing Wu, Jie Ma, and Shiqi Fan. An APF and MPC combined collaborative driving controller using vehicular communication technologies. *Chaos, Solitons and Fractals*, 89:232–242, 2015. ISSN 09600779.
- [77] Henk Wymeersch, Gabriel Rodrigues De Campos, Paolo Falcone, Lennart Svensson, and Erik G Ström. Challenges for cooperative ITS: Improving road safety through the integration of wireless communications, control, and positioning. In *2015 International Conference on Computing, Networking and Communications (ICNC)*, pages 573–578, 2015. ISBN 9781479969593.
- [78] C. Houben and S. Houben. Endowing advanced driver assistance systems with fault tolerance. *Annual Reviews in Control*, 39:58–67, 2015. ISSN 13675788.

References

- [79] Daniel Watzenig and Bernhard Brandstätter. *Comprehensive Energy Management–Eco Routing & Velocity Profiles*. Springer, 2017. ISBN 9783319025223.
- [80] Rajesh Rajamani. *Vehicle Dynamics and Control*. Springer Science \& Business Media, 2006. ISBN 9780387263960.
- [81] Chang Mook Kang, Seung Hi Lee, and Chung Choo Chung. Comparative evaluation of dynamic and kinematic vehicle models. In *2014 IEEE 53rd Annual Conference on Decision and Control (CDC)*, pages 648–653, 2014. ISBN 9781467360906.
- [82] Noor Hafizah, Amer Hairi, Khisbullah Hudha, and Zulkiffli Abdul. Modelling and Control Strategies in Path Tracking Control for Autonomous Ground Vehicles : A Review of State of the Art and Challenges. *Journal of Intelligent & Robotic Systems*, 86(2):225–254, 2016. ISSN 0921-0296.
- [83] William F Milliken, Douglas L Milliken, et al. *Race car vehicle dynamics*, volume 400. Society of Automotive Engineers Warrendale, 1995.
- [84] Chang-il Kim, Moon-sik Kim, and Kwang-soo Lee. Development of a Full Speed Range Path-following System for the Autonomous Vehicle. In *International Conference on Control, Automation and Systems (ICCAS 2015)*, number 15, pages 710–715, 2015. ISBN 9788993215090.
- [85] Dimitar Filev, Jianbo Lu, and Davor Hrovat. Future mobility: Integrating vehicle control with cloud computing. *American Society of Mechanical Engineers*, 135(3):S18, 2013.
- [86] Jarrod M Snider. Automatic Steering Methods for Autonomous Automobile Path Tracking. *Robotics Institute, Pittsburgh, PA, Tech. Rep. CMU-RITR-09-08*, 2009.
- [87] Aldo Sorniotti, Phil Barber, and Stefano De Pinto. Path Tracking for Automated Driving: A Tutorial on Control System Formulations and Ongoing Research. In *Automated Driving: Safer and More Efficient Future Driving*, pages 71–140. Springer, 2017. ISBN 978-3-319-31893-6.
- [88] Astrid Rupp and Michael Stolz. Survey on Control Schemes for Automated Driving on Highways. In *Automated Driving*, pages 43–69. Springer, 2017. ISBN 978-3-319-31893-6.
- [89] Gilles Tagne, Reine Talj, and Ali Charara. Design and Comparison of Robust Nonlinear Controllers for the Lateral Dynamics of Intelligent Vehicles. *IEEE Transactions on Intelligent Transportation Systems*, 17(3):796–809, 2016. ISSN 15249050.
- [90] T Besselmann and M Morari. Autonomous vehicle steering using explicit LPV-MPC. *2009 European Control Conference*, (1):2628–2633, 2009.

- [91] Salim Chaib, Mariana S Netto, and Said Mammar. Hinf, Adaptive, PID and Fuzzy Control: a Comparison of Controllers for Vehicle Lane Keeping. In *IEEE Intelligent Vehicles Symposium, 2004*, pages 139–144, 2004. ISBN 0-7803-8310-9.
- [92] Mehdi Jalalmaab, Mohammad Pirani, Baris Fidan, and Soo Jeon. Cooperative road condition estimation for an adaptive model predictive collision avoidance control strategy. *IEEE Intelligent Vehicles Symposium, Proceedings, 2016-Augus (Iv)*:1072–1077, 2016.
- [93] Shilp Dixit, Saber Fallah, Umberto Montanaro, Mehrdad Dianati, David Oxtoby, Tom Mizutani, and Alexandros Mouzakitis. Trajectory Planning for Autonomous High-Speed Overtaking using MPC with Terminal Set Constraints. In *2018 21st International Conference on Intelligent Transportation Systems (ITSC)*, pages 1061–1068, 2018.
- [94] Shilp Dixit, Umberto Montanaro, Mehrdad Dianati, David Oxtoby, Tom Mizutani, Alexandros Mouzakitis, and Saber Fallah. Trajectory planning for autonomous high-speed overtaking in structured environments using robust mpc. *IEEE Transactions on Intelligent Transportation Systems*, 2019.
- [95] P Raksincharoensak, T Ehira, K Shimono, and Y Tagawa. Autonomous Vehicle Trajectory Planning and Control Based on Virtual Disturbance Compensation via Simulation of Feedback Control Systems. In *International Symposium on Advanced Vehicle Control 2016*, 2016.
- [96] G Franze and W Lucia. A Receding Horizon Control Strategy for Autonomous Vehicles in Dynamic Environments. *IEEE Transactions on Control Systems Technology*, 24(2):695–702, 2016. ISSN 10636536.
- [97] Julia Nilsson, Paolo Falcone, Mohammad Ali, and Jonas Sjöberg. Receding horizon maneuver generation for automated highway driving. *Control Engineering Practice*, 41:124–133, 2015. ISSN 09670661.
- [98] Jingjing Jiang and Alessandro Astolfi. Shared-Control for a Rear-Wheel Drive Car: Dynamic Environments and Disturbance Rejection. *IEEE Transactions on Human-Machine Systems*, 47(5):723–734, 2017. ISSN 21682291.
- [99] Jingjing Jiang, Pierluigi Di Franco, and Alessandro Astolfi. Shared Control for the Kinematic and Dynamic Models of a Mobile Robot. *IEEE Trans. Contr. Sys. Techn.*, 24(6):2112–2124, 2016.
- [100] Daniel Limón, Ignacio Alvarado, Teodoro Alamo, and Eduardo F Camacho. MPC for tracking piecewise constant references for constrained linear systems. *Automatica*, 44(9):2382–2387, 2008. ISSN 14746670.
- [101] Ignacio Alvarado, Daniel Limón, Teodoro Alamo, Mirko Fiacchini, and Eduardo F Camacho. Robust tube based MPC for tracking of piece-wise constant references. In *2007 46th IEEE Conference on Decision and Control*, pages 1820–1825, 2007. ISBN 1424414989.

References

- [102] D. Limon, I. Alvarado, T. Alamo, and E. F. Camacho. Robust tube-based MPC for tracking of constrained linear systems with additive disturbances. *Journal of Process Control*, 20(3):248–260, 2010. ISSN 09591524.
- [103] Jan Marian Maciejowski. *Predictive control: with constraints*. Pearson education, 2002.
- [104] Andrey Fedotov, Valerii Patsko, and Varvara Turova. Reachable Sets for Simple Models of Car Motion. In *InTech. Recent Advances in Mobile Robotics*. IntechOpen, 2011.
- [105] Thomas D Gillespie. *Fundamentals of Vehicle Dynamics*. SAE International, 1997.
- [106] Rajesh Rajamani. Lateral vehicle dynamics. In *Vehicle Dynamics and Control*, chapter 2, pages 15–46. 2012. ISBN 9780387263960.
- [107] Philip Polack, Florent Altche, Brigitte DAndrea-Novel, and Arnaud De La Fortelle. The kinematic bicycle model: A consistent model for planning feasible trajectories for autonomous vehicles? In *IEEE Intelligent Vehicles Symposium*, pages 812–818, 2017. ISBN 9781509048045.
- [108] K. M. Madås, D., Nosratinia, M., Keshavarz, M., Sundström, P., Philppsen, R., Eidehall, A., & Dahlén. On path planning methods for automotive collision avoidance. In *Intelligent Vehicles Symposium (IV)*, pages 931–937, 2013. ISBN 9783902823625.
- [109] Alexander Brown and Sean Brennan. On the required complexity of vehicle dynamic models for use in simulation-based highway design. *Journal of Safety Research*, 49(February):105–112, 2014. ISSN 00224375.
- [110] James Blake Rawlings and David Q Mayne. *Model predictive control: Theory and design*. Nob Hill, 2009.
- [111] Sasa V Rakovic, Eric C Kerrigan, Konstantinos I Kouramas, and David Q Mayne. Invariant approximations of the minimal robust positively invariant set. *IEEE Transactions on Automatic Control*, 50(3):406–410, 2005.
- [112] Wilbur Langson, Ioannis Chryssochoos, SV Raković, and David Q Mayne. Robust model predictive control using tubes. *Automatica*, 40(1):125–133, 2004.
- [113] David Q Mayne, Maria M Seron, and SV Raković. Robust model predictive control of constrained linear systems with bounded disturbances. *Automatica*, 41(2):219–224, 2005.
- [114] Saša V Raković, Basil Kouvaritakis, Rolf Findeisen, and Mark Cannon. Homothetic tube model predictive control. *Automatica*, 48(8):1631–1638, 2012.
- [115] Elham Semsar-Kazerooni, Jan Verhaegh, Jeroen Ploeg, and Mohsen Alirezaei. Cooperative adaptive cruise control: An artificial potential field approach. In *2016 IEEE Intelligent Vehicles Symposium (IV)*, pages 361–367, 2016. ISBN 978-1-5090-1821-5.

- [116] E Semsar-Kazerooni, K Elferink, J Ploeg, and H Nijmeijer. Multi-objective platoon maneuvering using artificial potential fields. In *20th World Congress of the International Federation of Automatic Control*, pages 15571–15576, 2017.
- [117] Richard Volpe and Pradeep Khosla. Manipulator Control with Superquadric Artificial Potential Functions: Theory and Experiments. *IEEE Transactions on Systems, Man and Cybernetics*, 20(6):1423–1436, 1990. ISSN 21682909.
- [118] Julia Nilsson. *Automated Driving Maneuvers - Trajectory Planning via Convex Optimization in the Model Predictive Control Framework*. PhD thesis, 2016.
- [119] Jacopo Guanetti, Yeojun Kim, and Francesco Borrelli. Control of connected and automated vehicles: State of the art and future challenges. *Annual Reviews in Control*, (May), 2018. ISSN 1367-5788.
- [120] Jorge L Garriga and Masoud Soroush. Model predictive control tuning methods: A review. *Industrial & Engineering Chemistry Research*, 49(8):3505–3515, 2010.
- [121] Gesner A Nery Júnior, Márcio A F Martins, and Ricardo Kalid. A PSO-based optimal tuning strategy for constrained multivariable predictive controllers with model uncertainty. *ISA transactions*, 53(2):560–567, 2014.
- [122] Shilp Dixit, Umberto Montanaro, Mehrdad Dianati, Alexandros Mouzakitis, and Saber Fallah. Integral mrac with bounded switching gain for autonomous vehicle lateral tracking. *IEEE Transactions on Control Systems Technology*, under review.
- [123] Steven E. Shladover. PATH at 20—History and major milestones. *IEEE Transactions on Intelligent Transportation Systems*, 8(4):584–592, 2007. ISSN 15249050.
- [124] Sebastian Thrun, Mike Montemerlo, Hendrik Dahlkamp, David Stavens, Andrei Aron, James Diebel, Philip Fong, John Gale, Morgan Halpenny, and Gabriel Hoffmann. Stanley: The robot that won the DARPA Grand Challenge. *Journal of Field Robotics*, 23(9):661–692, 2015. ISSN 14746670.
- [125] Vito Cerone, Mario Milanese, and Diego Regruto. Combined automatic lane-keeping and driver’s steering through a 2-DOF control strategy. *IEEE Transactions on Control Systems Technology*, 17(1):135–142, 2009. ISSN 10636536.
- [126] Zhenji Lu, Barys Shyrokau, Boulaïd Boulkroune, Sebastiaan Van Aalst, and Riender Happee. Performance Benchmark of state-of-the-art Lateral Path-following Controllers. In *2018 IEEE 15th International Workshop on Advanced Motion Control (AMC)*, pages 541–546, 2018.
- [127] T. Keviczky, P. Falcone, F. Borrelli, J. Asgari, and D. Hrovat. Predictive control approach to autonomous vehicle steering. *2006 American Control Conference*, pages 4670–4675, 2006.

References

- [128] Paolo Falcone, H. Eric Tseng, Francesco Borrelli, Jahan Asgari, and Davor Hrovat. MPC-based yaw and lateral stabilisation via active front steering and braking. *Vehicle System Dynamics*, 46(March 2015):611–628, 2008. ISSN 0042-3114.
- [129] Hongxiao Yu, Jianmin Duan, Saied Taheri, Huan Cheng, and Zhiqian Qi. A model predictive control approach combined unscented Kalman filter vehicle state estimation in intelligent vehicle trajectory tracking. *Advances in Mechanical Engineering*, 7(5):1–14, 2015. ISSN 1687-8140.
- [130] Yang Cao, Fan Yu, and Zhe Luo. Generalized Predictive Control Based on Vehicle Path Following Strategy by Using Active Steering System. In *International Symposium on Advanced Vehicle Control 2016*, 2016.
- [131] Razvan C Rafaila, Gheorghe Livint, and Florin A Rusu. Multivariable Non-linear Predictive Control of Autonomous Vehicle Dynamics. In *2016 IEEE International Conference on Development and Application Systems (DAS)*, pages 97–102, 2016. ISBN 9781509019939.
- [132] P. Falcone, F. Borrelli, H. E. Tseng, J. Asgari, and D. Hrovat. Linear time-varying model predictive control and its application to active steering systems: Stability analysis and experimental validation. In *International Journal of Robust and Nonlinear Control*, volume 18, pages 862–875, 2008. ISBN 10498923\ r10991239.
- [133] P Falcone, F Borrelli, H.E.E Tseng, J Asgari, and D Hrovat. A hierarchical Model Predictive Control framework for autonomous ground vehicles. In *2008 American Control Conference*, pages 3719–3724, 2008. ISBN 978-1-4244-2078-0.
- [134] Thorsten Luettel, Michael Himmelsbach, and Hans Joachim Wuensche. Autonomous ground vehicles—Concepts and a path to the future. *Proceedings of the IEEE Special Centennial Issue*, 100:1831–1839, 2012. ISSN 0018-9219.
- [135] Mariusz Bojarski, Davide Del Testa, Daniel Dworakowski, Bernhard Firner, Beat Flepp, Prasoon Goyal, Lawrence D Jackel, Mathew Monfort, Urs Muller, Jiakai Zhang, and Others. End to end learning for self-driving cars. *arXiv preprint arXiv:1604.07316*, 2016.
- [136] Shuyang Du, Haoli Guo, and Andrew Simpson. Self-driving car steering angle prediction based on image recognition. *Department of Computer Science, Stanford University, Tech. Rep. CS231-626*, 2017.
- [137] Urs Muller, Jan Ben, Eric Cosatto, Beat Flepp, and Yann L Cun. Off-road obstacle avoidance through end-to-end learning. In *Advances in neural information processing systems*, pages 739–746, 2006.
- [138] Gang Tao. *Adaptive Control Design and Analysis*. John Wiley & Sons, 2003.
- [139] Mario Di Bernardo, Alessandro Di Gaeta, Umberto Montanaro, and Stefania Santini. Synthesis and experimental validation of the novel LQ-NEMCSI adaptive strategy on an electronic throttle valve. *IEEE Transactions on Control Systems Technology*, 18(6):1325–1337, 2010. ISSN 10636536.

- [140] Annamaria Buonomano, Umberto Montanaro, Adolfo Palombo, and Stefania Santini. Building temperature control using an enhanced MRAC approach. In *2015 European Control Conference (ECC)*, pages 3629–3634. IEEE, 2015.
- [141] Umberto Montanaro, Alessandro di Gaeta, and Veniero Giglio. An MRAC approach for tracking and ripple attenuation of the common rail pressure for GDI engines. *IFAC Proceedings Volumes*, 44(1):4173–4180, 2011.
- [142] Annamaria Buonomano, Umberto Montanaro, Adolfo Palombo, and Stefania Santini. Dynamic building energy performance analysis: A new adaptive control strategy for stringent thermohygrometric indoor air requirements. *Applied Energy*, 163:361–386, 2016. ISSN 03062619.
- [143] Umberto Montanaro and Josep M. Olm. Integral MRAC with Minimal Controller Synthesis and bounded adaptive gains: The continuous-time case. *Journal of the Franklin Institute*, 353(18):5040–5067, 2016. ISSN 00160032.
- [144] Annamaria Buonomano, Umberto Montanaro, Adolfo Palombo, and Stefania Santini. Temperature and humidity adaptive control in multi-enclosed thermal zones under unexpected external disturbances. *Energy and Buildings*, 135:263–285, 2017.
- [145] RH Byrne and CT Abdallah. Design of a model reference adaptive controller for vehicle road following. *Mathematical and computer modelling*, 22(4):343–354, 1995.
- [146] T Fukao, S Miyasaka, K Mori, N Adachi, and K Osuka. Active steering systems based on model reference adaptive nonlinear control. In *IEEE Intelligent Transportation Systems*, pages 502–507, 2001. ISBN 0-7803-7194-1.
- [147] Takanori Fukao, Shogo Miyasaka, Kenji Mori, Norihiko Adachi, and Koichi Osuka. Active steering systems based on model reference adaptive nonlinear control. *Vehicle System Dynamics*, 42(5):301–318, 2004. ISSN 00423114.
- [148] Zachary T Dydek, Anuradha M Annaswamy, and Eugene Lavretsky. Adaptive control and the NASA X-15-3 flight revisited. *IEEE Control Systems*, 30(3):32–48, 2010. ISSN 02721708.
- [149] Daniel Shevitz and Brad Paden. Lyapunov stability theory of nonsmooth systems. *IEEE Transactions on Automatic Control*, 39(9):1910–1914, 1994.
- [150] Nicholas Fischer, Rushikesh Kamalapurkar, and Warren E Dixon. LaSalle-Yoshizawa corollaries for nonsmooth systems. *IEEE Transactions on Automatic Control*, 58(9):2333–2338, 2001.
- [151] J Corts. Discontinuous dynamical systems-a tutorial on solutions, nonsmooth analysis, and stability. *IEEE Control Systems Magazine*, 28(3):36–73, 2008. ISSN 0272-1708.

References

- [152] Antoine Schmeitz, Jeroen Zegers, Jeroen Ploeg, and Mohsen Alirezaei. Towards a generic lateral control concept for cooperative automated driving theoretical and experimental evaluation. In *2017 5th IEEE International Conference on Models and Technologies for Intelligent Transportation Systems (MT-ITS)*, pages 134–139, 2017. ISBN 978-1-5090-6484-7.
- [153] Jorge Cortes. Discontinuous dynamical systems. *IEEE Control systems magazine*, 28(3):36–73, 2008. ISSN 1066033X.
- [154] Frank H Clarke. *Optimization and nonsmooth analysis*, volume 5. Siam, 1990.
- [155] Hassan K Khalil and JW Grizzle. *Nonlinear systems*. Prentice hall Upper Saddle River, NJ, 2 edition, 2002.
- [156] Xiao-wu Mu, Zhi-shuai Ding, and Gui-fang Cheng. Uniformly ultimate boundedness for discontinuous systems with time-delay. *Applied Mathematics and Mechanics (English Edition)*, 32(9):1187–1196, 2011. ISSN 02534827.
- [157] Chris Urmson, Joshua Anhalt, Drew Bagnell, Christopher Baker, Robert Bittner, M N Clark, John Dolan, Dave Duggins, Tugrul Galatali, Chris Geyer, Michele Gittleman, Sam Harbaugh, Martial Hebert, Thomas M Howard, Sascha Kolski, Alonso Kelly, Maxim Likhachev, Matt McNaughton, Nick Miller, Kevin Peterson, Brian Pilnick, Raj Rajkumar, Paul Rybski, Bryan Salesky, Young-Woo Seo, Sanjiv Singh, Jarrod Snider, Anthony Stentz, Ziv Wolkowicki, Jason Ziglar, Hong Bae, Thomas Brown, Daniel Demirish, Bakhtiar Litkouhi, Jim Nickolaou, Varsha Sadekar, Wende Zhang, Joshua Struble, Michael Taylor, Michael Darms, and Dave Ferguson. Autonomous Driving in Urban Environments: Boss and the Urban Challenge. *Journal of Field Robotics*, 25(8):425–466, 2008.
- [158] John Leonard, Jonathan How, Seth Teller, Mitch Berger, Stefan Campbell, Gaston Fiore, Luke Fletcher, Emilio Frazzoli, Albert Huang, Sertac Karaman, and Others. A perception-driven autonomous urban vehicle. *Journal of Field Robotics*, 25:727–774, 2008. ISSN 14746670.
- [159] M. Bertozzi, A. Broggi, A. Coati, and R. I. Fedriga. A 13,000 km Intercontinental Trip with Driverless Vehicles: The VIAC Experiment. *IEEE Intelligent Transportation Systems Magazine*, 5(1):28–41, 2013. ISSN 1939-1390.
- [160] Johan Andreasson. *On generic road vehicle motion modelling and control*. PhD thesis, KTH, 2006.
- [161] Q Wang and S Müller. A hierarchical controller for path planning and path following based on model predictive control. In *International Symposium on Advanced Vehicle Control 2016*, 2016.
- [162] Mingcong Cao, Rongrong Wang, Jinxiang Wang, and Nan Chen. An integrated mpc approach for fwia autonomous ground vehicles with emergency collision avoidance. In *2018 21st International Conference on Intelligent Transportation Systems (ITSC)*, pages 2432–2437. IEEE, 2018.

References

- [163] Jitendra Shah, Matt Best, Ahmed Benmimoun, and Mohsen Lakehal Ayat. Autonomous rear-end collision avoidance using an electric power steering system. *Proceedings of the Institution of Mechanical Engineers, Part D: Journal of Automobile Engineering*, 229(12):1638–1655, 2015.
- [164] Xiaohui Li, Zhenping Sun, Daxue Liu, Qi Zhu, and Zhenhua Huang. Combining Local Trajectory Planning and Tracking Control for Autonomous Ground Vehicles Navigating along a Reference Path. In *17th International IEEE Conference on Intelligent Transportation Systems (ITSC)*, pages 725–731, 2014. ISBN 978-1-4799-6078-1.
- [165] E Kim, J Kim, and M Sunwoo. Model predictive control strategy for smooth path tracking of autonomous vehicles with steering actuator dynamics. *International Journal of Automotive Technology*, 15(7):1155–1164, 2014.
- [166] Yiheng Wei, Yangsheng Hu, Yi Dai, and Yong Wang. A generalized padé approximation of time delay operator. *International Journal of Control, Automation and Systems*, 14(1):181–187, 2016.
- [167] Haitao Xing, Jeroen Ploeg, and Henk Nijmeijer. Padé approximation of delays in cooperative acc based on string stability requirements. *IEEE Transactions on Intelligent Vehicles*, 1(3):277–286, 2016.
- [168] Anastasios M. Lekkas, Andreas Reason Dahl, Morten Breivik, and Thor I. Fossen. Continuous-Curvature Path Generation Using Fermat’s Spiral. *Modeling, Identification and Control*, 34(4):183–198, 2014. ISSN 0332-7353.
- [169] Sampo Kuutti, Saber Fallah, Konstantinos Katsaros, Mehrdad Dianati, Francis Mccullough, and Alexandros Mouzakitis. A survey of the state-of-the-art localization techniques and their potentials for autonomous vehicle applications. *IEEE Internet of Things Journal*, 5(2):829–846, 2018.

Appendix

A

List of Parameters for Initialisation

Table A.1 Design Parameters: Environment and Situational Awareness

Symbol	Value	Units
Road Geometry		
N_{lanes}	2	-
w_{lane}	3.5	-
Subject Vehicle		
l_f	1.446	m
l_r	1.477	m
M	2412.503	kg
I_z	4715.977	kg m^2
C_f	3.4781×10^5	N rad^{-1}
C_r	3.4781×10^5	N rad^{-1}
Lead Vehicle		
$l_{\text{lv},l}$	4.1	m
$l_{\text{lv},w}$	1.7	m
v_{LV}	[22.22, 25]	m s^{-1}
Potential Field		
A_{car}	10	-
γ	0.2	-
ζ	3	-
A_{lane}	36	-
ϵ	$0.14 \cdot w_{\text{lane}}$	-
α	0.16	-
V_1	(100, 0)	m
V_2	(100, $N_{\text{lanes}} \cdot w_{\text{lane}}$)	m
V_3	(-60, $N_{\text{lanes}} \cdot w_{\text{lane}}$)	m
V_4	(-60, 0)	m

List of Parameters for Initialisation

Table A.2 Design Parameters: Robust MPC for Trajectory Planning

Symbol	Value	Units
Controller Parameters		
t_s	0.1	s
N	20	-
h_t	$N \cdot t_s$	s
Q	$\text{diag}(2 \times 10^{-2}, 1 \times 10^{-2}, 1 \times 10^1)$	-
R	$\text{diag}(1.5 \times 10^0, 2 \times 10^2)$	-
P	solution of (3.30)	-
T	$10^2 P$	-
K_Ω	$-R^{-1}B^T P$	-
K	$[0, 0, 2.2628; 0.2804, 0.9300, 0]$	-
System Constraints and Initialisation		
\mathcal{X}	$-[0; 0.035; -26.4] \leq x \leq [2 \cdot w_{\text{lane}}; 0.035; 33.3]$	-
$l_{\text{lv,w}}$	1.7	m
\mathcal{U}	$-[1.5; 0.02] \leq u \leq [1.5; 0.02]$	-
x_0	$[0.5 \cdot w_{\text{lane}}; 0; 25.67]$	-

Table A.3 Design Parameters: EMRAC for lateral tracking

Symbol	Value	Units
Nominal Controller Parameters		
$v_{x,\text{nom}}$	29.8611	m s^{-1}
K_X^*	$[-0.0615, -0.157, 0.03735, 4.4651]$	-
K_R^*	4.8145	-
Weighting Matrices for Adaptive Gains		
\mathcal{M}	0.0049	-
$\hat{\mathcal{M}}_{\phi_N}$	0.0105	-
ρ_X	$10^{-3}\mathcal{I}_4$	-
ρ_R	10^{-3}	-
ρ_I	$10^{-3}\mathcal{I}_4$	-
ρ_N	8×10^{-4}	-
α_X	$[42, 42, 420, 210]^T$	-
α_R	500	-
α_I	$[4.2, 4.2, 42, 21]^T$	-
α_N	0.35	-
β_X	$\alpha_X/20$	-
β_R	$\alpha_R/20$	-
β_I	$\alpha_I/20$	-
η_ϕ	2	-
η_{ϕ_N}	30	-

Table A.4 Design Parameters: EMRAC for lateral tracking: Test-track

Symbol	Value	Units
Steering Actuator System		
$\bar{\tau}_{\text{sa}}$	30×10^{-3}	s
Nominal Controller Parameters		
$v_{x,\text{nom}}$	15.2778	m s^{-1}
K_X^*	$[-0.0501, -0.6417, 1.5724, 14.6378, -9.7546]$	-
K_R^*	1.3756	-
Weighting Matrices for Adaptive Gains		
\mathcal{M}	17.6721	-
$\hat{\mathcal{M}}_{\phi_N}$	0.01	-
ρ_X	$10^{-3}\mathcal{I}_4$	-
ρ_R	10^{-3}	-
ρ_I	$10^{-3}\mathcal{I}_4$	-
ρ_N	8×10^{-4}	-
α_X	$[42, 42, 21, 42, 42]^T \times 10^{-2}$	-
α_R	1000	-
α_I	$[42, 42, 21, 42, 42]^T \times 10^{-3}$	-
α_N	0.05	-
β_X	$\alpha_X/20$	-
β_R	$\alpha_R/20$	-
β_I	$\alpha_I/20$	-
η_ϕ	20	-
η_{ϕ_N}	90	-

List of Parameters for Initialisation

Table A.5 Design Parameters: EMRAC for lateral tracking: Overtaking Manoeuvre

Symbol	Value	Units
Steering Actuator System		
$\bar{\tau}_{\text{sa}}$	30×10^{-3}	s
Nominal Controller Parameters		
$v_{x,\text{nom}}$	8.0146	m s^{-1}
K_X^*	$[-0.0788, -0.2392, 0.7501, 7.2248, -3.3778]$	-
K_R^*	15.3771	-
Weighting Matrices for Adaptive Gains		
\mathcal{M}	7	-
$\hat{\mathcal{M}}_{\phi_N}$	0.025	-
ρ_X	$10^{-3}\mathcal{I}_4$	-
ρ_R	10^{-3}	-
ρ_I	$10^{-3}\mathcal{I}_4$	-
ρ_N	8×10^{-4}	-
α_X	$[42, 42, 21, 42, 42]^T \times 10^{-5}$	-
α_R	1	-
α_I	$[42, 42, 21, 42, 42]^T \times 10^{-6}$	-
α_N	45	-
β_X	$\alpha_X/20$	-
β_R	$\alpha_R/20$	-
β_I	$\alpha_I/20$	-
η_ϕ	20	-
η_{ϕ_N}	95	-

Appendix **B**

Development of a Prediction Model



OR a discrete-time linear state-space system described by the equation given below

$$x(k+1) = Ax(k) + Bu(k), \quad k \in \mathbb{N} \quad (\text{B.1})$$

where k denotes the current time instant, $x(k) \in \mathbb{R}^n$ is the current state, and $u(k) \in \mathbb{R}^m$ is the current input. (B.1) can be utilised in an iterative manner to build a prediction model expressing the evolution of the system's state trajectories. A schematic of such a prediction model is presented in Figure B.1.

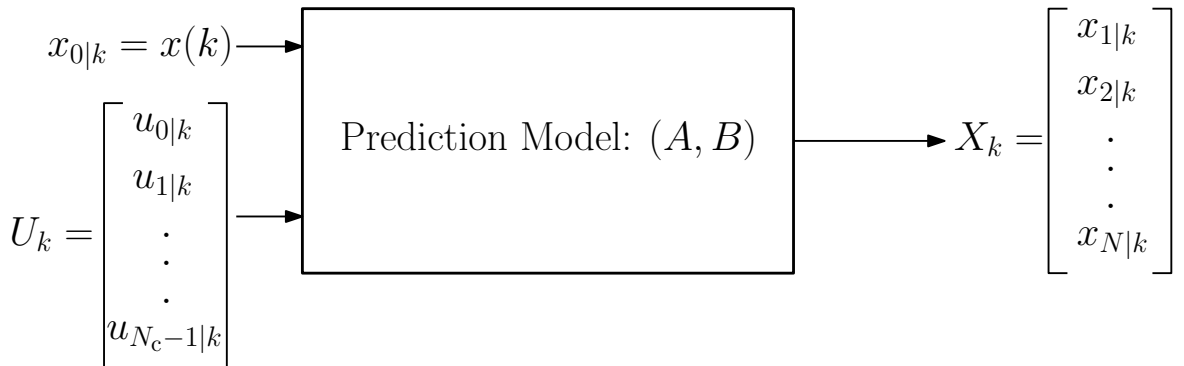


Figure B.1 Schematic of a prediction model

Development of a Prediction Model

$$\begin{aligned}
x_{1|k} &= Ax_{0|k} + Bu_{0|k} \\
x_{2|k} &= Ax_{1|k} + Bu_{1|k} \\
x_{3|k} &= Ax_{2|k} + Bu_{2|k} \\
&\vdots
\end{aligned} \tag{B.2}$$

(B.2) represent the future states of the system for a given initial condition and input. The future evolution of the states can be expressed in terms of initial state $x_{0|k}$ as shown below

$$\begin{aligned}
x_{1|k} &= Ax_{0|k} + Bu_{0|k} \\
x_{2|k} &= A(Ax_{0|k} + Bu_{0|k}) + Bu_{1|k} = A^2x_{0|k} + ABu_{0|k} + Bu_{1|k} \\
x_{3|k} &= A^3x_{0|k} + A^2Bu_{0|k} + ABu_{1|k} + Bu_{2|k} \\
&\vdots \\
x_{N|k} &= A^Nx_{0|k} + A^{N-1}Bu_{0|k} + \cdots ABu_{N-2|k} + Bu_{N-1|k}
\end{aligned} \tag{B.3}$$

where $u_{N_c} = u_{N_c+1} = \cdots = u_N$. Expressing (B.3) in matrix form gives rise to the expression below

$$\begin{bmatrix} x_{1|k} \\ x_{2|k} \\ \vdots \\ x_{N|k} \end{bmatrix} = \begin{bmatrix} A \\ A^2 \\ \vdots \\ A^N \end{bmatrix} x_{0|k} + \begin{bmatrix} B & \mathcal{O}_{n,m} & \cdots & \mathcal{O}_{n,m} \\ AB & B & \cdots & \mathcal{O}_{n,m} \\ \vdots & \vdots & \ddots & \vdots \\ A^{N-1}B & A^{N-2}B & \cdots & \mathcal{O}_{n,m} \end{bmatrix} \begin{bmatrix} u_{0|k} \\ u_{1|k} \\ \vdots \\ u_{N-1|k} \end{bmatrix} \tag{B.4}$$

By defining the matrices

$$\begin{aligned}
X_k &= \begin{bmatrix} x_{1|k} \\ x_{2|k} \\ \vdots \\ x_{N|k} \end{bmatrix}, \quad U_k = \begin{bmatrix} u_{0|k} \\ u_{1|k} \\ \vdots \\ u_{N_c|k} \end{bmatrix} \\
\Phi &= \begin{bmatrix} A \\ A^2 \\ \vdots \\ A^N \end{bmatrix}, \quad \Psi = \begin{bmatrix} B & \mathcal{O}_{n,m} & \cdots & \mathcal{O}_{n,m} \\ AB & B & \cdots & \mathcal{O}_{n,m} \\ \vdots & \vdots & \ddots & \vdots \\ A^{N-1}B & A^{N-2}B & \cdots & \mathcal{O}_{n,m} \end{bmatrix}
\end{aligned} \tag{B.5}$$

the prediction model in (B.4) is expressed in the compact form given below

$$X_k = \Phi x_{0|k} + \Psi U_k \quad (\text{B.6})$$

using, $x_{0|k} = x(k)$

$$X_k = \Phi x(k) + \Psi U_k \quad (\text{B.7})$$

where (B.7) is the prediction model expressed in its final compact matrix notation. Moreover, the following matrices are defined which will be used later while deriving the cost-function.

$$\Lambda = \begin{bmatrix} Q & & \\ & Q & \\ & & \ddots & \\ & & & P \end{bmatrix} \in \mathbb{R}^{nN \times nN}, \quad \Theta = \begin{bmatrix} R & & \\ & R & \\ & & \ddots & \\ & & & R \end{bmatrix} \in \mathbb{R}^{mN_c \times mN_c} \quad (\text{B.8})$$

Appendix C

Derivation of Cost Function: Nominal MPC

 N this chapter, the cost function described in (3.18) is simplified to express it as function of the decision variables $u_{\text{dv}} = (U_i, \theta)$ and parameters $x_{\text{par}} = (x_p, \hat{x})$. The main steps undertaken to perform this simplification are presented starting with the cost function given below.

$$V_N(U_i, \theta; x_p, \hat{x}) = \sum_{i=0}^{N-1} \left[\|x(i) - x_{ss}\|_Q^2 + \|u(i) - u_{ss}\|_R^2 \right] + \|x(N) - x_{ss}\|_P^2 + \|x_{ss} - \hat{x}\|_T^2 \quad (\text{C.1})$$

the expression can be expanded further as

$$\begin{aligned} V_N(U_i, \theta; x_p, \hat{x}) &= \sum_{i=0}^{N-1} [x(i)^T Q x(i)] + N[x_{ss}^T Q x_{ss}] - 2[x(i)^T Q x_{ss}] \\ &\quad + [u(i)^T R u(i)] + N[u_{ss}^T R u_{ss}] - 2[u(i)^T R u_{ss}] \\ &\quad + x(N)^T P x(N) + x_{ss}^T P x_{ss} - 2x(N)^T P x_{ss} \\ &\quad + x_{ss}^T T x_{ss} + \hat{x}^T T \hat{x} - 2x_{ss}^T T \hat{x} \end{aligned} \quad (\text{C.2})$$

collecting terms based on the prediction model in (B.5) and (B.8)

$$\begin{aligned} V_N(U_i, \theta; x_p, \hat{x}) &= x_p^T Q x_p + X_i^T \Lambda X_i + \theta^T J \theta \\ &\quad - 2x_p^T Q M_x \theta - 2X_i^T \Lambda J_N M_x \theta \\ &\quad + U_i^T \Theta U_i - 2U_i^T \Theta J_{N_c} M_u \theta + \hat{x}^T T \hat{x} - 2\theta^T M_x^T T \hat{x} \end{aligned} \quad (\text{C.3})$$

Derivation of Cost Function: Nominal MPC

where,

$$\begin{aligned} J &= M_\theta^T \begin{bmatrix} NQ + P + T & \mathcal{O} \\ \mathcal{O} & NR \end{bmatrix} M_\theta \\ J_{N_c} &= \begin{bmatrix} \mathcal{I}_{N_c} & \mathcal{I}_{N_c} & \cdots & \mathcal{I}_{N_c} \end{bmatrix}^T \\ J_N &= \begin{bmatrix} \mathcal{I}_N & \mathcal{I}_N & \cdots & \mathcal{I}_N \end{bmatrix}^T \end{aligned} \quad (\text{C.4})$$

using (B.7) in (C.3)

$$\begin{aligned} V_N(U_i, \theta; x_p, \hat{x}) &= x_p^T (Q + \Phi^T \Lambda \Phi) x_p + U_i^T (\Theta + \Psi^T \Lambda \Psi) U_i + \hat{x}^T T \hat{x} \\ &\quad + \theta^T J \theta + 2U_i^T \Psi^T \Lambda \Phi x_p - 2\theta^T (M_x^T Q + M_x^T J_N^T \Lambda \Phi) x_p \\ &\quad - 2U_i^T (\Psi^T \Lambda J_N M_x + \Theta J_{N_c} M_u) \theta - 2\theta^T M_x^T T \hat{x} \end{aligned} \quad (\text{C.5})$$

the equation is expressed using a compact matrix notation given below

$$\begin{aligned} V_N(U_i, \theta; x_p, \hat{x}) &= u_{dv}^T \begin{bmatrix} \Theta + \Psi^T \Lambda \Psi & -2\Psi^T \Lambda J_N M_x + \Theta J_{N_c} M_u \\ \mathcal{O} & J \end{bmatrix} u_{dv} \\ &\quad + u_{dv}^T \begin{bmatrix} 2\Psi^T \Lambda \Phi & \mathcal{O} \\ -2M_x (Q + J_N^T \Lambda \Phi) & -2M_x^T T \end{bmatrix} x_{par} \\ &\quad + x_{par}^T \begin{bmatrix} Q + \Phi^T \Lambda \Phi & \mathcal{O} \\ \mathcal{O} & T \end{bmatrix} x_{par} \end{aligned} \quad (\text{C.6})$$

(C.6) can be simplified further as

$$V_N(u_{dv}; x_{par}) = \frac{1}{2} u_{dv}^T \mathbf{G} u_{dv} + u_{dv}^T \mathbf{F} x_{par} + x_{par}^T \mathbf{L} x_{par} \quad (\text{C.7})$$

Thus, the equation above shows that V_N is a quadratic function of u_{dv} and x_{par} and commonly available solvers such as *quadprog*, *fmincon*, etc. can be used to solve the optimisation as a *qp* problem.

Appendix **D**

Derivation of Cost Function: Robust MPC

 N this chapter, the cost function described in (3.29) is simplified to express it as a quadratic function of the decision variables $u_{\text{dv}} = (\bar{x}, \bar{U}_i, \theta)$ and parameters $x_{\text{par}} = (x_p, \hat{x})$. The main steps undertaken to perform this simplification are presented starting with the cost function given below.

$$V_N(\bar{x}, \bar{U}_i, \theta; x_p, \hat{x}) = \sum_{i=0}^N \left[\|\bar{x}(i) - \bar{x}_{\text{ss}}\|_Q^2 + \|\bar{u}(i) - \bar{u}_{\text{ss}}\|_R^2 \right] + \|\bar{x}(N) - \bar{x}_{\text{ss}}\|_P^2 + \|\bar{x}_{\text{ss}} - \hat{x}\|_T^2 \quad (\text{D.1})$$

expanding the terms

$$\begin{aligned} V_N(\bar{x}, \bar{U}_i, \theta; x_p, \hat{x}) &= \sum_{i=0}^{N-1} [\bar{x}(i)^T Q \bar{x}(i)] + N[\bar{x}_{\text{ss}}^T Q \bar{x}_{\text{ss}}] - 2[\bar{x}(i)^T Q \bar{x}_{\text{ss}}] \\ &\quad + [\bar{u}(i)^T R \bar{u}(i)] + N[\bar{u}_{\text{ss}}^T R \bar{u}_{\text{ss}}] - 2[\bar{u}(i)^T R \bar{u}_{\text{ss}}] \\ &\quad + \bar{x}(N)^T P \bar{x}(N) + \bar{x}_{\text{ss}}^T P \bar{x}_{\text{ss}} - 2\bar{x}(N)^T P \bar{x}_{\text{ss}} \\ &\quad + \bar{x}_{\text{ss}}^T T \bar{x}_{\text{ss}} + \hat{x}^T T \hat{x} - 2\bar{x}_{\text{ss}}^T T \hat{x} \end{aligned} \quad (\text{D.2})$$

collecting terms based on the prediction model in (B.5) and (B.8)

$$\begin{aligned} V_N(\bar{x}, \bar{U}_i, \theta; x_p, \hat{x}) &= \bar{x}^T Q \bar{x} + \bar{X}_i^T \Lambda \bar{X}_i + \theta^T J \theta \\ &\quad - 2\bar{x}^T Q M_x \theta - 2\bar{X}_i^T \Lambda J_N M_x \theta \\ &\quad + \bar{U}_i^T \Theta \bar{U}_i - 2\bar{U}_i^T \Theta J_{N_c} M_u \theta + \hat{x}^T T \hat{x} - 2\theta^T M_x^T T \hat{x} \end{aligned} \quad (\text{D.3})$$

Derivation of Cost Function: Robust MPC

where,

$$\begin{aligned} J &= M_\theta^T \begin{bmatrix} NQ + P + T & \mathcal{O} \\ \mathcal{O} & NR \end{bmatrix} M_\theta \\ J_{N_c} &= \begin{bmatrix} \mathcal{I}_{N_c} & \mathcal{I}_{N_c} & \cdots & \mathcal{I}_{N_c} \end{bmatrix}^T \\ J_N &= \begin{bmatrix} \mathcal{I}_N & \mathcal{I}_N & \cdots & \mathcal{I}_N \end{bmatrix}^T \end{aligned} \quad (\text{D.4})$$

using (B.7) in (D.3)

$$\begin{aligned} V_N(\bar{x}, \bar{U}_i, \theta; x_p, \hat{x}) &= \bar{x}^T (Q + \Phi^T \Lambda \Phi) \bar{x} + \bar{U}_i^T (\Theta + \Psi^T \Lambda \Psi) \bar{U}_i + \hat{x}^T T \hat{x} \\ &\quad + \theta^T J \theta + 2\bar{U}_i^T \Psi^T \Lambda \Phi \bar{x} - 2\theta^T (M_x^T Q + M_x^T J_N^T \Lambda \Phi) \bar{x} \\ &\quad - 2\bar{U}_i^T (\Psi^T \Lambda J_N M_x + \Theta J_{N_c} M_u) \theta - 2\theta^T M_x^T T \hat{x} \end{aligned} \quad (\text{D.5})$$

the equation is expressed using a compact matrix notation given below

$$\begin{aligned} V_N(\bar{x}, \bar{U}_i, \theta; x_p, \hat{x}) &= u_{dv}^T \begin{bmatrix} Q + \Phi^T \Lambda \Phi & \mathcal{O} & \mathcal{O} \\ 2\Psi^T \Lambda \Phi & \Theta + \Psi^T \Lambda \Psi & -2\Psi^T \Lambda J_N M_x + \Theta J_{N_c} M_u \\ -2M_x (Q + J_N^T \Lambda \Phi) & \mathcal{O} & J \end{bmatrix} u_{dv} \\ &\quad + u_{dv}^T \begin{bmatrix} \mathcal{O} & \mathcal{O} \\ \mathcal{O} & \mathcal{O} \\ \mathcal{O} & -2M_x^T T \end{bmatrix} x_{par} \\ &\quad + x_{par}^T \begin{bmatrix} \mathcal{O} & \mathcal{O} \\ \mathcal{O} & T \end{bmatrix} x_{par} \end{aligned} \quad (\text{D.6})$$

As illustrated in Appendix C, (D.6) can be simplified further as

$$V_N(u_{dv}; x_{par}) = \frac{1}{2} u_{dv}^T \mathbf{G} u_{dv} + u_{dv}^T \mathbf{F} x_{par} + x_{par}^T \mathbf{L} x_{par} \quad (\text{D.7})$$

Thus, the equation above shows that V_N is a quadratic function of u_{dv} and x_{par} and commonly available solvers such as *quadprog*, *fmincon*, etc. can be used to solve the optimisation as a *qp* problem.

Appendix **E**

Frequency Response: Vehicle Lateral-Yaw Dynamics



The variation in lateral-yaw of a vehicle response to front steering angle for different longitudinal velocities is illustrated below.

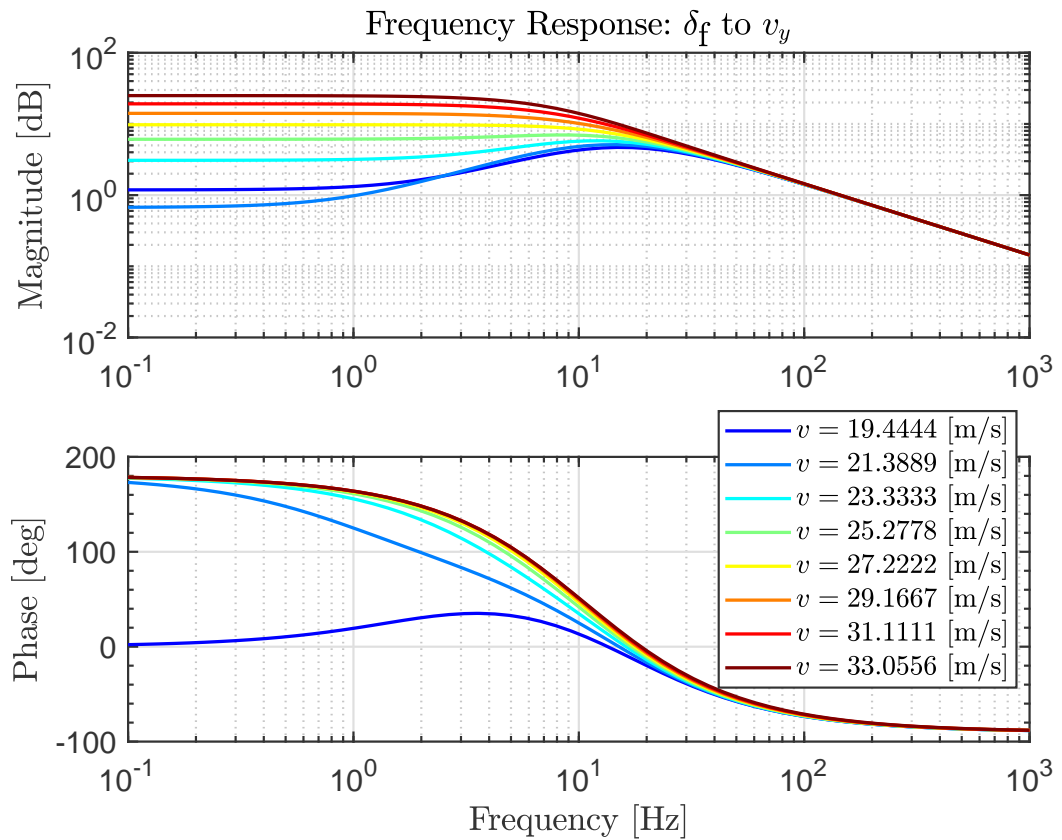


Figure E.1 Frequency Response Function: steering angle δ_f to lateral velocity v_y

Frequency Response: Vehicle Lateral-Yaw Dynamics

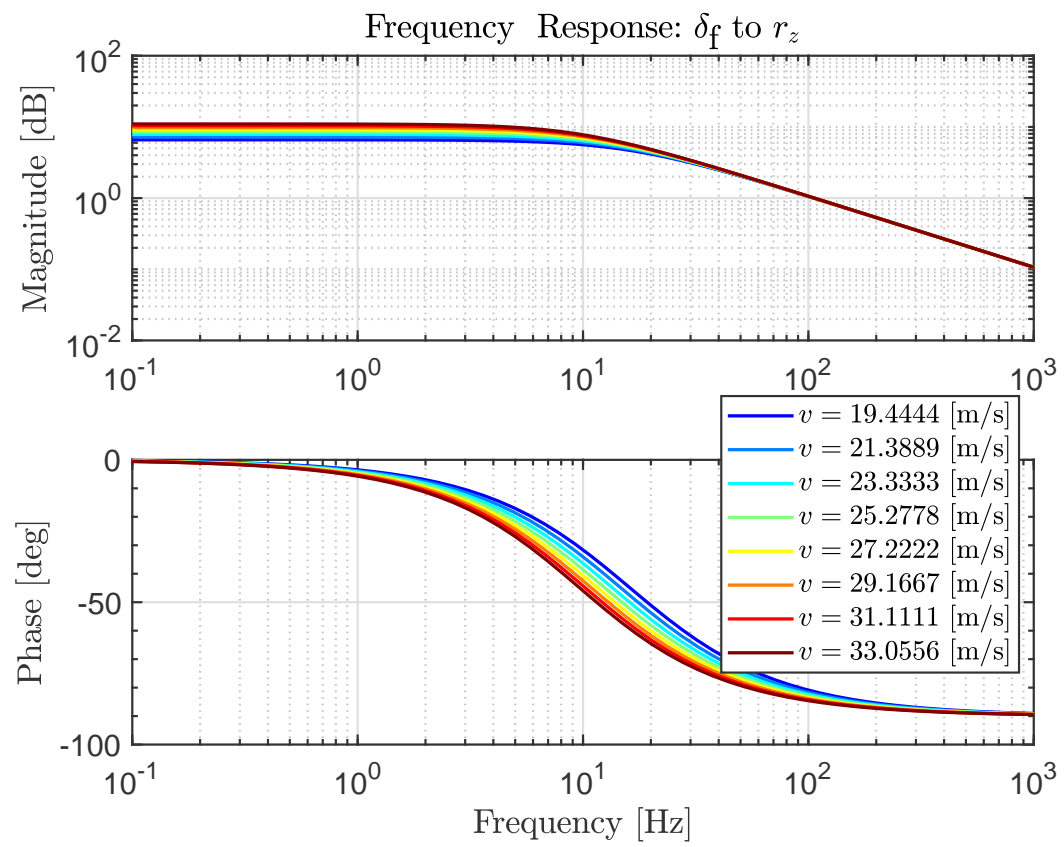


Figure E.2 Frequency Response Function: steering angle δ_f to yaw-rate r_z

Appendix F

Determination of Look-Ahead Distance

 HIS chapter provides a rationale behind the determination the look-ahead distance ξ_{la} . For the augmented path-tracking model described in (5.5) if the heading angle error ψ_e is assumed to be small, the chord lengths can be approximated as the arc length [106], see Figure F.1. This assumption can be used to define the lateral error at the look ahead point $\eta_{e,la}$ as

$$\eta_{e,la} = \eta_e + \xi_{la} * \psi_e \quad (\text{F.1})$$

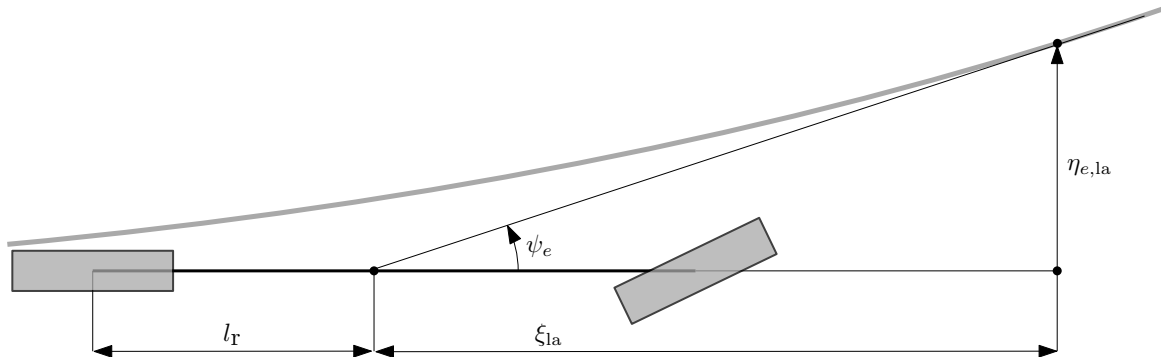


Figure F.1 Look-ahead distance ξ_{la} and lateral error $\eta_{e,la}$ at look-ahead point

Thus, from the output definition in (F.1) and the system dynamics in (5.5) a transfer function $G_{yu}(s)$ from input $u = \delta_{f,des}$ to the output $y = \eta_{e,la}$ is defined.

F.1 Medium-speed driving

The poles and zeros of $G_{yu}(s)$ for different values of look-ahead distance ξ_{la} are illustrated in Figure F.2. The model has been generated using 15.27 m s^{-1} as the longitudinal velocity. The plot shows that while the poles of the system are unaffected by the value of ξ_{la} , the damping for the conjugate zeros increases as ξ_{la} increases. Moreover, the non-minimum phase zero which introduced in the system as a result of the pure-time delay in the steering actuator and is not affected by ξ_{la} either. Thus, to prevent unwanted oscillations from entering the system, a look-ahead distance $\xi_{la} > 0$ is chosen for computing the reference curvature for the path-tracking problem presented in Section 5.4. The final value of the look-ahead distance ξ_{la} is obtained by tuning to achieve a suitable compromise between tracking accuracy (corner cutting) and smoothness of control action.

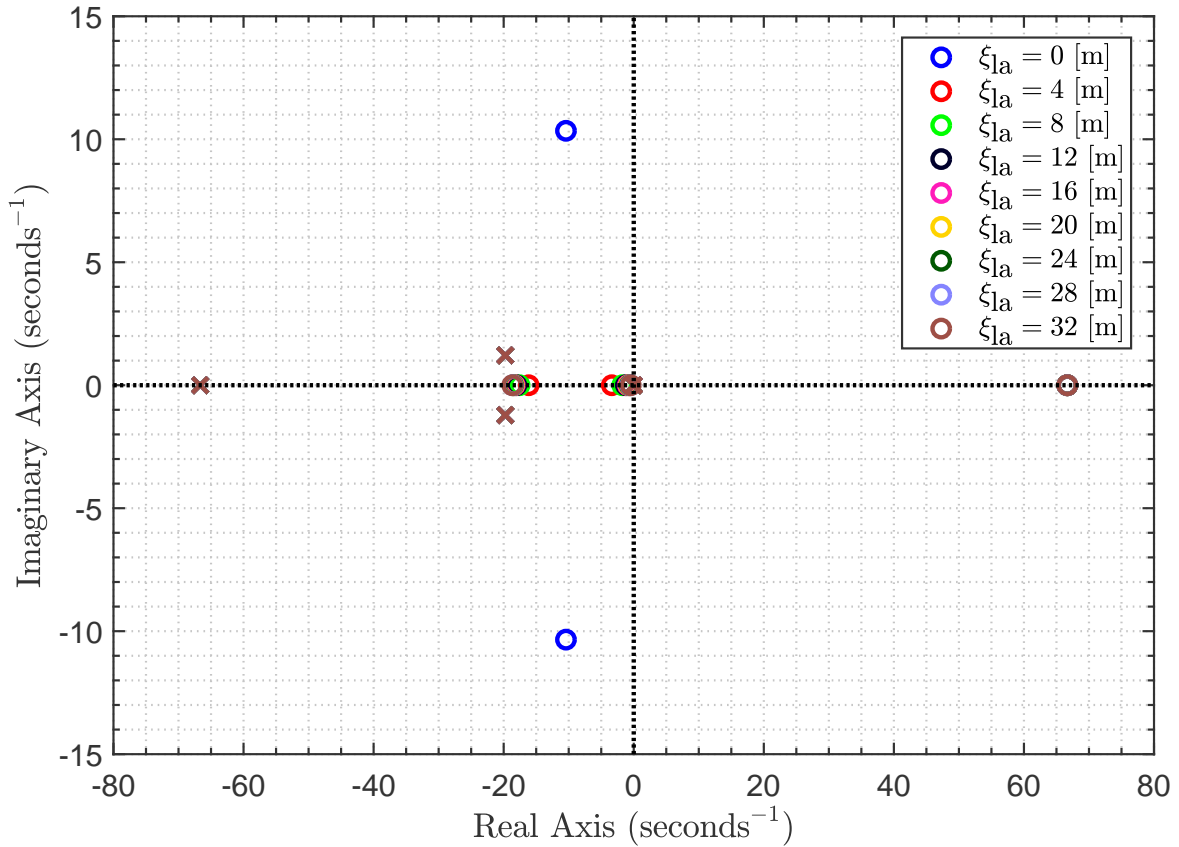


Figure F.2 Poles and Zeros of the system $G_{yu}(s)$ with $v_{x,\text{nom}} = 15.27 \text{ m s}^{-1}$ for different look-ahead distances

F.2 High-speed driving

The results and analysis from the section above are also performed for high-speed driving by defining the model $G_{yu}(s)$ using 29.18 m s^{-1} as the longitudinal velocity. Figure F.3 shows the poles and zeros of the system for increasing values of look-ahead distance ξ_{la} . The observations regarding the location of poles and the non-minimum phase zero are consistent and can also be seen in this figure. Furthermore, the plot shows that the damping of the conjugate zeros is worse which directly means that the look-ahead distance has to be much further at high-speeds to achieve similar values of damping in the system response. This insight it used to better tune the value of ξ_{la} for performing manoeuvres/tracking at high-speeds as required in Section 5.5. Consequently, just as the previous section the look-ahead distance ξ_{la} is tuned so that a suitable balance between accurate trajectory tracking and smooth system response is achieved.

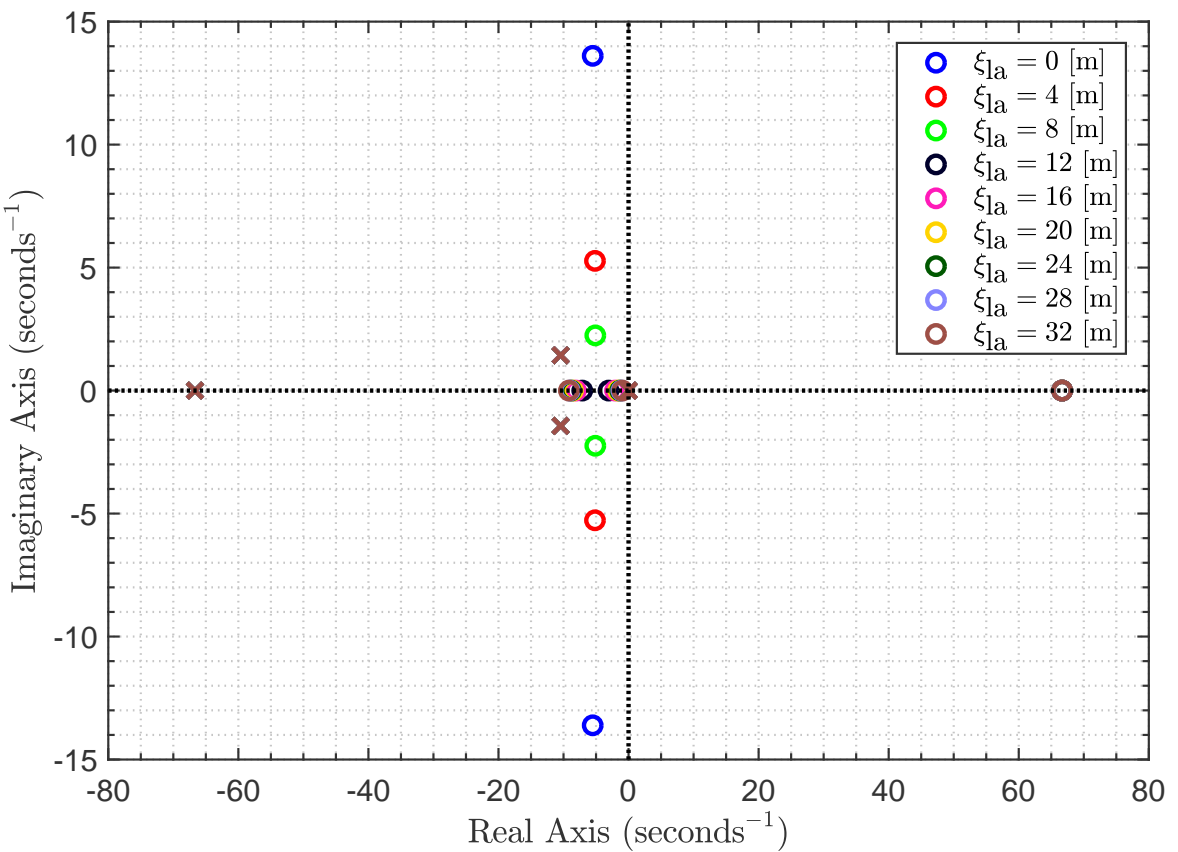


Figure F.3 Poles and Zeros of the system $G_{yu}(s)$ with $v_{x,nom} = 29.18 \text{ m s}^{-1}$ for different look-ahead distances

Design of Controllers for Reference Model

 HIS this chapter outlines the steps that are carried out to compute the nominal controllers for the reference model within the EMRAC framework. The nominal controllers consist of a nominal feedback controller K_X^* and a nominal feedforward controller K_R^* that are used to steer the dynamics of a system (5.5) towards the reference system (5.7). The control law used to achieve this is given below.

$$u(t) = K_X^*x(t) + K_R^*\kappa(t) \quad (\text{G.1})$$

G.1 Design of Reference Feedforward Controller: K_R^*

The feedforward term K_R is computed using the technique presented in [106] and it summarised below. The dynamics of the system (5.5) under state feedback K_X is given by

$$\dot{x} = (A + B_1K_X)x + B_2\kappa \quad (\text{G.2})$$

which can be further simplified by defining the matrix $A_m = (A + B_1K_X)$ resulting in the expression given below.

$$\dot{x} = A_m x + B_2\kappa \quad (\text{G.3})$$

It is noteworthy that due to the presence of the term $B_2\kappa$ while travelling on a curve, the error states will not converge to zero even though A_m is Hurwitz. This necessitates the need of a feedforward term u_{ff} (in addition to the feedback) to compensate for curved paths. The addition of u_{ff} to the control action results in the

Design of Controllers for Reference Model

closed-loop dynamics given below.

$$\dot{x} = A_m x + B_1 u_{ff} + B_2 \kappa \quad (\text{G.4})$$

By following steps similar to the ones presented in [106] (Chapter 3), a feedforward action can be computed that results in zero steady-state error for the lateral position $\eta_{e,ss}$ but cannot influence the steady-state error for the heading angle error $\psi_{e,ss} = 0$. This resultant u_{ff} obtained using the Symbolic Toolbox in MATLAB is a function of the model parameters in the matrices (A , B_1 , B_2), elements of the feedback control matrix K_X , and the curvature κ . The expression of the function is lengthy but by depicting it as K_R the feedforward action is presented in the compact form given below.

$$u_{ff} = K_R \kappa \quad (\text{G.5})$$

G.2 Design of Reference Feedback Controller: K_X^*

In (G.1), the feedback controller is a full state feedback law. The only prior condition for the design of the feedback law is that the resultant closed-loop system dynamics need to be stable (i.e., $(A + B_1 K_X)$ is Hurwitz). For this body of work, the feedback controller is designed using the procedure presented below.

where \mathcal{I} is an identity matrix of appropriate dimensions. For a given stabilizing feedback controller K_X , a feedforward controller K_R can be designed based on Section G.1. For the resultant closed-loop system given as

$$\dot{x} = (A + B_1 K_X) x + (B_1 K_R + B_2) \kappa \quad (\text{G.6})$$

the output equation is defined as

$$y = \mathcal{I}x \quad (\text{G.7})$$

where \mathcal{I} is an identity matrix of appropriate dimensions. The definition of the output vector is used to create transfer functions $G_{j1}(s)$ from input κ to the j^{th} output where $j \in \{1, \dots, 5\}$. For the closed-loop system (G.6), it is desirable to minimise the steady-state gain of the error outputs (i.e., η_e and ψ_e) and have favourable phase characteristics in high-frequency regions. Moreover, since the steering dynamics are modelled as Padé approximations, there is also some non-minimum phase behaviour introduced into dynamics of lateral velocity v_y and yaw-rate r_z . As a result, to reduce the negative effect due to zeros in the positive half of the complex plane it is necessary to push them as far as possible from the origin. A optimisation routine is utilised to calculate an appropriate feedback control action that considers

the requirements discussed above. The objectives for this optimisation routine can be formulated as

$$\begin{aligned}
 & \min V_{\text{ctrl}}(K_X) \\
 & V_{\text{ctrl}}(K_X) = -\sum_{j=1}^2 (\operatorname{Re}(z_{G_{j1}}^+))^2 + \sum_{k=3}^4 (G_{k1}(0))^2 + (\angle(G_{31}(\infty)))^2 \\
 & \text{subject to} \\
 & \operatorname{Re}(\lambda_i) < 0, \quad i = 0, 1, \dots, 5 \\
 & \frac{K_X(1, 4)}{K_X(1, 3)} \in [\xi_{\text{la,min}}, \xi_{\text{la,max}}]
 \end{aligned} \tag{G.8}$$

where $\operatorname{Re}(z_{G_{j1}}^+)$ represents the real part of the non-minimum phase zeros of the $G_{j1}(s)$ transfer function, $G_{.1}(0)$ represents the steady-state gain of the transfer function, $\angle(G_{.1}(\infty))$ represents the phase of the tranfer function as $s \rightarrow 0$, λ_i represents the i^{th} eigenvalue of the closed-loop matrix $A + B_1 K_X$, and $[\xi_{\text{la,min}}, \xi_{\text{la,max}}]$ represents the suitable range pf look-ahead distances which are obtained from Appendix F. The optimisation routine in (G.8) is solved using the MATLAB function *fmincon* and the resultant optimal feedback controller K_X^* that minimises the cost function is used as the feedback controller for the reference model.

G.3 Closed-loop Dynamics

The feedback controller from Section G.2 is used to calculate the appropriate feedforward action K_R^* . Thus, the resultant control law of the form (G.1) is obtained and the closed-loop dynamics are given as

$$\dot{x} = (A + B_1 K_X^*)x + (B_1 K_R^* + B_2)\kappa \tag{G.9}$$

where defining $A_m = (A + B_1 K_X^*)$ and $B_m = (B_1 K_R^* + B_2)$ expression given below

$$\dot{x} = A_m x + B_m \kappa \tag{G.10}$$

is obtained which describes the dynamics of the reference model.

Vita

Shilp Dixit was born in Rajasthan, India in 1989. He successfully completed his B.E in Information Technology from University of Mumbai, India in 2010. Subsequently he worked at Deloitte Consulting LLC. as a Business Analyst from 2010 to 2012. He then moved to the Engineering Research Center in Tata Motors where he worked on semi-active suspension controller. Shilp was a graduate student at Eindhoven University of Technology from 2013 to 2015 where he obtained his MSc. in Automotive Technology and worked under the supervision of Prof. Henk Nijmeijer. He joined Flanders Make, Belgium as an associate research engineer in 2016 and worked on various automotive projects such as waste heat recovery systems and motion control of semi-autonomous vehicles.

Since October 2016, Shilp has been a PhD researcher in the Department of Mechanical Sciences at University of Surrey, UK under the supervision of Dr. Saber Fallah and Dr. Umberto Montanaro. His research focuses on design of motion planning and control algorithms for the next generation of intelligent vehicles. His work was supported by Jaguar Land Rover and the UK-EPSRC grant EP/N01300X/1 as part of the jointly funded Towards Autonomy: Smart and Connected Control (TASCC) Programme. This thesis is a compilation of the work done during the PhD.

